UNIVERSITÉ DU LUXEMBOURG

PhD- FSTM-2023-030
The Faculty of Science, Technology and Medicine

DISSERTATION

Defence held on 08/03/2023 in Esch-sur-Alzette

to obtain the degree of

DOCTEUR DE L'UNIVERSITÉ DU LUXEMBOURG

EN *SCIENCES DE L'INGÉNIEUR*

by

Karl Nicolaus VAN ZWEEL
Born on 14 January 1988 in Heilbron, (South Africa)

OBSERVING UNSEEN FLOWLINES AND THEIR CONTRIBUTION TO NEAR STREAM ENDMEMBERS IN FORESTED HEADWATER CATCHMENTS

Dissertation defence committee

Dr Christophe Hissler, dissertation supervisor
Senior Researcher, Luxembourg Institute of Science and Technology (LIST)

Dr Julien Bouchez
Senior Researcher, CNRS, Institut de Physique du Globe de Paris

Dr Stéphane Bordas, Chairman
Professor, Université du Luxembourg

Dr Markus Hrachowitz
Associate Professor, Technical University of Delft

Dr Laurent Pfister, Vice Chairman
Professor, Université du Luxembourg, Luxembourg Institute of Science and Technology (LIST)

"Eventually, all things merge into one, and a river runs through it. The river was cut by the world's great flood and runs over rocks from the basement of time. On some of the rocks are timeless raindrops. Under the rocks are the words, and some of the words are theirs. I am haunted by waters."

— Norman Maclean, A River Runs Through It

Karl Nicolaus van Zweel

Observing unseen flowlines and their contribution to
near stream endmembers in forested headwater catchments

202 pages.

PhD thesis, University of Luxembourg (2023)
With references, with summary in English

PhD- FSTM-2023-030

Abstract

The general scope of the PhD research project falls within the framework of developing integrated catchment hydro-biogeochemical theories in the context of the Critical Zone (CZ). Significant advances in the understanding of water transit time theory, subsurface structure controls, and the quantification of catchment scale weathering rates have resulted in the convergence of classical biogeochemical and hydrological theories. This will potentially pave the way for a more mechanistic understanding of CZ because many challenges still exist. Perhaps the most difficult of all is a unifying hydro-biogeochemical theory that can compare catchments across gradients of climate, geology, and vegetation. Understanding the processes driving the evolution of chemical tracers as they move through space and time is of cardinal importance to validating mixing hypotheses and assisting in determining the residence time of water in CZ.

The specific aim of the study is to investigate what physical and biogeochemical processes are driving variations in observable endmembers in stream discharge as a function of the hydrological state at headwater catchment scale. This requires looking beyond what can be observed in the stream and what is called "unseen flowlines" in this thesis. The Weierbach Experimental Catchment (WEC) in Luxembourg provides a unique opportunity to study these processes, with an extensive biweekly groundwater chemistry dataset spanning over ten years. Additionally, WEC has been the subject of numerous published works in the domain of CZ science, adding to an already detailed hydrological and geochemical understanding of the system.

Multivariate analysis techniques were used to identify the unseen flowlines in the catchment. Together with the excising hydrological perception model and a geochemical modelling approach, these flowlines were rigorously investigated to understand what processes drive their respective manifestations in the system. The existing perceptual model for WEC was updated by the new findings and tested on 27 flood events to assess if it could adequately explain the $c - Q$ behaviour observed during these periods. The novelty of the study lies in the fact that it uses both data-driven modelling approaches and geochemical process-based modelling to look beyond what can be observed in the near-stream environment of headwaters.

General introduction

Context of the thesis

A better understanding of water resources is necessary, as evidenced by the floods of 2021 and the severe droughts that followed the next year in Western Europe. The need for a multi-disciplinary approach to the problem is greater than ever before to ensure consistent supplies of fresh water, protect lives and infrastructure from floods in a landscape that is ever changing due to human activity.

The definition of the critical zone (CZ) was a big step in this direction (Brantley et al., 2007; Anderson et al., 2007; Amundson et al., 2007; Brantley and White, 2009). The CZ, spanning from the top of the canopy to the fresh bedrock, can be viewed as the skin of the earth, where solids, gasses – and fluids interact. If we break down the CZ further into functional units, we can define catchments. Catchments are the fundamental functional units of the earth's surface where the structure of the regolith controls most of the fluid and energy exchanges. The regolith is the CZ's hidden part inside catchments, that encompasses all material from fresh rock to the atmosphere (Eggleton, 2001; Field et al., 2015; Sciences and Geosciences, 2001). Regolith is a major compartment of CZ where fluxes of water, energy, solutes and matter occur. The production of regolith from the original bedrock influences the chemistry of surface waters and buffers the atmospheric CO_2 concentration (Taylor et al., 2012; West et al., 2013; Berner and Maasch, 1996). The regolith is the terrestrial environmental compartment where most of the water exchanges occur. Its bio-physico-chemical properties drastically impact the water that percolates and/or stores in its different parts (organic and mineral soil horizons, weathered and/or fractured bedrock, etc.).The time frame in which these processes take place varies from minutes to millennia. One of the most important questions currently that we are faced with is how long does water stay and where?

Aims and objectives

The aim of the study is to investigate what physical and biogeochemical processes are driving variations in observable endmembers in stream discharge as a function of the hydrological state at headwater catchment scale. Understanding the processes driving the evolution of chemical tracers as they move through space and time is of cardinal

importance for understanding the residence time of water in *CZ*. A unique opportunity is afforded in the Weierbach Experimental Catchment (*WEC*) in Luxembourg for the study, with an extensive bi-weekly groundwater chemistry data set. Multivariate analysis techniques were used to identify hidden endmembers (flow lines) in the catchment. The existing perceptual model of the *WEC* was updated by the new findings and tested on 27 flood events to assess if it could adequately explain the $c - Q$ behaviour observed during these periods.

This new insight is presented in the framework of integrated hydro-biogeochemical theories. This PhD is embedded in the doctoral unit project FNR/PRIDE/HYDRO-CSI (coordinated by Prof. Laurent Pfister) and supervised by a collaboration between the University of Luxembourg/LIST (Dr. Christophe Hissler) and the Karlsruhe Institute of Technology (Prof. Erwin Zehe).

Thesis layout

The structure of the thesis deviates slightly from the classical structure of a PhD thesis in that the state of the art and the description of the study site are presented as two respective but complimentary chapters. This was done to provide readers who may not be so familiar with geochemistry with a perspective on current research problems within the framework of integrated hydro-geochemical theories. There have been important review papers (Hrachowitz et al., 2016; Li et al., 2021; Benettin et al., 2022) written about this task, but due to the length and breadth of the topic, chemical processes are rarely talked about in depth.

Chapter 1 explores the current state of the art in the context of integrated hydro-biogeochemical theories. The aim of the chapter is to give the reader a conceptual feel of the scope of the field by touching on well-established theory in the field of geochemistry and progressively discussing the advancements in our understanding of coupled hydro-geochemical processes that not only influence atmospheric CO_2 budgets but also play a key role in our ability to assess the influence of land use changes on catchment-scale water storage and solute export. The chapter concludes by synthesising a conceptual model that highlights the knowledge blocks required to build a numeric model of catchments.

Chapter 2 discusses the study site. The purpose of the discussion is to provide the reader with a concise but comprehensive overview of all the work that has been accomplished in *CZ* science. What is known about the *WEC* is critically evaluated in light of the knowledge blocks identified in Chapter 1. The chapter concludes with a discussion of the evolution of our understanding of the system and the contribution that this research can make.

A detailed discussion of the methodologies used during the study is provided in **Chapter 3**. The chapter is organised in accordance with the overall structure of the thesis. Critical

aspects of the methodology will be revisited in the respective chapters to refresh the reader.

In **Chapter 4**, the results of a multivariate analysis are explained, and classical graphical geochemical techniques are presented. The central hypothesis in this chapter states that the large variation in concentrations observed in solutes (SO_4^{2-}, Na^+, Ca^{2+}, and Mg^{2+}) is due to the mixing of shallow and deep flow lines during sampling. The underlying control can be attributed to a rapid decrease in vertical conductivity, and, as with $c - Q$ patterns in stream flow, the relative contribution of the respective flow lines will vary depending on the system's hydrologic state. If the system has a large enough set of data, it will be possible to separate the chemical signatures of the most important flow lines because their chemical compositions will be different enough to make this possible.

Hypotheses derived from the conceptual understanding of the updated hydro-biogeochemical perceptual model will be tested using synthetic experiments in **Chapter 5** (numerical geochemical models). The main hypothesis that will be tested in this chapter is that carbonate dissolution is the primary mechanism responsible for the increase in alkalinity that occurs as water moves deeper into the subsurface from the surface. The weathering of silicate minerals also contributes to alkalinity, albeit to a lesser extent. The primary contributor to the acidity in the system can be attributed to the oxidation of *DOC*. As a result, on a larger scale, the system can be understood as being driven by acid-base reactions. Linked to this is the secondary hypothesis that the dominant source of sulphate is surface input and not pyrite oxidation. In addition, surface fluxes of sulphide (S) are stored as sulphate (SO_4^{2-}) minerals, and the effect of sulphate reduction to pyrite can be disregarded.

In the final chapter (**Chapter 6**), a proof of concept for the work is presented to the reader. On the data set developed in Chapter 4, a supervised learning algorithm (commonly referred to as "machine learning") is trained. The model (Random Forest) is then used to classify chemical samples collected during 27 flood events in the WEC over a 10-year period. The results of this classification step are then evaluated in light of the current understanding of the hydrological processes underlying the generation of streamflow in the *WEC*. The chapter concludes with a discussion of the study's significance within the paradigm of integrated hydro-biogeochemical theories and the potential future research avenues that it may inspire.

Contents

Chapter 1

A brief geochemical perspective on integrated hydro-biochemical theories

1.1 Introduction

The common notion that surface water more closely resemble soil- or ground water than precipitation has led many authors (Langbein and Dawdy, 1964; Johnson et al., 1969; Buttle and Peters, 1997; Evans and Davies, 1998) to theorize that inference can be drawn about the magnitude and mobility of stored subsurface water by observing stream chemistry (Brooks et al., 2015). It is intuitive to assume that the extent of chemical evolution of water entering the *CZ* will be a function of the contact time the solute has with the host rock and soil, it is therefore fair to assume that a link can be made between stream chemistry and residence time of water in *CZ*. This task however has proven to be difficult and is one of the two central themes identified in the double paradox defined by Kirchner, 2003. The first part of the paradox asked the question how 'old water' is so rapidly mobilized, and the second part linked to this, is the spatial variability of the water chemistry of the water stored in the catchment. The question of the first part of the double paradox has been address in several publications including in the work by McDonnell and Beven (2014) . The second part of the paradox is where integrating geochemistry into hydrological studies can add value.

It has been the interest of many studies to link the hydrological- and biogeochemical functioning of *CZ* to concentration- discharge ($c - Q$) patterns observed in the outlet of a catchment. Evans and Davies (1998) compiled a series of taxonomic loops that aimed to describe different classes of episodic variation in dissolved solutes. This was done by making use of a 3-component conservative endmember-mixing model (precipitation, soil water and groundwater), relying on the assumption of no transient variability of endmember chemical signature in response to antecedent conditions (Chanat et al., 2002). The main uncertainty in this approach lies in characterizing the endmember solute concentration. McDonnell et al. (1991) has looked at addressing this variability in hydrograph separation using either a two-component model ($2CM$) or a three component model ($3CM$). Ladouche et al. (2001) investigated combining stable isotopes – and major elements tracers to distinguish between sources during endmember mixing. Aubert et al. (2002) took this one step further with the inclusion of $^{87}Sr/\ ^{86}Sr$ isotopic ratios and managed to show the influence of distinct contributing areas or reservoirs and that their relative contributions are a function of the hydrological state of the system. Godsey et al. (2009) evaluated several models aimed to describe $c - Q$ behaviour by making use of data from 59 geochemically diverse US catchments. All the catchments in the study showed nearly chemostatic behaviour if evaluated using the power law approach in the form $C = aQ^{-b}$. In this study it was furthermore found that most simplistic hydrological and geochemical models could be forced to approximately fit the observed concentration discharge relationship by assuming unrealistic or internally inconsistent parameter values.

The two most important methods that emerged and commonly used in stream flow separation is hydrograph separation (Klaus and McDonnell, 2013) and a multivariate approached

to end member mixing analysis that is now mostly referred to *EMMA* (Christophersen and Hooper, 1992). The major difference between these two techniques is the first aims to quantify temporal source components or stated in layman's terms distinguishing between pre-event and event water. *EMMA* on the other hand aims to distinguish between geographical sources or pools (Ali et al., 2010; Correa et al., 2017; Petelet-Giraud et al., 2018; Floriancic et al., 2019; Gillet et al., 2021). Both these techniques are based on the same four assumptions. Assumption 1: The stream water is a mixture of source solutions. Assumption 2: The mixing process is linear and only uses hydrodynamic mixing. Assumption 3: The tracers' solutions are conservative. Assumption 4: The concentration of the source solutions is extremely high.

Since the application of *EMMA* to model stream water as a mixture of soil water endmembers several decades ago (Hooper et al., 1990; Christophersen et al., 1990), this technique has been instrumental in the development of hydrological science, as tracers aided in the understanding of catchment integrated response of hydrological flow paths (Delsman et al., 2013). The use of tracers in *EMMA* has raised another important question: How many tracers to use? This has been addressed the work by Barthold et al. (2011). The authors evaluated how varying tracer set sizes and number of end members. It was found that models where in fact highly sensitive to tracer set sizes and composition. Furthermore, due to its ubiquity in *CZ*, it was demonstrated that major elements are not always useful tracers for distinguishing between sources. The main problem faced with *EMMA* lies exactly in the assumptions that is made for the techniques. A paper by Pelizardi et al. (2017) has shown the influence chemical reactions can have on the identification of endmembers (assumption 4). The dilemma then of this technique is how to decouple the chemical variance from the hydrodynamic mixing process (assumption 2).

It would be a logical step to start off by constructing a reaction path model between two endmembers to be able to decouple chemical variance from mixing variance along a mixing line between two endmembers in a system. This can be done by constructing an inverse model. An inverse model can be described as the process of deducing the geochemical reactions that are responsible for the change in the chemical composition of water along a flow path. It is necessary to conduct at least two chemical analyses of the water at different points along the flowline. Additionally, it is necessary to identify a set of mineral phases that are possibly reacting throughout the flow path. Mole-balance models are calculated using the results of the analyses and the phases. A series of mole transfers of phases and reactants is what makes up a mole-balance model. This model is used to account for the change in composition that occurs along the flow path. This methodology has been applied to a number of well-known investigations (Garrels and MacKenzie, 1967), and the documentation for it is extensive (Plummer et al., 1991a; Parkhurst and Charlton, 2008). This approach, on the other hand, is plagued by the same issue that plagues a large number of other modelling approaches in this area, and that issue is equifinality. The process of inverse modelling might result in multiple distinct models that are all capable of

adequately explaining the system. After that, the modeller is responsible for interpreting the data and determining which model is the most plausible option.

CZ science seeks to develop a mechanistic-predictive approach to explain $c-Q$ patterns observed in stream discharge (Chorover et al., 2017). Several seminal papers has hypothesized that the main mechanisms driving chemostatic behaviour are cation exchange (Hoagland et al., 2017; Herndon et al., 2015; Bao et al., 2017; Kim et al., 2014), seasonal dissolution/ precipitation of amorphous aluminosilicates (Anderson et al., 1997; Mulholland et al., 1990; Williams et al., 1993; Campbell et al., 1995) or change in reactive mineral surface area and decrease in weathering rates through chemical affinity effects (Clow and Mast, 2010; Li et al., 2017). With the improved understanding of these mechanisms and the coupling of solute transport (advection, dispersion, and diffusion), reactive transport models have developed into very useful tools to intemperate and understand the behaviour of *CZ* (Li et al., 2017). Reactive transport models (*RTM*) are for the most part complex, physically based models similar to distributed hydrological models and subsequently suffer the same limitations in terms of nonlinearity of scale, uniqueness, equifinality and uncertainty (Beven and Freer, 2001; Ebel and Loague, 2006). (Li et al., 2017) in a review paper on the role of *RTM*'s in the understanding of *CZ*, points out that complex process based models such as *RTM*'s are not necessary superior to parsimonious models (power law model etc.), but is required to tease apart the importance of individual controlling processes. Bao et al. (2017) developed a watershed hydrogeochemical code (*RT-Flux-PIHM*). The model couple hydrological processes (*PIHM*) and land-surface processes (*FLUX—Noah Land Surface Model*) with a multicomponent reactive transport model. Li et al. (2017) utilized the *RT-Flux-PIHM* code to show that in the modelled study area, Cl^- chemodynamic behaviour is governed by flushing of pore water, whereas the Mg^{2+} chemostatic behaviour can be attributed to clay dilution and cation exchange. Maher and Chamberlain (2014) proposed a model that relates weathering derived products to mean fluid travel time and the supply of fresh reactive material from erosion to downstream propagation. The model relies on the theory developed by Maher (2011) where the author showed that the weathering rate of granitic material depended most strongly on fluid residence time and fluid flow rate and depended weakly on material age. The implication of this is that there is a point in the trajectory path of a solute particle, as it moves though the system, where the chemical evolution of the solute is thermodynamically limited based on the solution's proximity to equilibrium. The decrease in reaction rate for a given mineral as a function of the linear approach to equilibrium can be seen in equation 1.1 (Lasaga, 1984; Appelo and Postma, 2006).

$$R = k\frac{A_0}{V}(\frac{m}{m_0})^n g(C) \tag{1.1}$$

In the rate equation R is the overall rate ($mol/L/s$), k is the specific rate ($mol/m^2/s$), A_0 is the initial surface area of the given solid mineral (m^2), V is the volume of the solution (m^3).

The factor $(m/m_0)^n$ accounts for the change in surface area, where m_0 is the initial moles and m the moles of solid for a given time. The exponent n in the factor is a function of the initial grain size distribution (Dixon and Hendrix, 1993). The function $g(C)$ accounts for the effects of proximity of the solution composition to equilibrium with the given mineral. Earlier work done by Maher (2011) showed that resident time of a solute relative to the residence time required for the solute to approach chemical equilibrium is the dominant mechanism controlling solute fluxes. Maher and Chamberlain (2014) then proceeded to develop a scaling approach to relate these two time scales. The model is fitted to recorded $c-Q$ data and use the Damköhler (D_a) number and mean travel time distribution as fitting parameters. The main uncertainties of all the reactive transport models are heterogeneity of reacting minerals that are contributing to the chemical evolution of the solute. In various studies the D_a-number is calculated for the weathering rate of specific mineral in a numerical reactive transport model (Maher, 2010; Maher, 2011; Maher and Chamberlain, 2014; Ameli et al., 2017). The goal of all these studies was to determine for what range of D_a-numbers catchment discharges will be sensitive to heterogeneity.

The link between the geochemical and catchment hydrological studies overlap strongly when looking at the residence time of a water particle in *CZ*. Currently the main research focus of hydrologists in the *CZ* is to understand the travel time distribution (TTD) of water in the regolith to the stream. It is well understood that TTD is time variable for a catchment and usually a mean travel time distribution is assumed, such is the case of the convolution integral approach. An alternative to this approach has developed in the recent past, with the notable change in thinking that the system can be conceptualized as a suite of storage components linked by fluxes that represent the perceived dominant processes of the catchment (Hrachowitz et al., 2016). This is in essence a semi-distributed hydrological modelling approach and therefore rely on so-called 'conservative' tracers (O-H stable isotopes) to calibrate the model. In the review paper by Abbott et al. (2016) the function of tracers and the information that can be obtained from tracer tests are discussed. What is of particular importance in the discussion of the note that the hydrological approach of determining travel time is either focused seasonal or event scales. This approach is very effective at predicting water discharges but cannot account for the velocity effect . What this means is that current geochemical modelling approaches that does consider the effect to travel time distributions, assume a mean travel time. Due these assumptions, these models can only give insight on continental scale (solutes liberated by weathering).

Several approaches have been briefly discussed to introduce the now very apparent need for integrated hydro-biogeochemical theories. In a review paper, Li et al. (2021) proposed a way forward . Most if not all review papers discuss and refer to studies that form part of the building blocks of a new theory, without going into detailed discussions about the fundamental theory these studies are based on. To give the reader a good conceptual view of the current state of art, selected biogeochemical processes will be discussed in more detail and integrated into a conceptual model in the section to follow.

1.2 Chemical evolution on the journey from recharge to discharge

The need for integrated hydro-geochemical theories is echoed in every recent study looking at the impacts on land use changes and the CO_2 balance in the atmosphere. It is well understood that hydrological -and biogeochemical processes are tightly coupled, dictating fluxes and storage of atmospheric CO_2. Recent work has shown that weathering rates of carbonates shales (underlies 20-25% of the Earth's land area) is highly responsive to environmental conditions.

On continental scale the most abundant cations and anions are Ca^{2+}, Mg^{2+} and Na^{+}, HCO_3^-, SO_4^{2-}, NO_3^- and Cl^-. The global concentrations of Na^{+}, SO_4^{2-}, and Cl^- in fresh groundwater approach the sigmoidal shape of a normal distribution, suggesting the global controls on the concentrations of these species are their respective availability in rocks, relatively slow rate of dissolution or biological processes (Davis and De Wiest, 1966; Appelo and Postma, 2006). Solutes like Ca^{2+}, SiO_2 and HCO_3^- seems to reach an asymptotic value, suggesting that these species reach a maximum concentration that are thermodynamically limited (Maher, 2011).

On catchment scale, the processes controlling the concentration of solutes are significantly more complex. Catchments integrate both hydrological-and biogeochemical transformation processes (Grathwohl et al., 2013), these processes are in most cases not in equilibrium and many are influenced by feedback mechanisms, causing non-linear relationships between processes. The most simplistic way to view the geochemical evolution of a solutes along its flow path from recharge to groundwater, is the change in type from $NaCl$-type - to Ca^{2+}-$HC0_3^-$-type water and then with time again to $NaCl$-type (sea water) with increasing age (Chebotarev, 1955).

Chebotarev (1955) concluded in a classic paper based on more than 10,000 chemical analyses of well samples from Australia that groundwater tends to chemically evolve toward the composition of seawater. He discovered that this evolution is typically accompanied by the regional changes in dominant anion species listed below:

$$Cl^- \rightarrow HCO_3^- + SO_4^{2-} \rightarrow SO_4^{2-} + Cl^- \rightarrow Cl^- + SO_4^{2-} \rightarrow Cl^- \tag{1.2}$$

The processes governing the evolution of infiltrating water can be broadly summarized as ion exchange, dissolution of primary minerals and precipitation/ dissolution of secondary minerals (Cherry and Freeze, 1979; Appelo and Postma, 2006). Generally, the evolution from Cl^--type water to HCO_3^- -type water with depth can be attributed to carbonate mineral dissolution in a response to dissolving CO_2 gas into soil solution (Appelo and Postma, 2006). Because calcite and dolomite are abundant in nearly all sedimentary basins, and because these minerals dissolve quickly when exposed to CO_2-charged groundwater,

HCO_3^- is almost always the dominant anion in recharge areas. Gypsum and anhydrite are far more soluble than calcite and dolomite, but far less so than chloride minerals like halite ($NaCl$) and sylvite (KCl). When calcite (or dolomite) and gypsum dissolve in fresh water at 25°C, the water becomes brackish, with total dissolved solids ranging between 2100 and 2400 (mg/L) for a P_{CO_2} range of 10^{-3} to 10^{-1} bar. Because SO_4^{2-} will be the dominant anion, we have effectively entered the SO_4^{2-} -HCO_3^- composition phase of the Chebotarev evolution sequence (Cherry and Freeze, 1979).

Before following the journey of a water particle through the CZ, flowlines and endmembers will be briefly defined, as in some discussions these two terms are used interchangeably, and depending on the context of some literature, these two terms may not mean the same thing. In the context of this work, a flowline is the path that water takes in the aquifer, defined as a continuous line that traces the maximum gradient on a potentiometric surface map.

According to most chemical literature, an endmember (also end-member or end member) is a mineral or chemical composition that is at the extreme end of a series in terms of the purity of its chemical composition. In the context of mixing models, this would imply an extreme set of tracer concentrations. In the context of this work, it is assumed that dominant flowlines exist and that these flowlines will have unique chemical compositions that can be thought of as endmembers of the water composition observed in streams.

This section aims to examine the relationships between 1) oxidation and reduction, 2) cation exchange, 3) mineral precipitation and dissolution, and 4) water mixing. This is done to give the reader an idea of how the various processes affect the chemical evolution of water as it flows through the CZ and is eventually discharged into the stream.

1.2.1 Atmospheric deposition

Studies that estimate recharge using Cl^-, presuming that it can be considered a conservative tracer, have already provided an extensive description of the contribution of both wet and dry deposition (Schoeller, 1960; Eriksson, 1960; Lerner et al., 1990; Edmunds and Gaye, 1994; Wood and Sanford, 1995; Wood, 1999). However, it has been demonstrated that Cl^- cannot be considered a conservative tracer in forested ecosystems (Viers et al., 2001; Öberg and Sandén, 2005; Bastviken et al., 2007; Svensson et al., 2012). Prompting the development of additional methods for determining the relative contributions of wet and dry deposition.

The origins of geogenic solutes (Ca^{2+}, Mg^{2+}, Na^+) are attributed to water-rock interactions in both hydrological and geochemical approaches to understanding groundwater evolution. However, only nitrogen (Paerl, 1997; Stadler et al., 2008) , chloride, and sulphur (Robertson et al., 1989) have received significant attention from geochemists, despite the importance of atmospheric deposition to the reactive mass balance of a catchment. For

this reason, groundwater geochemists have mostly focused on mineral weathering rates to characterise water's chemical evolution as it travels through a catchment. It appears that the hydrological community as a whole is unaware of the role that atmospheric deposition could play in solute export (Wood, 2019).

Given that the Earth's atmosphere is a closed system (Lequy et al., 2013), matter is recycled and either returns to the surface (wet or dry deposition), unchanged or is chemically altered. There are several methods for calculating both dry and wet deposition, this will however not be discussed here. Wet deposition refers to the transfer of atmospheric substances to the Earth's surface via precipitation (rain, snow, etc.) and is significantly simpler to quantify than dry deposition (Lindberg and Lovett, 1985; Lovett and Lindberg, 1993; Watanabe et al., 2008).

Dry deposition is the process whereby atmospheric particles or gases settle on surfaces without precipitation and can be influenced by various factors such as vegetation in forests. Vegetation can affect dry deposition by acting as a physical barrier to the particles, which can alter their trajectory and decrease their deposition rate (Lindberg et al., 1988; Saylor et al., 2019). While wet deposition measurements have reported uncertainties of around 20%, dry deposition estimates have reported uncertainties ranging from 30% to 75% (Lindberg et al., 1986; Lovett and Lindberg, 1993). The uncertainties in measuring atmospheric deposition have been estimated to be up to 30% for sulphur and up to 40% for nitrogen and the base cations (Na^+, K^+, Mg^{2+}, Ca^{2+}; Draaijers et al., 1996).

Calculating atmospheric deposition

In order to account for the contribution from atmospheric depositional flux (DF) with units ($100 \times mg/m^2/year$), a conversion to solute concentration (C_{depo}) is required, by dividing DF by the rainfall flux P with units ($m^3/m^2/year$):

$$C_{depo} = \frac{DF}{P} \tag{1.3}$$

The concentration C_{depo} does not represent the concentration that eventually find its way into the subsurface. To obtain the latter ($C_{recharge}$), one must account for solute concentration due to evapotranspiration. Under the assumption of steady state, a concentration ratio (CR) is used to obtain $C_{recharge}$. CR can be expressed as P divided by the annual vertical groundwater recharge flux q_v with units ($L^3/L^2/T$):

$$CR = \frac{P}{q_v} \tag{1.4}$$

$C_{recharge}$ can then be calculated by the following relationship:

$$C_{recharge} \times q_v = CR \times C_{depo} \tag{1.5}$$

In order to use this model to calculate $C_{recharge}$, P and q_v must be known. The estimation of dry deposition with aerosol models are complex and a detailed discussion falls beyond the scope of this work. What should be noted is that dry deposition contributes significant amounts of NO_x and SO_x (Butler and Likens, 1995), resulting in increased dry deposition in areas covered under conifer opposed to deciduous canopies (Fowler, 1980). Canopy-exchange makes estimating dry deposition on vegetation extremely difficult. The influence of vegetation effects were shown in a study by Galloway and Likens (1978) where the differences in chemical composition between wet-only rain gauges and bulk samplers where quit apparent.

To conclude the discussion on the importance of wet- and dry deposition on catchment scale mass balance calculations, it should be noted that roughly all elements are present as geogenic solutes in atmospheric deposition (Galloway et al., 1982; Berner and Maasch, 1996). In a recent study by Wood (2019) showed for 3 case studies that over 50% of major cations- and anions potentially originated from atmospheric deposition. This work highlights the potential source of elements that are generally thought of as having their origin below the surface.

Crossing the threshold now and moving below surface the next important processes that control the fate of solutes will be discussed.

1.2.2 Oxidation/Reductions

Reduction and oxidation (redox) is the main processes controlling the natural concentrations of O_2, NO_3^-, $Mn(IV)$, Fe^{3+}/Fe^{2+}, SO_4^{2-}, CH_4, CO_2 etc. in groundwater. Redox reactions occur through the transfer of electrons from one atom to another in an order that is predictable from standard equilibrium thermodynamics. This sequence is referred to the ecological succession of terminal electron-accepting processes (McMahon and Chapelle, 2008).

The rate at which electrons are transferred vary from one reaction to the next. The rate may sometimes be very slow but is sped up significantly by a microorganism catalyst. Microorganisms in groundwater obtain energy by catalysing redox processes. An example of this is the microbe *Desulfovibrio sp.* that produce enzymes to significantly speed up the reduction of sulphate where organic matter is the reductant (Appelo and Postma, 2006). The significance of this process of sequential reduction, is that redox processes may form segregated zones that are dominated by a single redox couple (McMahon and Chapelle, 2008). This behaviour is leveraged to get a better understanding of what the redox conditions are with depth in groundwater. The redox potential (E_h) controls the redox equilibria and can be theoretical calculated using the Nernst equation. A theoretical oxidation-reduction reaction can be expressed as (Appelo and Postma, 2006):

$$bB_{red} + cC_{ox} \longrightarrow dD_{ox} + gG_{red} \tag{1.6}$$

The lowercase letters in this expression represent the stoichiometric values of the reactants (concentrations are represented by capital letters). The subscripts indicate the reaction's oxidant and reductant. The respective half-reactions can then be expressed as:

$$bB_{red} \longrightarrow D_{ox} + ne^{-} \tag{1.7}$$

;and

$$gG_{red} \longrightarrow cC_{ox} + ne^{-} \tag{1.8}$$

Using the Nernst equation, the redox potential of this hypothetical reaction can then be calculated:

$$E = E^0 + \frac{RT}{nF} ln \frac{[D_{ox}]^d [G_{red}]^g}{[B_{red}]^b [C_{ox}]^c} \tag{1.9}$$

In equation 1.9 E^0 is the standard potential ($Volts$), where all substances are present at unit activity at 25°C and 1 atm. F is the Faraday's constant (96.42 $kJ/Volt$ gram equivalent), n is the number of electrons transferred in the reaction, R is the gas constant ($8.314 \times 10^{-3} kJ/deg/mol$) and T is the absolute temperature.

Unlike pH, E_h cannot be measured unambiguously in most natural waters. E_h measurements are performed by using an inert Pt-electrode over which H_2 gas is bubbled in a solution of pH = 0, this condition allows for equation 1.9 to be rewritten as:

$$E = E^0 + \frac{RT}{nF} ln \frac{[D_{ox}]^d}{[B_{red}]^b} \tag{1.10}$$

With equation 1.10, E of a solution can be calculated if the concentrations of the redox couples are known. E_h is related to E as follows:

$$E_h = E_{measured} + E_{ref} \tag{1.11}$$

where $E_{measured}$ is the measured probe response and E_{ref} is the potential of the reference electrode. Lindberg and Runnells (1984) compared field measured E_h with computed E_h for various redox couples (5.2). It was shown from the results that there is a significantly large variation between values calculated from analytical data and physical measurements,

making it very hard to interpret what is being measured by a redox probe in the field. Figure 5.2 shows that the E_h reading from the probe can range from $0.03V$ to $0.5V$ in a zone dominated by oxygen reduction, indicating that the Pt-probe is apparently unaffected by O_2 concentration. This is due to a lack of equilibrium between various redox species (Lindberg and Runnells, 1984). Theoretical and measured E_h values frequently differ due to the following factors:

- Dynamic conditions: Despite approaching a steady state, the regolith part above the capillary fringe will never achieve true thermodynamic equilibrium because two or more redox processes occur in parallel (Lindberg and Runnells, 1984; Markelova, 2016). Under these conditions, the recorded E_h is a mixed potential, with the dominant redox couples having the highest exchange currents dominating.
- Reversibility and electroactivity: The Pt-electrode system can only be used with electroactive redox couples that are truly reversible (Markelova, 2016).
- Contamination: The Pt-electrode is susceptible to some of the chemicals in the solution (Stumm and Morgan, 1970; Fiedler et al., 2007). Caution is thus required when interpreting field measured E_h values.

Electron acceptors/oxidants

To address the difficulties of obtaining quantitative values for E_h in groundwater through either using a Pt-electrode or analytical measurements, the process of ecological succession of terminal electron-accepting is used to get an approximation of what the redox conditions in a particular zone might be (Champ et al., 1979; Chapelle et al., 1996a; McMahon and Chapelle, 2008). The formation of these zones of single electron accepting processes or redox gradients are mainly vertical in recharge areas of unconfined aquifers dominated by natural sources of electron donors (McMahon et al., 2011). These respective processes generate distinctive end products (N_2, NH_4^+, Fe^{2+}, H_2S and CH_4). Tracking the consumption of electron acceptors and the generation of distinct end products along a flowline is the most reliable method for identifying the distribution of redox processes (Chapelle et al., 1996b). However, when sampling an aquifer using a pumping well, several flowlines may be intercepted and what is obtained is a mixed sampled of various redox zones (McMahon and Chapelle, 2008). A framework for assessing redox processes through a set of threshold values for electron acceptors was first developed by Chapelle et al. (1995) and later revised by Paschke et al. (2007)and further refined by McMahon and Chapelle (2008).

However, this method is only really useful in saturated conditions. Seasonal fluctuations in water levels have a significant impact on redox reactions in shallow subsurface horizons above the capillary fringe, resulting in frequent changes in E_h, which affect pH. Protons are produced during oxidation processes, which reduce pH, and consumed during reduction processes, which raise pH. Because the location of the oxic-anoxic interface changes due to fluctuating water table levels, the kinematics of these processes are critical for these zones

(Du Laing et al., 2009). The dynamics of trace metals in floodplain soils for instance,are driven by the redox chemistry of sulfur (S), iron (Fe), and manganese (Mn) (Griethuysen et al., 2005). Due to their direct control over metal binding (sorption) to the mineral and organic phases of soil, as well as their bioavailability, redox and pH are the dominant factors in the fate and transport of many metals (Frohne et al., 2011). Among the most extensively researched topics were metals in soils caused by S, Fe, and Mn redox chemistry (Frohne et al., 2011; Schulz-Zunkel et al., 2015).

Nitrate reduction

An important terminal electron acceptor in groundwater systems is nitrate. It has been the focus of countless studies as it is the most widespread and commonly found contaminant in groundwater systems (Strebel et al., 1985; Korom, 1992; Spalding and Exner, 1993; Feast et al., 1998; Tesoriero et al., 2000; Rivett et al., 2008; Beeson and Cook, 2004; Arndt et al., 2020; Hill, 2019). The significance of the increasing prevalence of nitrate in groundwater in the literature is that the processes controlling nitrate attenuation in the subsurface are well understood, with denitrification generally being accepted as the dominant process (Korom, 1992; Rivett et al., 2008).

The framework of redox zones from the study of Chapelle et al. (1995) grouped both O_2 and NO_3^{2-} reduction in the first zone. Later McMahon and Chapelle (2008) revised this framework to distinguish between O_2-and NO_3^-- reducing zones. However, in practice what can more commonly be expected is several redox reactions occurring simultaneously (McGuire et al., 2000). There are several reasons why this may be the case, ranging from spatial variation in geochemical conditions (Christensen et al., 2000), influence of microbial communities on biofilm scale (Yu and Bishop, 1998; Bishop and Yu, 1999), and the availability of other electron donor such as the coupled reduction of nitrate with pyrite oxidation (Kölle et al., 1983; Strebel et al., 1985; Postma et al., 1991).

$$5FeS_2 + 14NO_3^- + 4H^+ \rightarrow 7N_2 + 5Fe^{2+} + 10SO_4^{2-} + 2H_2O \tag{1.12}$$

$$5FeS_2 + NO_3^- + 7H_2O \rightarrow 5FeOOH + \frac{1}{2}N_2 + 9H^+ \tag{1.13}$$

Mn, *Fe* redox dynamics

Mn(IV) will be reduced before Fe^{3+} and SO_4^{2-} during the ecological succession process. However, these reactions occur simultaneously above the capillary fringe. Iron (Fe) compounds are common and get the most attention among the metals. They are also easy to change when the soil's E_h changes (Thompson et al., 2006; Mansfeldt et al., 2012).

In the absence of O_2, Fe^{3+} functions as a terminal electron acceptor, accepting electrons from microorganisms via metabolic oxidation of organic DOC (Mansfeldt et al., 2012).

The reduction of Fe^{3+} results in the release of Fe^{2+}, which is quickly oxidised once the soil re-aerates, resulting in simultaneous precipitation as *Fe* oxide (e.g., following water table drops) (Mansfeldt et al., 2012). As a result of temporal inundation and the formation of low E_h, *Fe* and *Mn* (hydr)oxides in the solid phase are reduced to Mn^{2+} and Fe^{2+}, which exist in the liquid phase as soluble metals and organic complexes (Reddy and DeLaune, 2008). Manganese oxides are most often (thermodynamically) very efficient electron acceptors (after O_2 and NO_3^-) in the soil respiration sequence, as suggested for the SHAFDAN soil aquifer treatment system in Israel (Goren et al., 2012). *Mn(IV)* dissolves to become mobile as Mn^{2+} in its reduced form and later solidifies as Mn-oxide in its oxidised form (Stumm et al., 1996; Reddy and DeLaune, 2008).Goren et al. (2012), and Oren et al. (2007) investigated the biogeochemical processes involved in Mn mobilisation, adsorption, and precipitation in the soil aquifer treatment system. Other metals that have received attention include *Sb* (Hockmann et al., 2014; Hockmann et al., 2015), *Ni* (Antić-Mladenović et al., 2011; Rinklebe et al., 2016), *Cu* (Xu et al., 2013; Kusonwiriyawong et al., 2016), *U* (Handley-Sidhu et al., 2009; Fu et al., 2018). The presence of MnO_2 in sediments indicates that the environment was highly oxidizing. Hematite, on the other hand, is stable over a much wider E_h range. In contact with hematite, dissolved Mn^{2+} is stable over a wide range, whereas Fe^{2+} is unstable in contact with MnO_2. Furthermore, rhodochrosite ($MnCO_3$) is stable over a wide E_h range, whereas the presence of siderite ($FeCO_3$) indicates that the conditions are strongly reducing (Appelo and Postma, 2006)

Electron donors/reductants

Dissolved organic matter (DOM) is an important component of the carbon cycle and aquatic biogeochemistry, eventually connecting terrestrial and aquatic ecosystems (Battin et al., 2009; Saraceno et al., 2009; Lee et al., 2016). Dissolved organic carbon (DOC) is the most abundant DOM component in forested stream ecosystems (McLaughlin and Kaplan, 2013), and also the most common electron donor (*reductant*) (Gillham and Cherry, 1978; Starr and Gillham, 1993; McMahon et al., 2011; Thurman, 2012). In headwater catchments, particularly those with predominant subsurface flow, the primary source of DOC is DOM leached by precipitation and transported to the stream (Boyer et al., 1997).

Flow systems that have an abundant source of natural electron donors could evolve quickly from a O_2-reducing environment further down the electron acceptor succession (Puckett et al., 2002), vice versa for systems that has a limited supply of electron donors may not evolve beyond the O_2-reducing phase (McMahon et al., 2004). Common redox reactions in which DOC is oxidised are presented in Table 1.1. In the following sections, the most important electron acceptors in this reaction will be discussed.

Table 1.1: Relevant redox reactions. Section a of the table shows balanced redox reactions. Section b shows common reduction and oxidation reactions in soil system at pH 7 for 25 °C. Adapted from Stumm et al. (1996).

Reductant	**Balanced equation**	**Section**
Aerobic oxidation (O_2/O_2^- redox couple)	$CH_2O + O_2 \rightarrow CO_2 + H_2O$	
Nitrate reduction (NO_3^-/N_2 redox couple)[1]	$5CH_2O + O_2 + NO_3^- \rightarrow 2N_2 + CO_2 + 3H_2O$	
Mn(IV) reduction ($Mn(IV)/Mn^{2+}$ redox couple)[2]	$CH_2O + 2MnO_2 + 4H^+ \rightarrow CO_2 + 2Mn^{2+} + 3H_2O$	
Microbial Fe reduction (Fe^{2+}/Fe^{3+} redox couple)[2]	$CH_2O + 4FeOOH + 8H^+ \rightarrow CO_2 + 4F2^{2+} + 7H_2O$	a
SO_4^{2-} reduction	$2CH_2O + SO_4^{2-} + 2H^+ \rightarrow 2CO_2 + H_2S + 2H_2O$	
NO_3^- reduction by pyrite[3]	$5FeS_2 + 14NO_3^- + 4H^+ \rightarrow 7N_2 + 2Fe^{2+} + 10SO_4^{2-} + 2H_2O$	
Fe^{3+} reduction	$10Fe^{2+} + 2NO_3^- + 14H_2O \rightarrow N_2 + 10FeOOH + 18H^+$	

Reduction	$E_h^0(V)$	**Oxidation**	$E_h^0(V)$	
Aerobic respiration				
$O_{2(g)} + 4H_2^+ + 4e^- \rightarrow 2H_2O$	0.811			
Denitrification				
$2NO_3^- + 12H^+ + 10e^- \rightarrow N_{2(g)} + 6H_2O$	0.811	$CH_2O + H_2O \rightarrow CO_{2(g)} + 4H^+ + 4e^-$	-0.484	b
Mn(IV) reduction				
$MnO_2(s) + 4H^+ + 2e^- \rightarrow Mn^{2+} + 2H_2O$	0.519			
SO_4^{2-} reduction				
$SO_4^{2-} + 9H^+ + 8e^- \rightarrow HS^- + 4H_2O$	-0.221			

123

[1] Bragan et al. (1997), Høgh-Jensen et al. (2004), Kölle et al. (1983), Korom (1992), Smith and Duff (1988), and Starr and Gillham (1993)

[2] Canfield et al. (1993)

[3] Kölle et al. (1983), Strebel et al. (1985), Van Beek et al. (1988), and Böhlke and Denver (1995)

1.2.3 Ion Exchange

When infiltrating water differs from what is already present in the soil solution, ion exchange reactions between dissolved cations and those sorbed to mineral surfaces can dramatically alter water chemistry (Appelo and Postma, 2006). Clay minerals, iron oxides, weathered primary minerals, and organic material make up the exchange complex in soil. The exchange complex can easily contain an amount of mobile cations that is 300 times greater than what is present in soil moisture per volume of wet sediment (Appelo and Postma, 2006). Thus, ion exchange can have a significant impact on estimating the solute export generated by primary mineral weathering, and solute velocities will differ (retardation), making inferences about chemical processes from stream water even more difficult.

Different plant species can strongly affect soil nutrient cycling. Soil base cation status and pH, for example, can differ between plant species (Lelong et al., 1990; Finzi et al., 1998a; Augusto et al., 2002; Dijkstra and Smits, 2002; Reich et al., 2005; Oostra et al., 2006). Furthermore, because plant species cause cation concentration divergence in soils (Alban, 1982; Lelong et al., 1990; Finzi et al., 1998b; Dijkstra and Smits, 2002; Reich et al., 2005), they may influence polyvalent cation "bridging" of negatively charged *SOM* to negatively charged clay particles, reducing its accessibility to decomposers (Oades, 1988; Muneer and Oades, 1989; Clough and Skjemstad, 2000). Polyvalent cations can also form direct complexes with *SOM* molecules, causing coagulation and reducing solubility (Oste et al., 2002). Thus, differences in the degree to which *SOM* is chemically stabilised could be caused by plant species' influence on cation chemistry. Common garden species have been observed to cause significant divergence in soil pH and exchangeable base cation status. Species with *Ca*-rich tissues can raised soil pH and enriched surface horizons in Ca^{2+}, promoting greater earthworm abundance and faster forest floor turnover (Reich et al., 2005; Hobbie et al., 2006). Because of its profound impact on a number of chemical reactions involving essential plant nutrients, phytotoxic elements, and pollutants, soil pH is regarded as the "master variable" of soil chemistry. pH influences the solubility of these elements, determining their biological availability and mobility either directly or indirectly (Penn and Camberato, 2019).

Anions can also be exchanged in soils for cations on the surface of soil minerals or organic matter. This exchange process is driven by differences in ionic concentration and affinity between the soil solution and the soil solid phase. According to Pansu and Gautheyrou (2006), anion exchange capacity (AEC) was rarely studied prior to 1975, owing to the fact that anions have a weaker influence on soil in temperate zones than cations, which link with negatively charged surfaces. SO_4^{2-} is one of the anions that can be exchanged in soils and can come from a variety of sources, including atmospheric deposition, plant roots, and mineral weathering; the latter two SO_4^{2-} sources will be discussed further in the following sections. Several factors influence SO_4^{2-} mobility in soils, including the presence

of cations that compete with SO_4^{2-} for exchange sites (Tabatabai, 1987), the pH of the soil solution (Adams and Rawajfih, 1977), and the chemical form of SO_4^{2-} in the soil solution (Churka Blum et al., 2013).

Under steady-state chemical conditions, the composition of a cation exchanger will be the same as that of the groundwater around it. When the composition of the water changes due to pollution, acidification, or change in vegetation influence (land use change), the cation exchanger readjusts its composition to the new groundwater concentrations. As a result, the exchanger serves as a temporary buffer that can completely change the concentrations in water via a process known as ion chromatography (Appelo and Postma, 2006).

At continental scale, dissolved Na^+ concentrations in rivers are used to derive the solute contribution from silicate weathering (Gaillardet et al., 1999). In a recent study by Tipper et al. (2020), it was shown that there is a major supply from exchange processes of non-silicate Na^+ to the CZ from ancient seawater that is weakly bounded to sedimentary rocks. The authors showed silicate weathering fluxes has been overestimated on global scale due to this phenomenon. The rate of ion exchange is rapid, and for the exchange of Na^+ for Ca^{2+}, the balanced reaction can be written as follows:

$$Na_2X + Ca^{2+} \leftrightarrow CaX + 2Na^+ \tag{1.14}$$

where X^{2-} represent the concentration of exchange sites, and analogue to mineral dissolution, the equilibrium among solute and exchangeable cations are calculated using the law of mass action. Cation exchange pools and its relative importance as a control on both soil and groundwater solute concentrations has been well documented (Fisher and Mullican, 1997). The most important behaviour however that pertain to the current discussion is the exchange of Na^+ for divalent cations Ca^{2+}. Both Hagmaier (1971) and Lee (1981) observed that as depth increased and ground water flowed away from recharge sources, calcium and magnesium cations shifted from dominant to subordinate cations in relation to total cations.

1.2.4 Dissolution/precipitation

The soil respiration

The main drivers of CO_2 production in soil is microbial activity (decay of labile organic matter) and root respiration (Amundson and Davidson, 1990; Hanson et al., 2000):

$$CH_2O + O_2 \rightarrow CO_2 + H_2O \tag{1.15}$$

These process are a major contributor to the carbon cycle (Raich and Potter, 1995) and is in turn dependant on soil water content and temperature (Reardon et al., 1979; Romero-

Mujalli et al., 2019). Most of the CO_2 produced in the soil escape to the atmosphere where it has a mean residence time of roughly 10 years (Appelo and Postma, 2006). The two most prominent sinks for atmospheric carbon are CO_2 consumption during rock weathering reactions and CO_2 uptake during photosynthesis and transformation to organic matter (Gaillardet et al., 1999), where it has a relatively short residence time of between 10 and a 100 years for temperate climates (Keller and Bacon, 1998). Given the relatively short timescales of these processes, land use changes can have an important effect on the CO_2 content of the atmosphere (Appelo and Postma, 2006; Li et al., 2008; Macpherson et al., 2008; Liu et al., 2018).

To appreciate the significance of CO_2 production as a pH regulator for soil water and groundwater, it is necessary to review the fundamental chemical interactions. In the last section about how oxidation of terminal electron acceptors leads to the formation of redox zones, it was shown that CO_2 ($CO_{2(g)}$) gas is a reaction product that dissolves in water according to Henry's law:

$$CO_{2(gas)} \rightarrow CO_{2(aq)} \tag{1.16}$$

and forms carbonic acid:

$$CO_{2(aq)} + H_2O \rightarrow H_2CO_3 \tag{1.17}$$

At $25°C$, dissolved CO_2 is 600 times more abundant than carbonic acid. To simplify calculations, most literature adopts the convention of summing these two species together, so the overall reaction becomes:

$$CO_{2(aq)} + H_2O \rightarrow H_2CO_3^* \tag{1.18}$$

where $H_2CO_3^* = CO_{2(aq)} + H_2CO_3$ (Appelo and Postma, 2006). Dissolved CO_2 represent a major hydronium ion (H_3O^+) supply in weathering reactions (Walker et al., 1981; BernerR et al., 1983; Calmels et al., 2014), and in unpolluted or natural systems, CO_2 production and root respiration are the primary proton donor processes (Appelo and Postma, 2006). Substantial work has been done to quantify weathering fluxes to understand the influence of CO_2 soil consumption on the atmospheric CO_2 balance (Bluth and Kump, 1994; Gaillardet et al., 1999; Hartmann et al., 2009; Goll et al., 2014; Hartmann et al., 2014). The partial pressure of CO_2 (P_{CO_2}), refers to the concentration of CO_2 in the gas phase. This parameter forms an important input in all the mechanical models used to quantify weathering fluxes (Roelandt et al., 2010; Beaulieu et al., 2012; Goddéris et al., 2013; Goddéris et al., 2006). The carbon acid system can be divided into two extreme cases: an open system and a closed system (Appelo and Postma, 2006).

An open system refers to a system that has a constant concentration boundary with regards to P_{CO_2}.This case will represent the unsaturated zone where soil gas is in equilibrium with the atmosphere. The carbonic acid concentration can be related to P_{CO_2} using a log transformation of the mass action equation:

$$log[H_2CO_3^*] = log[P_{CO_2}] - 1.5 \tag{1.19}$$

This implies for an open system at a given pH, if the P_{CO_2} is known, that all carbonic species can be defined.

A close system represents a case where the sum of the dissolved carbon species is considered constant, meaning no additional supply of CO_2 from the atmosphere. This means that the distribution of carbonate species can be defined as follows:

$$TIC = m_{H_2CO_3^*} + m_{HCO_3^-} + m_{CO_3^{2-}} \tag{1.20}$$

In the case of a closed system if two of the four variables are known ($Alkalinity$, pH, TIC and P_{CO_2}), the distribution of carbonate species can be calculated. Alkalinity is defined as the sum of equivalents of all dissociated weak acids:

$$Alkalinity = m_{HCO_3^-} + 2m_{CO_3^{2-}} \tag{1.21}$$

Seasonal P_{CO_2} fluctuations are observed and can range anywhere from atmospheric concentrations ($P_{CO_2} = 10^{-3.5}$) to two orders of magnitude higher ($P_{CO_2} = 10^{-1.5}$) depending on the vegetation cover (Reardon et al., 1979; Calmels et al., 2014). This range of P_{CO_2} -values would imply that the theoretical pH of soil solution (pure water) in equilibrium with a constant CO_2 pressure can range between 4.6 (upper limit of root respiration and organic matter degradation) and 5.6 (Appelo and Postma, 2006).

Carbonate weathering

Infiltrating water recharging to the deeper groundwater cause an increase in P_{CO_2}. This is however not the only potential source of CO_2 in groundwater. DOC can be transported in via groundwater (Albéric and Lepiller, 1998), by preferential flow paths, bypassing the soil horizon. Sediments containing DOC may also be a source (Keller and Bacon, 1998). Deeper sources may also play a role, for instance degassing of magma or thermal metamorphosis of oceanic carbonate rock (Etiope, 1999; Yoshimura et al., 2001; Chiodini et al., 1998; Chiodini et al., 1999; Herman and Lorah, 1987; Kohfahl et al., 2008; Yoshimura et al., 2004). The weathering of carbonate rocks is strongly influenced by P_{CO_2}. This statement may be intuitive, but for sake of being thorough, it will be briefly explained. The reaction between calcite and $CO_{2(g)}$ can be expressed as follows:

$$CO_{2(g)} + H_2O + CaCO_3 \rightarrow Ca^{2+} + 2HCO_3^- \tag{1.22}$$

The mass action for this reaction can be defined as:

$$\frac{[Ca^{2+}][HCO_3^-]^2}{[P_{CO_2}]} = 10^{-6.0} \tag{1.23}$$

The timescales of weathering of carbonate minerals can be highly dynamic. Calcite for instance may dissolve in a matter of hours, and just as easily precipitate again as a function of P_{CO_2} (Serrano-Ortiz et al., 2010; Roland et al., 2013; Calmels et al., 2014). The solubility of carbonate minerals can also be influenced by the presence of other types of minerals and for instance gypsum. The latter case has been well described when calcite, dolomite and gypsum are present and a process known as dolomitization occur (Back et al., 1983; Plummer et al., 1990; Cardenal et al., 1994; Saunders and Toran, 1994; Sacks et al., 1995; Capaccioni et al., 2001; Lopez-Chicano et al., 2001; Centrella et al., 2023). This process is driven by the common ion effect. When gypsum or anhydrite dissolves, Ca^{2+} concentration increase:

$$CaSO_4 \rightarrow Ca^{2+} + SO_4^{2-} \tag{1.24}$$

The increase in Ca^{2+} causes the calcite to precipitate, reducing the concentration of carbonates. The decrease in carbonates drives the dissolution of dolomite, increasing the concentration of Mg^{2+} and Ca^{2+}. Mixing of waters that are in equilibrium with a carbonate mineral but has different P_{CO_2} values may cause a subsaturation, driving dissolution of the mineral. In a recent study by Romero-Mujalli et al. (2019), the authors back-calculated the soil-rock P_{CO_2} using published spring water chemistry data , where carbonate minerals where considered an important lithological class. The calculations in the study assumed that alkalinity represents the spatio-temporal variation of CO_2. The argument why this could be assumed, is based on the relative fast rate of dissolution of calcite and subsequent equilibration with CO_2. Also, calcite precipitation due to CO_2 degassing was expected to be slow, based on the work by Szramek and Walter (2004). A filter criterion was defined to select data that was not influenced by sulphide oxidation ($\frac{[Ca^{2+}]}{[SO_4{}^{2-}]} > 10$) and silicate weathering ($\frac{[Ca^{2+}]}{[Na^{+}]} > 10$, Gaillardet et al. (1999)). The significance of these two processes on the concept of using alkalinity to back calculate soil-rock P_{CO_2} will be discussed in the sections to follow. It is however required to first discuss another process that can be a source of acidity in soil- and groundwater.

Table 1.2: Solubility of relevant carbonates. The K-values was obtained from Nordstrom et al. (1990). The balanced dissolution reactions was obtained from the PHREEQC.DAT database Parkhurst and Appelo (2013).

Mineral Name	formula	Dissolution reaction	$-log(K)$	Note
Calcite	$CaCO_3$	$CaCO_3 \leftrightarrow CO_3^{2-} + Ca^{2+}$	8.48	
Magnesite	$MgCO_3$	$MgCO_3 \leftrightarrow CO_3^{2-} + Mg^{2+}$	8.24	
Rhodochrosite	$MnCO_3$	$MnCO_3 \leftrightarrow CO_3^{2-} + Mn^{2+}$	11.13	redox sensitive
Siderite	$FeCO_3$	$FeCO_3 \leftrightarrow Fe_{2+} + CO_3^{2-}$	10.89	
Dolomite	$CaMg(CO_3)_2$	$CaMg(CO_3)_2 \leftrightarrow Ca^{2+} + Mg^{2+} + 2CO_3^{2-}$	17.09	
Strontianite	$SrCO_3$	$SrCO_3 \leftrightarrow CO_3^{2-} + Sr^{2+}$	9.27	
Witherite	$BaCO_3$	$BaCO_3 \leftrightarrow CO_3^{2-} + Ba^{2+}$	8.56	Can presipitate as Barite (relatively insoluble) if SO_4^{2-} is avaiable
Cerussite	$PbCO_3$	$PbCO_3 \leftrightarrow CO_3^{2-} + Pb^{2+}$	13.1	redox sensitive

Pyrite oxidation

Pyrite is the most common sulphide mineral in the crust of the Earth (Rickard and Luther, 2007). Sulfur (S) inputs to forest ecosystems originate primarily from mineral weathering, with sulphide minerals (primarily pyrite, FeS_2) and evaporite minerals, primarily gypsum ($CaSO_4 \cdot 2H_2O$) or anhydrite ($CaSO_4$), being the dominant minerals (Berner and Berner, 1996). Pyrite can undergo oxidative weathering directly via the reduction of atmospheric oxygen or indirectly via the reduction of iron-bearing minerals. The extreme acidity of acid mine drainage is caused by the latter oxidative process (Druschel et al., 2004). Additionally, atmospheric deposition and the decomposition of organic matter are also important sources. Pyrite weathering is the primary source of S in unpolluted systems Arkesteyn (1980). Therefore, it is obvious that pyrite oxidation is an essential regulator of biogeochemical processes. Organic and inorganic S are the two primary pools of S. The majority of the total S pool in soils consists of the organic fraction (Freney et al., 1975; Mitchell and Fuller, 1988).

When carbonate weathering is driven by sulfuric acid produced by oxidation of sulphide minerals, such as in the Mackenzie basin or in Taiwan (Calmels et al., 2007; Beaulieu et al., 2011; Tank et al., 2016), carbonate rocks are a source of geogenic carbon to the atmosphere. Invoked as a non-negligible source of CO_2 to the atmosphere during the Cenozoic, sulfuric acid-driven carbonate weathering can impact the carbon cycle over timescales as long as the sulphur residence time in the ocean (Torres et al., 2014). This source of geological CO_2 in the atmosphere would make carbonate weathering a potentially significant part of the long-term carbon cycle. Understanding the significance of sulfuric acid in silicate weathering reactions in terrestrial environments requires determining the source of sulphate in river systems. If the primary source of sulphate is the oxidative weathering of pyrite, then the pathway by which this occurs can exert control over the acidity generated or consumed (Calmels et al., 2007). The function of pyrite's oxidative

weathering in terrestrial weathering remains unclear, but what is clear is that it should be considered when dealing with the CO_2 consumption budget (chemical weathering) in a watershed (Hercod et al., 1998; Galy and France-Lanord, 1999; Anderson et al., 2000; Gaillardet et al., 2003; Millot et al., 2003; Spence and Telmer, 2005; Calmels et al., 2007; Lerman et al., 2007; Li et al., 2008).

The role that sulphide weathering plays in the long-term regulation of atmospheric oxygen makes it crucial to identify the source of sulphate in river systems and, consequently, the global ocean (Petsch and Berner, 1998). The rain component of the dissolved load can be estimated if the constant export of SO_4^{2-} from all hydro-systems reflects a constant input of SO_4^{2-} from the atmosphere (via wet and dry deposits). In a Central European catchment, Zimmermann et al. (2006) demonstrated that wet- and dry-deposits account for 37% and 63%, respectively, of the total SO_4^{2-} input. The significance of dry deposition is revealed by the compositional difference between rainwater collected by wet-only rain gauges, which are only open during rain, and rainwater collected by bulk samplers, which are always open (Galloway and Likens, 1978). Sulfur and oxygen isotopes are an effective method for determining the source of sulphate in river or groundwater systems (Karim and Veizer, 2000; Pawellekl et al., 2002; Calmels et al., 2007; Otero et al., 2008; Tuttle et al., 2009; Yuan and Mayer, 2012). Evaporite minerals like gypsum and anhydrite are typically enriched in heavy sulphur and oxygen isotopes (^{34}S and ^{18}O), whereas pyrite is enriched in the light sulphur isotope (^{32}S). Using mixing models based on this behaviour, sulphate sources in rivers have been quantified with success (Turchyn et al., 2013).

Silicate weathering

In the top part of the regolith (solum and transition to subsolum) material are generally depleted in geogenic material as this material will represent the weathered product from the bedrock (Brantley et al., 2007; Xiao et al., 2021). Here secondary source of alkalinity could be attributed to the weathering of silicates. In soils and shallow systems this process results in the net transfer of atmospheric CO_2 to dissolved HCO_3^- (Berner and Rao, 1996). Silicate weathering reactions consume acid, and in unpolluted systems (Appelo and Postma, 2006), the main source of protons is carbonic acid (driven by the oxidation of dissolved organic carbon) and organic acids.

$$2CO_2 + 3H_2O + CaAl_2Si2O_8 \rightarrow Ca^{2+} + 2HCO_3^- + Al_2Si_2O_5(OH)_4 \tag{1.25}$$

$$2CO_2 + 3H_2O + MgSiO_3 \rightarrow Mg^{2+} + 2HCO_3^- + H_4SiO_4 \tag{1.26}$$

$$2CO_2 + 11H_2O + 2NaAlSi_3O_8 \rightarrow 2Na^+ + 2HCO_3^- + H_4SiO_4 + Al_2Si_2O_5(OH)_4 \tag{1.27}$$

1.3 Mixing of flowlines

The final part of the discussion concerns mixing. Streams in catchments represent the integrators of a catchments, where hydrological – and geochemical process are observed as a convoluted signature in the form of a concentration-discharge plot. Substantial work has been done on the understanding of fundamental processes on the $c - Q$ relationship. Musolff et al. (2015) could relate nitrate export out of the Sauerbach catchment as a function of landscape units. On continental scale (Gaillardet et al., 1999) and catchment scale (White and Blum, 1995), $c - Q$ patterns were used to quantify chemical weathering. Landscape heterogeneity as the main driver causing contrasting $c - Q$ patterns in shale headwater catchments (Herndon et al., 2015; Schwab et al., 2017).

The study of $c - Q$ patterns in streams have a strong connection with what is observed in *EMMA*. The fundamental motivation for the development of *EMMA* was to find endmembers in stream water that could effectively describe the mixing space (U). In the initial development of *EMMA*, (Christophersen and Hooper, 1992; Christophersen et al., 1993), the authors used soil solution contributions to describe the concentrations observed in the stream. If we stop for a moment and think what the underlying structure is that both these methods are trying to quantify, an answer might be obtained by more recent work in the domain of travel time distributions of water and the contrasting chemical signature often observed between old and young water.

Variation of permeability with depth exerts a first order control on vertical connectivity (VC). In the case where permeability decrease sharply with depth (vertical conductivity is low), more than 95% percent of the water flow through the top 6 meters of the subsurface and has negligible interaction with reactive rock (Xiao et al., 2021). This control causes a chemical contrast between shallow – and deep water. Subsurface properties vary with depth, with shallow soils having generally magnitudes higher permeability compared to unweathered bedrock (Welch and Allen, 2014). In systems where soils are geogenic, soil materials are the product of weathering and subsequently depleted in geogenic solutes such as Ca^{2+} and Mg^{2+} (Jin et al., 2010; Brantley et al., 2013). Precipitation entering the system will rapidly flow through the soil layer and will have relatively young ages (less than a year), in contrast deep water will be much older and will have a higher concentration of geogenic solutes. If these flowlines meet in the stream and their respective relative contributions controls the $c - Q$ pattern in the stream. In the context of *EMMA*, the old -and young water each represent an endmember and their relative contributions to streamflow can be calculated by performing a mass balance using a conservative tracer. This is however where *EMMA* fails, as very few (if any) tracers in nature are conservative and are subject to variation due to ion exchange (Clow and Mast, 2010), thermodynamic constraints (Maher, 2011; Ameli et al., 2017), spatial heterogeneity of sources (Seibert et al., 2009; Winterdahl et al., 2014; Herndon et al., 2015), dilution effects(Bao et al., 2017) and residence time variations and rapid depletion of solute stores (Herndon et al.,

2015; Hoagland et al., 2017). It can now be seen that endmembers source water can vary with climate, land cover and geological condition (Woodruff et al., 2015; Schwab et al., 2017).

In a recent paper by (Zhi et al., 2019) tested the hypothesis that contrasting $c-Q$ patterns is shaped by switching of the dominance of the relative contribution of endmember source water under transient hydrogeological conditions and that the respective endmember contrasting chemical composition arose from subsurface biogeochemical heterogeneity. The influence of these processes may be intuitive given the discussion leading up to it, but what is however impactful about the work is a development of a model that relate the power law slope (b) to the extent of concentration contrast as a function of discharge. This model will be discussed in the next section in the perspective of integrated hydro-biogeochemical theories.

1.3.1 Towards Integrated hydro-biogeochemical theories

The need to understanding the linkage between travel time distributions and biogeochemical reactions across climate-and landscape gradients has been the central theme on which both classical geochemical studies and hydrological studies converged on in recent years. In the review paper by Hrachowitz et al. (2016) the importance of young water fractions and transit time distributions on solute export has been highlighted. In broad terms this concept comes down to exposure (reactive) time (Orth and Schügerl, 1972; Glassley et al., 2002; Seeboonruang and Ginn, 2006a; Seeboonruang and Ginn, 2006b). Transit time represent age of a water package regardless of how long that package was exposed to reactive material. Exposure time is defined as the time water particles are exposed to reactive materials. This links up again with the sub-surface architecture of a catchment and vertical conductivity.

It has been shown in recent work that vertical conductivity plays a big part in solute export. Sharp contrast in solute concentrations between young and old water could be expected in systems where vertical conductivity is low (Wen and Li, 2018; Xiao et al., 2021). Inferring from the previous discussion, contact time of water with reactive material is not the only major control on dissolution rates, therefore domain scale solute export depends on the relative magnitudes of transport and reaction time scales . The relative importance of particle travel time versus characteristic time of reaction rates can be related in the Damkölher number (D_a):

$$D_a = \frac{\tau_T}{\tau_R} \tag{1.28}$$

Where τ_T is the transport residence timescale and τ_R is the reaction timescale (Fogler, 2020). The application of the D_a-framework has been adopted from chemical engineering. In this field there are wide variation of definitions of D_a-numbers, furthermore some

confusion still exists about the different types of D_a-numbers and the physical meaning of the characteristic time dealing with mixing influence on liquid-phase chemical reactions (Rehage and Kind, 2021). To understand the significance of the D_a- number in the framework of solute export in catchments, a brief discussion is required about the studies leading up to the adoption of this concept in the paradigm of *CZ* science.

In homogeneous systems with regards to reactive mineral distribution and permeability, τ_T is the mean residence time of water. In heterogeneous systems however, the mean age of storage will typically be much older than the mean age of water leaving the system (Berghuijs and Kirchner, 2017). To complicate things further, the main difficulty of the D_a-number approach is to clearly define the characteristic time scale of reactions (τ_R). Only first-order decay reactions show a clear concentration dependence on time (Li et al., 2021). Denitrification studies have quantified τ_R by looking at the rate of depletion of nitrate along a known flow path (Ocampo et al., 2006; Zarnetske et al., 2011; Pinay et al., 2015). This approach is not applicable when defining D_a-numbers for weathering reactions, as reaction kinetics for weathering has been shown to not be scalable from lab-or plot scale to catchment scale (Yu and Hunt, 2017).

An initial approach to infer controls on stream solute fluxes has led many researchers to study concentration -discharge patterns (Langbein and Dawdy, 1964; Johnson et al., 1969; White and Blum, 1995; Buttle and Peters, 1997; Evans and Davies, 1998; Godsey et al., 2009; Stallard and Murphy, 2014). The main framework on which all these studies are designed around is based on the power law approach developed by (Johnson et al., 1969):

$$C = aQ^b \tag{1.29}$$

where C is the concentration of the solute under investigation and Q is the discharge of the stream. Godsey et al. (2009) evaluated several models aimed to describe $c - Q$ behaviour by making use of data from 59 geochemically diverse US catchments. The study showed 3 distinct behaviours in terms of *log* emphC *vs.* Q plots could be observed. A negative slope of the plot indicate dilution, a positive slope indicates enrichment and a near-zero slope indicates chemosatic behaviour. It has been theorizing that the main mechanisms driving chemostatic behaviour is 1) cation exchange, 2) flushing of soil – groundwater, 3) seasonal dissolution/precipitation of amorphous aluminosilicates, 4) change in reactive mineral surface area; and 5) decrease in weathering rates due to chemical affinity effect (Clow and Mast, 2010).

Maher and Chamberlain (2014) developed a model to relate the extent of chemical weathering rates as a function of physical heterogeneity. The model considers thermodynamic- and kinetic constraints (proximity to equilibrium, Maher (2011)), and links weathering fluxes to discharge and travel time (the model assumes an exponential travel time distribution).

The model calculates the D_a-number by fitting $c - Q$ data. In the model the D_a-number represent the ratio between fluid residence time (t_f) and the residence time required to reach equilibrium between secondary and primary mineral assemblage (T_{eq}) and can be defined as follows (Johnson and DePaolo, 1994; Steefel and Mäher, 2009; Maher, 2010; Maher and Chamberlain, 2014; Li et al., 2014):

$$D_a = \frac{t_f}{T_{eq}} = \frac{R_n L \phi}{q C_{max}} \tag{1.30}$$

In the denominator on the right-hand side of the equation, $C_{max}[mol/L]$ represent the maximum solute concentration, $q(m/yr)$ the specific discharge. In the numerator,$R_n[\frac{mol}{l} yr^{-1}]$ represent the reaction rate, $L(m)$ the flow path length and ϕ the effective porosity. Commonly advective velocity is used instead of q. The definition assumes q is equal to the area-normalized discharge, and ϕ allows for the conversion between velocity and specific flux (Wymore et al., 2017).

To describe the relationship between concentration and discharge, Wymore et al. (2017) factored out discharge (q) out of the D_a-number by defining a Damköhler coefficient (D_w):

$$D_W = D_a \times = \frac{L\phi}{T_{eq}} \tag{1.31}$$

The closed-form analytical solution for the advection-reaction equation for a heterogeneous reaction where the concentration of the solute along a flow path L, is a function of D_w, q and initial- and final concentrations C_0 and C_{max} respectively, is shown below. To see the full derivation, please refer to Maher and Chamberlain (2014). The equation accounts for the heterogeneity in travel times by assuming an exponential distribution for travel times (Małoszewski and Zuber, 1982; McGuire and McDonnell, 2006):

$$C = \frac{c_0}{1 + \frac{D_W}{q}} + C_{max} \frac{\frac{D_W}{q}}{1 + \frac{D_W}{q}} \tag{1.32}$$

The initial- and maximum concentrations required to solve the model. The initial concentration C_0 represent the concentration input from vegetation and dust deposition. In the modelling approach this value is assumed to be the asymptotic non-zero concentration observed during sustained increasing runoff. The maximum concentration represents the thermodynamic limit (equilibrium between secondary and primary mineral assemblage) and is taken as the asymptotic concentration at prolonged low flow conditions. Due to the assumptions on the travel time distributions, this model is not well suited for seasonal -or event time scale predictions (Wymore et al., 2017). The model has however been fitted to long term monitoring data and used to evaluate solute generating ability (D_w) across

landscape gradients (Maher, 2011; Maher and Chamberlain, 2014; Von Blanckenburg et al., 2015; Ibarra et al., 2016).

This brings us now to the $c-Q$ model of Zhi et al. (2019):

$$b = \frac{\delta_b C_{ratio}}{C_{ratio,\frac{1}{2}} + C_{ratio}} + b_{min} \tag{1.33}$$

where;

$$C_{ratio} = \frac{C_{SW}}{C_{GW}} \tag{1.34}$$

$$\delta_b = b_{max} - b_{min} \tag{1.35}$$

$$C_{ratio,\frac{1}{2}} = concentrationrationwhereb = \frac{1}{2}(b_{max} - b_{min}) \tag{1.36}$$

The authors show through sensitivity analysis that parameters b_{min}, b_{max} and $C_{ratio,\frac{1}{2}}$ in the model is governed by reaction kinetics and thermodynamics. The authors explain that the reaction characteristics amplify concentration differences between shallow and deep zones, which ultimately results in more pronounced flushing or dilution behavior. These findings align with what Ameli et al. (2017) showed at the hillslope scale. Minerals with high ratios of equilibrium concentration versus intrinsic weathering rate lead to dilution $c-Q$ patterns because more concentration contrasts can develop between shallow and deep zones. On the other hand, smaller ratios drive the system toward chemostasis due to low mineral solubility (low equilibrium concentrations) and relatively similar concentrations in shallow and deep zones.

Both models, in effect, fit the same data. The model proposed by Maher and Chamberlain (2014) must assume a *TTD*, which introduces an error and limits the model's applicability to specific situations. Furthermore, the model assumes that C_{min} and C_{max}x are the atmospheric concentration input and the thermodynamically limited maximum concentration, respectively. In a system where the shallow zone is sufficiently flushed during high flow, this assumption may be correct. However, the development of the model proposed by Zhi et al. (2019) demonstrates that chemical changes in the shallow flowlines, as well as the connection of upslope sources, can govern this concentration. The D_a-coefficient is calculated in the model of Maher and Chamberlain (2014); in the model of Zhi et al. (2019), the extent of control over concentration differences controlling the power law slope is quantified. If one considers what the D_a-coefficient informs about the system, one might conclude that it is the same information that the latter model seeks to convey. That is, the ratio of reaction time to travel time influences the chemistry in the stream.

1.4 Conclusion

Hydrological transport is elegantly explained in the review paper by Hrachowitz et al. (2016). To paraphrase, solutes applied homogeneously and instantly to a catchment will disperse on their way to the outlet. Thus, these solutes arrive at the exit late. For chemically conservative substances, these lags are caused by (1) differential flow velocity fields, (2) distinct flow path lengths, and (3) molecular diffusion. The breakthrough curve of solute arriving at the catchment outlet represents the catchment's integrated signature of flow path distributions. Thus, a completely conservative solute travels with water, subject to the same physical interactions in the flow domain as water.

Rarely, if ever, are natural tracers conservative. This means that natural tracers are controlled and transformed by additional processes before they reach the catchment outlet. If a boundary is drawn around a catchment, the simplest model to describe the system is a reactive mass balance (*accumulation* = *in* - *out* + *generation* - *consumption*). The coupled nature of hydrological transport and weathering (*accumulation*) has been extensively studied (Maher, 2010; Maher, 2011), whereas the *accumulation* (ion exchange, etc.) and *consumption* (phase transformation, plant uptake etc.) terms in numerical models still represent a substantial degree of uncertainty. In the main discussion, it was stressed that the functioning of the shallow horizons of the *CZ*, particularly those above the capillary fringe, is influenced by a multitude of biogeochemical processes. These processes are briefly summarized in a hypothetical representation shown in figure 1.1. The concentration of cations such as Ca^{2+}, Mg^{2+}, and Na^{+}, which are frequently used in weathering rate calculations, can vary greatly as a result of these processes. The large uncertainty of this zone is then propagated to the solute export quantification of deeper horizons. The vastly different reaction rates of these processes may have significant implications for mixing models. This is especially evident in the discussion of the mixing of young and old water in streams, as well as the underlying assumptions regarding the processes governing chemostatic behaviour. Furthermore given the fact that the largest contribution to streamflow are from shallow flowlines, it could be argued that the influence of biogeochemical processes active in the shallow horizons may be more important than the influence of weathering reactions.

To make progress in developing integrated hydro-biogeochemical theories, experimental catchments with well-understood hydrological functions are required. In addition, multidisciplinary research is necessary because processes are tightly coupled. In the next chapter, the study site will be discussed in detail to assess what information is currently available and how this knowledge and information can be leveraged in this thesis.

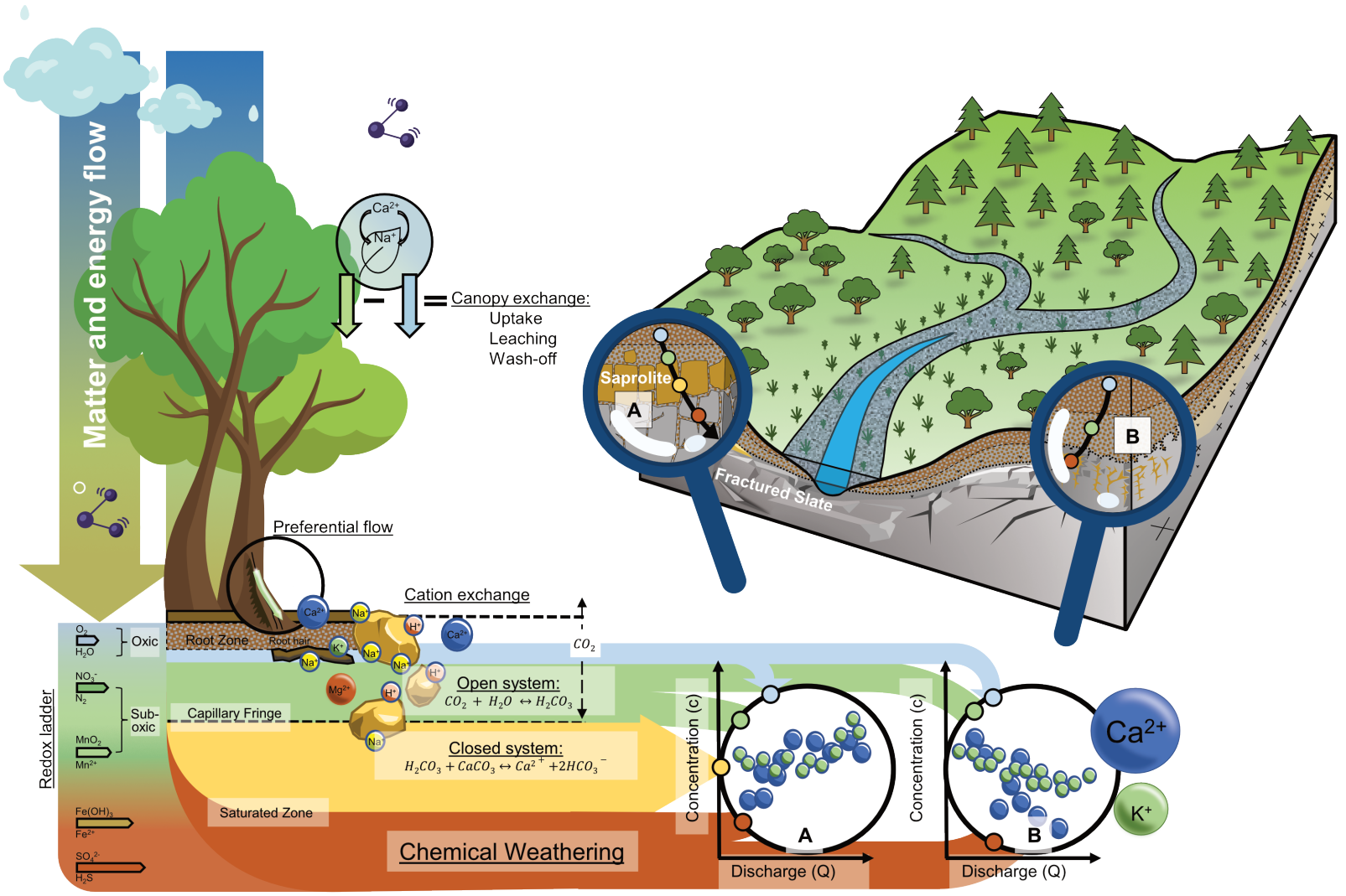

Figure 1.1: Uncovering the biogeochemical dynamics of a catchment: A Hypothetical Representation of Ca^{2+} and K^+ Concentration-Discharge Patterns in Soil and Deep Horizons at Sites A and B.

Chapter 2

Taking stock of what we know: The Weierbach Experimental Catchment

2.1 About the WEC

All of the research presented in this dissertation has been carried out within the Weierbach experimental catchment (*WEC*). An abstract model of the numerous coupled hydrogeological - and geochemical processes influencing concentration-discharge patterns in streams was developed in the previous chapter (figure 1.1). Recent process-based understanding (hydrologic- and biogeochemical processes) of the WEC is reviewed in this chapter. This will be done in order to evaluate the current extent of our understanding of the system and identify knowledge gaps that may can be addressed in this thesis.

The *WEC* is the most researched and instrumented experimental catchment in Luxembourg, with a long list of experimental studies (Klaus et al., 2015; Juilleret et al., 2016; Antonelli et al., 2017; Scaini et al., 2017; Glaser et al., 2018; Scaini et al., 2018; Schwab et al., 2018; Gourdol et al., 2021; Bonanno et al., 2021; Fabiani et al., 2022), modeling studies (Kavetski et al., 2011; Fenicia et al., 2014; Glaser et al., 2016; Carrer et al., 2019; Glaser et al., 2019; Bonanno et al., 2022) and biogeochemical studies (Moragues-Quiroga et al., 2017; Montemagno et al., 2022). It is also a *CZ* observatory that is recognised internationally (Hissler et al., 2021). Figure 2.2 is a timeline that shows how understanding and knowledge have slowly grown from 2002, when the first stream gauge was installed, until now. A theoretical curve of information gain is shown in the figure for both the hydrological and the biogeochemical functioning of the system. It is clear that studies seeking to understand the hydrological functioning of the catchment have made significant strides over the course of the past two decades, whereas our comprehension of the biogeochemical processes governing the system has progressed at a significantly more sluggish pace. In addition, very little progress has been made toward the development of a coherent perceptual hydrobiogeochemical model.

The catchment is located in the northwestern region of Luxembourg (Lat: 49.8273,Long: 5.7956), and it has an area of 45 *ha*. The *WEC* is a headwater catchment within the Alzette River basin in Luxembourg. The catchment is located in the Ardennes massif, which is distinguished by an elevated subhorizontal plateau and deep V-shaped valleys. A portion of the plateau of the catchment is technically not a plateau because it is classified as an "interfluve" (a higher region found between valleys). This region will be referred to as the secondary plateau for the remainder of the thesis, while the plateau of the catchment will be referred to as the primary plateau.

The catchment's stream network consists of three tributaries that converge into a single stream and is bordered by a highly dynamic riparian zone composed primarily of litter degradation material and colluvium from the hillslopes (Antonelli et al., 2020a; Antonelli et al., 2020b). The riparian area in the catchment is narrow, flat, and well-defined with some areas where the riparian zone widens (the average riparian zone area comprises of 1.2% of the catchment area, from Glaser et al. (2021). The plateau area is about 30 ha and

has slopes between 0° and 5°. The hillslope area is about 12 ha and has slopes between 5° and 44°. The hillslope area includes a riparian area representing about 0.4 ha (Rodriguez and Klaus, 2019).

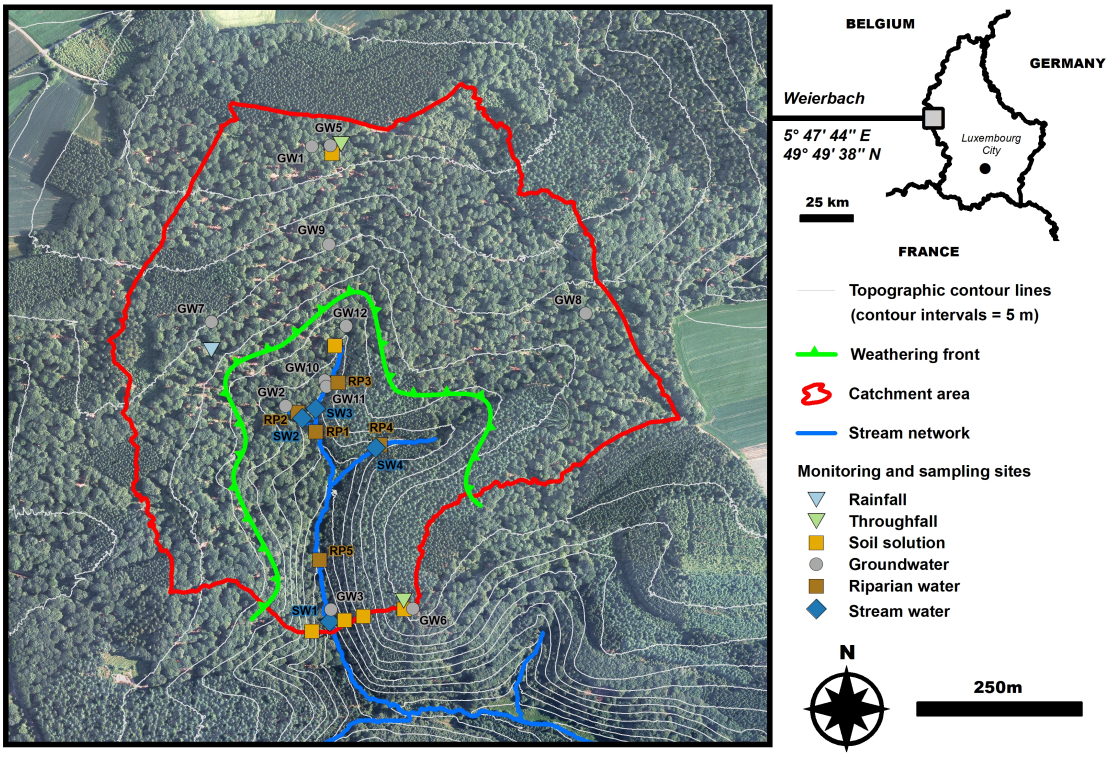

Figure 2.1: Map of the Weierbach catchment and its location in Luxembourg The map displays the locations where the six types of water samples were collected. The colours of the locations correspond to the respective sample colors. The green contour line indicates the basement of the chemical weathering front, as inferred from the subsurface exploration by Gourdol et al. (2021). Additionally indicated are the primary and secondary plateaus.

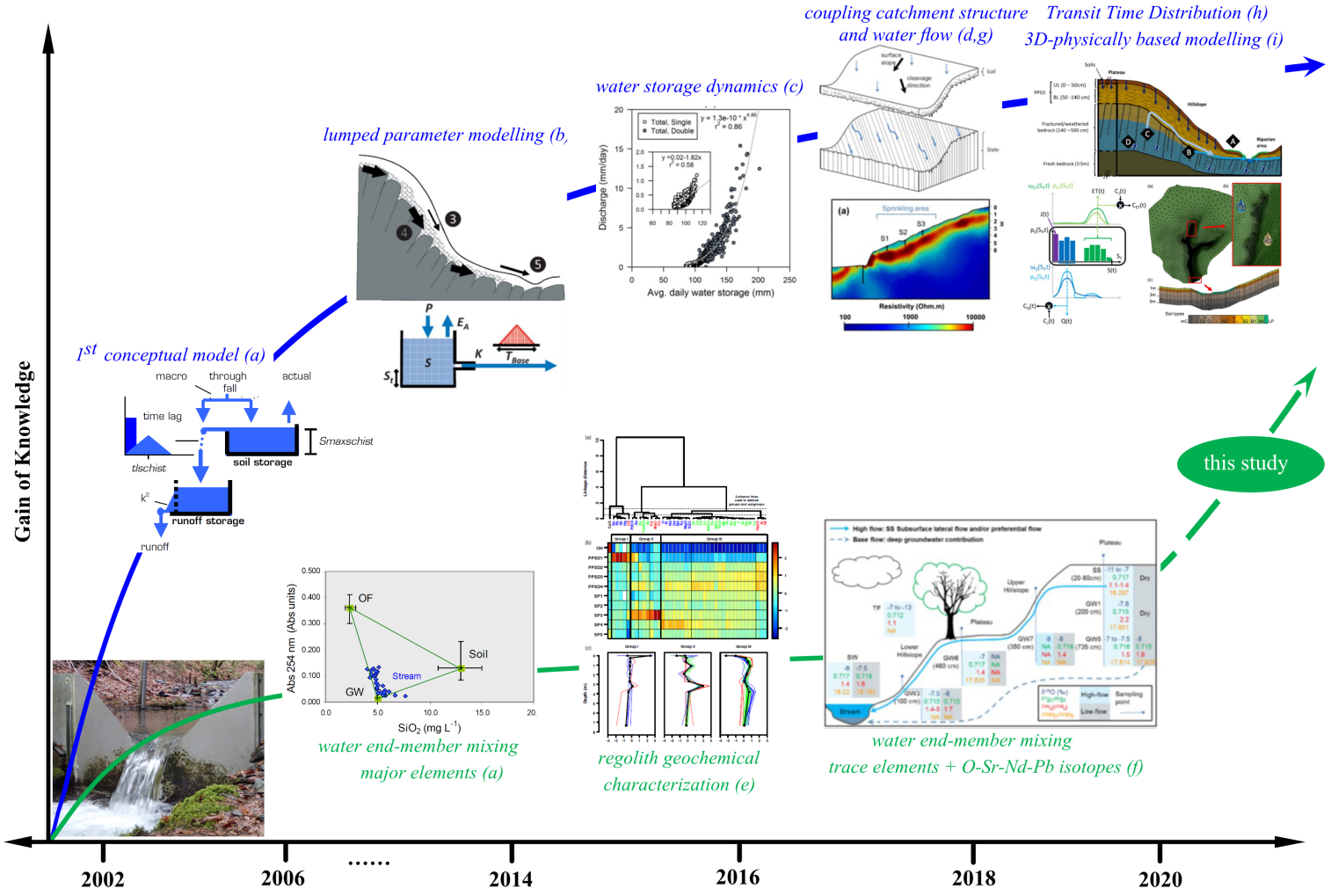

Figure 2.2: A timeline illustrating the rate of advancement in understanding of hydrological and biogeochemical processes over the past two decades. The figure was derived from a comprehensive list of published studies from the previous two decades. Hydrology (blue line) and geochemistry (green line) process understandings are depicted in chronological order: Figures from (a) Pfister et al., 2006 ; (b) Wrede et al. (2015); (c) Martínez-Carreras et al. (2016); (d) Scaini et al. (2017); (e) Moragues-Quiroga et al. (2017)(f); Moragues Quiroga (2018); (g) Scaini et al. (2018); (h) Rodriguez and Klaus (2019); I) Glaser et al. (2020)

2.1.1 Vegetation

The structure of the WEC's forest is the result of past and current management practices. Oak trees are evenly distributed throughout the area, whereas the density of beech trees increases from the plateau to the footslope and varies greatly between areas. The hillslope transect of the primary plateau is densely populated with a mixed forest consisting primarily of European beech trees (78% of the forest stand, 60% in basal area), as well as pedunculate and sessile oak hybrid trees (22% of the forest stand, 40% in basal area). The two oak species frequently produce hybrids that are phenologically difficult to distinguish (Fabiani et al., 2022). Shrubs are absent, and the understory is dominated by blueberries (*Vaccinium myrtillus*). The riparian zone is populated by a variety of short plants, including spinulose wood fern (*Dryopteris carthusiana*), yellow basalm (*Impatiens nolitangere*), opposite-leaved golden saxifrage (*Chrysopsis oppositifolium*), and woodsorrel (*Oxalis acetosella*; Martínez-Carreras et al., 2015). The vegetation of the secondary plateau consists primarily of Norway spruce and Douglas fir.

2.1.2 Regolith

The term "regolith" refers to the unconsolidated or secondary cemented cover that overlies more coherent bedrock. Weathering, erosion, transport, and/or deposition of older material results in the formation of regolith (Scott and Pain, 2009). Various models have been proposed to describe how weathering takes place in the *CZ*. Brantley et al. (2007) consider the *CZ* as a flow-through reactor (*FTR*). In net denudation or topographic steady state (uplift balanced by erosion), solid material enters the reactor through its lower boundary, solid sediment products are skimmed off the top by erosion, and dissolved products leak out through its porous sides. In contrast to the *FTR* model, a net depositional system adds new material to the surface. A piece of rock is believed to move vertically through this system, cracking and experiencing chemical weathering until it reaches the rock–regolith boundary. The fragment moves randomly as it is mechanically and biomechanically pushed through the soil and moved downslope (Mudd and Furbish, 2006; Kaste et al., 2007), undergoing abiotic weathering and biologically-driven nutrient extraction (Burford et al., 2003). The regolith covers the *CZ* and is the natural focus of rock and mineral decay. Saprolith is decayed bedrock that retains its structure and fabric if the regolith develops from in-situ bedrock. The "Saprolith" is divided in a lower part called Saprock and a upper part called Saprolite (Scott and Pain, 2009).

The *WEC* regolith is composed of 2 parts called *solum* and *subsolum* (Juilleret et al., 2016). In this thesis, we follow the definition of Juilleret et al. (2016), where the *solum* is defined as the upper part of the soil constituted by a *O*, *A* and *B* horizon, respectively (where pedogenic processes are dominant and where biota play an important role); the lower part is defined as *subsolum* where the original rock structure or fabric of the bedrock is preserved. The *WEC*'s *solum* (figure 2.3-b), consists on average of a stony silt loam

soil derived from periglacial solifluction deposits that is overlain on a schist substratum that has been weathered. A thin, dark organic surface horizon (O to A horizon, 0-8 cm on average) is followed by a cambic horizon (B horizon, 8-40 cm on average) with a well-developed angular blocky soil structure. The texture of the silt loam is inherited from the loess deposit and was mixed with schist clasts via solifluction, with the number of schist clasts increasing with depth.

A stratigraphic and geochemical characterization of the *WEC*'s regolith was conducted by (Moragues-Quiroga et al., 2017). The study combined mineralogical, major and trace element and Sr-Nd-Pb-U radiogenic isotope analyses to gain a deeper understanding of the primary plateau regolith characteristics and evolution, as can be seen in figure 2.3-b. Moragues-Quiroga et al. (2017) observed three distinct compartments that have different geochemical – and mineralogical characteristics as a function of contrasting evolutions. These respective processes are related to different atmospheric deposition events and seasonal water saturation dynamics.

The geology of the catchment is dominated by slates, phyllites and quartz of Devonian age (Kleber, 1997; Semmel and Terhorst, 2010)). During the last 10 years, extensive drilling and geophysics (*ERT*; Gourdol et al., 2021) campaigns has been conducted. The *WEC*'s deep subsurface exploration yielded more detail than is currently known. Figure 2.3-a depicts two processed composite images of the core. The blue demarcator on the core image depicts the lithological profile of the secondary plateau. This core image on the left (red demarcator) displays the primary plateau's profile. The colour difference between these two images (lithology colour) reveals the relative rates of chemical weathering between the two areas. Underneath the subsolum, saprolite is present on the primary plateau, and is absent on the secondary plateau (indicated by the green dashed contour line on figure 2.1). Figure 2.3-c shows the occurrence of saprolite, inferred from core description information and electrical resistivity survey by Gourdol et al. (2021), where red and blue tones indicate high resistivity and low resistivity, respectively. The green dashed contour line indicates the elevation of the basement of the chemical weathering front (where the colour changes from yellow to black-grey in the core images) that seems to be related to the occurrence of the saprolite in the catchment.

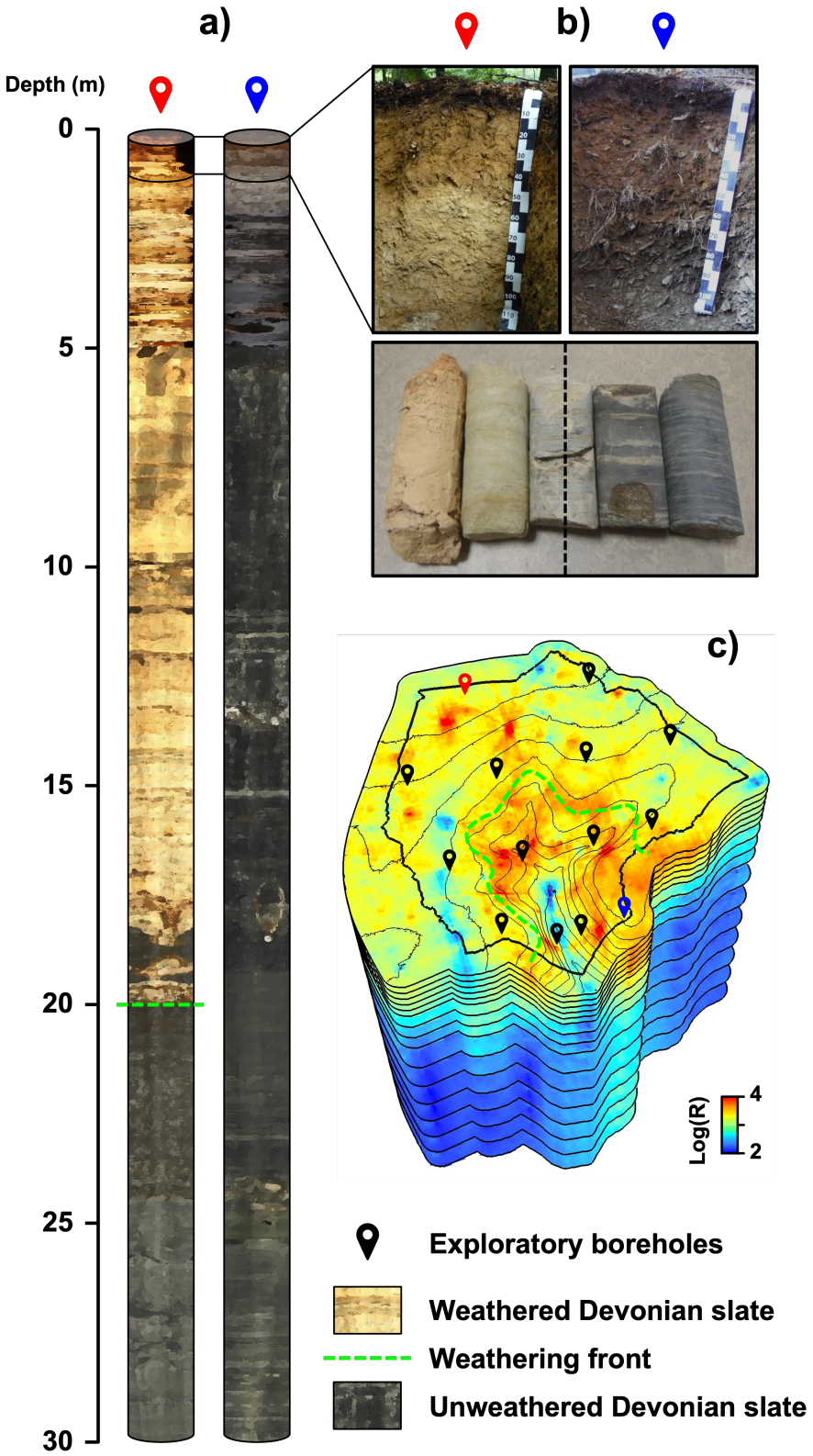

Figure 2.3: Structure of the regolith of the Weierbach Experimental Catchment. a) drilling cores at the primary (red) and secondary (blue) plateau locations. b) soil profiles described at the primary (red) and secondary (blue) plateaus. c) Interpolated depth slice calculated from the electrical resistivity survey (Gourdol et al., 2021)

2.1.3 Climate

The climate is semi-marine, and precipitation is evenly distributed throughout the year with an annual average of 953 mm (2006–2014; Pfister et al., 2017). Lower base flow occurs from July to September. This is due to higher losses through evapotranspiration (*PET* annual average of 593 mm for the period of 2006-2014, from Pfister et al., 2017). The average annual stream discharge is 478 mm. Streamflow can cease intermittently from upstream to downstream during dry conditions. During these conditions rainfall-runoff behaviour is characterized by a sharp, short-lasting discharged peak (Wrede et al., 2015). During wet conditions, a double peak behaviour is observed, where a single rapid discharge peak appear shortly after a rainfall event, followed by a broad, long-lasting second discharge peak that start a few hours after the onset of precipitation. The second peak largely outweigh the first peak in terms of volume (Martínez-Carreras et al., 2016; Scaini et al., 2018). Figure 2.4 show the daily total precipitation in the *WEC* and the daily mean discharge at *SW1* from late 2008 to 2022 .

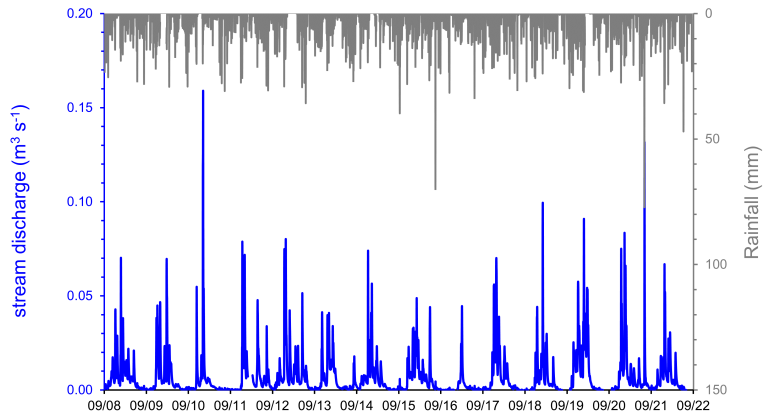

Figure 2.4: Daily total precipitation amount (mm/d) and daily mean discharge ($m^3\ s^-$) at *SW1*.

2.2 Hydrological Perceptual model

The first iteration of the current perceptual model of the main flow paths through the *WEC* was proposed in the study by Pfister et al., (2006), followed by Wrede et al. (2015). In the study a variety of field measurements and streamflow simulations was used to translate the experimental understanding into a qualitative perceptual model. This model was updated with a focus on storage controls by Martínez-Carreras et al. (2016). More recently, noteworthy advancement of the process-based understanding was described in a paper by Rodriguez and Klaus (2019). The Weierbach is a difficult case to understand in terms of streamflow generation as it has a double peak response in streamflow in winter and a single peak response that is remarkably concomitant with precipitation in summer (Wrede

et al., 2015). This is a widespread and poorly understood phenomenon (Martínez-Carreras et al., 2016).

The current understanding about the origin of the first peak in the double peak response is that it is caused by saturated excess flow from the riparian soils into the stream (Klaus et al., 2015; Glaser et al., 2016). This understanding is supported by the hydrograph separation and end-member mixing analysis studies (Martínez-Carreras et al., 2015; Wrede et al., 2015). This mechanism has also been proven by high frequency stream *DOC* observations (Schwab et al., 2018), thermal infrared imagery (Glaser et al., 2018) and diatom tracer studies (Pfister et al., 2010; Klaus et al., 2015; Antonelli et al., 2017; Pfister et al., 2017).

The second peak observed in the streamflow is attributed to lateral subsurface flow above the PPSD/weathered bedrock interface. This area is assumed to have a much higher lateral conductivity compared to the vertical conductivity in this zone. This is an important aspect of the Weierbach that makes studies on streamflow generation in this catchment very important. In a recent study by Xiao et al. (2021), the authors showed that permeability variations with depth is a first-order control on hydro-geochemical functioning. This fact has also been highlighted several other studies (Schoeneberger and Wysocki, 2005; Ghasemizade and Schirmer, 2013; Brooks et al., 2015). The implication of this controls is that for catchments that is characterised by a sharp decrease in permeability with depth, 95% of water flow though the top part of the subsurface, causing chemical contrasts between shallow and deep groundwaters. Furthermore, elongated mean transit times (*MTT*'s) and weathering rates are expected.

Understanding the subsurface structure of a catchment is still one of the largest knowledge gaps in CZ science (Hopp et al., 2009; Ameli et al., 2016; Hale and McDonnell, 2016; Zimmer and McGlynn, 2017; Zimmer and Gannon, 2018; Fan et al., 2019; Li et al., 2021).

A recent geophysics study that included the information from a recent large scale drilling program was conducted by Gourdol et al. (2021) in the *WEC*. The results of the study suggest that there is a deep chemical weathering front located on the primary plateau of the *WEC* that becomes less distinct at a specific contour line in the valley. This weathering front acts as a boundary between the saprolite and parent rock, exerting control over the hydrological processes within the catchment. The weathering front on the hillslopes is relatively shallow and fades out near the stream. However, the secondary plateau does not exhibit a chemical weathering front, but is characterized by extensive fracturing.

Even though great strides have been made in the process-based understanding of stream flow generation in the *WEC*, there are still some uncertainties in the understanding of these processes. In the case of the single peak response most of the studies suggest saturated overland flow, Jackisch et al. (2021) has shown that to a smaller extend fast subsurface flow lines may also contribute to this response. Martínez-Carreras et al. (2016) states that

both processes are likely to occur but the extent of participation of each is still uncertain. Strong evidence exist that the generation of the second delayed peak is controlled by storage-threshold mechanism observed by Martínez-Carreras et al. (2016). What this means practically is that the plateau and the stream are connected when the catchment is sufficiently wet, and the plateau play a dominant role in the generation of the second peak. The transfer of water from the plateau to the stream through various landscape units and their respective influence are still not well understood.

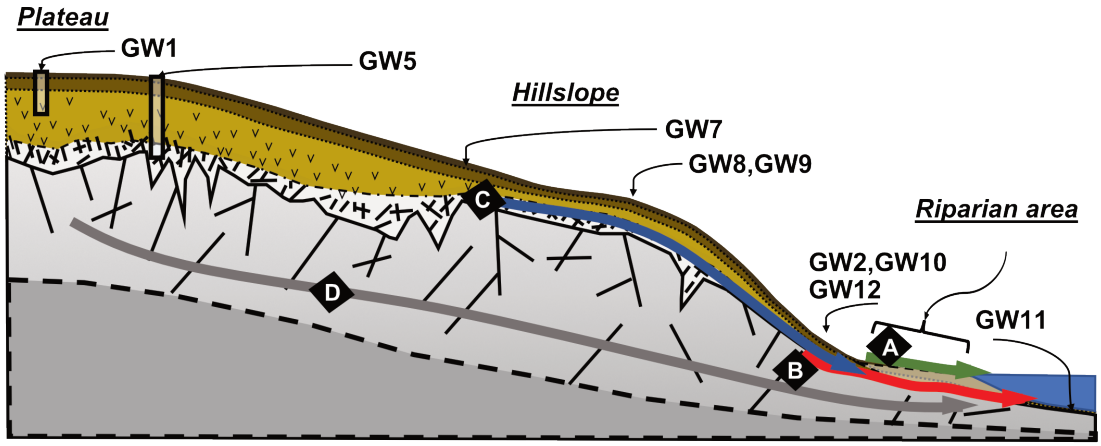

Figure 2.5: Current hydrological perceptual model of the WEC (adapted from Rodriguez and Klaus, 2019).The current respective contributions to stream flow are labelled as diamonds. Flow line A represent the near stream saturated excess flow from the riparian soils due to precipitation. Flow line B represent the Near-stream lateral subsurface saturated flow through the basal layer (BL) of the Pleistocene periglacial slope deposits ($PPSD$) activated after a bedrock storage threshold is exceeded. Flow line C is caused by the same mechanism as B, but activated upslope. Finally, flow line D represent deep groundwater contributions from upstream via flows through the weathered and fractured slate bedrock with a cleavage oriented partly parallel to the stream.

2.3 Hydro-biogeochemical understanding

A continues bi-weekly groundwater- and surface water physico-chemical parameter monitoring campaign has been running in the catchment since 2009. The monitoring network has been steadily growing from five boreholes in 2009 to 26 currently. Several shorter-term research projects have added to the extent of the current dataset. All these studies had the common goal of understanding water fluxes in different parts of the critical zone, resulting in an extensive set of observed parameters. Recently Hissler et al. (2021) published a portion of the current dataset. The hydro-chemical dataset was not included in this publication as it formed part of the current study.

The longest groundwater quality data are available for boreholes $GW1$-$GW13$. These boreholes are located along the hillslope catena. A detailed description about the borehole construction and instrumentation is given in chapter 4. The borehole depths range from 2.5 meters to 7 meters below surface and the first 1 meter is cased off.

Figure 2.6 shows a Piper diagram (Piper, 1944), comparing the groundwater ($GW1$-$GW13$) with rainwater, throughfall, soil solution, stream water and riparian water. Figure 2.6 show boxplots of the major cations, anions, pH and EC for the different sample sites. $GW2$, $GW5$, $GW10$ and $GW12$ have a relatively high variance in concentration of Ca^{2+}, Mg^{2+} compared to the other sample sites. This is also the case for alkalinity and EC. NO_3^- is also an interesting parameter to take note of. It can be seen from figure 2.6 that high variance in this parameter is observed for sample sites on the secondary plateau ($GW3$, $GW6$) relative to the other sample sites. The current understanding of the subsurface architecture of the WEC may explain the high variance observed in some of the boreholes and not in others. Due to the variability in the depth of the weathered zone from the plateau to the stream, one can imagine that stratification in storage, storativity and transmissivity with depth will occur moving from the plateau to the stream. This will imply that when sampled, boreholes intercepting several flow lines will render a water sample that is a mixture of the respective flow lines. By this logic, boreholes that intercept several dominant flow lines will show a higher degree of variation in chemistry data.

Even though substantial work has been done in terms of geochemical description of potential geochemical processes units such as the regolith evolution (Moragues-Quiroga et al., 2017), impact of litter degradation (Montemagno et al., 2022), mixing of flow lines (Martínez-Carreras et al., 2016), no robust geochemical model currently exists of the WEC. Several uncertainties are still to be addressed.

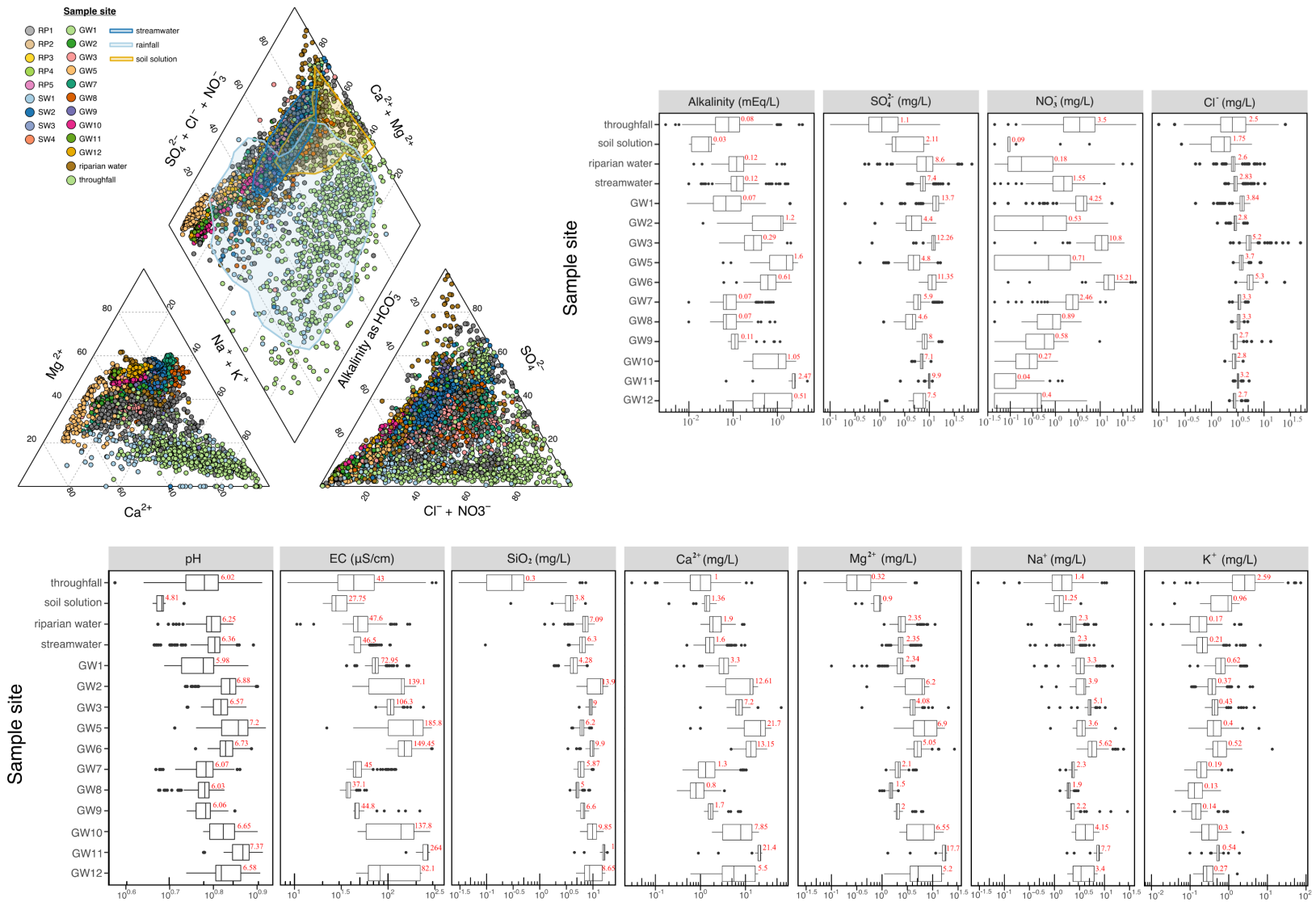

Figure 2.6: Overview of *WEC* hydrochemical data The left-top Piper diagram shows the sample sites' chemical composition (relative concentrations of major cations and anions). Box plots reveal the variance and median of the major water sample types (throughfall, soil solution, riparian water, stream water, and groundwater).

2.4 Conclusions

The *WEC* is the ideal testbed for the advancement of integrated hydro-biogeochemical theories through the development of new concepts. The *WEC* provides over two decades of information on the hydrological processes of the system. The subsurface of the *WEC* has also been extensively explored. A comprehensive and long-running biweekly hydrochemical data set contributes to the abundance of knowledge and opportunity presented.

Possibly, the geochemical understanding of the system is not as advanced, providing an opportunity for this study. Due to the abundance of data (hydrological and geochemical), both data-driven modelling approaches and geochemical process-based modelling can be used to gain a better understanding of the coupled nature of the processes controlling $c - Q$ patterns in streams. In the next chapter, we'll talk in depth about the methods used in this thesis.

Chapter 3

Methodology

3.1 Introduction

Throughout the course of the study, a variety of data sets were utilized. As part of an ongoing monitoring programme, certain data sets were gathered while the study was being conducted and included in the final analysis (sampling of groundwater, riparian water, surface water, rainfall, and throughfall). A weekly frequency campaign that was planned for one year was also put into effect to provide higher resolution on key aspects of trends that were observed in the long-term monitoring programme. This was done in order to provide more accurate information. the specifics of which are covered in this chapter's discussion.

3.2 Data collection

3.2.1 Long term monitoring

The study made use of an existing monitoring programme in operation since 2009 (figure 2.1). Since then, the monitoring network has expanded from five groundwater wells to a dense grid of twenty-six groundwater wells. Since 2009, the groundwater wells $GW1$, $GW2$, $GW3$, $GW5$, and $GW6$ have been routinely sampled. Since 2014 and 2015, $GW7$ and $GW8$ have been part of the monitoring network. More recently, $GW9$, $GW10$, $GW11$, $GW12$, and $GW13$ have been installed, and data from 2019 onwards is available. $GW14$–$GW27$ are the most recent wells drilled in 2021. These wells lack complete equipment and are sampled every six weeks using a bailer and do not form part of the study.

The borehole information are shown in table 3.1 below. The equipped boreholes are sampled with a peristaltic pump. Historically, the sampling procedure involved pumping the borehole for a few minutes and then filling the sample cup. This is still debatable if accurate samples are taken, as this procedure may introduce additional variance in the data as a result of the boreholes not being sufficiently purged. However, it is operationally necessary, as some boreholes only provide wellbore storage during dry months and may be pumped dry before a sample can be collected. Water level measurements are recorded continuously in 15-minute increments for the equipped boreholes ($GW1$-$GW13$).

Table 3.1: Borehole information. Figure 2.1 shows the locations of the boreholes.

BH Name	Standpipe (cm)	Depth (cm)	Depth below surface (cm)	Well screen depth below surface (cm)	Weekly sampling	bi-weekly sampling
GW1	32	252	220	152	x	x
GW2	35	230	195	136	x	x
GW3	32	254	222	160	x	x
GW5	33	753	720	382	x	x
GW6	29	473	444	350		x
GW7	18	555	537	400	x	x
GW8	20	520	500	-		x
GW9	28	656	628	-	x	x
GW10	31	330	299	-	x	x
GW11	30	130	100	-	x	x
GW12	40	345	305	-	x	x
GW13	9	795	786	-		x

Precipitation was collected using a 3-liter Palmex rain sampler, which minimises gas transfer between the bottle headspace and the open atmosphere in order to reduce water evaporation. To collect and quantify throughfall, Benoit plastic collectors (400 cm^2 interception area) were installed close to the older trees (deciduous, Douglas, and Spruce) to collect and quantify throughfall. The soil solution was measured at six sites dispersed throughout the catchment. The bulk of the samples were taken from 2009-04-09 to 2014-09-17, with six more samples between 2015 and present. Riparian waters are collected from riparian soils at a depth of 10cm. As part of the biweekly monitoring programme, stream water is sampled at four locations throughout the catchment. This is accomplished by collecting a random sample at each site. During the sampling, the EC is also measured using a WTW® TetraCon® 925 probe.

3.2.2 Weekly frequency sampling

A weekly frequency monitoring campaign was designed to add additional resolution on key potential processes observed upon initial analysis of the long-term existing database. At the time of the study boreholes GW9 to GW13 was recently drilled and equipped. The campaign was planned for one year with a sampling frequency of one week time increments. Boreholes $GW6$ and $GW8$ did not form part of the weekly sampling campaign.

Using a flow-through cell system, electrical conductivity (EC), dissolved oxygen (DO), redox potential (ORP), and pH were measured at each sampling event (figure 3.1). Before sampling a borehole, the probes were given five minutes to record a datum reading of EC ranging from 0.1 to 1.7 ($\mu S/cm$) after the system was flushed with one litre of milliQ water. After this, the borehole was purged while the values of the four parameters were continuously recorded in one-minute increments. Using two WTW® Multi 3630 IDS data loggers, this was accomplished. When the EC reading remained stable for several minutes, a groundwater sample was collected, and it was assumed that the borehole was homogeneous. After collecting the water sample, the flow-through system was sealed, and the probes were given 20 minutes to equilibrate with the solution in the cells prior to obtaining the final readings for the four parameters. In addition to the four parameters,

pumping time, the water level prior to and immediately after pumping, and the amount of water extracted from the well were also recorded. The following are the probes used for each of the four physical parameters:

- EC: WTW® TetraCon® 925;
- DO: WTW® FDO® 925;
- ORP: WTW® SenTix® ORP-T 900;
- pH: WTW® SenTix® 940.

The pH probe was calibrated at each sampling event in the field. HACH Singlet™ Solution Packs were used for a two-point calibration in the field.

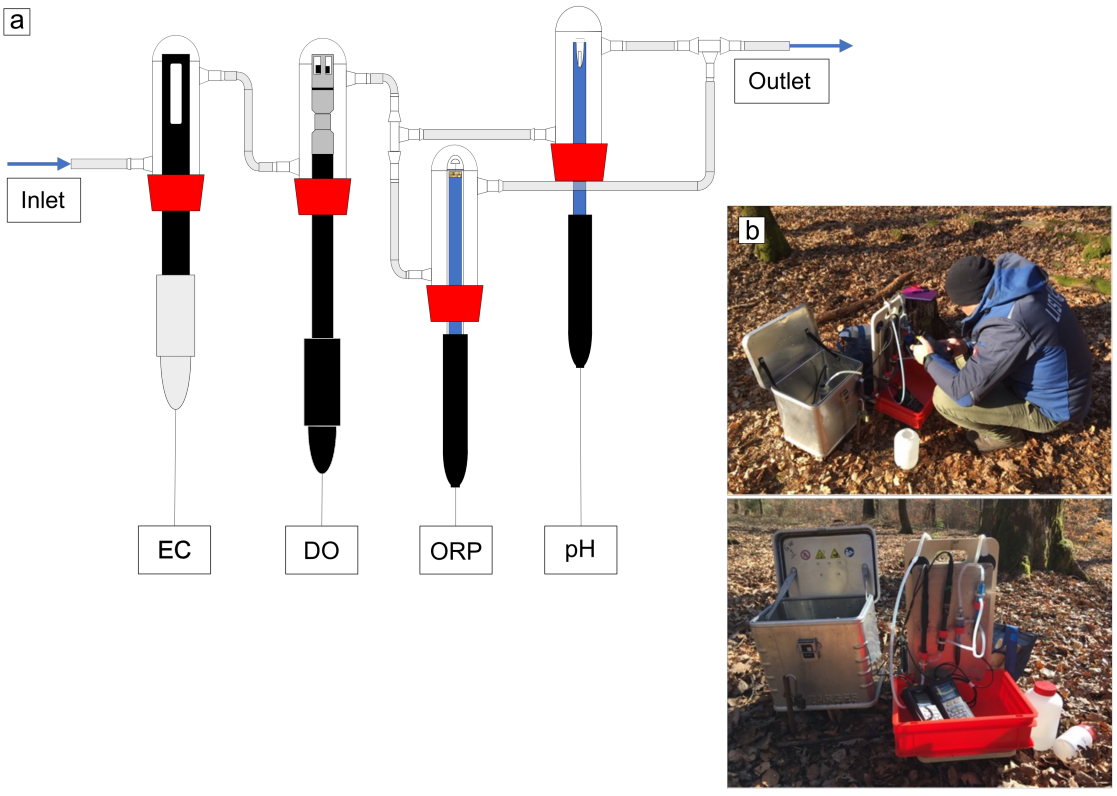

Figure 3.1: Schematic (a) of the flow-through cell used to measure in-situ electrical conductivity (*EC*), dissolved oxygen (*DO*), oxidation-reduction potential (*ORP*), and pH. The *ORP* and pH probes were placed in parallel to avoid interfering with one another. Two WTW® Multi 3630 IDS data loggers were used to automatically record the probe data. (b) shows two photos of the setup in the WEC.

3.3 Laboratory analysis

3.3.1 Pre-processing

All water samples were filtered in the LIST laboratory shortly after collection. A vacuum system and 0.45 µm Cellulose Acetate membrane filters, manufactured by Sartorius (type 111, 47 mm diameter), was used. During pre-processing of the samples EC was measured using a TetraCon® 925 probe.

3.3.2 Analysis

From 2009 to 2022, all collected samples were subjected to a complete water chemical composition analysis using the same protocols and analytical facilities. Table 3.2 shows the quantification limit for all analyses. The quantitative blank values were always less than the quantification limit.

The pH and alkalinity were measured using a Mettler Toledo equipment with $0.01N\ HCl$ up to pH 4.5. Dissolved Organic Carbon (DOC) was analyzed using a Teledyn-Tekmar Apollo 9000 system. The dissolved silica (SiO_2) and HPO_4^{3-} concentrations and the absorbance at 254 nm ($Abs254$) were measured using spectrophotometry with a Skalar© continuous flow analyzer SAN^{++}. The major cation (Na^+, K^+, Ca^{2+}, Mg^{2+}, NH_4^+) and anion (Cl^-, NO_3^-, SO_4^{2-}) concentrations were analyzed using ionic chromatography (Dionex ICS-5000 dual channel).

The total content of trace metals (Al, Fe, Mn, Ba, Sr) were analysed with a Quadrupole ICP-MS (Agilent 7900) associated with an ISIS 3 (Agilent) injection system. The analyses were conducted in He mode and ^{103}Rh and ^{185}Re were used as internal standards. The calibration standards were prepared with Multi elements ICP standard solutions (CHEM-LAB Analytical) diluted in HNO_3 1%. The analytical blank values were less than 1% of the lowest sample concentrations for all elements. For all elements, the quantification limit are given in Table 3.2.

Table 3.2: Quantification limit of the analytical methods used for the major elements.

Parameter (mg/L)	Na^+	K^+	Ca^{2+}	Mg^{2+}	NH_4^+	Cl^-	NO_3^-	SO_4^{2-}	SiO_2	HPO_4^{3-}	DOC
DL	0.1	0.02	0.2	0.1	0.01	0.1	0.02	0.1	0.1	0.05	0.1
Parameter ($\mu g/L$)	Al	Fe	Mn	Ba	Sr						
DL	4.02	1	0.1	0.05	0.025						

3.4 Available data

The first stream gauge in the WEC was installed in 2002 (Hissler et al., 2021). Since then, there has been a multitude of studies in the WEC (see chapter 2). Currently

extensive data is available for rainfall, throughfall, soil volumetric water, groundwater levels and discharge. During 2009 several interdisciplinary studies was initiated, and intense monitoring started. The information pertaining to all the projects that have contributed to the present comprehensive dataset is presented in table 3.3. The table also includes a listing of the number of samples that were used in this study as well as the types of samples that were used.

Table 3.3: Data sources of hydrochemical data

Date	Project	groundwater	rainfall	riparian water	snow	soil solution	stream water	throughfall
2009	MSc. Thomas Blaise (CRPGL)	10	8	0	0	18	15	0
2010-2012	BIGSTREAM	106	39	12	4	62	119	24
2011-2014	SOWAT	219	80	72	1	369	233	209
2012-2018	CAOS	89	12	10	0	2	52	36
2014-2018	AFR Cristina	124	21	21	0	22	79	72
2016-2017	BIOTRANS	251	43	41	0	0	182	129
2018-2023	HYDRO-CSI	1176	64	235	0	2	273	211
2019-2022	EFFECT	120	17	12	0	0	70	51

Data processing and validation were necessary because the data set had developed over the course of a number of years and in response to a variety of projects. The methods used to achieve this goal will be discussed in the following sections.

3.4.1 Detectable limit

Several variables in the current database contain censored values. Censored values are those that are below or above the detection limit (DL) of the instrument or method employed. Because the entire data set used in this study ranges from 2009 to the present, data were generated through a series of laboratory measurements with varying detectable limits due to instrument and user changes. Farnham et al. (2002) proposes the following replacements for censored data: For data sets with a single or multiple DL values, replacing $< DL$ with $\frac{1}{2}DL$ yields the best performance in PCA's; parameters with $< DL$ values exceeding 30% yield poor PCA performance. In order to avoid ignoring these results during data processing (a value of "DL" is a result) and to be able to conduct multivariate statistical studies, it was decided to adhere to the criteria of Farnham et al. (2002). The median of the various DL was utilised, which was typically the minimum.

When examining central tendency and dispersion for the various variables, we used MEDIAN rather than MEAN because the data are generally skewed and, therefore, the former provides a more reliable estimate (Reimann et al., 2011).

3.4.2 Data-gap filling

In the context of Moragues Quiroga (2018)'s PhD research, parameters with more than 70% values above the detection limit were utilised in various multivariate analyses (MVA), data quality checks (ion balance), and describing the physicochemical parameter behaviour

of the respective sample sites. For the *MVA* phase of this investigation, it was determined that only major cations (Ca^{2+}, Mg^{2+}, Na^{+}, and K^{+}), major anions (alkalinity, Cl^{-}, SO_4^{2-}, and NO_3^{-}), and SiO_2 would be employed. In the analysis, only observations with a complete set of measured (not calculated) parameters were considered.

Regression imputation

It was found that absorbent (*A254*) had a very good correlation with *DOC* in several instances, with stream water ($SW1$) samples having the best correlation ($R^2 = 0.85$ and a p-value less than 2.2×10^{-16}). This relationship does not hold true for samples with low *DOC* concentrations, so *DOC* was calculated only for subsets (sample types) with an R^2 greater than 0.8 and a significantly low p-value.

The `lm_()` function in the `stats_package` (version 4.2.2) in R (Team et al., n.d.) was used to fit linear regression models for $GW1$ and $GW5$. The results are shown as a time series plot in chapter 5.

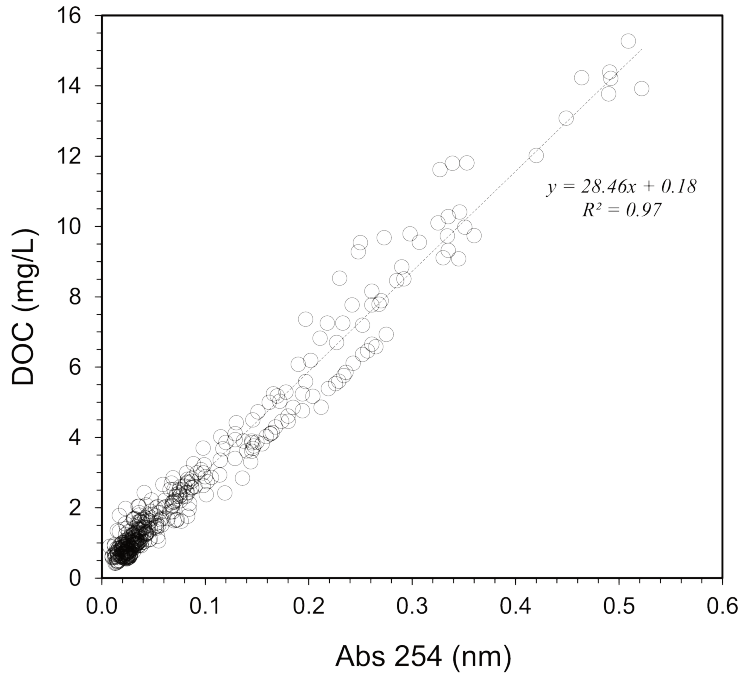

Figure 3.2: Plot of *DOC* (mg/L) *vs. A254* (nm) showing strong correlation between the two variables. The high degree of agreement between the two measurements supports the use of *A254* as a proxy for *DOC*.

Alkalinity

Missing alkalinity values were calculated as the charge balance difference between the sum of the cation change and the sum of the measured anions. This approach was based on the observation that, with the exception of rainfall and soil solutions, all sample types had

relatively low ion charge balance errors. Figure 3.4 shows the ionic balance percentage (equation 3.1) for the water sample types. Generally, ground- and stream- waters fall inside the ±10% boundary, whereas the rain and soil solutions show a larger proportion of observations outside this threshold.

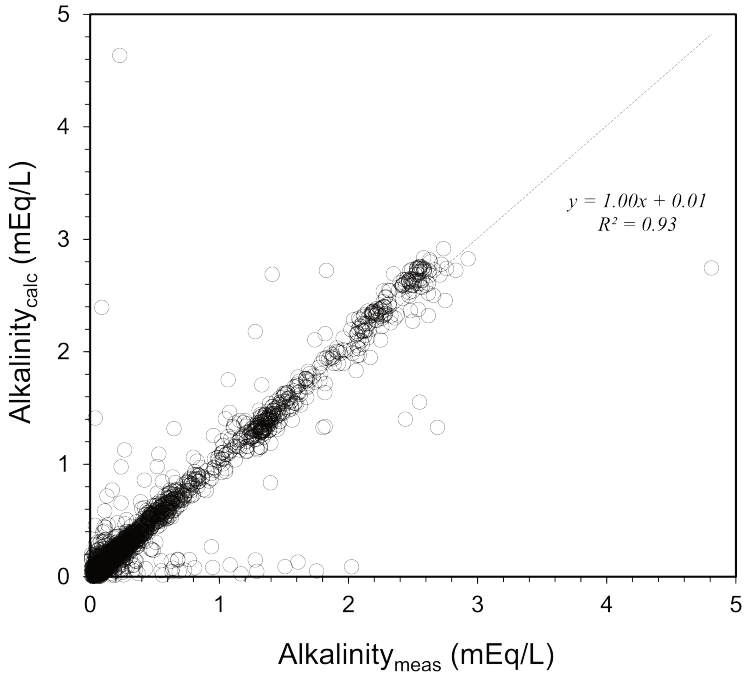

Figure 3.3: Comparison of calculated and measured alkalinity values. The calculated alkalinity (assuming ion balance error $\leq 10\%$) is shown to closely match the measured alkalinity, supporting the assumption that the difference between cations and anions can be accounted for by missing alkalinity.

$$E.B = \frac{(Sum\ of\ cations\ - Sum\ of\ anions)}{(Sum\ of\ cations\ + Sum\ of\ anions)} \times 100 \tag{3.1}$$

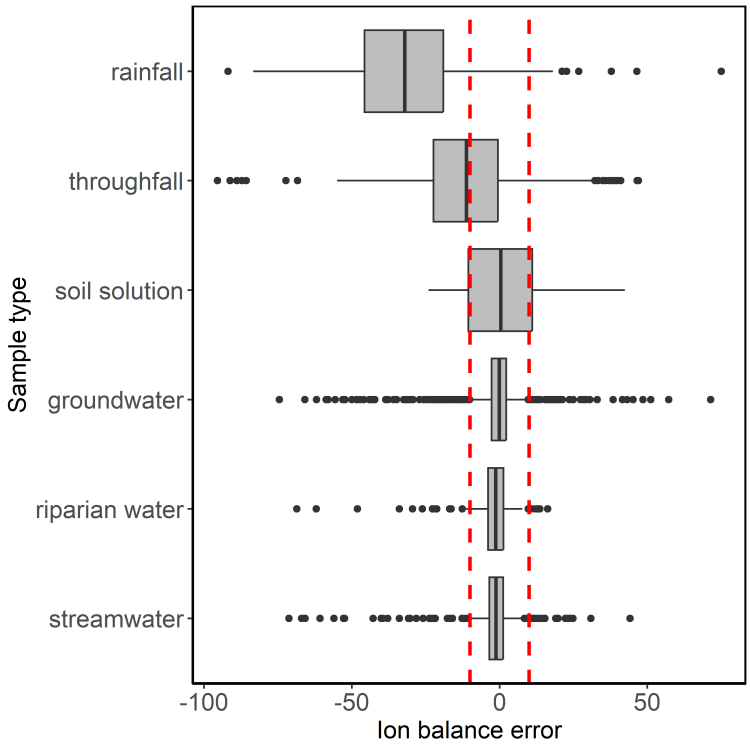

Figure 3.4: Ionic balance percentage box plots for the Weierbach waters The red dashed lines represent ±10% limits. The black line in each box represents the data's median; the upper and lower limits of the boxes represent the interquartile range (IQR); the whiskers represent the first and third quantiles ±1.5 times the IQR; and the points represent outliers beyond the whiskers' range.

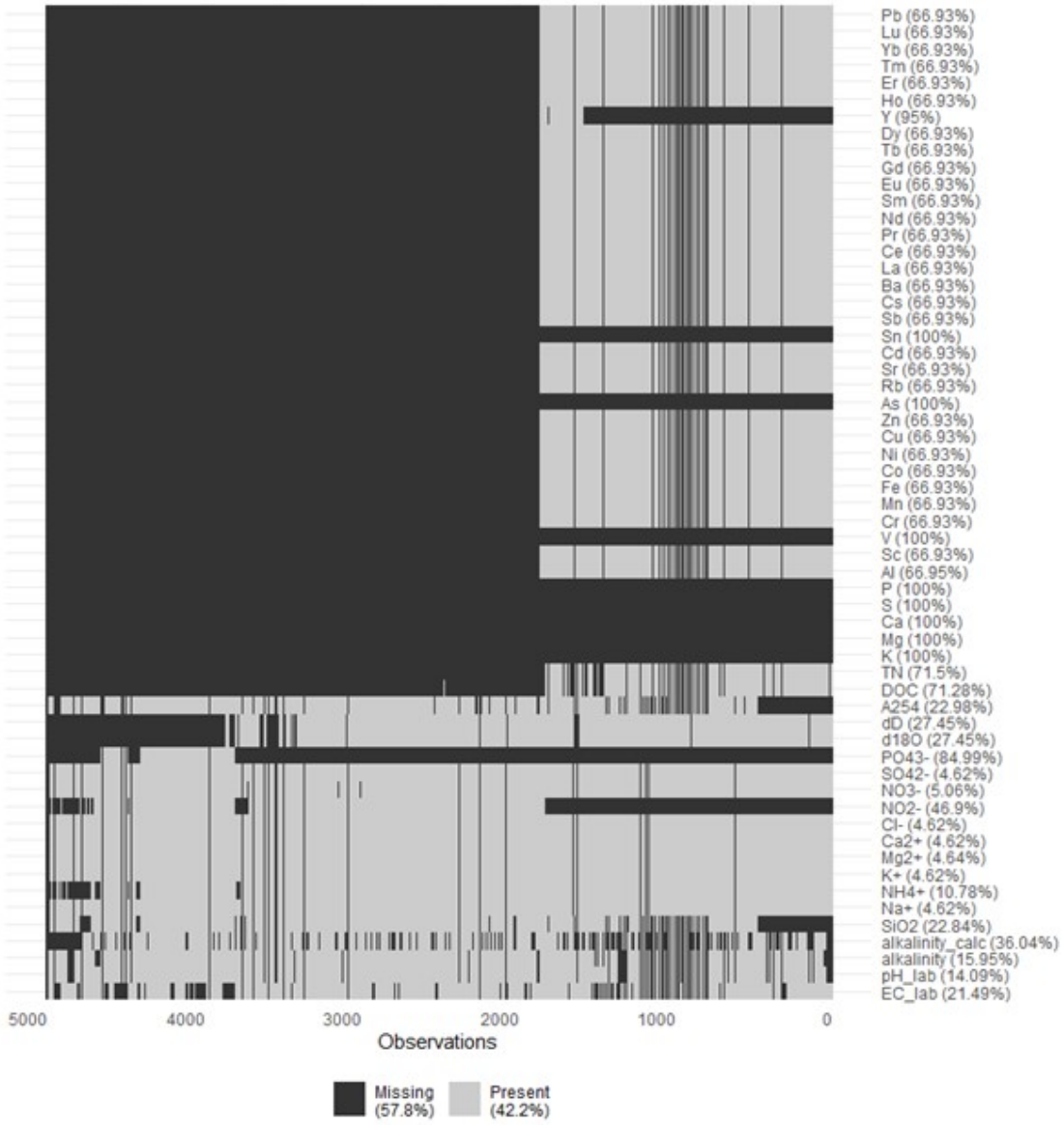

Figure 3.5: Presentation of the available and missing data in the *WEC* chemical database, including water samples from 2009 to 20222.

3.5 Multivariate statistical analysis

Due to the high volume of diverse data that is available spanning over almost a decade, there are many chemical- and physical variables that characterise each sampling point. To make sense of all the data, a multivariate statistical approach is used. The steps taken in this approach is discussed in detail below.

3.5.1 Hierarchical clustering

Hierarchical clustering (Hartigan, 1975; Kaufman and Rousseeuw, 2009), also known as hierarchical cluster analysis (*HCA*), aims to partition observations into groups or clusters using either an agglomerative (bottom-up) or a divisive (top-down) approach to group observations such that the pairwise dissimilarities of observations grouped together tend to be smaller than those of observations belonging to a different group (Hastie, 2009). *HCA* is one of the most widely used clustering methods in Earth sciences (Davis and Sampson, 1986; Schot and Van der Wal, 1992; Bini et al., 2011; Levitan et al., 2015), and is frequently employed in hydrochemical research (Güler et al., 2002; Güler and Thyne, 2004; Cloutier et al., 2008). *HCA* does not require a predetermined number of clusters, but rather a measure of dissimilarity or linkage. For consistency and comparability of results obtained by Moragues Quiroga (2018), the Ward's method (Ward, 1963) was selected as the linkage rule. The Pearson correlation distance (1 - Pearson correlation coefficient) was retained for the linkage distance, as it is suitable for clustering variables (Reimann et al., 2011). Before clustering, the samples were log-transformed to account for the highly positively skewed distributions of the parameters, and then the parameters were normalised by calculating their z-scores (Reimann et al., 2011):

$$Z_i = \frac{x_i - \bar{x}}{s} \tag{3.2}$$

where Z_i is the standard score for sample i, x_i is the value of the sample i, $\bar{x}$ is the mean and s is the standard deviation. This was done to ensure that each parameter is weighted equally and do not skew the Manhattan distance calculations (Judd, 1980; Templ et al., 2008).

The `hclust()` function (Langfelder and Horvath, 2012) in R was used to perform the calculations.

3.5.2 Principal component analysis

To deal with the curse of dimensionality (Bellman, 1961), principal component analysis (*PCA*) was performed on the z-transformed dataset. *PCA* is a multivariate statistical technique, one of the oldest multivariate techniques and one of the first to be introduced by Pearson (1901) and Hotelling (1933) independently. *PCA* attempts to reduce the dimensionality of a multivariate dataset while preserving as much of the data's original variation as possible (Everitt and Hothorn, 2011). This is accomplished by transforming the dataset into a new set of variables (principal components, or *PC*'s) that are linear combinations of the original variables, are uncorrelated with one another, and are ordered such that the *PC*'s account for the variance in the original dataset in descending order of importance (*PC* 1 explains the most variance, and so on). This step usually follows *HCA* and is seen in many studies (Melloul and Collin, 1992; Winter et al., 2000; Güler et al.,

2002; Güler and Thyne, 2004; Thyne et al., 2004; Cloutier et al., 2008). *HCA* is used to first cluster the samples in most workflows observed in studies utilising multivariate statistics. The following step is to perform a PCA to reduce the dimensionality of a complex dataset and uncover underlying data structures (Davis and Sampson, 1986). This procedure was followed, and the data was labelled according to the *HCA* cluster number. As previously stated, the variance in the original dataset can only be fully described by the entire set of *PC*'s, but not all PCs are useful for understanding the underlying structure of the data. Various formal and informal techniques are available to select the number of *PC*'s to retain (Kaiser, 1958; Cattell, 1966; Farmer, 1971; Jolliffe, 2002; Everitt and Hothorn, 2011). A scree diagram (Cattell, 1966) was used in the study. In this technique, the *PC*'s are plotted against their respective proportions of variance. The 'elbow' method is then applied to the number of components chosen (change in slope).

To sum up, a *PCA* is a method for reducing a multidimensional dataset to a new set of axes (*PC*'s). The *PC*'s are orthogonal (covariance between *PC*'s is 0) and, in descending order, account for the most variability in the multivariate space. The sample was then orthogonally plotted against *PC*'s, yielding new points known as scores. Furthermore, the *PC* loadings (eigenvectors) show the *PC*'s relationship to the scores on the plot.

The `prcompt()` function in the `stats_package` (version 4.2.2) in R was used to perform the calculations.

3.6 PHREEQC

PHREEQC (original acronym— *pH-REdox-EQuilibrium*) is a computer program that was developed to carry out a wide variety of aqueous geochemical calculations. It is written in the programming languages C and C++. PHREEQC is capable of implementing a number of distinct kinds of aqueous models, including two ion-association aqueous models (the model developed at Lawrence Livermore National Laboratory and WATEQ4F), a Pitzer specific-ion-interaction aqueous model, and the aqueous model developed using the Specific ion Interaction Theory (Parkhurst and Appelo, 2013). Many researchers and practitioners regard it as the tool of choice for a wide range of geochemical problems. Its open source nature, the ability to programme arbitrary kinetic laws for chemical reactions, and a thorough implementation of the Pitzer formalism for concentrated solutions all contribute to its success and longevity in many fields of hydrogeochemistry and geochemical modelling (De Lucia and Kühn, 2013). PHREEQC can model a wide variety of hydrochemical processes; however, for the purposes of this work, only the relevant PHREEQC functions (*keyword data blocks*) will be discussed in terms of data requirements and the physical principles on which the functions are based.

3.6.1 Speciation modelling

PHREEQC can be used to compute saturation indices, aqueous species distributions, and the density and specific conductance of a given solution composition. PHREEQC accounts for the nonideality of aqueous solutions by using ion-association, Pitzer, or SIT (Specific ion Interaction Theory) equations to calculate solute activities.

A brief overview of the processes in a multi-component solution will explain why PHREEQC is needed. For a general reversible chemical reaction;

$$aA + bB \leftrightarrow cC + dD \tag{3.3}$$

the law of mass action can be expressed as:

$$K = \frac{[C]^c[D]^d}{[A]^a[D]^d} \tag{3.4}$$

K represents the equilibrium constant in the expression. Using molar concentrations, the law of mass action cannot calculate the solubility of minerals. The law of mass action only applies to ion activity (amounts in square brackets), which is the total concentration measured after correcting for electrostatic shielding and aqueous complexes. Ion pairs or complexes can form in water. Complexation reduces the activity of "free" ions in water, thereby increasing mineral solubility and trace metal mobility. The activities of solutions with a small number of solutes can be calculated manually, but as the number of solutes increases, the calculations become more laborious. Fortunately, PHREEQC can assist with these calculations.

PHREEQC requires temperature, pH, redox state (pe), element concentrations, and valence states as input parameters to run a speciation model. The pe;

$$pe = -log[e^-] = \frac{E_h}{0.059} \tag{3.5}$$

can either be defined in the input, or a redox couple can be defined for PHREEQC to calculate the pe. In this work the O_2/H_2O redox couple will be used to calculate all E_h (pe) values. The justification for doing so is discussed in detail in Chapter 5. This data set's default units are ppm (units identifier). The PHREEQC.DAT database was used for the calculations. The saturation indices (SI) of potential mineral phases that may control the chemical composition of the solution were calculated using speciation modeling. SI can be defined as:

$$SI = log(\Omega) \tag{3.6}$$

where Ω is the saturation state. The saturation state is defined as ratio between Ion Activity Product (IAP, the numerator in equation 3.4) and the equilibrium constant K. This ratio shows the proximity to equilibrium for a given dissolving phase. Changes in saturation state can help identify which geochemical reactions are important in controlling water chemistry and distinguish different stages of hydrochemical evolution. The results obtained from the PHREEQC speciation models are presented in Chapter 5.

3.6.2 Inverse modelling and forward-inverse modelling

Predicting water composition and modelling weathering reactions necessitates the use of either a forward or inverse modelling approach (Plummer, 1992). Inverse modelling attempts to account for chemical changes that occur as water moves along a flow path (Plummer et al., 1994). This method is used to quantify the geochemical reactions that occur along a groundwater system flowline. Major elements and isotopes are used to delineate flowlines in the aquifer and infer physical and chemical processes controlling water chemistry (Eberts and George, 2000; Plummer et al., 1991b; Güler and Thyne, 2004; André et al., 2005). Simple mass and charge balance constraints can be used to determine which reactions are mathematically consistent with the data (Zhu, Anderson, et al., 2002), but they do not directly test whether any particular reaction is thermodynamically favourable. To address this issue, the inverse modelling code NETPATH (Plummer et al., 1991b; Plummer et al., 1994) and later an inverse model function (Parkhurst and Appelo, 2013) in PHREEQC, based on NETPATH, were developed. The modelling software was created to solve an inverse reactive mass balance with user-defined uncertainties (analytical uncertainties associated with each component). PHREEQC can generate families of inverse models with associated maxima and minima that each reaction can potentially contribute to. Inverse models necessitate the definition of a set of solutions (equivalent to a speciation model), which in the case of a reaction path model means an initial and final solution, and endmembers in the case of a mixing model. In order to solve the mass balance, PHREEQC also requires user-defined mineral phases that can be dissolved or allowed to precipitate. Ion exchange can also be incorporated. It should be noted that most of these types of model inputs are based on pre-existing conceptual geochemical models, which were often formed by first running speciation models. As a result, model results are frequently accepted or rejected based on a conceptual understanding of the system. Previous research using the mass and charge balance inverse modelling approach includes Garrels and MacKenzie (1967), Chapelle and Lovley (1990), Murphy and Schramke (1998), Sharif et al. (2008), and Dhiman and Keshari (2006).

An alternative strategy to inverse modelling is a forward-inverse approach. This approach entails performing a large number of forward models to identify the reactions that may explain the chemical change as water travels from point A to point B in a flowline. For parameter estimation, least-squares error minimization or similar approaches can be used, a strategy used by generic inverse models such as CXTFIT (Toride and Leij, 1995; Tang

et al., 2010) and PEST (Tonkin and Doherty, 2009). Conceptually, this approach is nothing more than a Monte Carlo model. With the integration of PHREEQC in the R environment, several studies have used a Monte Carlo approach to inverse modelling to gain insight about the potential processes governing water chemistry in aquifers. Conducting Monte Carlo simulations to systematically sample the parameter space can yield additional information from the data. However, a brute-force Monte Carlo approach may be inefficient in identifying an optimal parameter set that accurately reproduces the measured data. McNab Jr. (2014) proposed a strategy based on the Metropolis-Hastings algorithm (Metropolis et al., 1953), and the author tested this approach on two case studies (Garrels and MacKenzie, 1967; Chapelle and Lovley, 1990; Murphy and Schramke, 1998), included in the PHREEQC manual, obtaining similar results.

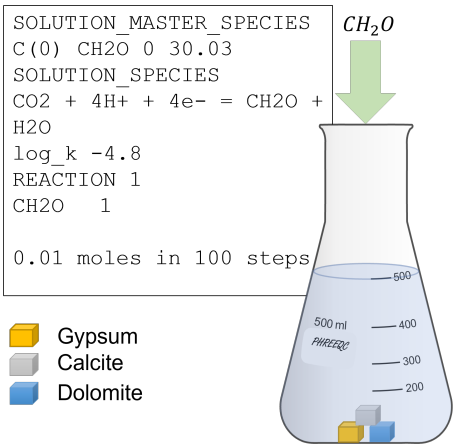

Figure 3.6: PHREEQC batch reaction. A code example is shown with a conceptual drawing of what the model represents. Acetate is added to a solution that is in contact with mineral phases that can dissolve. Acetate is allowed to be oxidized, prompting the dissolution of calcite and dolomite. Gypsum dissolution influence the solubility of calcite due to the common ion effect.

An hypothesis regarding the geochemical functioning of the system was put to the test in this investigation by employing the forward-inverse approach. A more in-depth discussion of the selection of secondary mineral phases to be used as inputs for the model is presented in Chapter 5. This section will provide a high-level summary of the process that was used to construct the model.

The `phreeqc` library in RStudio (Racine, 2012), was used to create the model. The platform-independent interface between R and PHREEQC provides high-level functions to setup and run geochemical simulations, collect and manipulate results, and perform simple tasks without programming. Complex tasks can be efficiently coded using the provided fundamental building blocks. High-level functions create and manipulate standard PHREEQC input scripts, which are tightly coupled with PHREEQC and evaluated. Thus,

the coupling requires good knowledge of R and PHREEQC syntax (De Lucia and Kühn, 2013).

The strategy requires the execution of a large number of forward models (10,000 simulations). Figure 3.6 depicts the PHREEQC model's fundamental input. The PHREEQC model is conceptually a batch reactor in which the amounts of mineral phases and *DOC* (in the model, acetate was used) vary for each model run. Input parameters are sampled at random from an *a priori distribution*. All parameter distributions were assumed to be Gaussian, with means corresponding to the observed means from the total WEC hydrochemical data set for each parameter. This model has several flaws, the most obvious of which is how the model's uncertainty is assessed. With further development of this approach, this limitation can be overcome. Following the methodology proposed by McNab Jr. (2014) could be one possible path. Another promising option is to incorporate the method developed recently by Bonanno et al. (2022). Tracer data sets from experiments conducted in the WEC were used in the study to improve parameter identifiability and process interpretation in transient storage models. The model's second major flaw is its assumptions about parameter distributions. The normality assumption may be valid in flowlines where one chemical process controlling the parameter is dominant. This behaviour is visible on a continental scale (Davis and De Wiest, 1966). This is not true of shallow flowlines (which are discussed in detail in Chapter 5). The standard deviations were assumed, but they may or may not be realistic.

The modelling approach provides insight into the biogeochemical functioning of the system despite its limitations. The model was only used to determine whether *DOC* oxidation is the primary source of acidity in the system.

3.7 Random forest model

Random Forest (*RF*) is a well-known machine learning algorithm that is applied to both regression and classification problems (Genuer et al., 2017). It is based on the concept of ensemble learning, which involves combining different classifiers to solve a complex problem and improve the model's performance . *RF* is a supervised algorithm that is used to make predictions based on labeled data. It is defined by Breiman (2001) as a learning method for classification and regression that is based on the Classification and Regression Trees (CART) method.

In the study discussed in Chapter 6, a Random Forest (*RF*) model was used to classify water samples collected from the stream at *SW1* during 27 flood events over a period of two decades. The dataset used to train the model consisted of chemical parameter concentration-based labels, including major cations, anions, and SiO_2. The *RF* model was chosen for its relative simplicity in comparison to more complex models, making it easier to set up and interpret the results. The *RF* model was constructed using the `randomForest`

package (Liaw and Wiener, 2002) in RStudio. It is a bagging procedure (opposed to the boosting method; Bartlett et al., 1998) and involves building each tree independently using a bootstrap sample of the dataset. In this case, instead of bootstrapping, k-fold cross-validation was used in the construction process. Cross-validation is a technique similar to bootstrapping that involves selecting samples without replacement and ensuring that there are no repeated elements in each subset. In this study, the model was constructed using 5 folds and 3 repeats. The default of 500 trees was kept. The dataset developed in Chapter 4 was split into a 70/30 training/testing set. The *RF* model was trained on the 70% subset using k-fold cross-validation and the remaining 30% was used to test the model. The model achieved an accuracy of 92.72%. It was then used to classify an unseen dataset containing water chemistry data from 27 flood events.

Chapter 4

Identifying unseen flowlines

4.1 Introduction

To link $c-Q$ patterns in stream discharge to bio-geochemical functioning in the catchment, the main contributing flowlines must be identified. Multivariate statistical techniques can be used to leverage the vast data set spanning over ten years. Previous work in the WEC considered the stream's endmembers or sources to be reservoirs, with each reservoir having a district chemistry.

In this chapter, we expand on this idea by defining flow lines that pass through these reservoirs. The current understanding differs from the previous model in that dominant or prominent endmembers are chemically altered versions of endmembers that cannot be observed directly in stream chemistry. We propose using all available parameters to define the dominant flowlines and when these flowlines are dominant.

Major cations and anions are available throughout the dataset's time span. Only data from 2009 to 2016 is available for trace elements. There are 51 sample sites, 39 parameters with 1173 complete observations, and 2583 complete for major ions in the current complete database. The data was compiled from several studies conducted over the last decade (chapter 2 and 4), and the parameters recorded during these studies differ.

Understanding the system and developing a coherent conceptual model turn the analysis into a multivariate problem. To independently quantify endmembers or flow lines using chemical parameter correlations, you need to do a number of different multivariate statistical analyses.

4.1.1 Research questions

The main research questions that will be addressed in this chapter are concerned with determining the origin of near stream endmembers. Shallow and deep flowlines are well known to converge at the lowest point of a catchment. It is therefore reasonable to assume that near stream endmembers will be made up of flowline mixtures, with the most dominant flowlines contributing to the endmember's chemical composition. Thus, the question is whether endmembers of endmembers can be accurately identified in the WEC.

4.1.2 Hypotheses

The central hypothesis of this chapter is that the large variation in concentrations of geogenic solutes (SO_4^{2-}, Na^+, Ca^{2+}, and Mg^{2+}) observed during groundwater borehole sampling is due to mixing of shallow and deep flow lines. The underlying control can be attributed to a rapid decrease in vertical conductivity, and, as with $c-Q$ patterns in stream flow, the relative contribution of the respective flow lines will vary depending on the system's hydrologic state. If the system has a sufficiently large data set, it will be

possible to isolate the chemical signatures of dominant flow lines because their chemical compositions will be sufficiently different to allow separation.

4.2 Hierarchical cluster analysis

Figure 4.1 depicts the main results of the hierarchical cluster analysis (HCA) performed on 2583 groundwater, riparian, and surface water samples. The samples were classified based on a visual inspection of the dendrogram, and the decision to draw the phenon line across the dendrogram to form six clusters was based on perceptual model understanding (Rodriguez and Klaus, 2019) and is thus subjective. The chosen "pruning distance" implies that all samples below the line belong to the same clusters; the phenon line effectively determines the number of clusters identified by the HCA process. To identify subgroups within the six main clusters, a secondary line was drawn at linkage distance 13.

Based on the perceptual model, the six clusters are attributed to the following flowlines in the system:

4.2.1 Cluster 1 - Deep groundwater

This cluster accounts for 12% ($n = 322$) of all observations and is classified as Ca^{2+}-Mg^{2+}-HCO_3^- -type water. It has the highest concentrations (mg/l) of Ca^{2+} (18.24±5.51), Mg^{2+} (11.19±4.41), alkalinity (91.86±27.29), and SiO_2 (13.24±3.70) . This cluster should be assigned to a flow line associated with primary mineral weathering in the system. The occurrence of this cluster is most common in $GW2$, $GW5$, $GW10$, $GW11$, and $GW12$ (figure 2.1). This corresponds to the system's perceptual model understanding, as these boreholes will intercept the deepest flow lines and thus represent water with the longest residence time. Cluster 1 ($C1$) subgroups have stiff diagrams with an increasing trend in both Ca^{2+} and Mg^{2+} as you move from $C1.1$ to $C1.3$. The change in Ca^{2+}/Mg^{2+} ratios ($C1.3$) is, however, significant.

4.2.2 Cluster 2 - Secondary plateau fracture flow

Cluster 2 ($n = 374$) is associated with the secondary plateau ($GW3$ and $GW6$, figure 2.1) and is a Ca^{2+}-HCO_3^- -type water. Based on the work done by Gourdol et al. (2021), this plateau has a shallow weathering front and is highly fractured in comparison to the primary plateau (figure 2.3). This cluster exhibits similar behaviour to cluster 1 in terms of Ca^{2+} (8.88 ±5.14), Mg^{2+} (4.55 ±1.94), alkalinity (20.72 ±17.45), and SiO_2 (9.15 ±1.2), but at lower concentrations (mg/l) and with significantly greater variance. This is to be expected given that the secondary plateau's highly fractured nature reduces water residence time. Cluster 2 ($C2$) also has higher concentrations of Cl^-, NO_3^-, and SO_4^{2-}. The significance of these parameters will be discussed in the section that follows. The

stiff plot shape differs significantly between $C2$ subgroups. This is due to an increase in alkalinity and Ca^{2+}, as opposed to a decrease in SO_4^{2-} and Mg^{2+} concentrations.

4.2.3 Cluster 3 - Flowline B

This cluster ($C3, n = 448$), is associated with the near-stream lateral subsurface saturated flow through the basal layer (BL) of the Pleistocene periglacial slope deposits ($PPSD$), activated after a bedrock storage threshold is exceeded (Rodriguez and Klaus, 2019). This cluster can be observed in $GW7 - GW12$,$RP1, 3, 4$ and $RP5$. $C3$ (figure 2.1) and is a Mg^{2+}-HCO_3^- -type water. This however changes when observing the subgroups within the cluster. SO_4^{2-} concentration (mg/l) increase significantly moving from $C3.1$ to $C3.2$. A 50% decrease in alkalinity is also observed.

4.2.4 Cluster 4 - Primary plateau intermediate groundwater

The shape of the stiff diagram (Ca^{2+}-HCO_3^- -type water) suggests that this cluster is chemically related to the deep groundwater cluster ($C1$). However, this cluster has lower concentrations (mg/l) of alkalinity (47.72 $\pm$28.15), Ca^{2+} (13.17 $\pm$8.48), Mg^{2+} (5.22 $\pm$2.02), and SiO_2 (7.7 $\pm$2.48). In this cluster, no subgroups were found to be significantly different. This cluster can be found in $GW2$, $GW5$, $GW7$, $GW10$, and $GW12$.

4.2.5 Cluster 5 - Primary plateau shallow groundwater

Cluster 5 is associated with the shallow groundwater of the main plateau and dominates the $GW1$ samples. This cluster is very interesting in terms of biogeochemical evolution because it represents vertical recharge on the primary plateau. This cluster is distinguished by a low alkalinity concentration (mg/l) and high concentrations of NO_3^- (3.72 $\pm$2.42) and SO_4^{2-} (13.06 $\pm$3.08). The water can be classified as Ca^{2+}-SO_4^{2-} dominant. This cluster, like $C4$, has no significantly different subgroups and can be found in $GW1$, $RP3$, and $RP5$.

4.2.6 Cluster 6 - Primary slope shallow groundwater

Cluster 6 is the largest, accounting for 43% ($n = 1123$) of the data. This cluster represents stream water and riparian water, and it is also prevalent in $GW7$, $GW8$, and $GW9$. It is reasonable to assume that this cluster represents a flow line similar to $C3$, with the added chemical influence of the catchment's soil layers. Because the soil layers are very acidic, this will also explain the decrease in alkalinity in this cluster compared to $C3$. The Mg^{2+}-$SO4^{2-}$ signature dominates the cluster. This cluster, on the other hand, had the most significantly different subgroups, with three of them Mg^{2+}-HCO_3^- dominant and one ($C6.3$) showing a Mg^{2+}-SO_4^{2-} dominant signature.

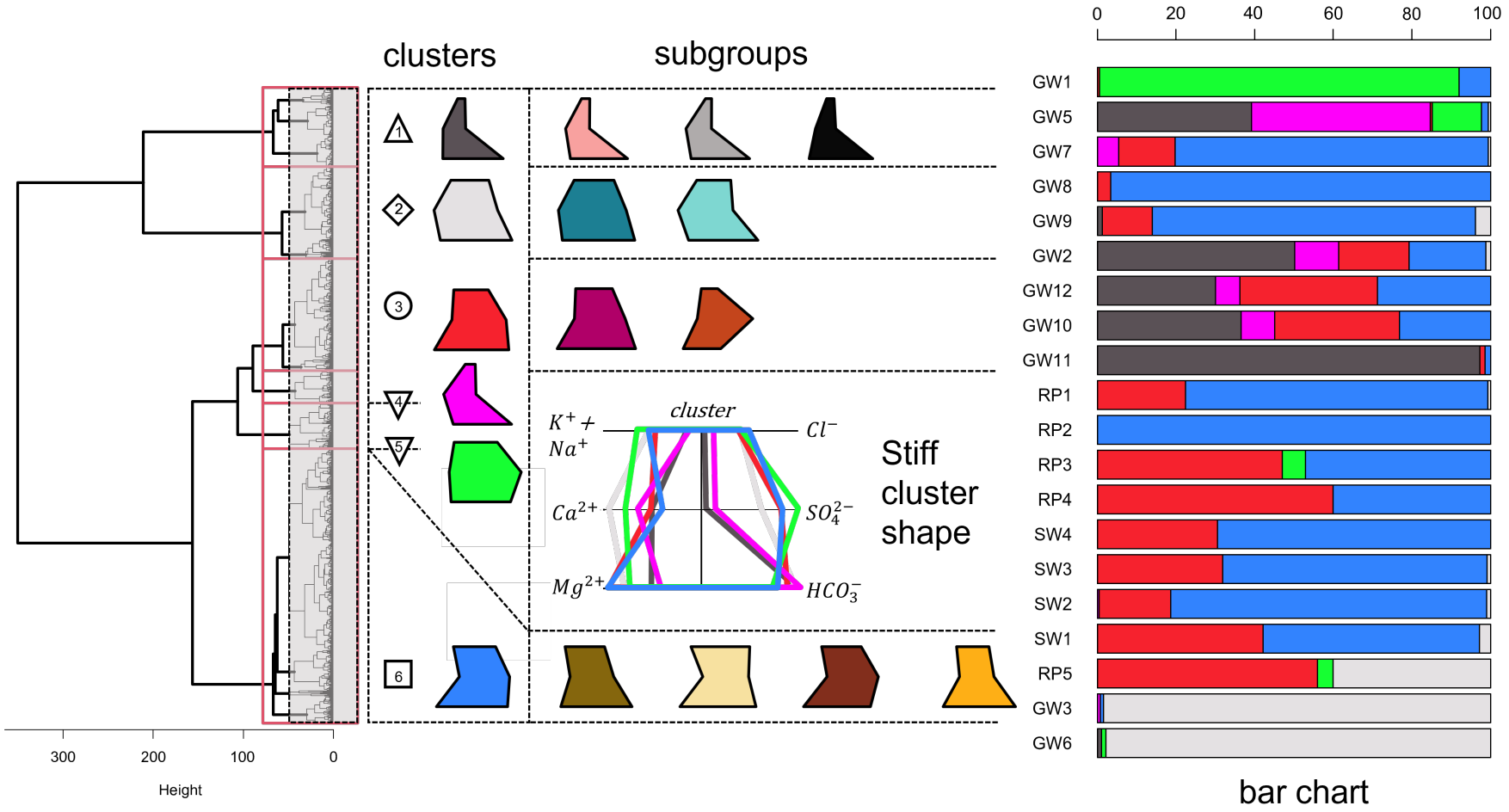

Figure 4.1: Groundwater, riparian water, and stream water (figure 2.1) are all shown on this dendogram. The dendogram illustrates how the observation can be broken down into six primary groupings. On the right-hand side of the graphic is a bar chart that illustrates the relative frequency of the occurrence of each of the corresponding primary clusters. In order to clearly differentiate the subgroups from the main clusters, both the main clusters and the subgroups are portrayed as stiff shapes (Stiff, 1951). There are six main clusters and thirteen subgroups.

4.3 Principle component analysis

The *HCA*-labeled data was used to perform a principal component analysis (*PCA*). This was done for two reasons. The first reason was to see if a *HCA* could identify potential endmembers in the system following the methodology in the framework of EMMA, and the second was to gain insight into potential processes causing the data variance. Some aspects of EMMA discussed in Chapter 1 are briefly mentioned. Hydrochemical data such as stable isotopes and major-and-trace ion chemistry are typically used to calculate mixing ratios. Christophersen and Hooper (1992) proposed a two-step procedure for systematising preliminary mixing analyses, which evolved into the EMMA methodology. The goal of EMMA is to determine the smallest number of endmembers mixing in the system in order to explain chemical variability assuming conservative mixing.

The first step is to identify the endmembers that are mixed in the water samples. This is a conceptual step that involves determining the smallest number of endmembers that explain the observed variability in a dataset and aids in determining the composition of these potential endmembers (Christophersen and Hooper, 1992; Christophersen et al., 1993). By performing dimensional reduction on the data, this is possible. *PCA*'s are also used in many studies to investigate chemical-and mixing processes in aquifers (Güler et al., 2002; Cloutier et al., 2008; King et al., 2014; Thyne et al., 2004; Melloul and Collin, 1992; Li and Zeng, 2017). It is difficult to visualise and interpret a large number of chemical analyses from various species. Instead of studying a dataset potentially as large as the number of species, it would suffice to analyse their projections on a space with much smaller dimensions. For large data sets, the use of graphical techniques proved to have limitations when compared to multivariate methods (Güler et al., 2002). *PCA* can be used to reduce data and assess the continuity, overlap and similarity of data clusters. This technique, strictly speaking, is not a multivariate statistical technique but rather a mathematical manipulation that may provide some insight into the structure of the data matrix by reducing the dimensions of the data matrix (Davis and Sampson, 1986).

The second step in *EMMA* is to calculate the mixing ratios for the identified endmembers in the mixtures based on conservative species concentrations. When endmember concentrations are unknown, it is a mechanical step that can be done by constrained linear least squares (Christophersen et al., 1990), separately for each sample; by non-linear optimization, taking into account all mixtures (Carrera et al., 2004); or geometrically based on the information of two or n-principal component mixing (Laaksoharju et al., 2008). This step will not be done in this section, as it falls outside the scope of this section, an the interest in performing a *PCA* was rather to assess if if the flowlines identified in the *HCA* made sense.

A *PCA* biplot of the loadings of the six main clusters for the first two principle components (*PC*'s) is shown in figure 4.2-a. A *PCA* biplot of the loadings of the 13 subgroups is

shown in figures 4.2–b. The methodology for the *PCA* is discussed in detail in Chapter 3, but specific points relevant to the results will be mentioned. Loading plots are shown in figures 4.2-c and 4.2-d. ($PC2$ *vs.* $PC1$ and $PC3$ *vs.* $PC2$, respectively). Following an examination of a scree plot for the analysis and the "elbow" rule, it was decided that only the first three PCs would be investigated. The first three PCs account for 80% of the variance in the data. Clusters 3 and 6 contain the majority of the *WEC*'s stream and riparian water (figure 4.1-bar chart). According to the loading vectors (figures 4.2–c), the deep groundwater cluster (cluster 1) moves away from these two clusters. This is due to an increase in SiO_2, alkalinity, Ca^{2+}, and Mg^{2+} (silicate mineral weathering and carbonate mineral dissolution). The water from the secondary plateau (cluster 2) has a similar enrichment in these solutes but a higher Cl^- and NO_3^- input. In terms of NO_3^- and SO_4^{2-} variance, the shallow groundwater on the primary plateau (cluster 5) and deep groundwater ($C2.1$, $GW3$) from the secondary plateau exhibit similar behaviour.

Looking at the subgroups further, the surface water has two dominant subgroups: $C3.1$ in summer and $C6.3$ in winter (this behaviour will be discussed in detail in the last chapter). Following the principles of interpreting the PCA from *EMMA*, subgroups $C4$, $C6.2$, and $C6.4$ could be argued to be potential near-steam endmembers that can explain the chemical composition of the stream water. Figures 4.2-d depict the importance of $PC3$ in comparison to $PC2$. $PC3$ is most closely related to riparian water and accounts for 8.5% of the variation in the data. This behaviour will be covered in greater detail later in this chapter. The results of the *PCA* make it clear that the *HCA* might be able to correctly identify some of the probable near stream endmembers. In addition, the interpretation of the loading vectors seems to correspond to our preliminary conceptual geochemical understanding of the system (chapter 2). In order to verify the accuracy of this interpretation, a traditional geochemical approach (Güler et al., 2002) will be utilised. This approach will be used to test our most updated conceptual understanding and to determine whether or not the clusters and subgroups described in section 4.2 make logical sense.

Before delving too deeply into the interpretation of chemical processes that may have resulted in the manifestation of the subgroups, the following section will show the relationship between water level and the occurrence of these subgroups. To reiterate, the subgroups observed are interpreted as dominant flowlines in the context of this work. Another logical check would be to see if these flowlines appear in a sequence that is consistent with the current perceptual hydrological model.

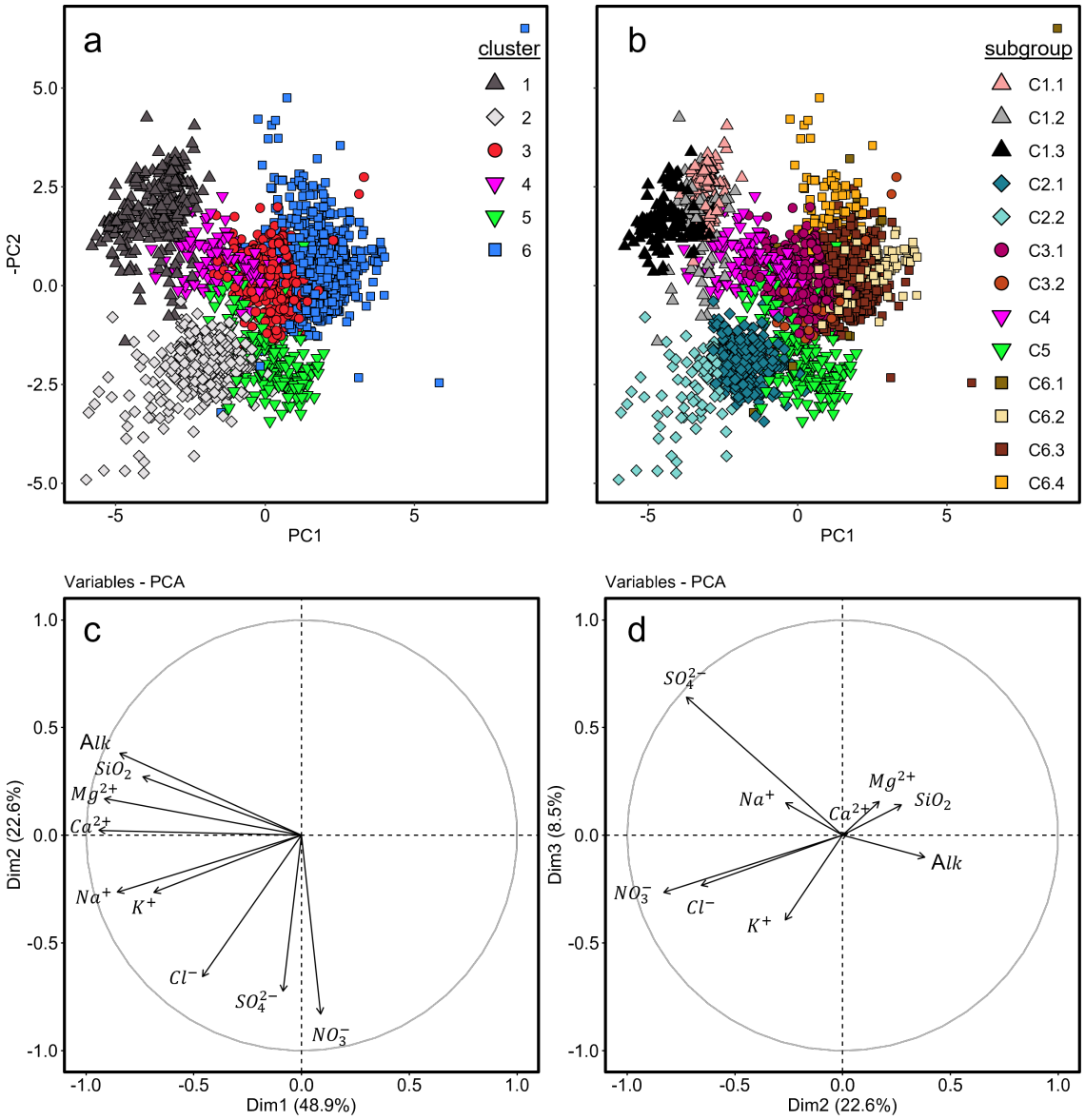

Figure 4.2: Projection of hydrochemical parameters (loadings) and observations (scores) on the principle components 1 and 2 space, including clusters corresponding to *HCA* results (figure 4.1). In biplot a, the colour code corresponds to the six major clusters. The colour codes in biplot b correspond to the 13 subgroups.

4.4 Flowline (subgroup) behaviour as a function of water level

The boreholes used in the study, as mentioned in the previous section, intercept multiple flow lines, and the relative contributions of the flow lines to the sample taken will be a function of the system's hydrological state. To see if this was the case, scaled Ca^{2+}/Mg^{2+} ratios (mean set to zero and unit variance) versus water level were plotted for the sampled

boreholes. This ratio was chosen because water chemistry is frequently evaluated using a biplot of Mg^{2+} *vs.* Ca^{2+} (Na^{+} normalised) and compared to theoretical ranges for carbonate, silicate, and evaporite lithologies (Schlesinger et al., 1982; Gaillardet et al., 1999; Stewart et al., 2022). In the case of the *WEC*, we anticipate that Mg^{2+} and Ca^{2+} concentrations will be influenced by a variety of sources. Thus, clusters with a high variance in this ratio indicate the involvement of multiple processes. As the scaled ratio variance decreases, it is reasonable to assume that a dominant process is influencing the ratio and, by extension, the concentrations of Mg^{2+} and Ca^{2+}.

The depth profile of the scaled ratios for plot 7 is depicted in figure 4.3-a (primary plateau, $GW1$, and $GW5$). There is a change in the ratio in $GW1$ for a water level depth of 2.1 metres, which coincides with a change in the dominant subgroup in $GW5$. Given that $GW1$ has a depth of only 2.52 metres (table 3.1), it is reasonable to assume that $GW1$ will not intercept subgroup $C1.2$. It is worth noting that subgroup $C6.1$ occurs at water levels lower than 2.1 metres in $GW1$. This subgroup is closely related to the soil solution and can be attributed to preferential flow from a shallower horizon through the borehole's gravel pack or possibly other preferential flow paths. In extremely wet conditions, $GW5$ behaves similarly to $GW1$, but as the system dries out, subgroup $C4$ takes over, followed by $C1.2$.

The behaviour of $GW7$, $GW8$, and $GW9$ is depicted in figure 4.3-b. $GW7$ shows distinct regions where subgroups are predominate. Subgroup $C6.3$ is dominant in extremely wet conditions, followed by $C6.2$, and finally $C3.1$. In dry conditions, subgroup $C4$ is also visible in $GW7$. In $GW8$, only subgroup $C6.2$ is found. In wet conditions, $GW9$ shows a clear dominance of subgroup $C6.3$, with a slightly less visible trend towards $C3.1$ when the system dries out. The presence of subgroups $C2.1$ and $C2.2$ is due to HCA misidentification. Figure 4.3-c depicts the boreholes located near the stream. $GW2$ and $GW10$ are not depicted here, but will be discussed further separately. $GW11$ is in the stream and would theoretically intercept the deepest flow line currently visible in the system. It is not surprising, then, that subgroup $C1.3$ dominates the samples collected from $GW11$. Borehole $GW12$ is close to $SW3$ and shows a trend toward subgroup $C1.3$ dominance as the water level in the borehole decreases. Figures 4.3–d show the depth profiles of the scaled ratios for $GW3$ and $GW6$, respectively. $GW6$ is located on the secondary plateau and dries out in the summer. $GW3$ is located near the stream ($SW1$). As mentioned in the description of the study site (figure 2.3), the weathering front on the secondary plateau is very shallow. It is interesting to note that the scaled Ca^{2+}/Mg^{2+} ratio for $GW3$ becomes stable when the water level in this borehole drops below 2 meters.

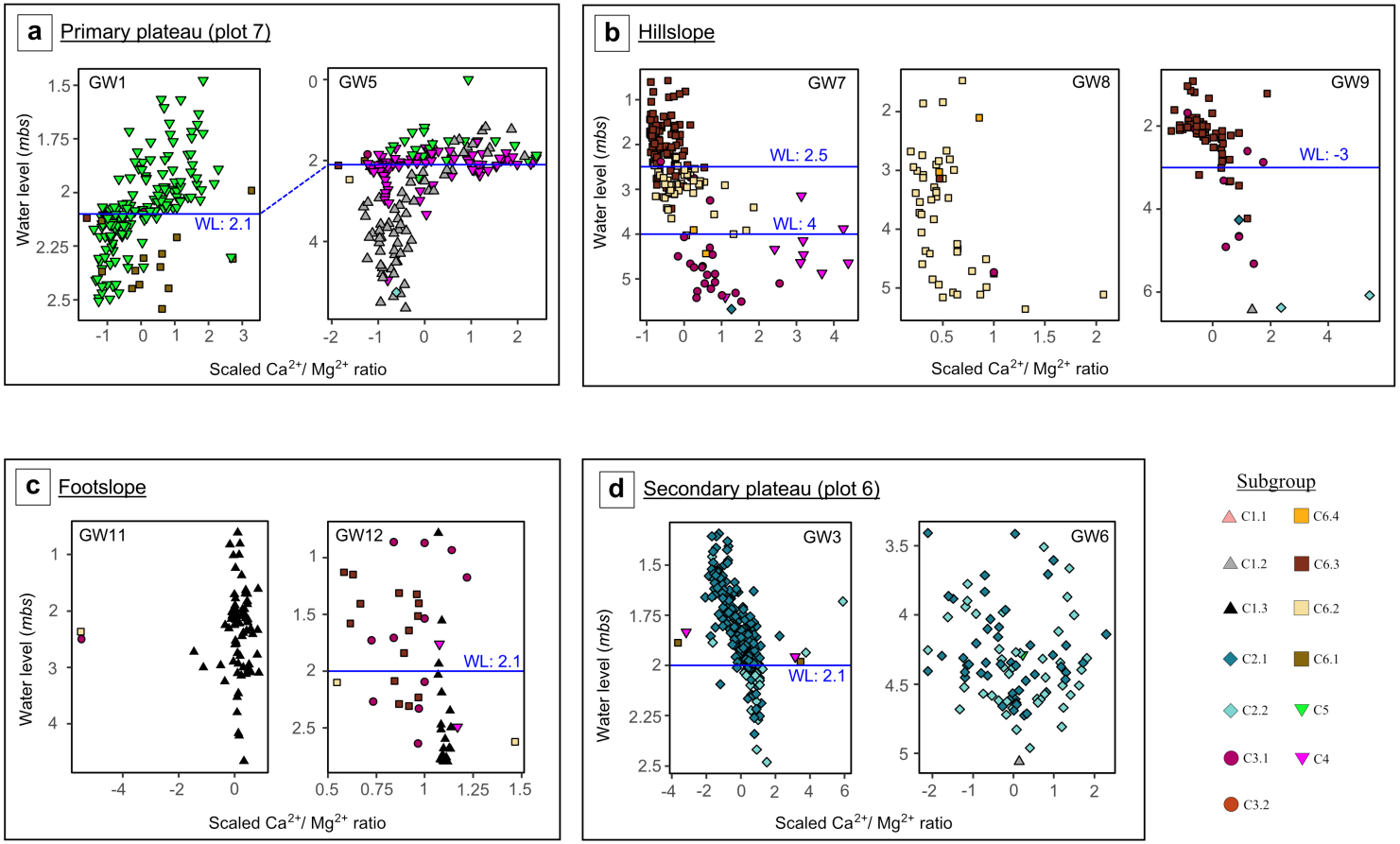

Figure 4.3: Water level *vs.* scaled Ca^{2+}/Mg^{2+} ratio for boreholes $GW1$–$GW9$, $GW11$, and $GW12$. The ratio-depth profiles are presented in separate plots that correspond to the landscape units in which these boreholes are situated (figure 2.1). The subgroups described in Section 4.2, are reflected visually by the colours and styles of the dots (figure 4.1). The water levels that are indicated by the blue horizontal lines in a borehole plots are those that correspond to a transition in a dominant subgroup. This transitional zone was classified solely based on the results of a visual examination.

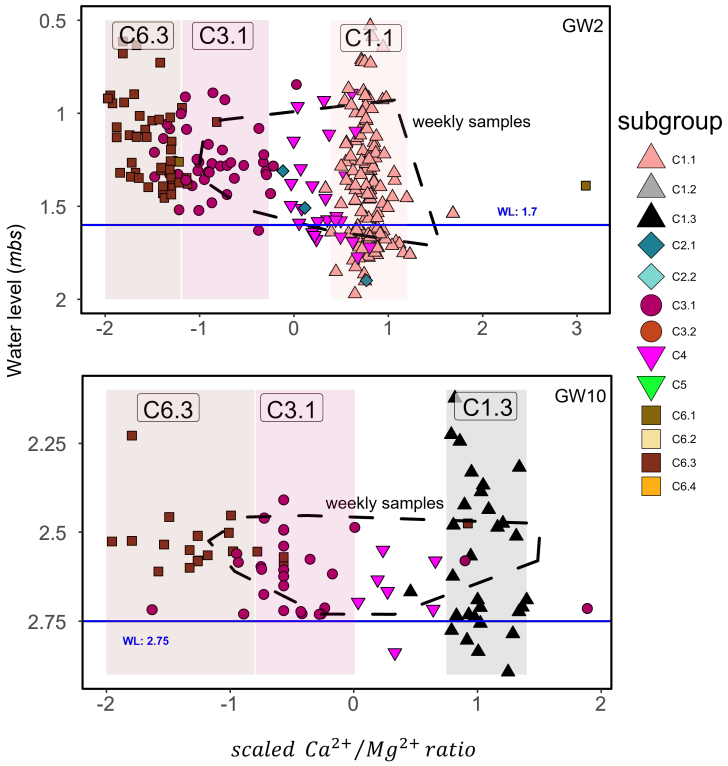

Figure 4.4: Water level *vs.* scaled Ca^{2+}/Mg^{2+} ratio for boreholes $GW2$ and $GW10$. These two boreholes are close to $SW2$ and $SW3$ (footslope, figure 2.1). The subgroups identified in these boreholes are denoted by the corresponding colour and marker shape. The horizontal blue lines indicate the depth (metres below surface) at which the subgroups associated with the deep flowlines become dominant. Above these depths, no clear correlation between the dominant subgroup and water level was observed. The polygons represent the samples collected during the most recent weekly campaign.

Figure 4.4 show the scaled ratio - depth trends for $GW2$ and $GW10$. Both boreholes are located close to $SW2$ and $SW3$, and represent locations where flow lines will converge (lowest point in the catchment). $GW2$ is relatively shallow (table 3.1) and it is therefore reasonable to assume it will not intercept subgroup $C1.3$. There is no clear correlation between water level and the subgroups. It was initially attributed to the difference in sampling protocol between the weekly – and bi-weekly campaigns. The bi-weekly protocol purges the borehole for a very short amount of time before the sample is taken, in contrast, during the weekly campaign the boreholes were purged until the EC stabilized before a sample was taken. It can be seen from the figures that there is no significant difference between the two sets of samples in $GW2$ and $GW10$. Considering the relative proximity of these wells to the stream and the fact that the deep flow lines will be relatively shallow at this location, it can be argued the dominance of one subgroup over another in a sample taken from $GW2$ and $GW10$ will be very sensitive to rainfall events. Rapid infiltration of rainwater through the soil may cause the dominance of cluster $C6.3$.

The results show that there are patterns emerging when looking at the occurrence of subgroups or flowlines as a function of water level in boreholes. The next step will be to determine whether these flowlines exhibit chemical behaviour that can be interpreted given our current knowledge of the system.

4.5 Chemical significance of clusters

To determine whether the clusters and subgroups identified (flowlines) in the *HCA*- and *PCA*-steps have any significance in terms of the biogeochemical functioning of the system, a closer examination of how subgroups interact in the system was required. Ratios between parameters can be used to gain a preliminary understanding of potential relationships. This approach is most likely the most basic step in interpreting hydro-chemical data. This principle is used in a number of well-known diagnostic plots in the field of geochemistry (Stiff, Schoeller, Durov, and Gibbs diagrams, to name a few). The Gibbs diagram is a popular diagnostic diagram (Gibbs, 1970). This diagram has been extensively used for the interpretation of groundwater (720 times as of mid 2017; Marandi and Shand, 2018). The diagnostic diagram was originally developed to interpret the key processes controlling surface water chemistry and may not be applicable to groundwater (Marandi and Shand, 2018). Gibbs diagrams show mechanisms that are controlling chemical composition of surface water on a global scale, therefore only showing mechanisms observable in surface water. One of the main criticisms of using Gibbs diagrams to interpret geochemical processes in groundwater systems is that the diagram does not incorporate the influence of SO_4^{2-}. As discussed in Chapter 1, the increase of SO_4^{2-} in groundwater chemical composition has a significant implication for the interpretation of the solubility of carbonate minerals. The importance of the latter is that the Gibbs diagram interpretation argues that solutions mainly have two extreme endmembers. A Na^+-Cl^--type water and a Ca^{2+}-HCO_3^--type water. The first is due to atmospheric deposition, and the latter is due to the dissolution or weathering of carbonate or silicate rocks. The third mechanism discussed by Gibbs (1970) is evaporative processes, which cause solutions to plot towards the seawater endmember in the diagram. For the purposes of the discussion. A combination of plots will be used and will be sequentially discussed.

Figure 4.5-a shows the diamond plot of a Piper diagram. This plot represents the projections from the cation- and anion-ternary plots. It is effectively a matrix transformation of (SO_4^{2-} + Cl^-+NO_3^-/ total anions) and (Na^+ + K^+/total cations). The plot shows 50% two-dimensional kernel density estimated (*2d KDE*) clusters of the 13 subgroups. Additionally, rainwater, soil solution, streamwater, and throughfall are also shown (95% *2d KDE* clusters for soil solution, streamwater, and rainwater). The conceptual reactive pathway from the surface to the subsurface is indicated by a path from **A** to **B** to **C**. The two respective "legs" of this path will be discussed with the aid of biplots.

Figure 4.5-c shows a biplot of alkalinity and SO_4^{2-} *vs.* Ca^{2+} and Mg^{2+}. This plot shows that the dissolution of carbonate- and sulphate minerals, both of which are secondary minerals, controls the concentration of these solutes. It would imply that the system will be extremely sensitive to surface input. The plot shows that as water moves from **A** to **C**, the variance decreases and eventually converges to a single dominant process in terms of the system's source of alkalinity. It is common practice to plot Mg^{2+} vs. Ca^{2+} (Na^{+}-normalized, figure 4.5-b). This is done in order to compare the data to the theoretical range of lithologies discussed in the previous section (carbonate, silicate, and evaporites). There is a compositional shift between throughfall and soil water. This shift is due to an increase in Mg^{2+}'s relative contribution. The shallow groundwater subgroups ($C6.2$ and $C6.3$) deviate significantly from the plot's overall slope. It can be seen that as Ca^{2+} concentration increases, Mg^{2+} concentration remains relatively constant. This behaviour is consistent in subgroup $C6.3$ but not in $C6.3$. Ion exchange is the dominant geochemical process that could explain this behaviour. This section will be followed by a more in-depth discussion.

Subgroups shift from an endmember (**A**) with a high relative contribution of Na^{+} to an endmember with a low relative contribution of Na^{+} (**C**) (figure 4.5-c). This is typical of carbonate dissolution as infiltrating water moves from the surface to deeper horizons in the subsurface (Chebotarev, 1955). It is worth noting, however, that the system's deepest groundwater ($GW11$, subgroup $C1.3$) and groundwater from the secondary plateau deviate from this linear trend. This would imply that silicate mineral weathering could cause chemical changes in the groundwater. The Gibbs-Anion plot (figure 4.5-e) confirms that the main source of alkalinity in the system can be attributed to carbonate dissolution. This can be deduced by a simple logical exercise: if Cl^{-} is assumed to be conservative and a bicarbonate mineral is allowed to dissolve as water travels deeper into the subsurface, at some point the solution will reach saturation with the carbonate mineral, thus a nonlinear increase in alkalinity can be expected. This is an oversimplification of the system, of course, and more attention to this process will be given in the next chapter. However, what is interesting is that the influence of vegetation can be directly observed here. The secondary plateau is covered by a mixture between Spruce and Douglas fir, and elevated Cl^{-} inputs observed under these canopy types account for the plot's deviation from the overall trend. The Gibbs-Anion plot also confirms that subgroups $C1.3$, $C2.1$, and $C2.2$ are chemically altered by silicate mineral weathering.

In summary, figure 4.5 depicts several potentially identifiable chemical processes occurring concurrently in the shallow horizons (moving from **A** to **B**). 1) Vegetation cycling; 2) atmospheric deposition; 3) ion exchange; 4) silicate weathering; and 5) secondary mineral dissolution and precipitation are the main processes. In these horizons, the high variation seen when moving from **A** (throughfall) to **B** (soil solution and shallow groundwater) is caused by the lack of dominance of one process over another. The variance observed decreases as water moves deeper into the subsurface due to the emergence of dominant

processes controlling water chemistry. This behaviour is visible when water moves from **B**, where alkalinity contributes around 50%–60%, to **C** (deep groundwater), where alkalinity is the dominant major anion (80%–90%). A Piper diagram of the subgroups reveals this pattern of behaviour quite clearly. This information is not presented in this chapter, but it is available in Appendix B. The chemical processes will be broken down in great detail in the subsequent sections of this article. Based on the diamond plot, the order of the discussion is going to more or less follow the path that water particles take as they travel from the surface (**A**) to the deep groundwater (**C**).

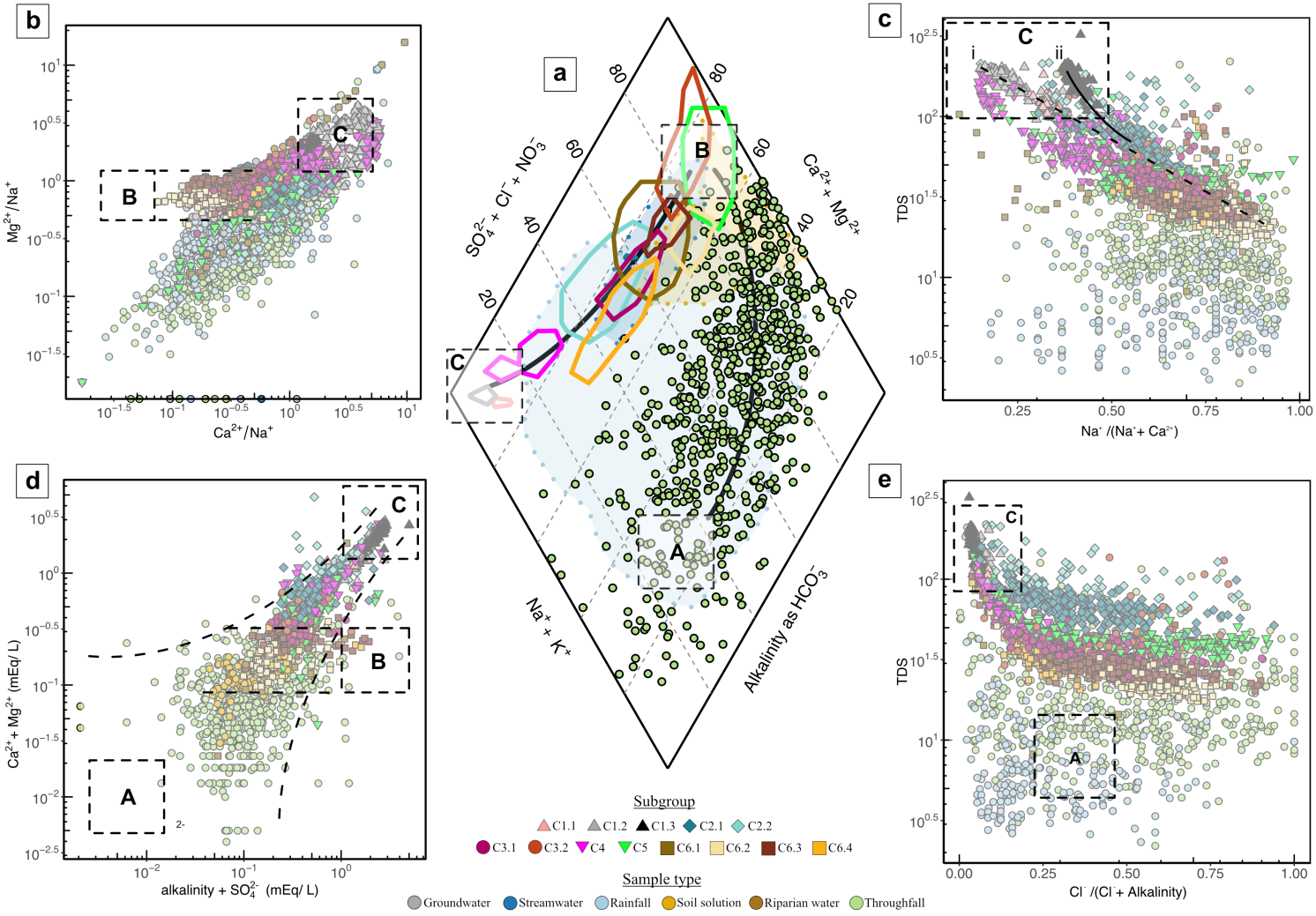

Figure 4.5: Subgroups are explained chemically. Piper diagram, diamond plot (a): The polygons are the 13 subgroups' 50% *2D KDE* clusters. Polygon colours match legend subgroup colours. Soil solution and rainfall are indicated by shaded areas with filled colours corresponding to each sample type's colour in the legend. **A**, **B**, and **C** boxes with a black line indicate a reaction path. b) Mg^{2+} *vs.* Ca^{2+}; and d) $Ca^{2+} + Mg^{2+}$ *vs.* alkalinity + SO_4^{2-} (mEq/L) show this path in increments. Gibbs plots are plots c and e. Lines *i* and *ii* in plot c show the reaction path of carbonate dissolution and silicate weathering respectively.

4.5.1 Soil solution and shallow flow lines

The reaction path from **A** to **B** will be discussed in this section. It can be seen from figure 4.5-b that the Mg^{2+} concentration increases relative to the Ca^{2+} concentration as thoughfall infiltrates into the subsurface. This increase can be due to secondary mineral dissolution or ion exchange. The exact source of Mg^{2+} is uncertain, but the relative decrease in Na^{+} can be adequately explained by the influence of ion exchange.

A total of 434 soil solution samples were collected from 2009 to 2021 from 8 sample sites at depths ranging from 10 cm to 60 cm (number of samples: 10 cm = 18, 20 cm = 193, 40 cm = 38, and 60 cm = 185). These samples were collected during the wet period of the WEC, as the soil dries out in the summer and no soil solution could be collected. A total of 732 throughfall samples were collected from 3 sample sites from 2010 to 2022. There is variation in parameters between sites across the whole depth profile. The variation in soil solution concentrations could be attributed to several factors, but the most important are soil type, vegetation cover, and soil saturation. Due to the relatively high infiltration rates observed in the catchment, it is also expected that throughfall and rainfall will have a large influence on the solutes observed in the soil.

The surface water mostly comprises cluster 6 (primary slope shallow groundwater) or cluster 3 (flowline B), with cluster 6 being dominant when the catchment is wet and vice versa. To understand the influence of throughfall on the flowlines and how it is chemically transformed as it moves through the soil layers, the 4 subgroups identified within cluster 6 must be investigated. These clusters represent the system when it is close to or fully saturated. By inspecting subgroup $C6.4$, it was observed that all the samples contained in this subgroup were from the riparian zone. It is well understood that the riparian zone chemically functions differently compared to the soils, so this subgroup was omitted from the comparison. The occurrence of the three subgroups observed in cluster 6 can be explained by ion exchange, the main chemical process occurring in the soil layers. The distinction between these three subgroups is primarily due to residence time. This was perhaps already somewhat evident from the piper diagram and the subgroup behaviour in wells $GW2$, $GW7$, and $GW9$. This behaviour will now be discussed in the context of the hydrological perception model.

In the previous work done in the *WEC*, the second peak in the stream flow response was attributed to lateral subsurface flow above the *PPSD*/weathered bedrock interface (Fenicia et al., 2014; Martínez-Carreras et al., 2016; Wrede et al., 2015). The authors argued that this flowline is fed by infiltration during rainfall and that a certain storage threshold must be exceeded before the flowline is connected to the stream. The significance of this behaviour would imply that before the critical threshold is exceeded, rainfall and throughfall will infiltrate vertically through the soil and will recharge the groundwater. The residence time of these solutes in the soil layers will be relatively small compared to when threshold is exceeded, and solutes flow laterally through the shallow layers to the

stream. Figure 4.6-a show a ternary plot of the relative concentrations of the major cations. This plot also forms part of the bottom left ternary section of the Piper diagram. It can be seen that the soil solution (10cm – 60 cm) forms a triangle in the plot. The bottom right of the triangle is dominated by solutes that has a relatively high concentration of Na^+ and K^+, as the solutes move vertically through the soil (figure 4.6-b), K^+ is intercepted by vegetation and Na^+ is exchanged for Ca^{2+} on cations exchange sites. Due to the dissolution/precipitation of secondary minerals and the weathering of primary minerals the $Ca^{2+}/\ Mg^{2+}$ ratio may vary. The influence of throughfall and rainfall can also be observed on the soil solution (green area and blue contour lines). Subgroups $C6.3$ and $C6.2$ plot on the grey shaded triangle. These solutes are enriched in Mg^{2+} and depleted in Na^+ and K^+. The offset between $C6.2$ and $C6.3$ on the Mg^{2+}-K^+ + Na^+ axis would imply that $C6.3$ has a larger residence time or exposure time in the soil compared to $C6.2$ (greater extent of ion exchange). It should also be noted that subgroup $C6.1$ plot in the soil solution triangle and it would be reasonable to assume that this group represent throughfall that finds its way into the deeper horizons via preferential flow paths. This is further corroborated by the fact that this subgroup is only observed when the system is dry (figure 4.3, $GW1$).

A last point to mention and the starting point of the next section, is the variance on the Ca^{2+}- Mg^{2+} axis. It can be observed that both subgroups $C6.3$ and $C6.2$ has similar variance in terms of the ratio between Ca^{2+} and Mg^{2+}. If the assumption is then correct that solutes related to $C6.3$ spend more time in the soil compared to $C6.2$, two potential conclusions can be drawn. The first is that reactions controlling the $Ca^{2+}/\ Mg^{2+}$ - ratio occur instantaneous relative to the rate of ion exchange. This could be explained by the dissolution/precipitation of secondary minerals, with the main source of these secondary minerals being input from the atmosphere as dust deposition. The second potential process is weathering of primary minerals that will be thermodynamically limited (equation 1.1) in summer due to build-up of reaction products in the interstitial water in the soil pores, and the subsequent flushing of these reaction products in winter. Both processes are equally plausible and in a previous mineralogical study (Moragues-Quiroga et al., 2017), three distinct groups (major-and trace elements) with different origins could be observed in the regolith profile, with one group that could clearly be linked to atmosphere-derived origin.

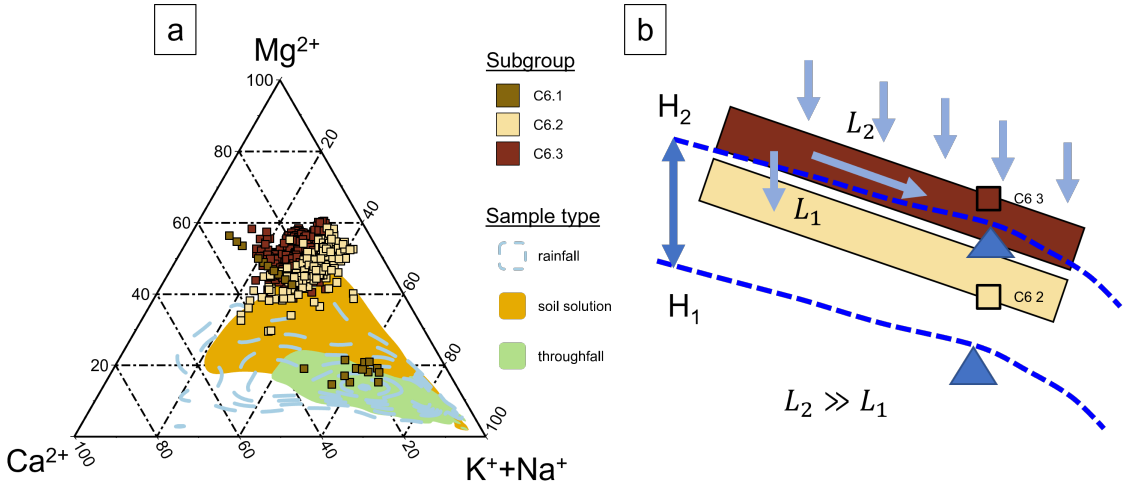

Figure 4.6: Ternary diagram (a) of the relative cation composition of subgroups $C6.1$, $C6.2$, and $C6.3$ compared to sample types: soil solution ($n = 434$), throughfall ($n = 732$), and rainwater ($n = 284$). For soil solution and throughfall, filled polygons are used, while rainfall is represented by a density-contoured area. A schematic (b) of the potential process causing the difference in relative cation composition, where L_{1-2} refers to flowline length and H_{1-2} to water level.

4.5.2 Silicate mineral weathering vs. carbonate mineral dissolution

As we move from point **A** to point **C** in figure 4.5, the primary source of alkalinity will be discussed. Given that the rate of dissolution of carbonate minerals is significantly higher than the rate of weathering of silicate minerals, and also taking into account the fact that the rates of mineral weathering become progressively slower as one moves deeper into the earth, There is sufficient evidence to support the hypothesis that the weathering of silicate minerals will function as a secondary source of alkalinity in the system.

As discussed in Chapter 1, silicate mineral weathering can consume acids. The problem is however that the rates at which these reactions occur is much slower than of carbonate mineral dissolution, making it difficult to quantify the contributions of alkalinity from these respective reactions. To distinguish between the contribution of Ca^{2+} and Mg^{2+} from carbonate dissolution and contributions from the liberation from silicate mineral weathering, strontium (Sr) and barium (Ba) can be used as tracers. Both are alkaline metals and strong lithophile elements (Kaleem et al., 2021), and like calcium and radium (Ra), only occur as divalent oxidation states in natural waters (Jaremalm et al., 2013). Ba and Sr has contrasting behaviour when it comes to weathering as Sr prefers to form admixture in the Ca^{2+}-bearing Plagioclase Feldspars (Hikov, 2004), whereas Ba may exist as Hyalophane, an intermediate member of Ortohoclase (Kaleem et al., 2021). The use of Ba^{2+}/Sr^{2+} and Ca^{2+}/Sr^{2+} ratios as tracers in mix models relies on the contrasting weathering susceptibility of the respective minerals these two elements occur in. Generally

K^+-minerals are more resistant to weathering compared to Ca^{2+}-minerals (Land et al., 2000).

Figure 4.7 show the median Ba^{2+} and Sr^{2+} concentration with depth. The concentration of Ba^{2+} increases from 2.26 ($\mu g/L$) in the throughfall to 47.4 ($\mu g/L$) at 40 cm depth, where it decreases again to 4.57 ($\mu g/L$) in $GW5$. From table 1.2, Witherite could be a potential source of Ba^{2+}, this however would imply that a similar trend will be observed in Sr^{2+} concentration with depth. This is not the case; thus, only other plausible source would be that Ba^{2+} is liberated in the weathering of Orthoclase ($KAlSi_3O_8$). This explanation is further strengthened by the fact that 40-60 cm is the main rooting depth, and would coincide with increased concentrations in organic acids. The influence of low molecular weight organic acids on the accelerated weathering of rocks-and clay minerals are well known (Wei et al., 2011; Kong et al., 2014), and most probably is responsible for this horizon of increased weathering. This also prove that primary mineral weathering still takes place in the soil (opposed to autogenic soils, where the soil is highly weathered) and can be considered as one of the chemical processes contributing to the larger variation in solute concentrations observed in the shallower horizons.

Regarding the contribution of geogenic solutes caused by silicate mineral weathering, little more can be said. Due to the uncertainty of the sources of many of the parameters that could be used as tracers (conservative tracers) to estimate the contribution of the weathering component to solute export from the catchment, performing a reactive mass balance will not provide much insight. The purpose of this study is to confirm that silicate mineral weathering can be considered a secondary process in catchment acidification buffering. The next step, which will be discussed in the subsequent section, is to determine which processes regulate the system's primary acidity source.

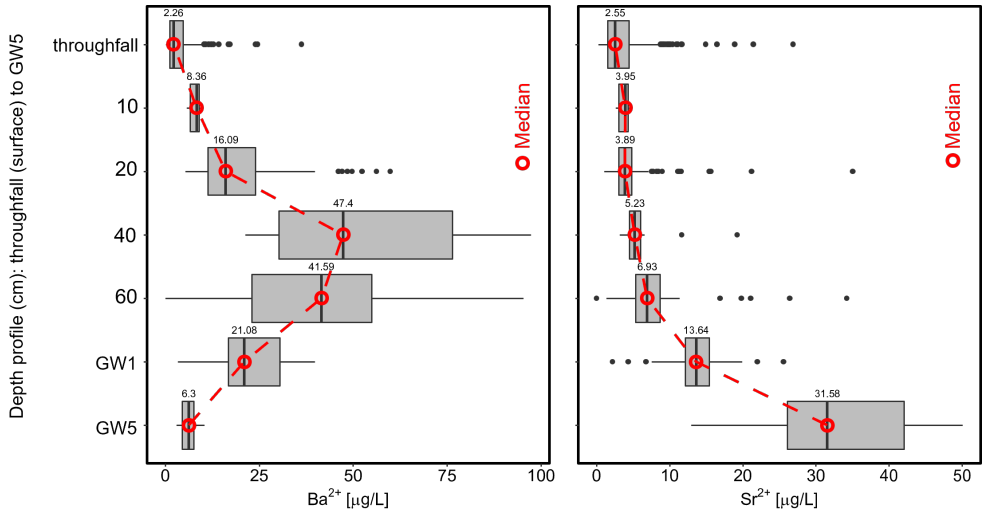

Figure 4.7: Box plots depict the depth profile of Ba^{2+} and Sr^{2+} concentration ($\mu g/L$) on the primary plateau (plot 7: $GW1$ and $GW5$).The black line (also indicated by red circles) in each box represents the data's median; the upper and lower limits of the boxes represent the interquartile range (IQR); the whiskers represent the first and third quantiles ± 1.5 times the IQR; and the points represent outliers beyond the whiskers' range. The throughfall and soil solution values are calculated using aggregated data (not divided by location).

4.5.3 Redox sensitive species and preferential flow paths

It is reasonable to assume that only two processes are capable of controlling the acidity of the *WEC*. The first is the oxidation of pyrite. This process may explain the Mg^{2+}-SO_4^{2-}-type water observed in shallow flowlines (cluster 6, figure 4.5). However, no pyrite was discovered during the mineralogical analysis of the *WEC* regolith (Moragues-Quiroga et al., 2017). The second process is a consequence of soil respiration and organic acids. Looking at redox-sensitive species allows for the observation of the latter.

Table 1.1 displays common redox reactions observed in soil solutions. In the majority of these reactions, dissolved organic carbon (*DOC*, represented as acetate) is oxidised, and as discussed in Chapter 1, redox reactions are the primary natural process that controls the concentrations of dissolved oxygen (*DO*), *DOC*, and NO_3^- in groundwater. The depth profiles of NO_3^- and *DOC* are depicted in figure 4.8–a, respectively. The *DOC* was computed using absorbent measurement data (*A254*). The effective measurement of *DOC* concentrations in samples with low concentrations has proven challenging. As a result, *A254* was used as a proxy. In chapter 3, a detailed discussion of how the *DOC* concentrations were calculated is presented.

Following the natural ecological succession of terminal electron-accepting processes (McMahon and Chapelle, 2008), *DOC* will be oxidized by first reducing $O_{2(aq)}$. Only in anoxic condition will NO_3^- be reduced. In both depth profiles a reduction with depth is observed. What is however visible is the impact of preferential flow paths. There is a distinct increase

in NO_3^- in $GW1$ (figure 4.8-a,I). This is however not so evident in the DOC depth profile due to the reduction rate of DOC compared to NO_3^-. Figure 4.8-b (III & IV), show time series trends of the 1 year weekly monitoring campaign. In both $GW1$ and $GW5$, NO_3^- and DOC appears to have an inverse response. This can be explained by the fact that DOC is rapidly transported from the surface with new water, causing a dilution of the resident NO_3^- concentration. The DOC is then oxidized, causing carbonate minerals to dissolve. This is evident from the increase in Ca^{2+} in response to a decrease in DOC. SO_4^{2-} shows an inverse trend compared to Ca^{2+}. This could imply that SO_4^{2-} that is transported from the top is precipitated as sulphate minerals.

The key observations of this section is that high DOC levels coincide with recharge events (meaning rainfall events). As the DO concentration is rapidly consumed by DOC oxidation, it is not always possible to use DO to identify these events. As there is always sufficient DO to act as an electron receptor, NO_3^- seems to be primarily stored in the deeper horizons. However, it is clear that NO_3^- levels in $GW1$ decrease in dry conditions. This does not appear to be the case with $GW5$. Ca^{2+} and alkalinity have an inverse relationship to DOC. This would imply that DOC oxidation is the driving force behind carbonate mineral dissolution. SO_4^{2-}, like NO_3^-, appears to be diluted by the arrival of surface water pulses. This would indicate that SO_4^{2-} is stored as sulphate minerals in the deeper horizons. Several possible sources of SO_4^{2-} exist: deposition from the surface and input from vegetation, sulphate mineral dissolution, and pyrite oxidation, as mentioned at the beginning of the section. Given that gypsum will affect the mobility of Ca^{2+}, the system's primary source of SO_4^{2-} must be identified. Ca^{2+} and SO_4^{2-} dynamics observed in the system will be discussed in the following section. As water moves from point **B** to point **C** (figure 4.5-a), the predominant cation shifts from Mg^{2+} to Ca^{2+}, and the predominant anion shifts from SO_4^{2-} to HCO_3^-.

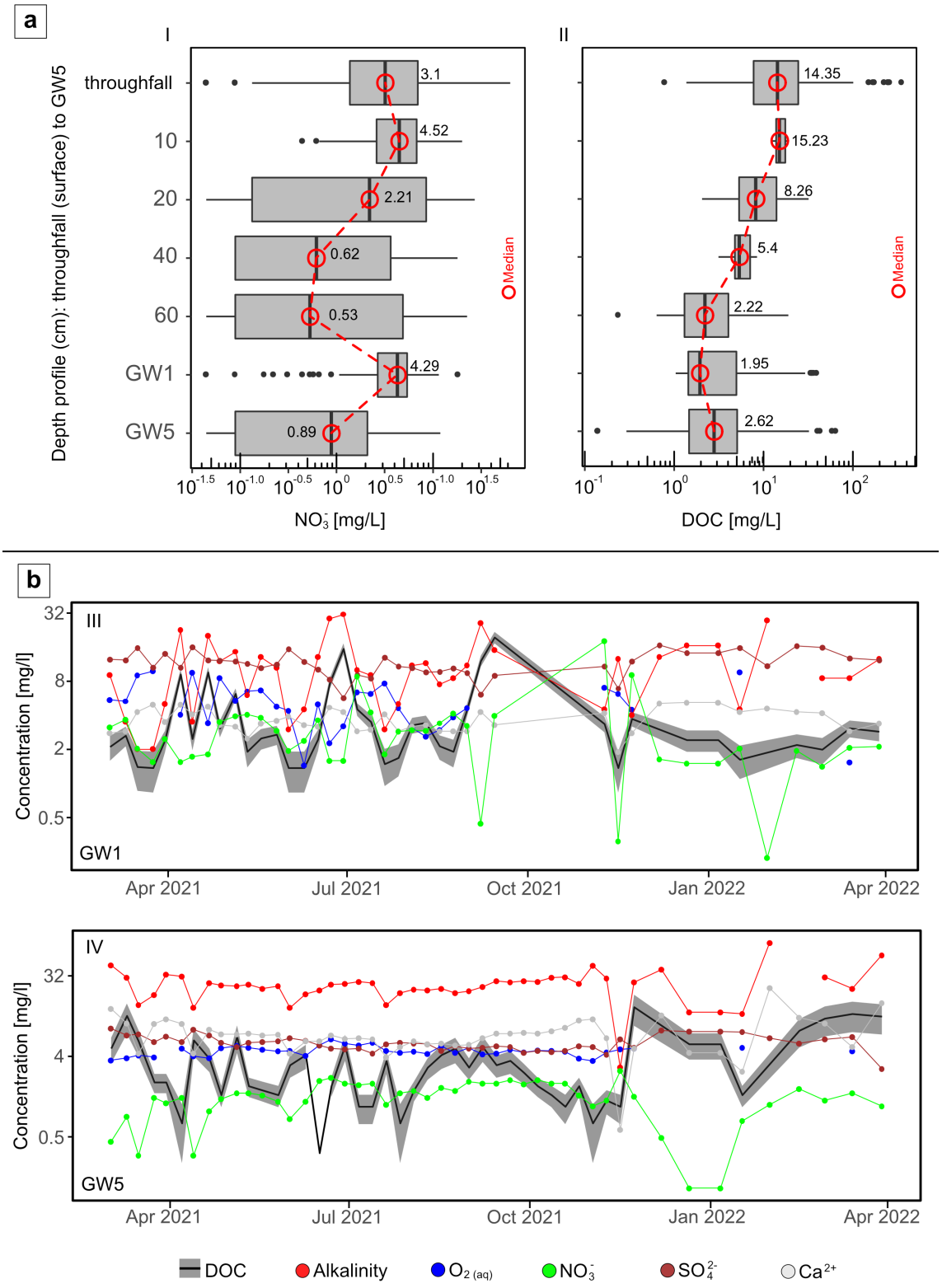

Figure 4.8: Box plots (a) depict the depth profile of NO_3^- and DOC concentration on the primary plateau (plot 7: $GW1$ and $GW5$). The black line (also indicated by red circles) in each box represents the data's median; the upper and lower limits of the boxes represent the interquartile range (IQR); the whiskers represent the first and third quantiles ± 1.5 times the IQR; and the points represent outliers beyond the whiskers' range. Time series plot (b) of concentration of DOC (calculated), alkalinity, DO, NO_3^-, SO_4^{2-} and Ca^{2+} for the one year weekly sampling campaign.

4.5.4 Calcium and Sulphate dynamics

Figure 4.9-a shows the depth profiles (box plots) of SO_4^{2-} and Ca^{2+} concentrations in the soil water and groundwater. The median concentrations for each depth are indicated on the plots. It can be observed that SO_4^{2-} increases with depth in the soil layers (surface to 40 cm), compared to Ca^{2+}, which seems to remain relatively static. A substantial decrease in SO_4^{2-} is observed when moving from $GW1$ to $GW5$. This coincides with a large increase in Ca^{2+} concentration. Figure B.2 in Appendix B shows the concentration profile of total sulphur ($S\%$, expressed as a percentage) for the primary plateau and the secondary plateau. From these figures, it can be observed that the litter has the highest concentration, followed by the soil. Some $S\%$ was observed in the slate, but significantly less compared to the litter. This could be interpreted to mean that the majority of the $S\%$ comes from the surface, where it is sequentially transformed to SO_4^{2-} and eventually stored as gypsum in the deep horizons.

Figure 4.9-b depicts the sequential sampling conducted at $GW5$. Figure 4.9-b-IV illustrates the correlation between major cations, anions, and EC. Only Ca^{2+} and Mg^{2+} were found to be correlated with EC. R^2 for Ca^{2+} *vs.* EC was 0.98, having a p-vale of 2×10^{-16}. R^2 for Mg^{2+} *vs.* EC was 0.8 a with a similar p-vale. However, the increase in Ca^{2+} concentration was significantly greater than that of Mg^{2+}. Ca^{2+} concentration was calculated as a function of EC using a linear regression model. Figure 4.9-b-III depicts the change in Ca^{2+} concentration over time, compared to the change in pH over the pumping duration. The pH trend exhibits a titration curve, and the point of equivalence coincides with the highest Ca^{2+} concentration in the time series. This figure demonstrates the significance of carbonate mineral buffering for pH control in the system and supports the findings of figure 4.8.

From the set of plots, it may be concluded that gypsum will exert a secondary control on the mobility of Ca^{2+}. Going forward, it can be assumed that acid-base reactions (titration) will be the primary control of Ca^{2+} mobility.

Now that the primary chemical processes observed along the reaction pathway from **A** to **B** to **C** have been discussed in order, the chemical functioning of the riparian zone can be discussed. This part of the landscape seems to act chemically very differently from the rest of the system and will be discussed in the section to follow.

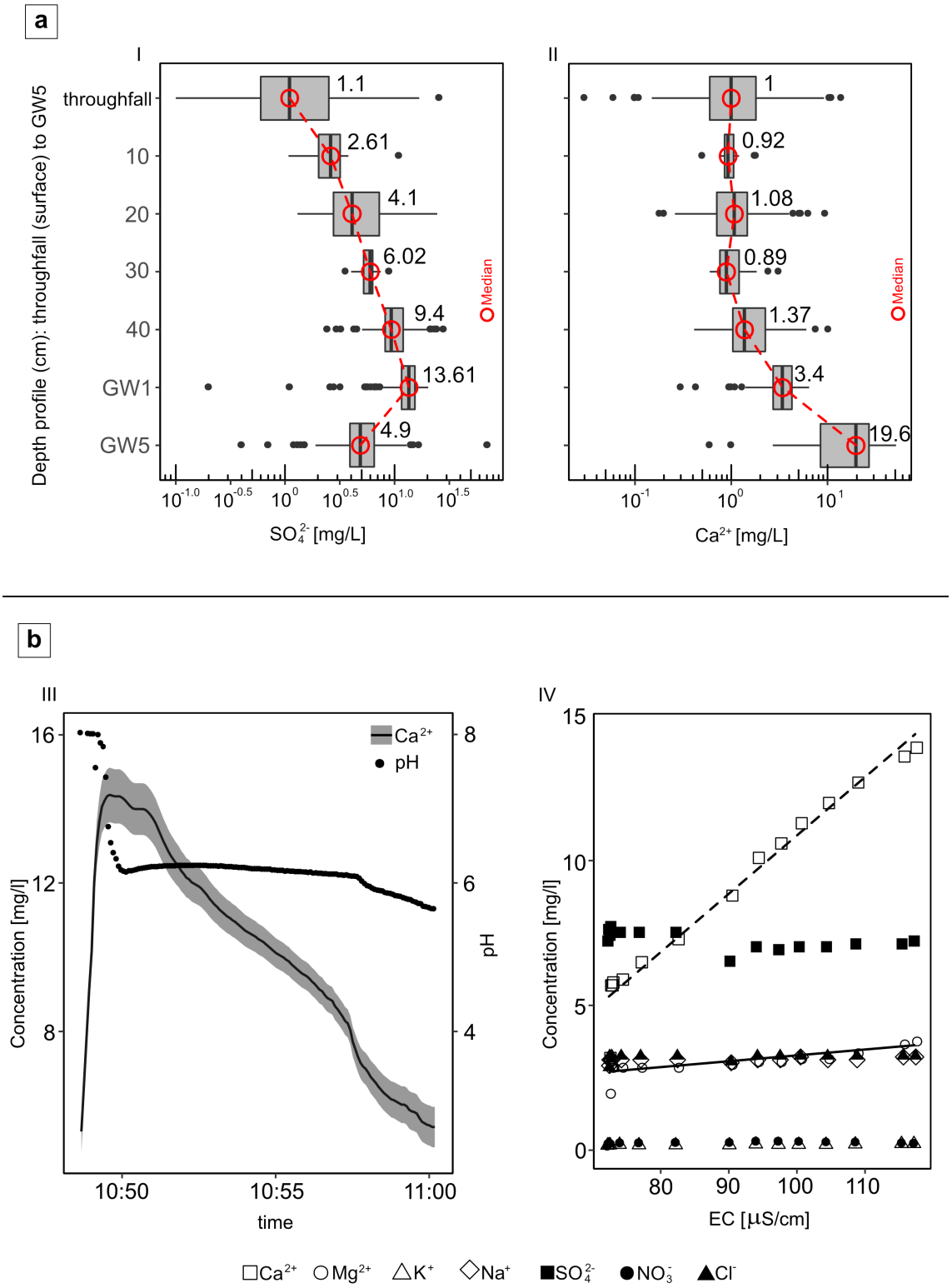

Figure 4.9: Box plots (a) depict the depth profile of SO_4^{2-} and Ca^{2+} concentration on the primary plateau (plot 7: $GW1$ and $GW5$). The black line (also indicated by red circles) in each box represents the data's median; the upper and lower limits of the boxes represent the interquartile range (IQR); the whiskers represent the first and third quantiles ± 1.5 times the IQR; and the points represent outliers beyond the whiskers' range. Time series plot of sequential sampling (b); III) of concentration of calculated Ca^{2+} and measured pH; IV) concentration major cations and anions (with the exception of alkalinity).

4.5.5 Riparian water

The riparian water has two distinct signals that can be attributed to seasonality. When the catchment is wet it will be reasonable to assume that the solutes observed in the riparian soils will be close to what is observed in flow line C and D (subgroup $C6.3$ and $C3.1$). When the catchment is dry, the riparian zone stays saturated to a large degree and then it could be expected that a solutes will be stored as secondary minerals as the interstitial solution becomes supersaturated with respect to these solutes, due to the drying out of riparian soils during summer.

Figure 4.10 displays the seasonal trends. The multivariate linear regression of SO_4^{2-} versus Ca^{2+}, Mg^{2+}, and SiO_2 yields an R^2 of 0.94 and a p-value less than 2×10^{-16} for the dry season chemical pattern and an R^2 of 0.67 and a similar p-value, indicating a strong correlation. The correlation matrices in figure 4.10 illustrate the relationship between these parameters. In figure 4.10-c, subgroups $C3.2$, $C6.4$, $C3.1$, and $C4$ are superimposed on soil solution, throughfall, and riparian water. It can be observed that the manifestation of subgroup $C6.4$ is caused by the mixing of throughfall with what is stored in the riparian zone. An anion-ternary plot (with endmembers SO_4^{2-}, alkalinity, and Cl^- plus NO_3^-) of soil solution, stream water, and throughfall is displayed in Figure 4.10-a. Overlapping subgroups $C3.2$, $C6.4$, $C3.1$, and $C4$ are removed and a schematic of the ternary diagram is depicted in figure 4.10-b. This diagram illustrates that subgroup $C3.2$ originates in the the stream water polygon and evolves into the plot's SO_4^{2-} endmember. This can also be seen in figure 4.10-c, where the relationship between SO_4^{2-} and Ca^{2+} is very strong (indicated by regression line I). In reverse, subgroup $C6.4$ evolves from stream water to the plot's alkalinity endmember, deviating from the groundwater trend (moving from subgroup $C4$ to subgroup $C3.1$), due to a greater relative contribution of Cl^- and NO_3^-. The regression line of SO_4^{2-} versus Ca^{2+} for subgroup $C6.4$ is depicted as line II in figure 4.10-c.

Flow line B (subgroup $C3.1$) must also traverse the riparian soils before entering the stream, based on the observations made regarding the predominant subgroups in the stream discharge. Residence time in riparian soils will determine whether solutes chemically evolve to represent riparian water or remain chemically related to solutes observed in subgroup $C3.1$. The flux from flow line B to the stream will determine the solute retention time in the riparian zone. Because throughfall during rain events flushes out resident pore water, subgroup $C6.4$ will be seen during transition periods (when the system is getting wetter or drier and is more likely to be quickly recharged). The following section will provide a more comprehensive description of this mixing process as well as an updated conceptual understanding of the system's processes.

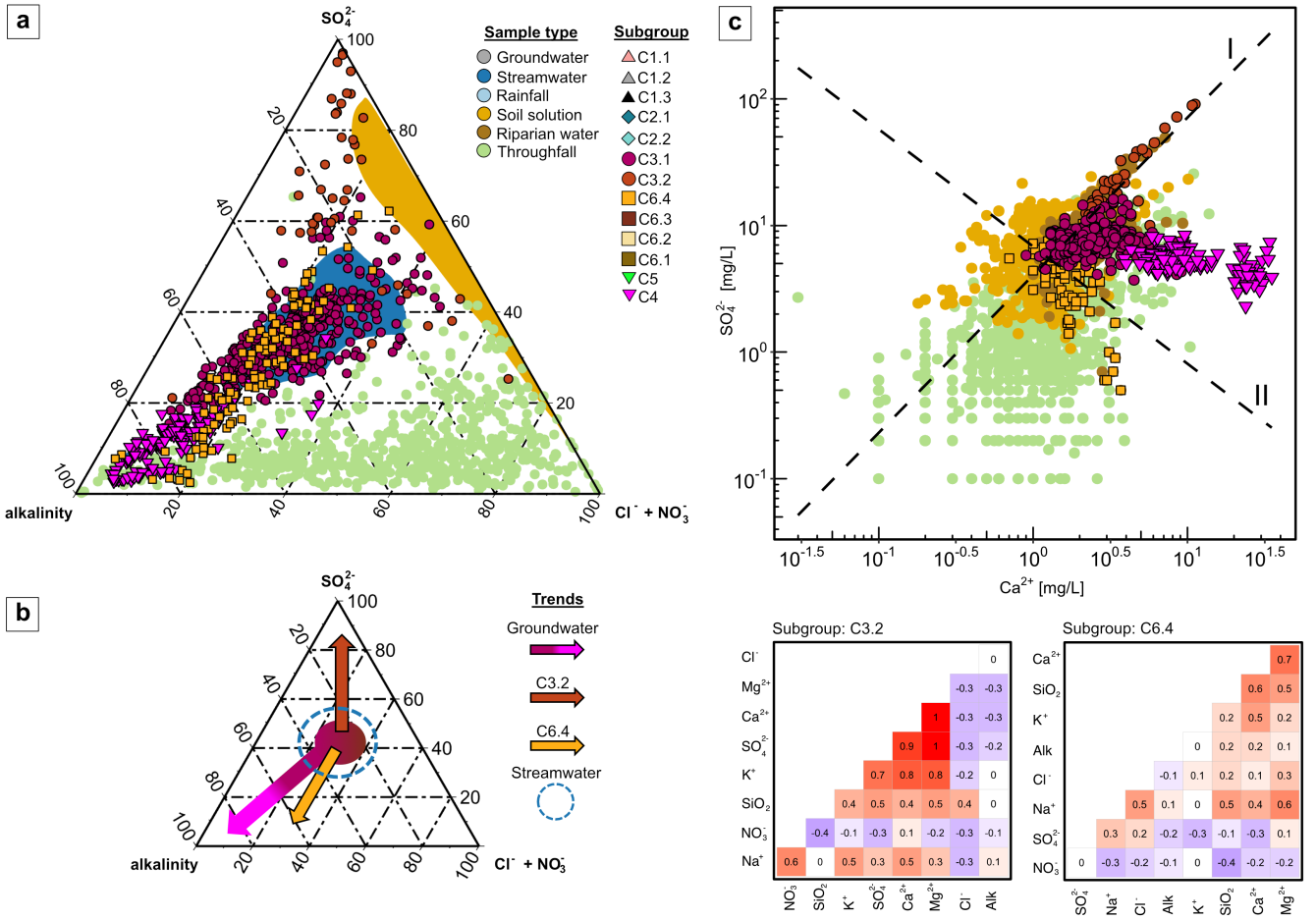

Figure 4.10: Anion ternary plot (a), illustrating the relative concentrations (mEq/L) of alkalinity, SO_4^{2-}, and $Cl^- + NO_3^-$, and (b), illustrating the subgroup trends for the anion ternary plot. A biplot (c) of SO_4^{2-} *vs.* Ca^{2+} illustrates the relationship between these two parameters for subgroups associated with the riparian zone, superimposed on riparian water, soil solution, and throughfall. Also shown are the correlation matrices for subgroups $C3.2$ and $C6.4$.

4.6 Synthesis

Figure 4.11 depicts a conceptual model of *WEC* mixing. The origins of the various subgroups are indicated (catchment units). To restate, flowlines were referred to as "subgroups" in the preceding discussions in the chapter. Conceptually, flowlines are endmembers, but endmembers are not necessarily flowlines. In the context of this discussion, "endmember" refers to a point in a mixing plane that forms one end of a range or series consisting of similar members. In this chapter, it is assumed that flowlines have distinct chemical signatures that are governed by a set of dominant biogeochemical processes linked to specific locations within the system. Catchment units will now be discussed in relation to these locations.

4.6.1 Weathered zone on the primary plateau

The weathered zone on the primary plateau functions as a semi-perched aquifer with a permeable base. Recharge (throughfall and rainwater) infiltrates vertically and chemically evolves sequentially to $C5$, $C4$, and $C1.2$. The dissolution of carbonate minerals is the primary biogeochemical process driving this sequential formation of subgroups. Subgroup $C4$ water flows laterally from the primary plateau to the stream when the phreatic head rises above the threshold caused by the contact of the weathering front and the fresh bedrock (figure 2.1). In contrast, when the phreatic head in the perched aquifer in the weathered zone falls below a certain threshold, it is no longer hydraulically connected to the hillslope, and subgroup $C4$ is no longer detectable in boreholes on the hillslope. During hydrological conditions in which the plateau is connected to the stream, water from cluster $C4$ flows rapidly through the fractured zone of the bedrock without being significantly altered chemically. Based on the presence of this subgroup in boreholes $GW2$, $GW10$, and $GW12$, this observation can be made. From the perched aquifer, water associated with subgroup $C1.2$ infiltrates vertically into the fresh bedrock, leaking into the bedrock. This water is thought to take the longest route to the stream and has changed chemically to subgroup $C1.3$ due to primary mineral weathering.

4.6.2 Hillslope

$GW7$ and $GW9$ are near the elevation that governs the connection between the perched aquifer on the plateau and the remainder of the catchment downslope (the base of the primary plateau weathering front). Infiltration descending vertically seems to mix with subgroup $C4$ to form subgroup $C3.1$. This is the beginning of flowline B in the perceptual model (figure 2.5). As the system saturates, water begins to flow laterally in the shallow flowlines, and subgroup $C6.3$ emerges as the dominant flowline (flowline C). Only subgroup $C6.2$ (vertical infiltration) is observed at $GW8$, which is located further away from the weathered zone's cutoff elevation. A secondary deep groundwater flowline is formed by water infiltrating vertically into the bedrock on a hillslope (subgroup $C1.1$). It is likely that

this flowline is a continuation of the deep flowline emanating from the primary plateau, mixed with water infiltrating vertically on the hillslope. This flowline exits the catchment through the riparian soil during wet conditions and presumably directly into the stream during extreme drought.

4.6.3 Riparian soils

Under low flow conditions, the riparian soils exhibit an intriguing behaviour and influence on the water observed in the stream. Under wet conditions, the flux from shallow flowlines C ($C6.3$) is sufficient to prevent chemical alteration. Upon drying of the catchment, the same behaviour is observed for flowline B (subgroup $C3.1$). If the flux from flowline B is low enough in dry conditions, subgroup $C3.1$ is chemically transformed as secondary minerals precipitate due to the supersaturation of the pore water. This water is diluted by throughfall when the system re-wets, forming subgroup $C6.4$. The occurrence of these subgroups in the stream will be detailed in the following chapter.

4.6.4 Secondary plateau

On occasion, during dry conditions, the secondary plateau's contribution to $SW1$'s streamflow is observed (figure 4.1). The plateau is highly fractured and has a very shallow weathering front. It does not demonstrate the same perched aquifer behaviour observed on the primary plateau. Therefore, it is plausible to argue that these flowlines are chemically defined by weathering processes and chemical input from the surface. It is anticipated that deep groundwater flowlines originating from the secondary plateau are younger than flowlines of comparable depth originating from the primary plateau. Given that higher concentrations of solutes are associated with weathering reactions, this may appear counter-intuitive. The assumption is based on the fact that the secondary plateau is highly fractured, however (Gourdol et al., 2021). It is also expected that the chemical signature observed in subgroups $C2.1$ and $C2.2$ will be highly susceptible to variation in chemical parameters due to input from the surface.

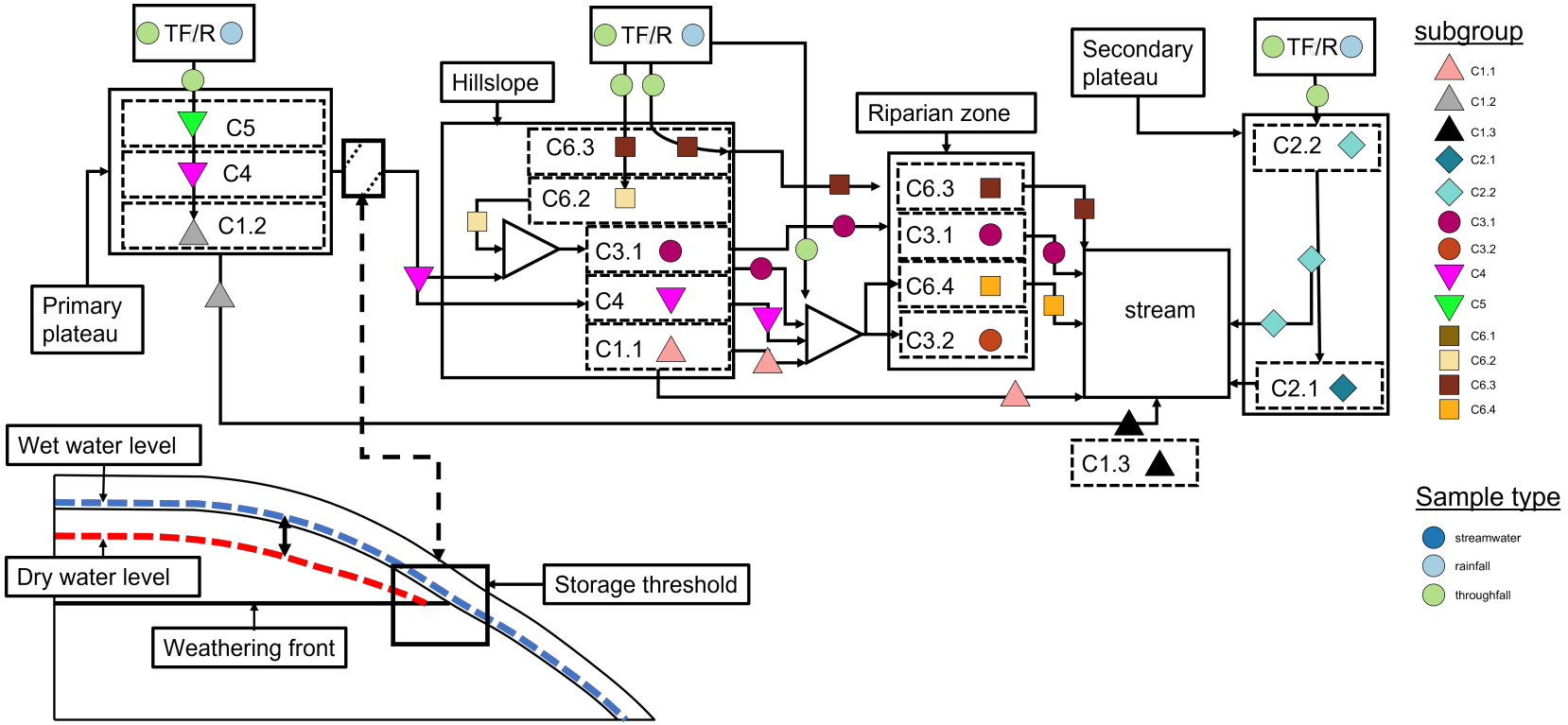

Figure 4.11: Schematic representation of the origins of subgroups. In addition, the convergence of these theoretical flowlines to create new flowlines or endmembers is depicted. The critical storage threshold behaviour and the subsequent activation and deactivation of subgroup $C4$ are depicted in a theoretical cross section of the primary plateau.

4.7 Conclusions

To briefly conclude this chapter, a few observations will be made. This chapter's primary objective was to use multivariate analysis to identify dominant flowlines in the WEC. The identified flowlines or endmembers were evaluated using standard geochemical graphical techniques (classification plots). It was discovered that the subgroup's behaviour was consistent with the current hydrological perceptual model. Only two major flowlines were found to be connected to streamflow generation. The first is subgroup $C6.3$, which is associated with lateral flow in the system's shallow horizons (flowline C, figure 2.5). $C3.1$ is the second dominant flowline (flowline B). This flowline appears to be a mixture of the vertically infiltrating recharge (subgroup $C6.2$), flow line C, and water originating from the primary plateau ($C4$).

In this thesis, the occurrence and behaviour of flowline $C4$ are intriguing and not fully resolved. Based on core drilling and geophysical survey results (not presented in this thesis), there is no significant difference between the hydrological conductivity of the primary and secondary plateaus. Evidently, the presence of saprolite is associated with the dissimilar chemical signatures observed between the two catchment units. Regarding mechanical weathering, there is essentially no difference. However, the extent of chemical weathering varies greatly (Chapter 2, *WEC*'s regolith description). According to the research of Brantley et al. (2013), chemical weathering appears to create and expand pores in weathering rock. This may suggest that the storage capacity of the primary plateau is significantly greater than that of the secondary plateau. The intermittent occurrence of flowline $C4$ is associated with storage in the primary plateau, and when this storage threshold is exceeded, it appears that flowline $C4$ is connected to the stream, mixing with subgroups $C6.2$ and $C6.3$ to form flowline B.

To pave the way for future research, it is necessary to comprehend the geochemical behaviour of potential tracers in the system. Ca^{2+} mobility in the system is significantly affected by the dissolution of carbonate minerals, as demonstrated in this chapter. The chemical processes underlying this behaviour will be examined in greater depth in the following chapter.

Chapter 5

Titration at Catchment scale

5.1 Introduction

In the previous chapter, a conceptual geochemical model was developed based on existing knowledge of the *WEC*'s hydrological functioning. Several dominant chemical processes, some of which may be obvious, were identified. The chemical processes that govern the behaviour of natural tracers will be investigated to aid in the future development of the proposed mixing model. Hypotheses derived from the conceptual understanding of the updated hydro-biogeochemical perceptual model will be tested using synthetic experiments in this chapter (numerical geochemical models). The following section outlines the hypotheses that will be tested in this chapter.

5.1.1 Hypotheses

- Carbonate dissolution is the primary mechanism responsible for the increase in alkalinity that occurs when water travels from the surface deeper into the subsurface. Silicate mineral weathering also contributes to alkalinity, albeit to a lesser extent. The oxidation of *DOC* can be credited as being the primary contributor to the acidity that is present in the system. As a result, the system can be understood on a more global level as being driven by acid-base reactions.
- It is possible to determine that the material that enters the system from the surface is the primary contributor of sulfate to the system (dust deposition and vegetation cycling). It is possible to ignore the reduction of sulfate to pyrite because the vast majority of sulfate is stored in the form of sulfate minerals.

The results will be presented in a manner that is organised into groups in accordance with the subgroups that were defined in the prior chapter. A table that provides a brief explanation of the meaning of the subgroups in the context of the conceptual understanding of the *WEC*, is presented below in order to help the reader refresh their memory.

Table 5.1: Description of clusters and subgroups (distinction between types of endmembers). The flowlines correspond to what is depicted in figure 2.5.

HCA -Chapter 4 Cluster	HCA -Chapter 4 Subgroup	Description	Perceptual model -Chapter 2 & 4 Classification
C1	*C1.1*	Deep flowline on the hillslope.	**Flowline D**
	C1.2	Deep flowline on the primary plateau.	
	C1.3	Flowline D (Deepest observable flowline).	
C2	*C2.1*	Flowlines associated with the secondary plateau.	**Flowline**
	C2.2		
C3	*C3.1*	Flowline B (Near-stream lateral subsurface saturated flow through the basal layer of the Pleistocene periglacial slope deposits *PPSD*).	**Flowline B**
	C3.2	Riparian water during dry conditions.	**Endmember** related to a water store.
C4	*C4*	Flowline originating from the primary plateau and forms an endmember of flowline B.	**Flowline**
C5	*C5*	Water infiltrating vertically on the primary plateau, heavily influenced by biogeochemical processes.	**Endmember** related to a water store.
C6	*C6.1*	Recharge that has followed preferential flow paths to deeper horizons.	**Flowline** (preferential flow)
	C6.2	Vertically infiltrating water similar to flowline C, but spend less time in contact with the shallow horizons of the regolith.	**Flowline**
	C6.3	Flowline C.	
	C6.4	Water stored in the riparian zone that is pushed out during precipitation events in dry conditions.	**Endmember** related to a water store.

5.2 PHREEQC speciation modelling

As discussed in Chapter 3, a set of physical and chemical parameters must be defined in order to model the species distribution in a solution. These parameters will be discussed in the following section before the model results are presented. The first critical parameter to consider is the redox state that will be used to define the solution.

5.2.1 Available data for modelling

The labelled data set defined in the preceding chapter contains 2591 complete sets of observations for major ions (Ca^{2+}, Mg^{2+}, K^{+}, Na^{+}, $alkalinity$, SO_4^{2-}, Cl^{-}, and NO_3^{-}), SiO_2, and pH. A subset of 798 labelled observations contain a complete set of major ions and minor elements (Al,Mn,Fe, and Ba) concentrations. There are a total of 377 field in-situ parameters ($E_{h(field)}$, $O_{2(aq,field)}$, EC, pH, and temperature) measurements. Figure 5.1 below depicts how observations are distributed amongst the subgroups.

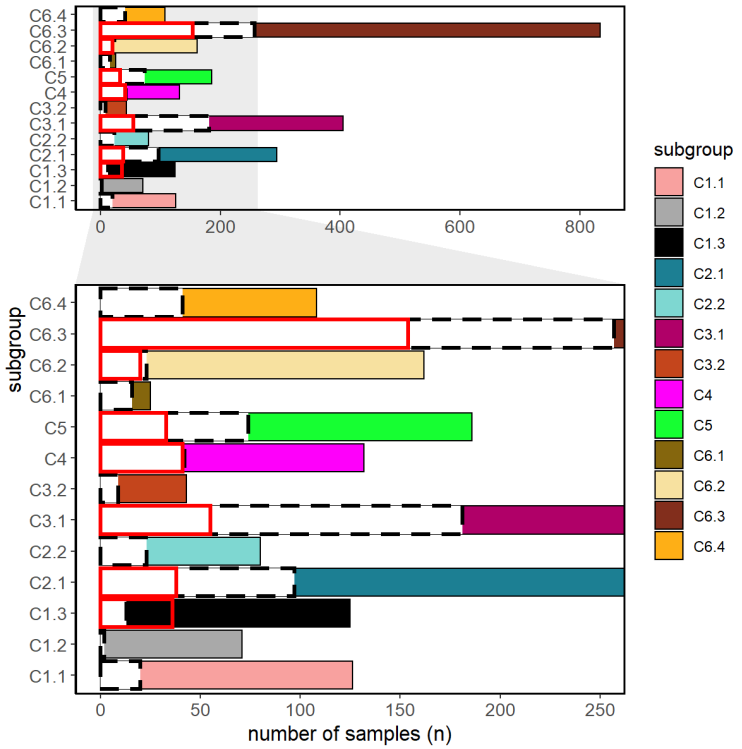

Figure 5.1: Bar chart showing the number of observations per subgroup containing major - and minor element concentrations (unfilled box with dashed border) compared to the complete labeled data set (containing the 9 main parameters used to cluster the data). The red boxes show the number of observations per subgroup, that contain field parameter data ($E_{h(field)}$, $O_{2(aq,field)}$).

5.2.2 Redox conditions

In Chapter 1, the importance of oxidation/reduction (redox) reactions was thoroughly discussed. A brief recap of the main ideas will be discussed before delving into the results for this topic.

Redox potential (E_h) refers to the chemical reaction in which electrons are transferred from (electron donors to electron acceptors). E_h can characterize the intensity of the oxidizing and reducing status in the unsaturated zone, just like in liquid solutions. The theoretical upper and lower boundaries of oxidation and reduction intensities are determined by the intensity of water oxidation (to oxygen) and reduction (to hydrogen gas), which typically range between -1 and $1\ V$.

Figure 5.2 compares groundwater field measured E_h values to E_h values calculated using the Nerst equation (equation 1.9) from Lindberg and Runnells (1984). The graph also displays the field measured E_h values from the weekly campaign, calculated from DO concentrations using PHREEQC.

Theoretical E_h values were computed using the assumption that $O_{2(aq)}/H_2O$ is the dominant redox couple. Based on the dissolved oxygen (DO) concentration measurements, this assumption was made. The median values for the various subgroups ranged from 1.1 ± 0.35 (mg/l) for $C1.3$ (deep groundwater) to 8.6 ± 0.35 (mg/l) for $C6.2$, indicating that the system is always oxic. According to the redox ladder, nitrate can only be reduced when the system becomes hypoxic.

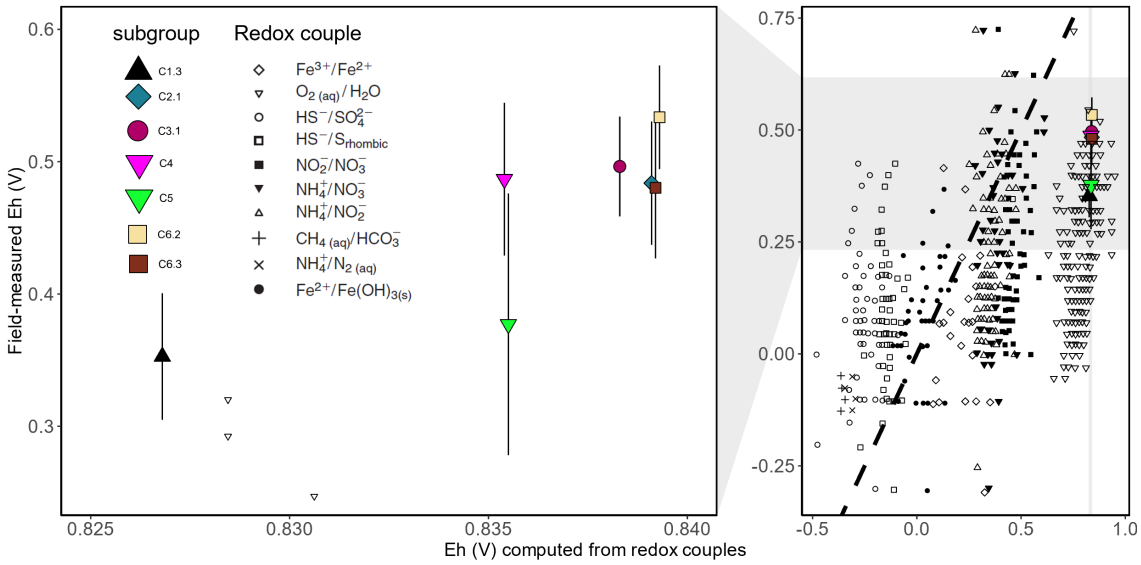

Figure 5.2: Weekly field measured Eh vs. theoretically calculated E_h (E_h in V), superimposed on a comparison of groundwater field E_h measurements with potentials calculated for individual redox species adapted from (Lindberg and Runnells, 1984)). Fe^{2+}/Fe^{3+} is the only couple that has good agreement between field measured and calculated E_h values (shown by the dashed regression line).

In natural shallow systems, water can only be oxidized/reduced under extremely oxidizing/reducing conditions, and the actual lower and upper E_h boundaries are governed by CO_2 reduction to methane (CH_4) and the presence of O_2, respectively. The two sources of acidity in the most near-surface environments are carbon dioxide from the atmosphere and organic acids formed by decaying organic matter, resulting in an acid pH range of 5–6. Acid sulfate soils have lower pH values, with values as low as 4 occasionally recorded (DeLaune and Reddy, 2005). The lower bound for pH in natural shallow environments can then be assumed to be this low pH value. The pH limit's upper bound is associated with CO_2-free water in contact with carbonate rocks, where pH levels as high as 10 have been recorded. An upper limit of 9 is reasonable for most surface waters (DeLaune and Reddy, 2005).

Using E_h values, one can determine the dominant redox couple in a system. Because multiple electron donors can drive multiple redox reactions at the same time, systems rarely have strict redox boundaries in practise. The redox state of the soil and the unsaturated zone can vary greatly (Mansfeldt, 2003; Fiedler et al., 2007). It can be oxidizing, weakly reducing, moderately reducing, or strongly reducing (≥ 400, $200 - 400$, $100 - 200$, and $-100\ mV$, respectively).

Figure 5.3 shows the in-situ pH *vs.* E_h measurements taken throughout the one-year weekly campaign. The following formula is used to calculate the graph's upper E_h bound (water stability line):

$$E_h = (20.60 - pH) \times 0.059 \tag{5.1}$$

The relationship shown below is used to calculate the lower E_h bound (lower limit of water stability):

$$E_h = -0.059 \times pH \tag{5.2}$$

Both equations are derived from the oxidation and reduction half-reactions of water oxidized with oxygen. The zones (oxidizing, weakly reducing, moderately reducing, and strongly reducing) are based on the redox zoning in soils adapted from the review paper by Zhang and Furman (2021). Only subgroups $C5$ and $C1.3$ are seen to exhibit weakly reducing behavior, with subgroup $C5$ exhibiting a preference for moderately reducing conditions.

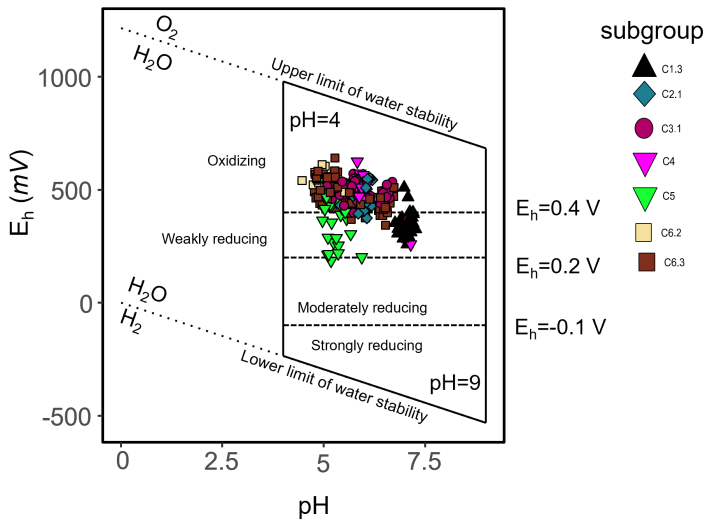

Figure 5.3: E_h-pH diagram depicting weekly in-situ field observations collected over the course of a year. The zones depicted on the graph are adapted from Zhang and Furman (2021). The upper and lower bounds represent the E_h - and pH stability ranges for water in natural environments.

In the context of the conceptual geochemical model, this behavior makes sense. Water that has been chemically altered by redox reactions is represented by subgroup $C5$. The pH and dissolved oxygen concentrations fluctuate in response to DOC, as shown in the previous chapter (figure 4.8). So, we can assume that when DOC is oxidized, the measured E_h will go down. Lower values in subgroup $C1.3$ are also reasonable, given that this group represents the deepest flowline.

5.2.3 PHREEQC speciation model results

Figure 5.4-a shows a heatmap of the modelling results obtained from PHREEQC for the complete data set. Of the 2591 observations in this data set, 2022 models converged successfully given the uncertainties in the data (electrical charge balance error of 5% or lower, pH, and *pe*). PHREEQC determines all potential phases for a given E_h and pH. The saturation indices (SI) of these phases are shown as a gradient of colour in a range between -25 (dark blue) and 0 (dark red).

To recap, a SI value of 0 indicates that the solution is in equilibrium with the respective phase, and values less than 0 indicate the degree of sub-saturation. The figure shows that the SI of dolomite increases with depth, rising from -9±1.3 in subgroups associated with shallow flowlines to close to -1.8±0.9 in the three subgroups associated with deep flowlines ($C1.1$–$C1.3$). Calcite showed a less pronounced but still increasing saturation trend as it moved from shallow to deeper groundwater, ranging from -5±0.73 to -0.7±0.6.

An interesting trend is the occurrence of saturation of magnesium silicate minerals in the deeper groundwater. The minerals associated with silica (quartz and chalcedony) were either close to saturation or super saturated for all the models . This is an overestimation because aluminium was not defined in the models, and it can be expected that the weathering of clay minerals due to acidic soils will play a significant role in silica mobility in the system.

The model results for the subset that contains complete parameter sets for both major- and minor-element concentrations are shown in Figure 5.4-b. A total of 610 models successfully converged. As seen in the previous set of modelling results, dolomite and calcite both showed an increase in SI with depth (moving from the shallow flowlines $C6.2$ to the deepest flowline $C1.3$). Dolomite has a SI range of -9.6±1.14 to -2±0.36. The SI of calcite increased from -5±0.7 to -1.1±0.18.

Both primary minerals and clay minerals show an increase in saturation, according to the models. These values should be used with caution because it is expected that the Al and Fe concentration obtained from laboratory analysis represents the total concentrations (ICP-MS analysis) in the sample. *Al*- and *Fe*-oxides may have a higher affinity for soil organic matter (SOM) than other mineral surfaces, such as clay minerals (Jones and Edwards, 1998; Kaiser and Zech, 1998; Kaiser et al., 2002). Thus concentration observed for these elements may associated with SOM and not with clay mineral weathering.

Because *Fe*-oxides and hydroxides have a high specific surface area (Kaiser and Guggenberger, 2003), positive relationships between SOM and *Fe*-oxides is often observed (Kaiser and Guggenberger, 2003; Kleber et al., 2005). As cations, Fe^{3+} and Al^{3+} can bind with organic ligands such as carboxylic groups in acidic soils, to form organo-mineral complexes (Higashi, 1983; Boudot et al., 1989) and stabilise SOM via cation bridges (Oades, 1988;

Lützow et al., 2006) via a direct bond formation between SOM and either Al^{3+} or Fe^{3+} at the surface (Duckworth et al., 2008; Mikutta et al., 2007).

Unlike Fe^{3+}, which exists in a variety of oxides with amphoteric surfaces on which organic anions are adsorbed, Al^{3+}'s interaction with organic materials is more likely to be electrostatic (Oades, 1988). As a result, it is expected that the activities of Al^{3+} and Fe^{3+} will be overestimated in the models, and the subsequent supersaturation of phases associated with these elements will be interpreted accordingly. What is intriguing is the increase in chlorite saturation with depth. The geochemical characterization of the regolith revealed the presence of chamosite, the Fe^{2+}-end member of the chlorite group (Moragues-Quiroga et al., 2017).

The deep flowline subgroups show a significant increase in Mn-oxide mineral SI values. This is consistent with current system understanding, as these flowlines will be older, resulting in less dissolved O_2 and a reduction in $Mn(IV)$.

The speciation modelling results confirm the current conceptual geochemical model developed in the previous chapter. There are some phases predicted by the models that merit further investigation. The first is the presence of alunite with high saturation in shallow flowlines and subsaturation in deep flowlines; the second is the presence of magnesium silicate minerals. The latter is commonly associated with tillite weathering (cemented tillite contains fragments of the underlying ultramafic complex and from the glacial deposits). Figure 4.5 shows that the ratio of Mg^{2+} to Ca^{2+} has shifted (normalized for Na^{+}) moving from throughfall to the subsurface. It is still unknown whether the system contains dolomite or if the carbonate minerals responsible for the system's buffer are Mg-calcite. At this point, the source of Mg^{2+} is also unknown.

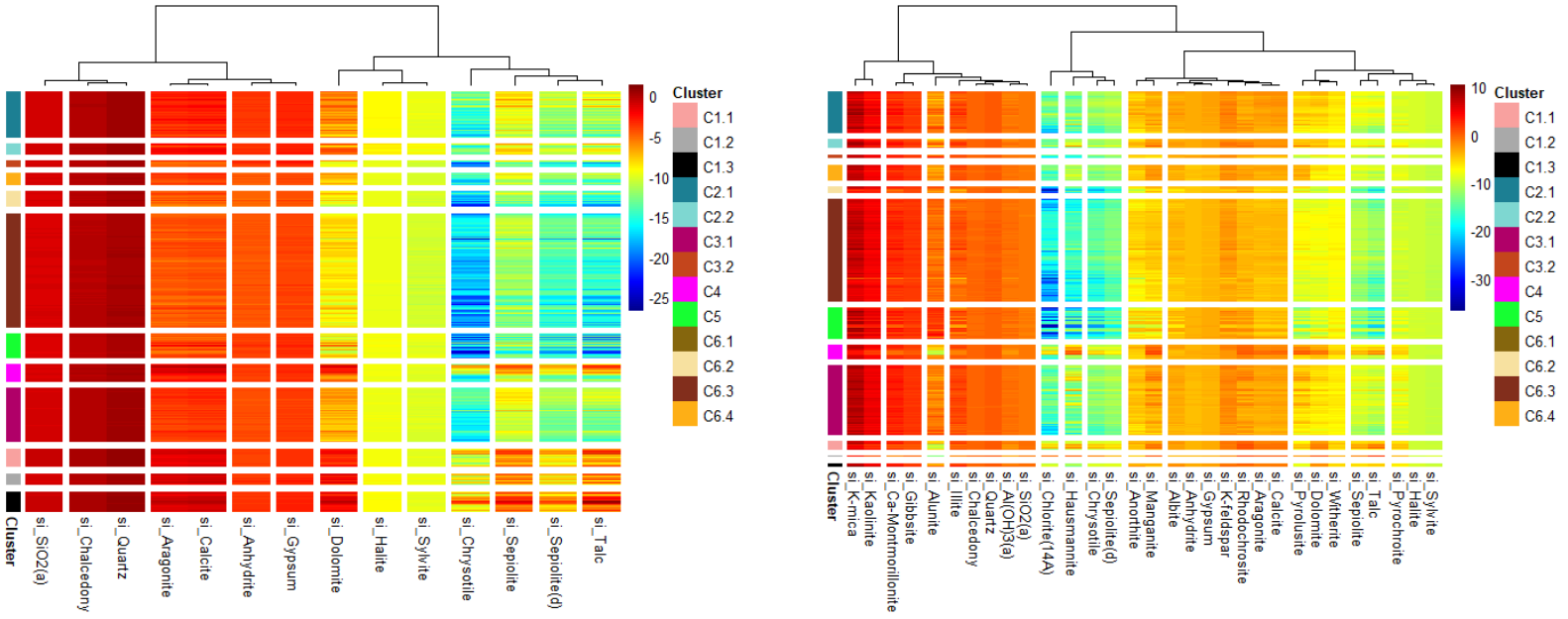

(**a**) Heat map A

(**b**) Heat map B

Figure 5.4: Heat maps of modelled *SI* values. Heat map A shows the saturation indices (*SI*) of phases for 2022 models for the complete labelled data set ($n_{C1.1} = 107$, $n_{C1.2} = 67$, $n_{C1.3} = 120$, $n_{C2.1} = 266$, $n_{C2.2} = 62$,$n_{C3.1} = 310$, $n_{C3.2} = 35$, $n_{C4} = 102$, $n_{C5} = 140$, $n_{C6.1} = 3$, $n_{C6.2} = 91$, $n_{C6.3} = 649$ and $n_{C6.4} = 70$). Heat map B displays the *SI* values for a subset of the labelled data ($n = 798$: $n_{C1.1} = 17$, $n_{C1.2} = 2$, $n_{C1.3} = 8$, $n_{C2.1} = 83$, $n_{C3.2} = 8$,$n_{C4} = 28$, $n_{C5} = 62$, $n_{C6.1} = 1$, $n_{C6.2} = 12$, $n_{C6.3} = 202$, $n_{C6.4} = 32$). The *SI* values are displayed on a colour scale ranging from dark blue to dark red. This range is between 0 and -25 for heat map A, and between 10 and -30 for heat map B.

5.3 Forward-inverse modelling

At this point, it is increasingly clear that the geochemical functioning of the system can be conceptualised as an acid-base tritiation process at catchment scale. Since the pH of the shallow flowlines is lower, the acidic soils have obviously had an impact. This acidity is largely buffered by carbonate minerals and, to a lesser extent, by the weathering of silicate minerals as water gradually penetrates deeper horizons of the subsurface. In shallow natural systems, organic acids, DOC oxidation, and pyrite oxidation are typically the only three sources of acidity.

Figure 4.1 shows that the initial main cluster ($cluster3$) associated with the shallow flowlines ($C6.1$-$C6.4$) was a Mg^{2+}-SO_4^{2-}-type dominant water on average. The main cluster ($cluster1$) represents deep flowlines with Ca^{2+}-HCO_3^- dominant water.

This is a well-known pattern that has been described in numerous studies. Ca^{2+}-SO_4^{2-}-HCO_3^- groundwaters and stream waters are frequently produced as a byproduct of pyrite oxidation when calcite weathers (Berner and Berner, 1987). The oxidation of trace amounts of pyrite, which is common in carbonate lithologies, produces sulfuric acid, which is then neutralised by calcium carbonate matrix dissolution. Under oxidising conditions, pyrite oxidation is often rapid and is typically controlled by microorganisms (Moses et al., 1987; Stumm et al., 1996; Chandra and Gerson, 2010). Calcium carbonate dissolution in response to pyrite oxidation and calcium carbonate weathering caused by soil CO_2 produced by microorganisms and organic degradation cause two distinct weathering fluxes.

One of the study's major uncertainties is determining the source of acidity. Figure 4.8 in the previous chapter demonstrated that there appears to be a relationship between DOC and alkalinity. The mineralogy study found no pyrite during the regolith characterization. Furthermore, it is very likely that all of the SO_4^{2-} observed in the system can be attributed to surface input. To determine whether the acid produced by DOC oxidation is sufficient to explain the trends observed in Ca^{2+}, Mg^{2+}, and SO_4^{2-}.

5.3.1 Acid -Base reactions

In order to determine whether the oxidation of DOC could produce sufficient acidity to explain the titration behaviour observed in the catchment, a synthetic experiment was created to test the hypothesis that pyrite oxidation is not the primary driver of carbonate mineral dissolution. The Forward-inverse model (FIM) methodology, including how it was set up and how it was run, is described in detail in Chapter 3.

The results that were obtained from the simulation are compared to the results that were obtained from the PHREEQC speciation modelling in figure 5.5. The figure presents the relationship between pH and the partial pressure of CO_2 (P_{CO_2}). The grey dots represent the results of 10,000 iterations of the model. As can be seen from the figure, the predicted

values of the *FIM* simulations and the values of the PHREEQC speciation modelling are, for the most part, in agreement with one another.

The *FIM* does not predict effectively the behaviour that is observed in the shallow flowlines ($C6.2$, $C6.3$, and $C5$). One of the main failures of the model is that it cannot account for the influence of organic acids. Despite the fact that the *FIM* could not describe the entire range of pH vs. P_{CO_2} relationships observed in the speciation models, the general trends could be reproduced, supporting the observations made in figure 4.8 that *DOC* oxidation is the primary driver of carbonate mineral dissolution.

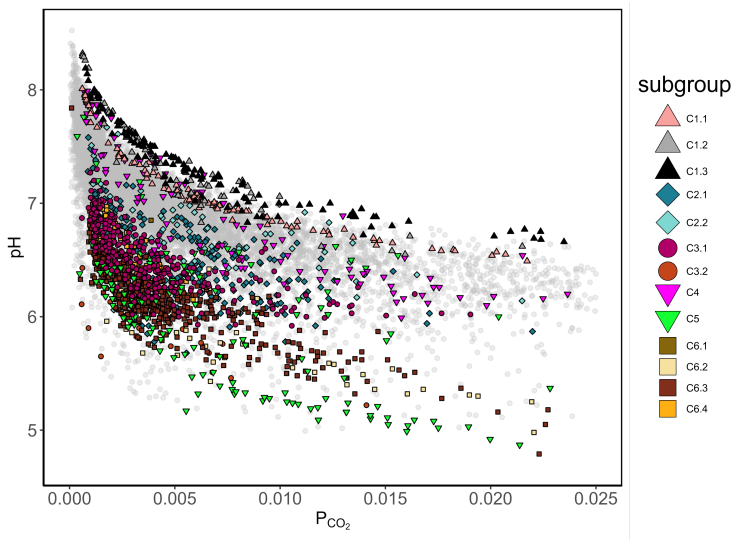

Figure 5.5: pH vs. P_{CO_2} The graph shows a biplot of pH vs. the partial pressure of $CO_{2,gas}$. The grey markers represent the results ($n = 10,000$) obtained from the forward-inverse model (*FIM*) simulation. The results obtained from the PHREEQC speciation models ($n = 2022$) are overlaid.

5.3.2 Common ion effect

Some minerals undergo rapid transformations when exposed to water. This is particularly true for "soluble" minerals such as gypsum, anhydrite, halite, fluorite, and the majority of carbonate minerals. In comparison to the residence time of groundwater, equilibrium will be reached relatively quickly (Appelo and Postma, 2006). Other minerals, typically silicates, react so slowly that equilibrium is never reached at low temperatures, necessitating consideration of reaction kinetics.

The concept of the law of mass action and the influence that the solubility of minerals sharing a common ion can have on each other is discussed in Chapters 11 & 3. When gypsum or anhydrite dissolves, Ca^{2+} concentration rises, causing calcite to precipitate and lowering carbonate concentration. The decrease in carbonates causes dolomite to dissolve, increasing the concentrations of Mg^{2+} and Ca^{2+} (dedolomitization). Mixing

waters that are in equilibrium with a carbonate mineral but have different P_{CO_2} values may result in subsaturation, causing mineral dissolution. As a result, estimating the relative contributions of flowlines during mixing is not as simple as using the concentrations of say Ca^{2+} in a mass balance.

The sources of the solutes that will be used as tracers must be well defined in order to test the mixing hypothesis developed in the previous chapter. The overarching mixing model developed in this work is still limited in several ways. The primary source of Mg^{2+} and SO_4^{2-} in the system is unknown. The dynamics of Ca^{2+} are linked to this uncertainty. The relationship between Ca^{2+} and $SI_{calcite}$ is depicted in figure 5.6-a. $SI_{calcite}$ approaches 0 as it moves deeper into the subsurface from the shallow flowlines. figure 5.4 has already demonstrated this. This relationship allows us to conclude that Ca^{2+} behaviour will be strongly related to P_{CO_2}.

The relationship between SI_{gypsum} and SO_4^{2-} is depicted in Figure 5.6-b. As can be seen, the *FIM* is unable to adequately explain the source of SO_4^{2-} in the shallow flowlines ($C6.2$, $C6.3$, $C3.1$ and $C5$). The speciation models for the subset data (which included Al concentrations) suggested that alunite ($KAl_3(SO_4)_2(OH)_6$), could be a SO_4^{2-} source in the system's shallow horizons. This is a reasonable assumption to make. Adsorption has been shown to remove a large portion of the SO_4^{2-} input to soils. Soil adsorptive capacity, on the other hand, decreases as pH decreases (Adams and Rawajfih, 1977). In arid regions, SO_4^{2-} is stored as gypsum. SO_4^{2-} retention in acid soils, such as the soils found in the *WEC*, may be caused by positively charged *Fe*- and *Al*-hydroxy-sulphates. This assumption is reinforced by the fact that the system's soil matrix and litter contain a much higher concentration of total $S\%$ than the deeper horizons (shown in figure B.2). There is still a large amount of uncertainty about the origin and mobility of SO_4^{2-} in the system, which is an important piece of the puzzle given the influence of pyrite oxidation on slate weathering rates.

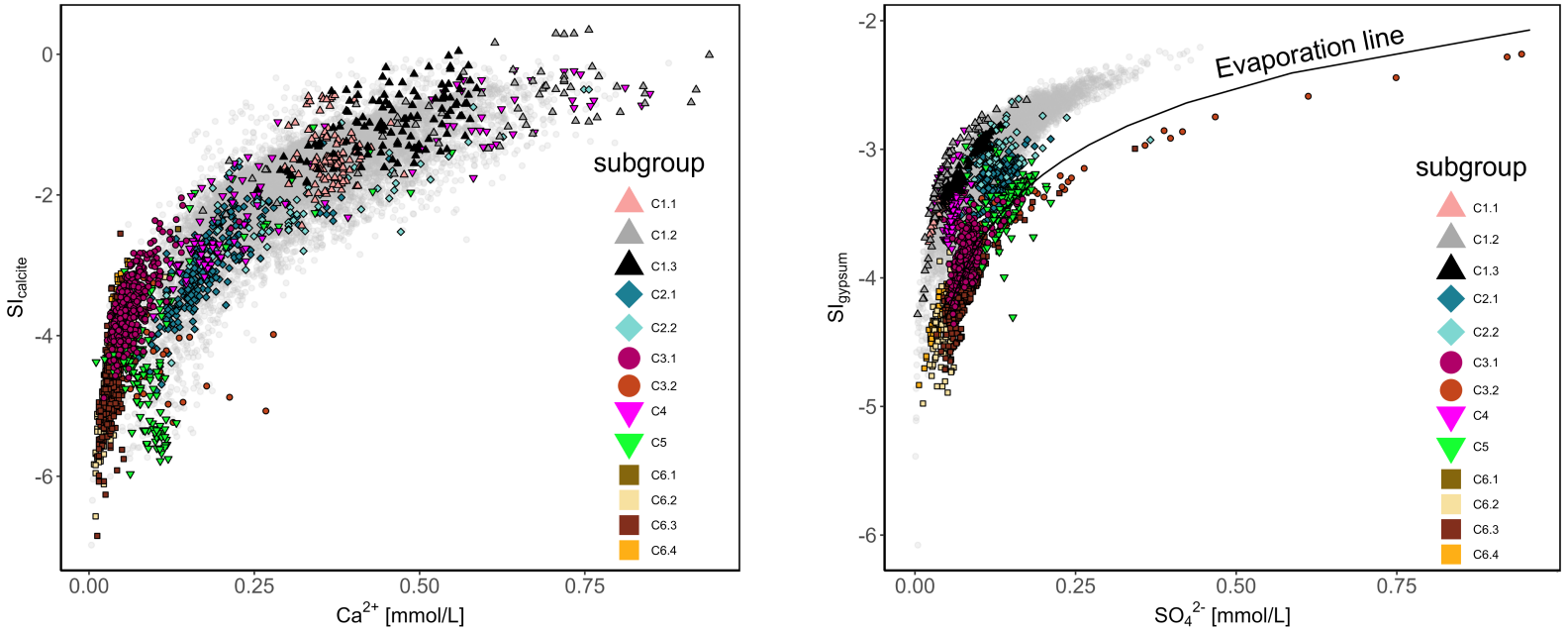

(**a**) scatter plot A

(**b**) scatter plot B

Figure 5.6: *SI vs.* ion activity $[mmol/L]$. Scatter plot A depicts the relationship between $SI_{calcite}$ and Ca^{2+} activity as predicted by 10,000 simulations (FIM). The PHREEQC speciation model results ($n = 2022$) are overlaid on these values. Similar to plot A, scatter plot B depicts the relationship between SI_{gypsum} and SO_4^{2-} activity, with the results of the speciation models superimposed.The black line in scatter plot B represents a curve obtained by sequentially removing (evaporating) pure water from a theoretical solution that represents the centroid of subgroup $C3.1$.

5.4 Conclusion

The work that is presented in this chapter serves as an initial step toward understanding the governing geochemical processes in the system and how these processes are coupled to hydrological processes. The understanding that is gained from this initial step is necessary for further progress.

Even though the PHREEQC speciation modelling and forward-inverse models provided some insight into which potential mineral phases may be controlling the chemical composition of the subgroups, the forward-inverse models failed to adequately explain the sources of SO_4^{2-} in the system; as a result, we are unable to either accept or reject the hypothesis that was presented at the beginning of the chapter. However, the forward inverse models do provide a reasonable explanation for the behaviour of Ca^{2+} and SO_4^{2-} in the flowlines that are deeper. It is possible that in the future, the models will be improved by testing additional mineral phases that were observed in the results of PHREEQC speciation modelling. The *FIM* method can also be used to test alternative hypotheses regarding the possible sources of the solutes that are used as traces. The approach that is being taken right now involves simplifying the system by limiting it to a single source of acidity (the oxidation of DOC), in addition to the dissolution of calcite, dolomite, and gypsum. These assumptions about the system could provide an explanation for the global control of pH within the system, providing encouraging initial results that support the hypothesis that the dissolution of carbonate minerals may be the primary source of alkalinity within the system. Moreover, these assumptions about the system could provide evidence for the hypothesis.

The results shown in figure 4.2 demonstrate that the subgroups $C6.2$, $C6.3$ (flowline C), and $C4$ can all be construed as endmembers of the subgroup $C3.1$ (flowline B). Given that the generation of streamflow in the WEC appears to be controlled by shallow flowlines, it is a valid argument that the chemistry of the stream will be controlled by biogeochemical processes associated with horizons at the same level as these flowlines. In addition, it is possible that deep flowlines do not make a significant contribution to the chemical composition of the stream, with the sole exception of the subgroup $C4$, as shown by the findings presented in Chapter 4. According to the findings, it is still necessary to determine the sources of $Mg2+$ and SO_4^{2-} in the shallow horizons. This is something that is made clear by the findings.

To supplement the findings presented in this and previous chapters, a data-driven modelling approach will be presented in the final chapter of this work. The chapter that follows will serve as a proof of concept to this thesis.

Chapter 6

Connecting the dots

6.1 Concentration-discharge patterns

Before starting the introduction of this chapter, table 6.1 is presented once more. This table was discussed in the prior chapter and is only presented to provide the reader with a quick review of the meaning of the subgroups. It is important to note that not all the flowlines in the subgroup are flowlines. Some of the subgroups consist of water that comes from regions that are governed by chemical processes that are analogous to one another. *C5* is a good illustration of this kind of subgroup. Although *GW1* and *GW5* are the most common locations in which *C5* is observed, the riparian zone also showed the occurrence of this subgroup. Similarly, subgroup *C6.4* is not associated with a flowline; rather, it is water that has been stored in the riparian zone and is flushed out into the stream during precipitation in dry conditions.

Table 6.1: Description of clusters and subgroups (distinction between types of endmembers). The flowlines correspond to what is depicted in figure 2.5.

HCA -Chapter 4 Cluster	Subgroup	Description	Perceptual model -Chapter 2 & 4 Classification
C1	*C1.1*	Deep flowline on the hillslope.	**Flowline D**
	C1.2	Deep flowline on the primary plateau.	
	C1.3	Flowline D (Deepest observable flowline).	
C2	*C2.1*	Flowlines associated with the secondary plateau.	**Flowline**
	C2.2		
C3	*C3.1*	Flowline B (Near-stream lateral subsurface saturated flow through the basal layer of the Pleistocene periglacial slope deposits *PPSD*).	**Flowline B**
	C3.2	Riparian water during dry conditions.	**Endmember** related to a water store.
C4	*C4*	Flowline originating from the primary plateau and forms an endmember of flowline B.	**Flowline**
C5	*C5*	Water infiltrating vertically on the primary plateau, heavily influenced by biogeochemical processes.	**Endmember** related to a water store.
C6	*C6.1*	Recharge that has followed preferential flow paths to deeper horizons.	**Flowline** (preferential flow)
	C6.2	Vertically infiltrating water similar to flowline C, but spend less time in contact with the shallow horizons of the regolith.	**Flowline**
	C6.3	Flowline C.	
	C6.4	Water stored in the riparian zone that is pushed out during precipitation events in dry conditions.	**Endmember** related to a water store.

Returning to where the discussion ended in the first chapter, the overarching theme of the thesis seeks to understand $c - Q$ relationships in forested hillslope catchments. Studies on $c - Q$ patterns in streams has been around for a long time (Johnson et al., 1969; Evans and Davies, 1998), and has seen renewed interest recently (Zhi et al., 2019; Stewart et al., 2022). This renewed interest was primarily motivated by mounting evidence that the mechanism responsible for the diverse patterns observed in c-Q measurements is related to the changing dominance of endmember sources contributing to stream chemistry (Zhi et al., 2019). This mechanism is strongly linked to the transit time estimations in catchments. In the review paper on the subject (Benettin et al., 2022), the authors give a comprehensive review of the most recent state of the art in the field. The paper discusses the typical pattern of streamflow, which consists of a greater proportion of young water during wet periods and a smaller proportion during dry periods (Birkel and Soulsby, 2015; Hrachowitz et al., 2015; Knapp et al., 2019). This is also shown by Xiao et al. (2021). The authors showed the first order control of permeability variations with depth on vertical conductivity.

The implication of this control is that more than 95% of water flows in the top 6 meters of the surface.

EMMA and the interpretation of $c-Q$ behaviour are dependent on the fact that the mixture (stream water) consists of endmembers with significantly different chemical compositions. In accordance with the hypothesis tested by Zhi et al. (2019), the dissimilar chemical composition of endmembers is a result of subsurface biogeochemical heterogeneity. In this particular study, two major endmembers or flowlines are assumed: shallow soil water and deep groundwater, with the relative contribution of each endmember to streamflow varying according to wet and dry conditions. This is referred to as the "shallow and deep hypothesis" by Stewart et al. (2022). Stewart et al. (2022) state that there are very few data sets that can be used to test this hypothesis, and to date, this hypothesis has only been tested using a synthetic experiment (numerical modelling) by Zhi et al. (2019), and more recently by Stewart et al. (2022). The second study was required to estimate soil water and groundwater concentrations based on average stream concentrations, similar to the procedure used by Maher and Chamberlain (2014) to determine C_0 and C_{max} from streamflow. The assumption behind the latter is that during extremely high flow, stream water represents the solute load contribution from atmospheric input, and during extremely low flow, the solute load contribution from weathering, where the weathering reaction has reached an thermodynamic limit. This concept was introduced by Maher (2011), and represent the point is a solute trajectory where equilibrium between the solution and the dissolving mineral phase is reached.

As a result of the data set developed in this work, this hypothesis can now be thoroughly tested, which is one of the novel aspects of the research presented in this thesis. The "shallow and deep hypothesis" was not directly tested, but some preliminary results that will show that the idea works will be shown briefly.

6.1.1 Proof of concept

The respective mean daily discharges for *SW1* through *SW4* are represented in figure 6.1. The water samples that were taken bi-weekly from 2011 to 2022 from the stream and labelled with the hierarchical clustering analysis (Chapter 4), are superimposed on the time series at the point in time that corresponds to the time that the water samples were taken.

During high flows, subgroup *C6.3* dominates the chemical composition of the stream water. This subgroup is hypothesised to represent flowline C in the current perceptual model of the *WEC* (figure 2.5). Subgroup *C3.1* becomes dominant as the system dries out and the discharge decreases. It is hypothesised that this subgroup represents flowline B. This flowline is activated when the bedrock storage threshold is exceeded (Rodriguez and Klaus, 2019). Chapter 4's findings suggest that the activation of flowline *C4* combined

with infiltrating water on the hillslope (*C6.2*) and lateral flowing water is responsible for the occurrence of this flowline (flowline C; *C6.3*).

Observations of subgroups *C2.1* and *C2.2* during periods of low flow in *SW1* are consistent with the close proximity of *GW3* to the sampling point of *SW1*. The water chemistry of *GW3* link this borehole to the secondary plateau. However, the presence of subgroup *C2.2* in the *SW2* and *SW4* can be explained by the fact that *C2.2* and *C1.1* are chemically similar and the hierarchical clustering potentially misidentified these samples. Additionally, the presence of flowline A can be observed (subgroup *C6.4*). Flowline A is assumed to represent the near-stream contributions caused by saturated overland flow from riparian soils, according to the current conceptual understanding of the *WEC* (Rodriguez and Klaus, 2019). The current interpretation of the data from chapter 4, would suggest that this flowline represents rather the water that is displaced during rainfall events and is stored in the riparian soils (figure 4.10). It should be noted that under persistently low flow conditions, the dominant subgroup in the stream (*SW2* and *SW3*) changes from *C3.1* to *C6.4* and then back to *C3.1* as the system becomes wetter. This demonstrates the effect of the riparian zone on the stream's water chemistry during dry periods.

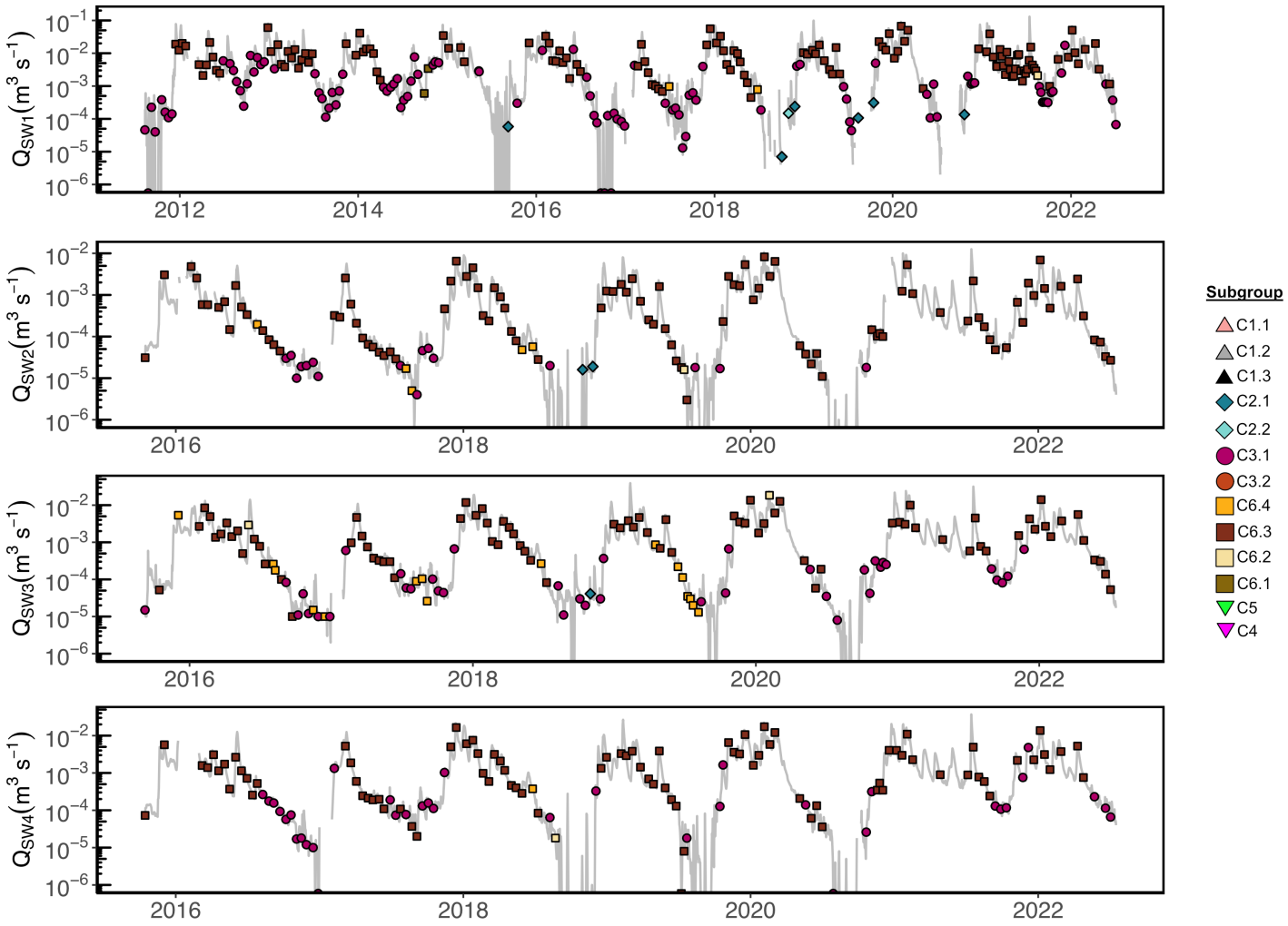

Figure 6.1: Time series plot of mean daily discharge of stream water sample sites $SW1 - SW4$ (grey line) with bi-weekly sampled points indicated. The coloured points correspond to the subgroups discussed in Chapter 4, demonstrating the variation in discharge between the subgroups over time.

Endmembers of endmembers

Comparing catchments over gradients of land use, climate, and geology yields complementary information from the Damköhler number and the power law approach. Even though both strategies use $c - Q$ data, the two approaches have different underlying concepts and methods of calculation.

The power law approach (Equation 1.29) is used to characterise the scaling relationship between discharge and solute concentration in a catchment, which is described by the parameter b (scaling exponent). It is possible to infer catchment properties and processes based on the value of b. The Damkölher number (D_a) has been proposed to be the key to comparing catchments with different properties (climatic *vs.* lithologic weathering controls; Ibarra et al., 2016). By utilising $c - Q$ patterns, it offers a metric that can be used to infer the resistance to dilution, similar to the information gained from the b-value in the power law. To refresh the reader's memory, a brief review of this unitless number will be provided as an extension of the Chapter 1 discussion. The D_a-number is a dimensionless quantity used to compare the rates of chemical reactions and fluid transport in a system. Calculating and interpreting the significance of this non-unique number has proven difficult. Two catchments may have the same D_a-number but very different τ_T or τ_R (equation 1.28). This implies that catchments will exhibit vastly different responses to variations in discharge or runoff (Ibarra et al., 2016).

Other potential pitfalls that can be deduced from literature include limitations in accuracy, where the D_a-number may not reflect the actual time scales of reaction and transport processes in a system; the non-homogeneous nature of natural systems and the D_a-number's applicability, as the ratio can only be applied to homogeneous systems with constant reaction rates. The D_a-number must be calculated using knowledge of the system's reaction rate, fluid velocity, and spatial scale. The accuracy of the D_a-number depends a lot on how accurate these input parameters are, which may be unknown or hard to measure in some systems. To account for temporal and spatial variability of these parameters, three potential permutations of the approach can be applied. The first is to calculate instantaneous D_a-numbers by calculating the reaction time scale to fluid transport time scale ratio at a given point in the system. This approach would probably render a result analogue to TTD's, where a distribution of these instantaneous D_a-number is obtained, that will most probably vary with time. The second approach involves spatially averaging the D_a-number, which is the ratio of the reaction time scale to the fluid transport time scale, over the entire system while taking into account the spatial distribution of the concentration and fluid velocity fields. This approach would represent use cases where the chemical parameters associated with the reaction used in the calculation is uniformly distributed in the catchment and a mean transit time can accurately be assumed. The final approach averages the temporal effect, by accounting for the variable input of both water and reactants into the system over a period of time. D_a-numbers is calculated

incrementally over this time period and an average D_a-number is calculated for the time period.

Current approaches using $c - Q$ data in streams to calculate D_a-numbers such as the model proposed by Maher and Chamberlain (2014) may be subject to the pitfalls discussed above. The recent model proposed by Zhi et al. (2019) may be a potential solution to understanding which data in the $c - Q$ trends must be used to parameterize the model of Maher and Chamberlain (2014). Figure 6.2 show a brief comparison of the model of Zhi et al. (2019) compared to the power law approach. This model is very similar to what has been shown by Bouchez et al. (2017). Similar in concept to what is proposed by Zhi et al. (2019), Bouchez et al. (2017) demonstrated that the b value in a $c - Q$ power law relationship can be estimated based on the combination of two sources. They exemplified this through the mixing of two hypothetical tributaries at a confluence point. The authors could also show the offset in timing of the peak in discharge between these tow sources at the mixing point could explain hysteresis loops observed in $c - Q$ patterns for a conservative tracer.

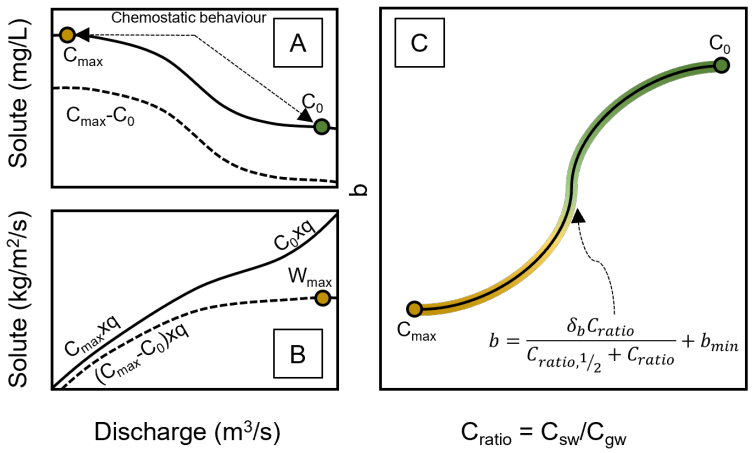

Figure 6.2: Schematic diagram comparing various modelling approaches. Figures A and B have been adapted from Ibarra et al. (2016). The illustration depicts a hypothetical $c - Q$ plot (solid line). The $c - Q$ relationship is corrected for atmospheric input (C_0) and represented by a dashed line. Figure B illustrates the export of solutes from the catchment. The dashed line denotes the solute load exported due to weathering, with W_{max} representing a plateau of the weathering flux due to the thermodynamic limit (Maher, 2011), with chemostatic behaviour indicated on A. Figure C (adapted from Zhi et al., 2019), illustrates the relationship between the power law exponent b and the ratio of groundwater to soil water concentration. The colour gradient depicting the mixing between these two endmembers.

The assumptions of "pure" endmembers (soil water and groundwater) must be valid for both approaches depicted in figure 6.2. But in reality, what is observed in streams are only near stream endmembers. The findings of Chapter 4 suggest that this assumption is not

always valid. The *WEC* flowline B (subgroup *C3.1*) includes both "unseen" and observable flowline endmembers (*C4*, *C6.2*, and *C6.3*). This implies that using subgroup *C3.1* for model fitting could lead to a biased understanding of the system, as it is hypothesised that flowline B (subgroup *C3.1*) would exhibit hysteresis behaviour due to differences in the contributions of the three assumed endmembers of flowline B.

Meybeck and Moatar (2012) proposed a method for segmenting $c - Q$ curves according to the stream's median flow (q_{50}). Thereby, the authors were able to define nine distinct $c - Q$ modalities. Using this method, Moatar et al. (2017) analysed long-term data from 293 monitoring stations in France. The authors discovered that 84% of all catchment-element combinations were chemodynamic (opposed to chemostatic, where the power law exponent is close to 0; Godsey et al., 2009) for at least 50% of the hydrographs, and 60% of combinations had nonlinear $c - Q$ curves. The manifestation of the controls (change in degree of contribution of endmembers to streamflow), on the b-value in the power law proposed by Zhi et al. (2019), is evident from the results of the two studies. Moatar et al. (2017) determined that two to three of the nine $c - Q$ modalities manifested for each parameter and were stable over time. The authors hypothesised that intrinsic and extrinsic elemental properties, such as solubility, reactivity, and source dynamics, are the primary determinants of the basic $c - Q$ template for each parameter. Chemodynamic behaviour can manifest as "flat," "up," and "down" trends (Godsey et al., 2009; Moatar et al., 2017). An increase in concentration with discharge (up) may indicate that the stream becomes hydraulically connected to areas that store water with a higher solute concentration. Decreasing concentration with discharge (down) may indicate flushing, in which the rate of removal exceeds the rate of solute release (source limited; Meybeck and Moatar, 2012). Lastly, "flat" behaviour may imply that the source is uniformly distributed, i.e., there is no significant difference in the different endmembers that control the system.

Figure 6.3 depicts the $c - Q$ patterns (log-log plot) for *SW1*'s major cations, anions (excluding alkalinity) and *DOC*. The classified data (subgroups) from the *HCA* step are superimposed on the plot. In cases where there was no inflection in the $c - Q$ trend, the total dataset's linear regression line (black line) is displayed. In cases where an inflection was observed, the regression lines of subgroups *C3.1* and *C6.3* are depicted (the colour of the line corresponds to the subgroup's legend color). The metrics of the regression is shown in table 6.2. The concentration of Ca^{2+} decreased with increasing discharge, corresponding to a type I modality (Meybeck and Moatar, 2012). Moatar et al. (2017) found that 26% of catchments in their study showed this $c-Q$ pattern. Given the acid-base titration behaviour described in Chapter 5, this would make sense. Due to the dissolution of carbonate minerals, Ca^{2+} concentration rises with increasing depth. During periods of low flow, Ca^{2+} concentrations will be higher, and vice versa. Na^{+} is the only major cation exhibiting a $c - Q$ curve with an inflection. This behaviour is intriguing and may suggest that the source of Na^{+} is controlled by primary weathering, as suggested by the flushing of

Na^+ observed in the trend of subgroup *C3.1*. Uncertainty remains regarding the primary control of Na^+ in the system. The main uncertainty lies in quantifying how much of the Na^+ is originating from primary mineral weathering and how much is dynamically released from the catchment's exchange complex. Furthermore can this exchange complex be assumed to be constant in composition over time?

The $c-Q$ patterns of redox-sensitive species (DOC and NO_3^-) are distinguishably distinct. According to Meybeck and Moatar (2012), DOC exhibits a F type modality, where at low flow the concentration of DOC does not change with discharge until an inflection point is reached (subgroup *C6.3* becomes dominant). When the inflection point in the trend is reach, DOC concentration decrease with discharge. NO_3^-, on the other hand, exhibits a concentration increase with discharge up until the inflection point, after which there is still an increase, albeit with a smaller gradient. SO_4^{2-} appears to exhibit a type D modality in which the concentration of SO_4^{2-} remains constant until subgroup *C6.3* becomes dominant, after which a concentration increase is observed. Close to half (48%) of the cases studied by Moatar et al. (2017) revealed this behaviour. The $c-Q$ pattern of SO_4^{2-} could be explained by the thesis's assumption that the majority of SO_4^{2-} in the catchment originates from the surface and given that the highest $S\%$ (figure B.2) is observed in the litter, the increasing concentration of SO_4^{2-} with high discharge will make sense as flowlines in shallow horizons extend upward into the catchment. The $c-Q$ pattern of Cl^- appears to be "flat", which would make sense given the fact that this solute will be distributed relatively homogeneously over the catchment and any chemical alterations will occur in the soil, which is also assumed to be homogeneous across the whole catchment.

The preceding discussion was not intended to present additional results regarding the potential hydro-biogeochemical functioning of the system, but rather to illustrate the potential error that can be made by relying solely on stream water chemistry. Conclusions drawn from the change in slope (b) in regression lines of $c-Q$ patterns may not reflect the whole truth. Given that the latter behaviour is caused by variations in permeability with depth (Xiao et al., 2021), one could argue that this behaviour is not unique to the *WEC*. Therefore, it is essential to identify the endmembers of near-stream endmembers.

Table 6.2: $c-Q$ regression line information related to figure 6.3.

Parameter	Total dataset			C3.1			C6.3			Chemodynamic
(mg/L)	R^2	b	*p-value*	R^2	b	*p-value*	R^2	b	*p-value*	behaviour
Ca^{2+}	0.613	-0.126	<2.2E-16	0.562	-0.125	<2.2E-16	0.147	-0.052	7.75E-06	Down
Mg^{2+}	0.341	-0.055	<2.2E-16	0.373	-0.057	3.04E-11	0.003	0.005	5.12E-01	Down
K^+	0.102	-0.096	1.23E-08	0.000	0.003	9.06E-01	0.023	0.058	8.47E-02	Flat
Na^+	0.376	-0.068	<2.2E-16	0.597	-0.065	<2.2E-16	0.012	-0.006	2.28E-01	Down/Flat
DOC^*	0.209	-0.146	6.63E-14	0.025	-0.048	1.34E-01	0.190	-0.233	3.12E-07	Flat/Down
Cl^-	0.069	-0.029	3.62E-06	0.190	-0.043	7.94E-06	0.102	0.039	2.45E-04	Flat
NO_3^-	0.216	0.250	<2.2E-16	0.489	0.520	1.69E-15	0.303	0.312	1.71E-11	Up/Up
SO_4^{2-}	0.003	0.007	3.12E-01	0.017	0.010	2.09E-01	0.201	0.054	1.14E-07	Flat/Up

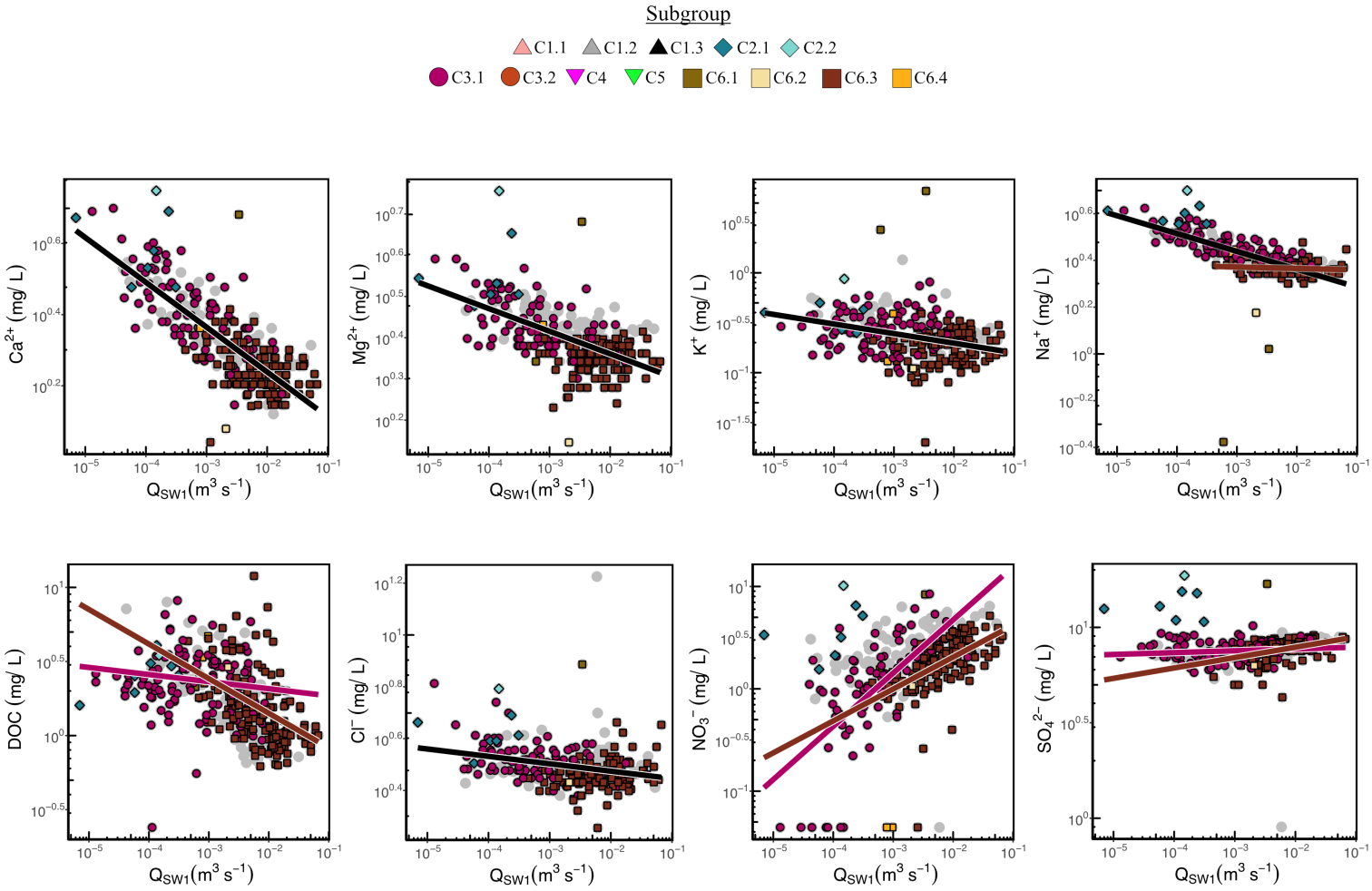

Figure 6.3: $c - Q$ on a log-log scale for the total bi-weekly dataset (grey) and the labelled data from SW1 (from Chapter 4). Regression lines are shown for the total dataset (in black) and for subsets *C3.1* and *C6.3* (in colored lines), providing a visual comparison of the relationship between concentration and discharge between the subgroups.

Potential of data driven models

The main question now is what to make of this classified dataset? How can the work that has been presented in this thesis aid in future research? To open a potential door for the future, a Random Forest (*RM*) model was trained on the labelled dataset and tested on an unseen dataset comprising of 27 flood events recorded over the last two decades in the *WEC*. The purpose of the exercise was to see if this method could be used to classify future samples.

One of the big attractions of using machine learning (*ML*) in catchment studies is its ability to identify the most important variables that influence water chemistry, streamflow generation, and weathering. For example, using *RM* or support vector machine (*SVM*) algorithms, researchers can identify the main drivers of water chemistry (Jadhav et al., 2015; Sakaa et al., 2022),and predict streamflow generation (Peng et al., 2020; Hagen et al., 2021; Sahraei et al., 2021) with good accuracy. Another advantage of using *ML* algorithms is that it can handle non-linear relationships between variables, which are often present in catchment studies. Nonlinear storage-discharge relationships (Botter et al., 2009; Kirchner, 2009), and nonlinearity in response to a threshold value (D'Amario et al., 2019), are two examples.

Even though the use of *ML* algorithms in forested catchment studies has become more prevalent, several limitations remain. The first and most obvious concern is data quality. The quality of the model is only as good as the data used to train it. Catchments are complex systems, and a multidisciplinary approach is required to comprehend them, as demonstrated by all recent review articles on the critical zone (Li et al., 2021; Benettin et al., 2022). Numerous data sets may lack information on processes that interact with the parameters a researcher wishes to investigate. In addition, there is no clear method for selecting the optimal *ML* algorithm, and different algorithms may produce varying results. As physically-based models, *ML* models are susceptible to overfitting. This defeats the purpose of the exercise, as *ML* models are typically employed to determine which parameters are driving processes of interest. The lack of physical comprehension provided by these models is most likely the method's most criticised aspect.

Despite these limitations, *ML* models can aid in the analysis or comprehension of catchments. A brief initial result of applying a *RM* model to the dataset created for this thesis will be presented in figure 6.4 and 6.3. A time series of *SW1* discharge measurements taken at 15-minute intervals over the past two decades is depicted in the figure. The 27 flood events are also represented by different-coloured markers on the graph. These markers correspond to the classification of the *RM* classifier, which was used to classify flood events according to their chemical characteristics. In terms of the relative contributions of flowlines C and B, a classifier enables a more in-depth understanding of the flood events. Appendix C provides a magnified view of every individual flood.

Figure 6.5 presents the $c - Q$ patterns of several water quality parameters (Ca^{2+}, Mg^{2+}, K^{+}, Na^{+}, SiO_2, Cl^{-}, NO_3^{-}, and SO_4^{2-}) on a log-log scale. The total biweekly data for the *SW1* is plotted, providing an overview of the typical concentration-discharge relationships for each parameter. Overlain on the plots are the labelled data from 27 flood events, which highlight the changes in water quality during these events. It is interesting to observe that mainly two subgroups (*C3.1* and *C6.3*) are observed in the biweekly data of *SW1*. The presence of subgroup *C5* is also observed in the flood data. This is intriguing because it appears that this subgroup is an endmember in terms of the *EMMA* framework (figure 4.2). This subgroup, however, is mostly found in *GW1*, which is located on the primary plateau and is relatively far from the stream (figure 2.1). In some cases, the subgroup was also observed in riparian samples. The potential for explaining hysteresis behaviour in the stream is the final thought on these preliminary results. Appendix C (figure C.8) contains an enlarged version of the NO_3^{-} $c - Q$ plot. It is clear that subgroup *C3.1* exhibits a potential hysteresis trend. In the closing remarks of this thesis, the potential significance of this trend will be discussed in the future on the subject of $c - Q$ patterns in catchments.

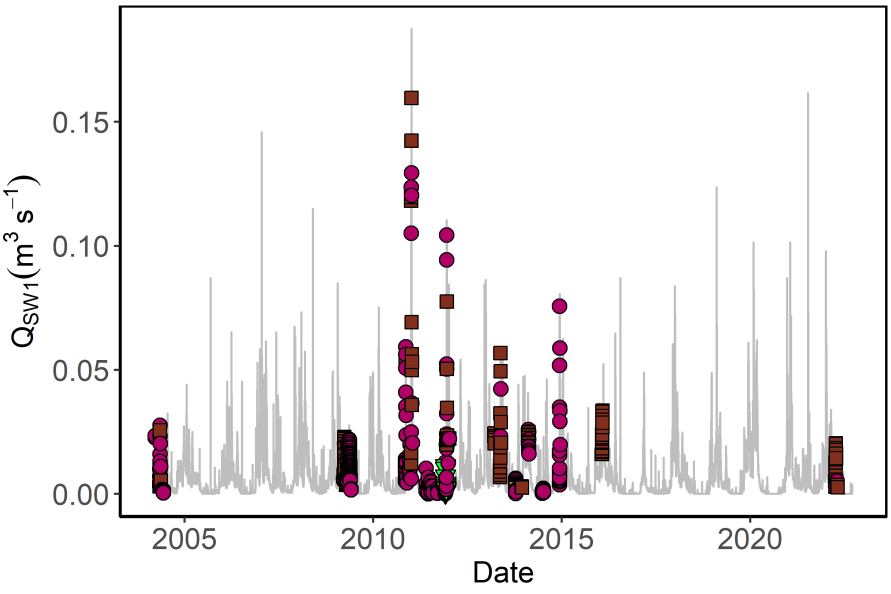

Figure 6.4: Time series of discharge at *SW1* from 2004 to 2022. The water samples that were collected throughout the 27 flood events and labelled with a Random Forest classifier are overlaid with the sample times that they were collected. Appendix C contains a zoomed-in view of each individual flood's time series trend.

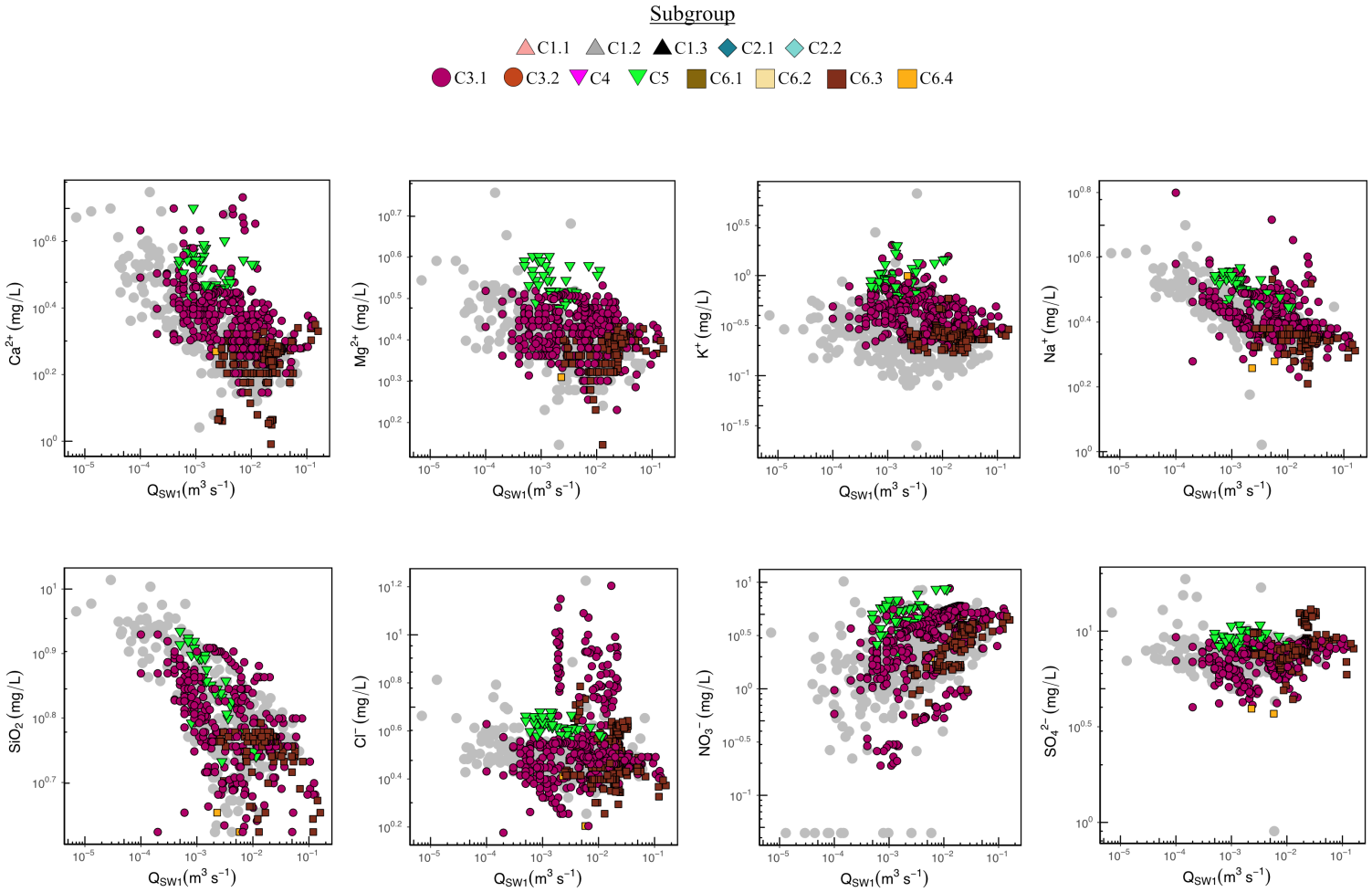

Figure 6.5: $c - Q$ plot on a log-log scale for the total bi-weekly dataset of *SW1* (grey) and the labelled data from the 27 flood events (classified using the Random Forest model trained on the dataset developed in Chapter 4).

6.2 Conclusion

The purpose of this chapter was not to present more results regarding the main body of work of the thesis, but rather to give the reader a sense of the applicability of the results of the study. Preliminary results were presented that will be used to pose a new hypothesis about potential controls on the power law slope (b) in forested headwater catchments and avenues of research to go about to test this hypothesis with the dataset developed in this work.

A few brief points about this chapter will just be re-iterated for the sake of clarity. The first is the significance of hysteresis loops on our understanding of concentration discharge behaviour. Hysteresis loops in concentration-discharge patterns in streams occur when the relationship between stream discharge and chemical concentration deviates from linearity. In the context of the discussion this would represent the inflection point in the $c - Q$ curve. This deviation can suggest that the catchment is undergoing non-linear processes such as retention and release of solutes from soils or changes in the sources of water to the stream. Hysteresis loops can also indicate the presence of different hydrologic pathways and mixing of waters in the catchment as shown in the study Bouchez et al. (2017). This phenomenon was not evident in the bi-weekly $c - Q$ trends, but it may appear in the high-frequency observations collected during the flood event. This raises two crucial questions: Are the b values calculated by fitting bi-weekly $c - Q$ patterns truly reflecting the chemical behavior of parameters, or are they simply reflecting the interplay of contributions from unseen flowlines to near-stream endmembers? Additionally, is the assumption that the stream is fed by groundwater during low flow conditions accurate? The bi-weekly sampling never captures the full range of discharge variability and mostly measures low flows, whereas the flood events reveal chemical signatures associated with shallow water stores and flowlines.

This question has bearing on how we interpret $c - Q$ patterns and how we go about parameterizing models to calculate D_a-numbers. With the most significant implication being that we may assume that a chemical element may present chemodynamic behaviour (Moatar et al., 2017), where in actuality it may just be attributed to flowlines mixing within the catchment.

Chapter 7

General conclusion

7.1 General Conclusion

In this section, the aim is to provide a comprehensive overview of the key conclusions derived from the research presented in the thesis. The work presented here represents the product of many years' worth of laborious effort put in by researchers who came before it. This including an extensive bi-weekly hydrochemical monitoring campaign spanning over a decade in the *WEC*. The study also benefited greatly from various other datasets generated by researchers working on complementary subjects within the catchment. This wealth of data and information provided a solid foundation for the analysis and conclusions drawn in the thesis.

The study was initially aimed at providing more quantitative results regarding the biogeochemical functioning of the system. However, it was soon realized that a qualitative understanding of the system was necessary before more quantifiable results could be obtained. While the results of this study are a step forward in understanding the critical zone and its processes, it should be seen as a starting point for further research. It is my hope that the work presented in this thesis will provide a framework for future researchers to build upon, leading to more in-depth and quantitative insights into the biogeochemical functioning of the system.

7.2 Main findings

The study's main findings will be presented sequentially, following the structure and workflow outlined in the thesis. The results will be presented in accordance with the steps and processes described in the methodology section, allowing for a clear and concise discussion of the findings and their relevance to the research questions and objectives. This method will provide a logical and organised overview of the results, making it easier for the reader to follow the study's progress and comprehend the significance of the findings. The focus will be on the progression of the research and the conclusions that can be drawn from the data, rather than on individual pieces of information in isolation, by presenting the results in this manner.

7.2.1 *WEC* Database

In this step of the workflow, a dataset of over 10 years of hydrochemical monitoring data was collated into a database. This database provided a comprehensive initial understanding of the water quality temporally and spatially (figure 2.6). The database comprises of groundwater, stream water, throughfall, soil water, and rainwater samples, totalling over 5000 observations at the time of writing. Of these observations, over half have complete sets of observations for major cations, major anions, and SiO_2. The database is comprehensive, including 70 variables for sample sites spread across the catchment. The large number of

observations and the breadth of the variables included provide a thorough representation of the water quality in the catchment and serve as a valuable resource for further research and analysis. This dataset will be published soon after the PhD defence as geodatabase paper. This will allow to open it to additional research questions that could come from abroad.

7.2.2 *WEC* Weekly monitoring dataset

A one-year monitoring campaign was conducted to collect data on four physical parameters, which include electrical conductivity (EC), dissolved oxygen (DO), pH, and oxidation-reduction potential (ORP), from a total of 10 sample points (9 boreholes and one stream water sample point). Trends in dissolved oxygen and redox potential (ORP) over time provided valuable insight into the processes controlling redox conditions in the groundwater. The collection of water samples at each monitoring point added another dimension to the analysis, and the combination of physical parameters and water samples contributed to the development of a detailed picture of the water quality dynamics in the system. This monitoring effort has yielded a wealth of data that provides a deeper understanding of the processes controlling the system's redox zonation.

7.2.3 Multivariate analysis

Chapter 4 of the thesis presents the results of classifying a subset of the total database (2583 observations) of groundwater, stream water, and riparian water using hierarchical clustering analysis (HCA). Initially, 6 main clusters were observed with the HCA, but these clusters were further divided into 13 subclusters (referred to as subgroups in the thesis) through further analysis. A principal component analysis (PCA) was then conducted on the labelled data to assess if potential endmembers could be identified in accordance with the method used in end-member mixing analysis ($EMMA$). Geochemical graphical techniques were used to interpret the trends observed in these subgroups. The results showed that HCA was able to identify flowlines and water stores (in this thesis both are referred to as endmembers) with chemically unique signatures. This led to an update of the current conceptual hydrological model of the system and new insight into the hydrological mechanism connecting the plateau to the stream during. The most significant result of this chapter is that groundwater data revealed the presence of unseen endmembers (flowlines) which play a large role in the variance observed in near-stream endmembers.

7.2.4 Geochemical numerical modelling

In **Chapter 5**, the numerical geochemical code PHREEQC was utilized to identify the mineral phases controlling the chemical signature of each subgroup from Chapter 4. The redox condition was defined by analysing the time series data from a year-long weekly monitoring campaign, which showed that $O_{2(aq)}/H_2O$ -redox couple, with only two

subgroups displaying weakly reducing behaviour due to the oxidation of *DOC*. PHREEQC was used to create over 2,000 speciation models based on major cations and anions, as well as 800 additional models that incorporated additional chemical parameters such as *Mn*, *Ba*, *Al*, and *Fe*. The saturation indices calculated by PHREEQC were used to determine potential mineral phases that could be controlling the mobility of solutes of interest or also called natural tracers. A forward-inverse modelling approach was then applied to test the hypothesis that the oxidation of *DOC* is the main driver of Ca^{2+} mobility in the system. The models provided sufficient evidence in favour of this hypothesis; thus, it was not rejected. However, the hypothesis regarding the source of SO_4^{2-} in the system could not be supported or rejected due to the limited ability of the model to explain the source in the shallow horizons of the regolith.

7.2.5 Proof of concept

Chapter 6 provides a proof of concept that subgroups identified in Chapter 4 are in line with the conceptual hydrological understanding of the system and can accurately predict $c - Q$ inflection patterns. A Random Forest model was trained on the Chapter 4 dataset, achieving 93% accuracy on the test dataset. The model was used to classify over 600 chemical analysis sets collected during 27 flood events over two decades in the *WEC*. The results showed that a subgroup (*C5*) associated with shallow groundwater on the plateau and the riparian water can be observed in the stream during specific events, which was not observable on bi-weekly timescale. The results also provided evidence that the chemical variance in the near-stream endmember during dry conditions could be explained by mixing of flowlines, suggesting that chemical parameters perceived to vary due to chemical processes may only vary due to the mixing of unseen flowlines.

7.3 Novelty of the study

The study presented in this thesis offers important insights for those seeking to study the Critical Zone. Two key takeaways are highlighted.

Firstly, we provide a thorough dataset that spans a long period of time, but only touch on the surface of its potential by using basic chemical parameters. One criticism of machine learning algorithms is their lack of process-based understanding they provide, but in this thesis, we take a step forward in exploring the underlying trends of the data. This dataset can be further enhanced by incorporating various physical parameters relevant to hydrology, thus enabling the use of both data-driven and physically-based models to test new theories in the *WEC* critical zone in the future.

Secondly, the thesis proposes a potential approach for testing geochemical hypotheses in the *WEC*. Although the modelling approach is not new, applying it to improve our

understanding of biogeochemical processes in the *WEC* provides an additional means to comprehend the coupled nature of reaction and transport processes.

7.4 Potential future research

Perhaps a fitting way to conclude this thesis is not with an epilogue or satisfactory ending where all the readers' questions are addressed, but rather stating a slightly altered version of the "shallow and deep hypothesis" (Stewart et al., 2022). The results presented in this thesis would suggest that there are mainly two potential controls on the power law slope (b). Thus the following hypothesis is posed:

"Vertical Connectivity is the primary control on the power law slope (b) in c-Q patterns, a secondary control is the extent of occurrence of saprolite in a catchment, and the storage capacity associated with it. Hysteresis loops observed in streams can be linked to the dynamic change in relative contribution of the water stored in the saprolite due to hydrological conditions."

In order to test the hypothesis, the extent of uncertainty of biogeochemical processes active in the shallow flowlines must be quantified in more detail. In the past a tracer (commonly Na^+) or multiple normalizing ions was used to account for the variation in concentrations of solutes that was assumed to be geogenic (Ca^{2+} and Mg^{2+} for example). There are however several processes that may influence the concentration of such tracers. The first is what is deposited on the catchment surface, if these sources of atmospheric deposition (wet and dry) are not properly accounted for in weathering rate calculations, the results can be biased, leading to an overestimation or underestimation of the weathering rate. The *WEC* potentially can be used as a testbed. During the chemical analysis, trends in anions where observed that could potentially be attributed to differences in vegetation spatially. This was not investigated further but does merit a closer look.

The following step is to define the capacity of the shallow system to store these elements and to understand to what extent the concentrations of solutes may vary due to this storage. When analysing $c - Q$ patterns in forested headwater catchments, it is vital to understand the dynamics of cation and anion exchange in soil. These processes have the potential to influence the soil's ability to retain these tracers to such an extent that it influences our interpretation of $c - Q$ patterns. These processes affect the chemical composition of groundwater and surface water runoff, which in turn impacts the chemical signature of water as a whole. When the soil becomes acidic, soils with a high cation exchange capacity are able to exchange cations, such as Ca^{2+}, Mg^{2+}, and Na^+, for other ones, such as hydrogen and aluminium. Anions, such as NO_3^- and SO_4^{2-}, are retained by soils through anion exchange processes. A deeper insight of these exchange dynamics can shed light on the effects of various land-use activities on the water quality of these systems. In the *WEC* the dominant source of SO_4^{2-} is still unclear, but some preliminary findings

may suggest that it could be linked to ion exchange in the soil. Given the behaviour of NO_3^- and SO_4^{2-} in the system, quantifying the relative importance of the dynamics of cation and anion exchange in soils are central to developing new theories on methodologies to calculate the D_a-number for example.

Moving deeper into the subsurface, saprolite storage can significantly affect $c-Q$ dynamics in streams because saprolite is a horizon that is rich in clay and minerals and acts as a long-term store of nutrients and solutes. The *WEC*'s unique composition of two landscape units, one containing saprolite (primary plateau) and the other not (secondary plateau), with a comparable vertical permeability, makes it an excellent experimental catchment to examine the impact of saprolite on $c-Q$ patterns. The presence of saprolite in a catchment can affect the timing and volume of water discharge into streams, which in turn can influence the concentration of solutes and nutrients in the stream water. The amount of water and nutrients released from saprolite storage into streams can vary depending on the soil conditions, precipitation patterns, and land-use activities in the catchment. For example, increased rainfall can lead to an increase in water discharge from saprolite storage, which can result in a pulse of high-concentration water in streams. This is potentially what is shown with the occurrence of subgroup *C4* in boreholes close to the footslope (*GW2* and *GW10*). This behaviour can also potentially be related to the critical storage threshold shown discussed by Martínez-Carreras et al. (2016). On the other hand, during dry conditions, reduced amounts of water are released from saprolite storage, leading to low-flow periods with reduced contribution from the primary plateau. This will cause flowline B to become chemically similar to flowline C, due to mixing of these two flowlines in the slope of the catchment. Understanding the role of saprolite storage in affecting concentration discharge dynamics is crucial for predicting and managing water quality in forested headwater catchments (Callahan et al., 2022).

I would like to conclude this thesis with an informal exchange I had with my supervisor Christophe Hissler several months before writing this conclusion. I believe this best describe my hopes for this work:

Me: *"Hi Christophe, I am just checking in. I have been reworking Chapter 1 to fit in with chapter 2. Both are now I would say a bit more coherent. I still need to add some stuff to really make the connection clear. As for the theory on EMMA, Da-numbers and c-Q relations in streams, I think I finally formed sound argument to unify all of these theories. I would really like to develop this concept in the framework of my thesis, as I did some preliminary analysis, and the results look promising. I foresee that I will not have time during my PhD to really proof all of the stuff I think is happening, but I believe this will lay the groundwork for PhD's to follow to really make a difference as the more I write the more I come to realise that the WEC is a truly unique opportunity to develop these integrated hydro-biogeochemical theories"*

Christophe Hissler: *"This last sentence should appear in the conclusion/perspective of the thesis"*

I have no illusions about the weaknesses of my thesis, and I wish I had more time to address them. My hope however is that I done enough to contribute in a small way to the advancement of the field of Critical Zone science.

Appendix A

Additional information about Chapter 2

A.1 Hydrochemical data

Table A.1: Hydrochemical data statistics of 10 year biweekly data set

Parameter	**Sample site**	GW1	GW2	GW3	GW5	GW6	GW7	GW8	GW9	GW10	GW11	GW12	riparian water	stream water
	sample number	176	82	251	256	176	94	167	117	79	73	80	222	810
Alkalinity (mEq/l)	Median	0.07	1.09	0.28	1.5	0.58	0.07	0.07	0.1	0.37	2.44	0.44	0.12	0.12
	Mean	0.13	0.84	0.33	1.44	0.69	0.14	0.11	0.15	0.85	2.34	0.87	0.16	0.15
	SD	0.19	0.56	0.22	0.8	0.46	0.17	0.12	0.17	0.71	0.5	0.85	0.15	0.13
units: (mg/l)														
SiO_2	Median	4.28	13.47	9.04	6.11	9.9	5.83	5.03	6.3	8.35	15.8	7.78	6.9	6.3
	Mean	4.43	11.6	9.05	6.27	9.62	6.21	5.23	6.41	9.23	15.65	9.5	6.99	6.47
	SD	0.95	4.02	0.82	1.11	1.75	1.41	0.84	0.79	2.43	2.05	4.09	1.59	1.15
Na^+	Median	3.3	3.8	5	3.3	5.4	2.3	1.9	2.2	2.95	7.5	2.8	2.29	2.3
	Mean	3.69	3.44	5.06	3.57	6.89	2.32	1.97	2.89	4.03	7.32	3.73	2.56	2.37
	SD	1.68	0.88	0.78	1.4	4.14	0.23	0.24	3.32	1.84	1.05	1.83	0.86	0.44
K^+	Median	0.63	0.36	0.43	0.35	0.48	0.19	0.13	0.13	0.24	0.54	0.25	0.18	0.21
	Mean	0.77	0.42	0.5	0.48	0.81	0.23	0.16	0.18	0.35	0.54	0.3	0.23	0.26
	SD	0.58	0.39	0.39	0.52	1.4	0.14	0.11	0.18	0.3	0.19	0.2	0.25	0.32
Mg^{2+}	Median	2.4	6	4	6.1	4.9	2.1	1.5	2	3.7	17.4	4.25	2.3	2.3
	Mean	2.3	4.99	4.16	7.59	5.65	2.13	1.52	2.23	6.25	16.59	7.34	2.75	2.4
	SD	0.68	2.14	1.36	4.32	2.85	0.51	0.23	0.81	4.19	2.9	5.46	1.69	0.45
Ca^{2+}	Median	3.3	12.1	7.06	20.7	12.8	1.3	0.7	1.6	3.8	21	4.2	1.9	1.6
	Mean	3.37	9.42	7.49	18.53	13.69	2.03	0.94	1.95	7.55	20	7.62	2.35	1.78
	SD	1.12	5.72	3.94	9.87	5.5	2.11	0.6	1.21	5.87	3.69	6.31	1.45	0.78
Cl^-	Median	3.8	2.8	5.1	3.7	5.24	3.3	3.3	2.7	2.7	3.1	2.7	2.6	2.8
	Mean	3.75	2.82	5.61	3.75	5.56	3.39	3.31	3.07	2.7	3.21	2.8	2.76	2.94
	SD	0.82	0.33	3.77	0.83	2.31	0.42	0.36	1.49	0.37	0.35	0.46	1.08	0.57
NO_3^-	Median	4.07	0.66	10.62	0.8	15.6	2.35	0.66	0.53	0.35	0.04	0.4	0.18	1.55
	Mean	4.04	1.1	11.52	1.76	18.32	2.52	0.9	0.69	0.32	0.14	0.44	1.89	1.74
	SD	2.28	1.67	5.76	2.38	10.4	1.52	0.67	1.09	0.2	0.23	0.65	5.3	1.24
SO_4^{2-}	Median	13.56	4.65	12.3	4.9	11.3	5.9	4.6	8.1	7.2	10	7.9	8.45	7.4
	Mean	12.96	5.23	12.18	5.6	11.78	6.42	4.4	8.64	7.13	9.86	7.13	10.71	7.45
	SD	3.55	2.01	1.79	2.79	3.13	2.54	1.14	2.22	0.87	1.24	2	11.67	1.54

Appendix B

Additional information about Chapter 4 & 5

B.1 Main hypothesis

The existing knowledge of the subsurface architecture of the WEC might be able to explain the high variance that was observed in some of the boreholes but not in others (figure 2.6). It is necessary to have a detailed conversation about drawdown curves while pumping in order to adequately explain this statement. The first person to mathematically describe the cone that forms in aquifers as a result of pumping was Theis (1935), who did so as follows:

$$s(r,t) = \frac{Q}{4\pi T} W(u) \tag{B.1}$$

where $s(r,t)$ is the drawdown at distance r at time t since the pumping of the borehole commenced. $Q[\frac{m^3}{t}]$ is the discharge rate and $W(u)$ is the well function of Theis. This function is dependent on two intrinsic properties of the aquifer, transmissivity and storativity respectively. Storativity (S) can be described as the additional release of water from storage due to an increase or decrease in hydraulic head, while transmissivity (T) is a function of the hydraulic conductivity of material ($T = conductivity \times auifer\ thickness$). Drawdown is proportional to the pumping rate, and inverse proportional to aquifer transmissivity and storativity (Cherry and Freeze, 1979).

Due to the variability in the depth of the weathered zone from the plateau to the stream, one can imagine that stratification in storage, storativity and transmissivity with depth will occur moving from the plateau to the stream. This will imply that when sampled, boreholes intercepting several flowlines will render a water sample that is a mixture of the respective flowlines, and the proportion of mixing will be a function of the shape of the cone of depression that will form due to pumping (figure B.1).

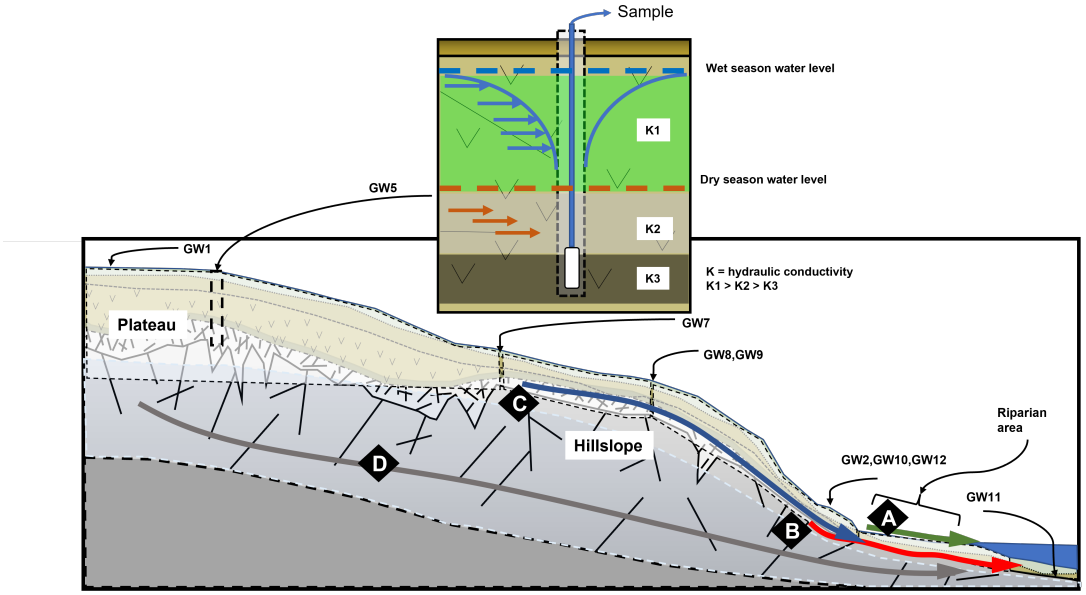

Figure B.1: The most recent iteration of the WEC's hydrological perceptual model (Rodriguez and Klaus, 2019). The figure is described in detail in Chapter 2. A depth profile of a borehole is represented by the diagram that can be found in the middle of the figure. The diagram illustrates how a cone of depression can develop as a result of prolonged abstraction. The cone of depression will play a role in determining the relative contributions of the stratified layers of water.

As discussed in Chapter 1, permeability variation with depth exerts a first-order control on vertical connectivity (VC). In the case where permeability decreases sharply with depth (vertical conductivity is low), more than 95% of the water flows through the top 6 metres of the subsurface and has negligible interaction with reactive rock (Xiao et al., 2021). This control causes a chemical contrast between shallow and deep water. Subsurface properties vary with depth, with shallow soils having generally higher permeability compared to unweathered bedrock (Welch and Allen, 2014). It is therefore highly likely that dominant flowlines can be observed from the *WEC*'s expansive data set by utilizing multivariate statistical techniques as discussed by Güler et al. (2002).

B.2 Calcium and Sulphate dynamics

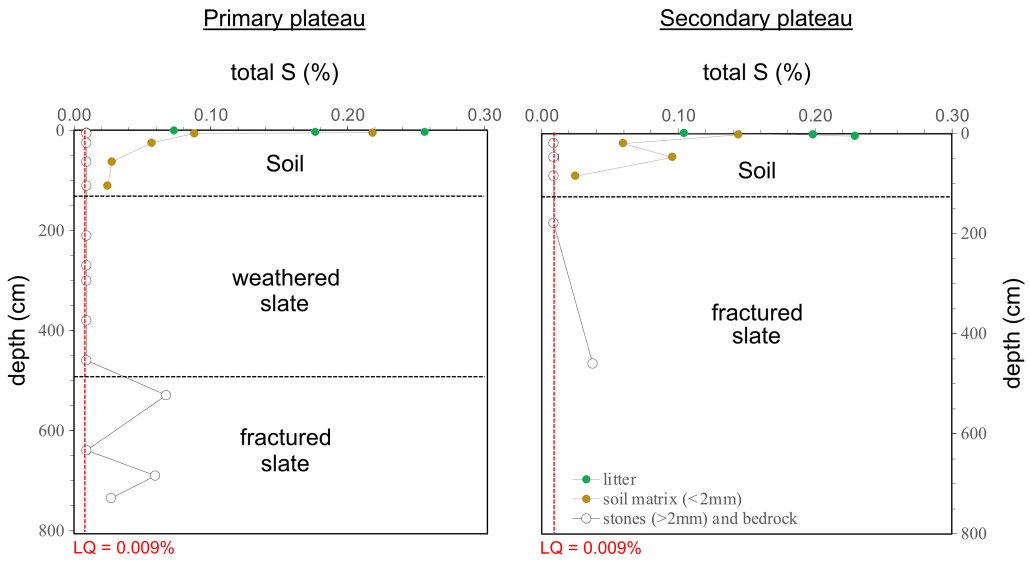

Figure B.2: The total percentage S concentration depth profile. Weathering profile 5 is located on the primary plateau (plot 7, close to $GW1$ and $GW5$). Weathering profile 6 is located on the secondary plateau (close to $GW6$).

B.3 Piper diagram of subgroups

The Piper diagram below presents the labeled data from Chapter 4. Additionally, enlargements of the two ion ternary diagrams are shown and compared to sample types. This including stream water, soil water, throughfall, and rainwater. These diagrams provide a visual representation of the chemical composition of the different sample types and subgroups and help to identify patterns and relationships among the various ions.

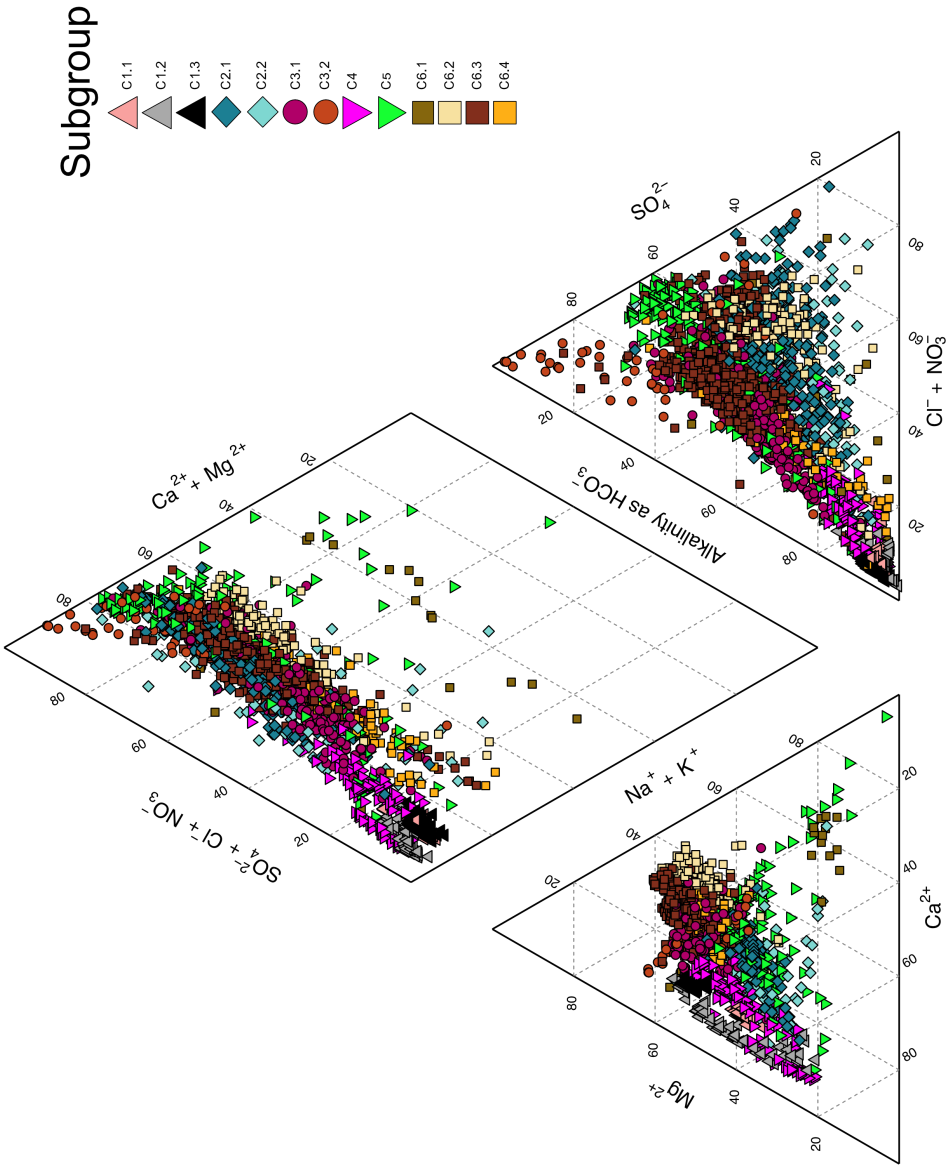

Figure B.3: Piper diagram depicting the subgroups identified in Chapter 4.

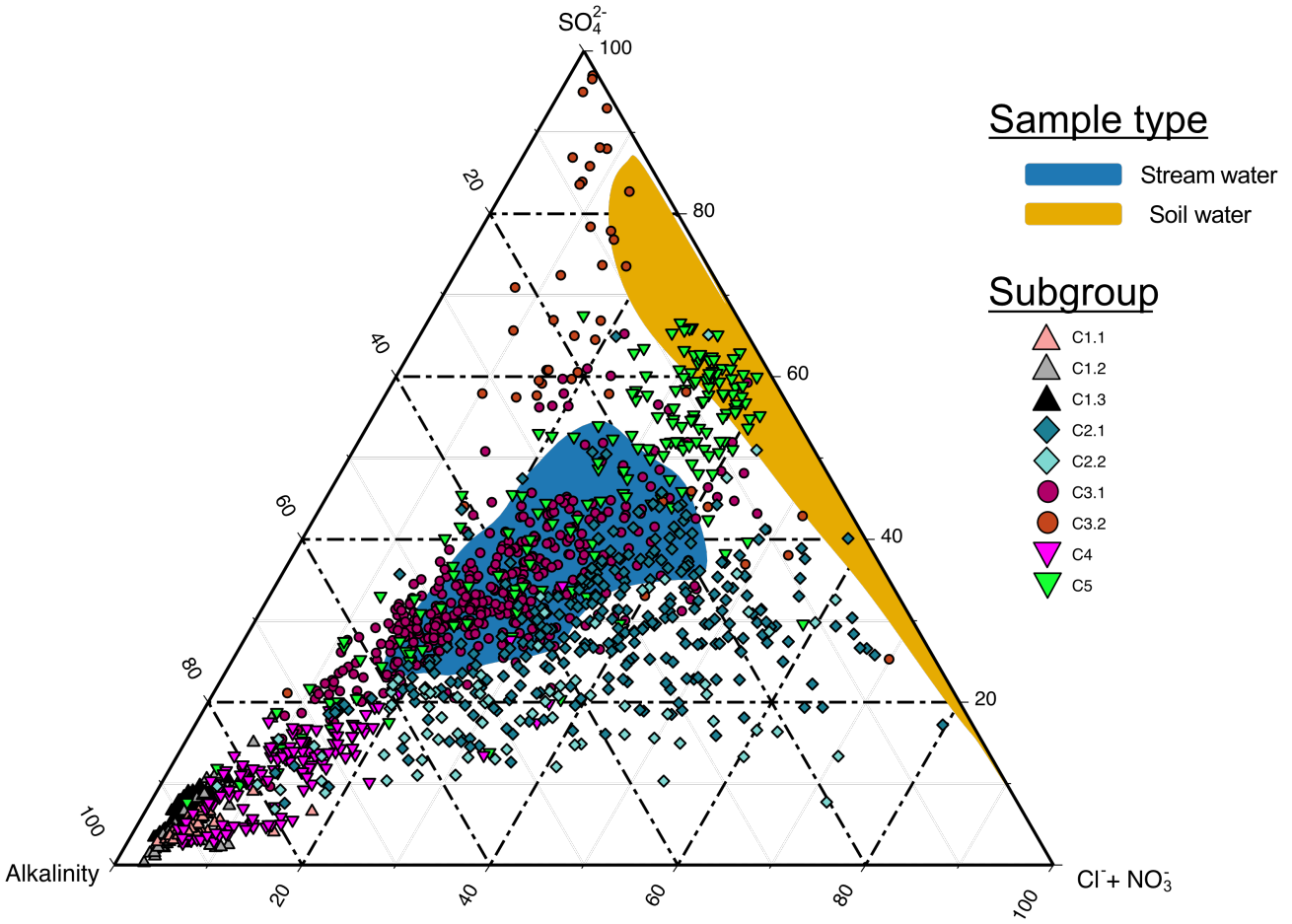

Figure B.4: Ternary diagram of anions identified in Chapter 4.

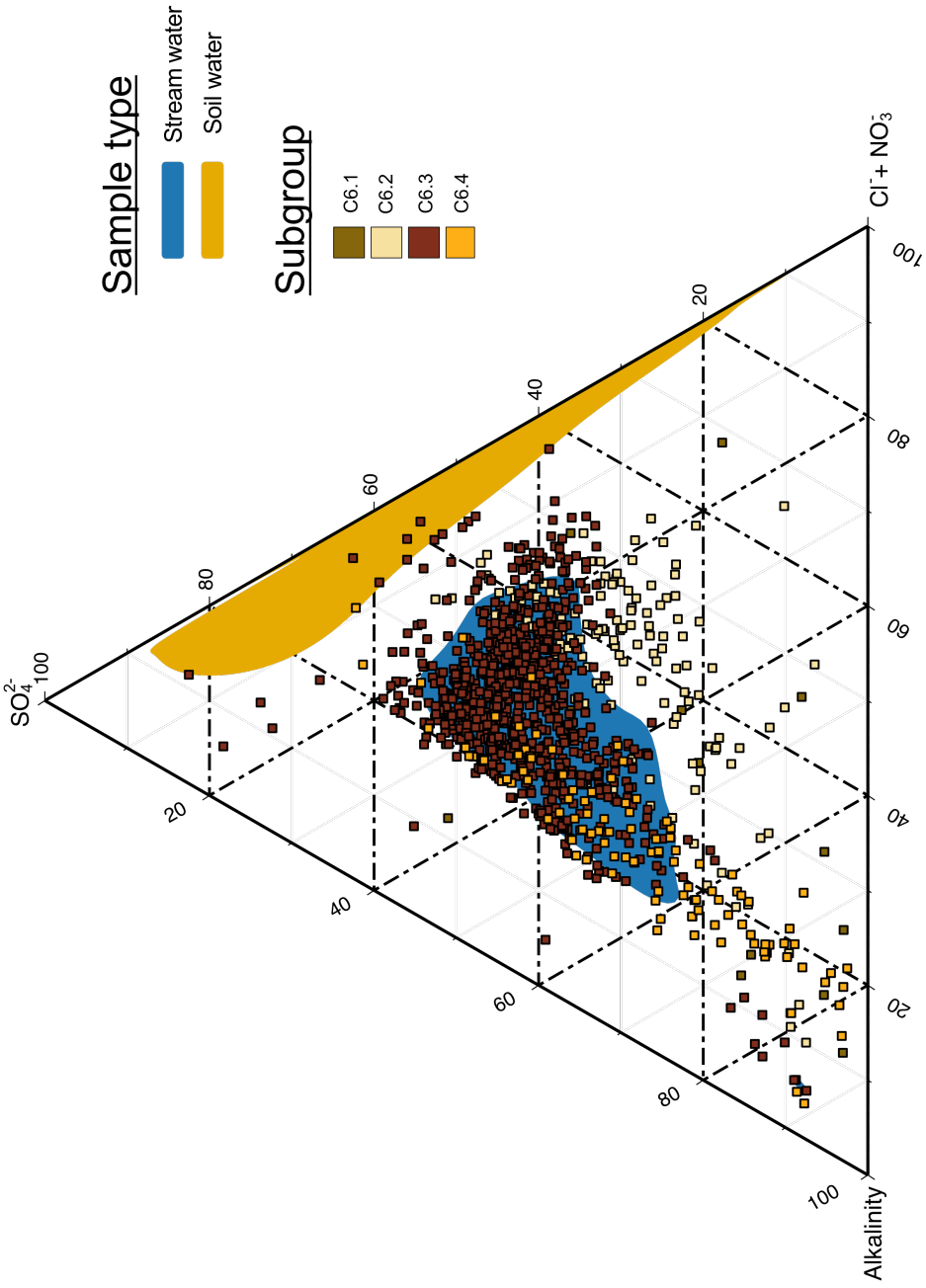

Figure B.5: Ternary diagram of anions identified in Chapter 4.

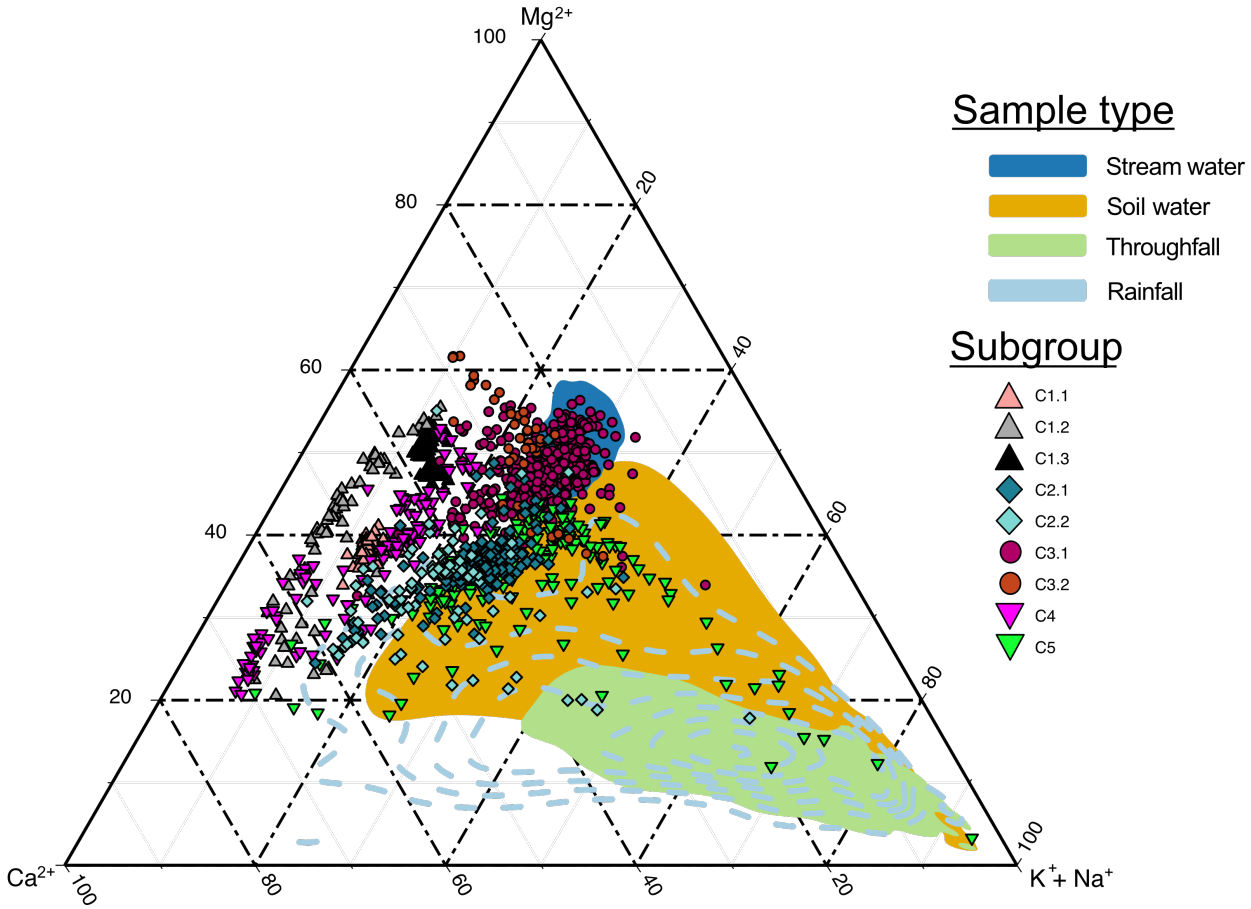

Figure B.6: Ternary diagram of cations identified in Chapter 4.

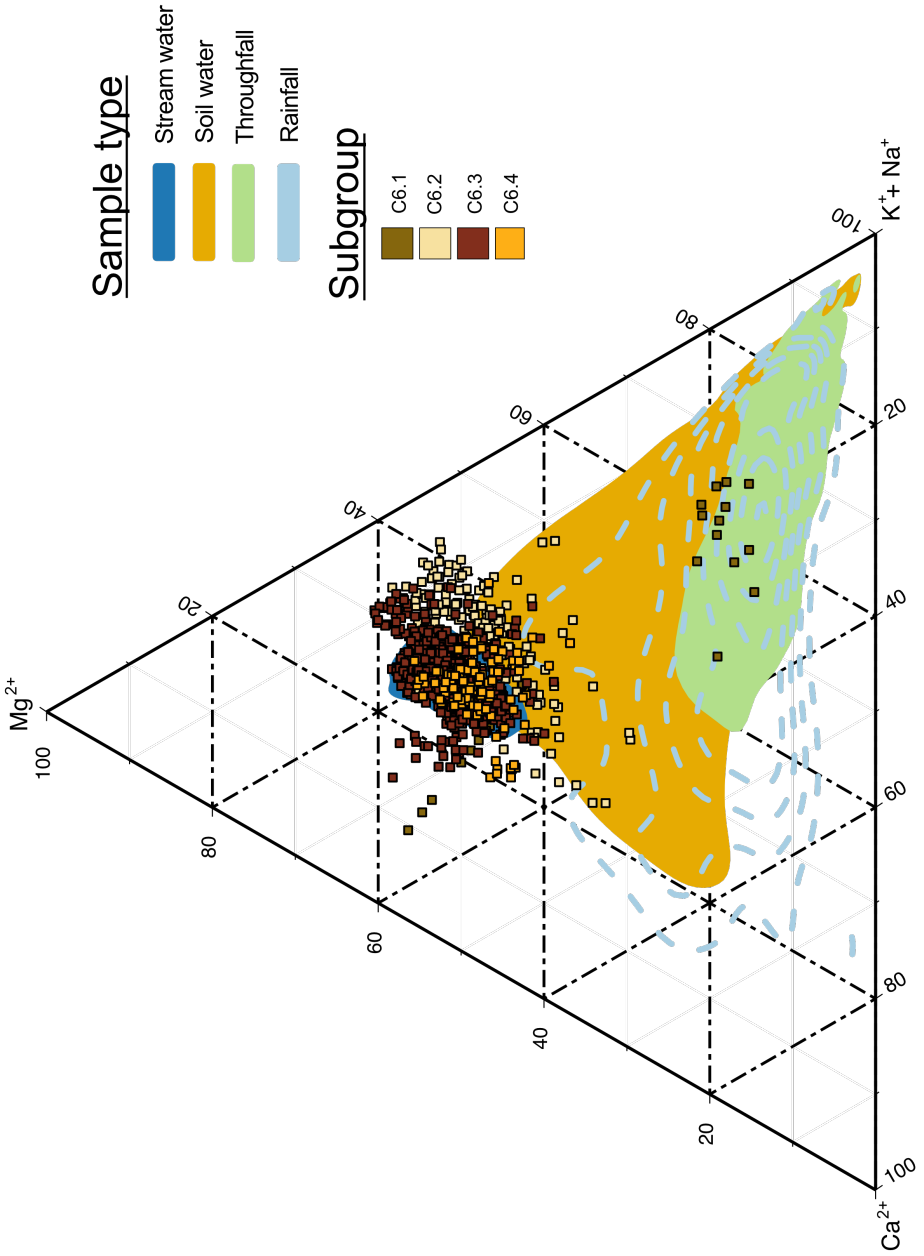

Figure B.7: Ternary diagram of cations identified in Chapter 4.

B.4 Weekly physical parameter measurements

The time series of the four physical parameters that was measured on a weekly basis is shown in the four figures below. Dissolved oxygen (DO), electrical conductivity (EC), redox potential (E_h), and pH) trends over the course of the one-year weekly sampling is shown for the 9 boreholes and *SW1*. A loess curve fit is also shown for boreholes that are associated with the different catchment landscape units and outlet (primary plateau, hillslope, and stream water). The study found that the sample site *GW11* has the lowest dissolved oxygen concentration. *GW1* and *GW5* exhibit a cyclic trend in their dissolved oxygen levels, which can be linked to input from recharge. The redox trends show two distinct signals, one of a reductive environment and one of a more variable oxic zone, which is consistent with the dissolved oxygen observations.

Figure B.8: Time series of the *DO* (*mg/L*) concentration for the 10 sample sites, with a loess curve fit superimposed to show trends. The figure highlights that the sample site *GW11* has the lowest dissolved oxygen concentration, while *GW1* and *GW5* show a cyclic trend that can be interpreted as input from recharge.

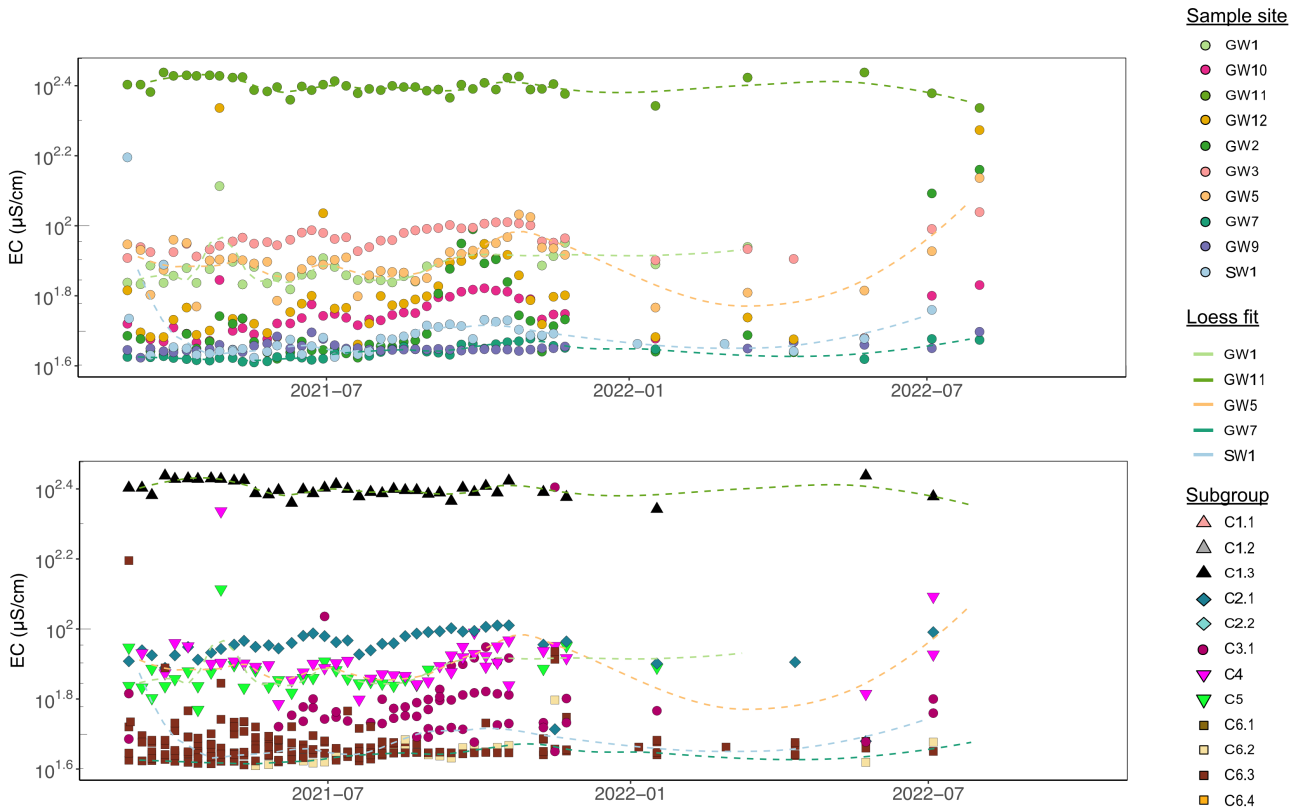

Figure B.9: Time series of the EC $(\mu S/cm)$ for the five sample sites, with a loess curve fit to highlight trends.

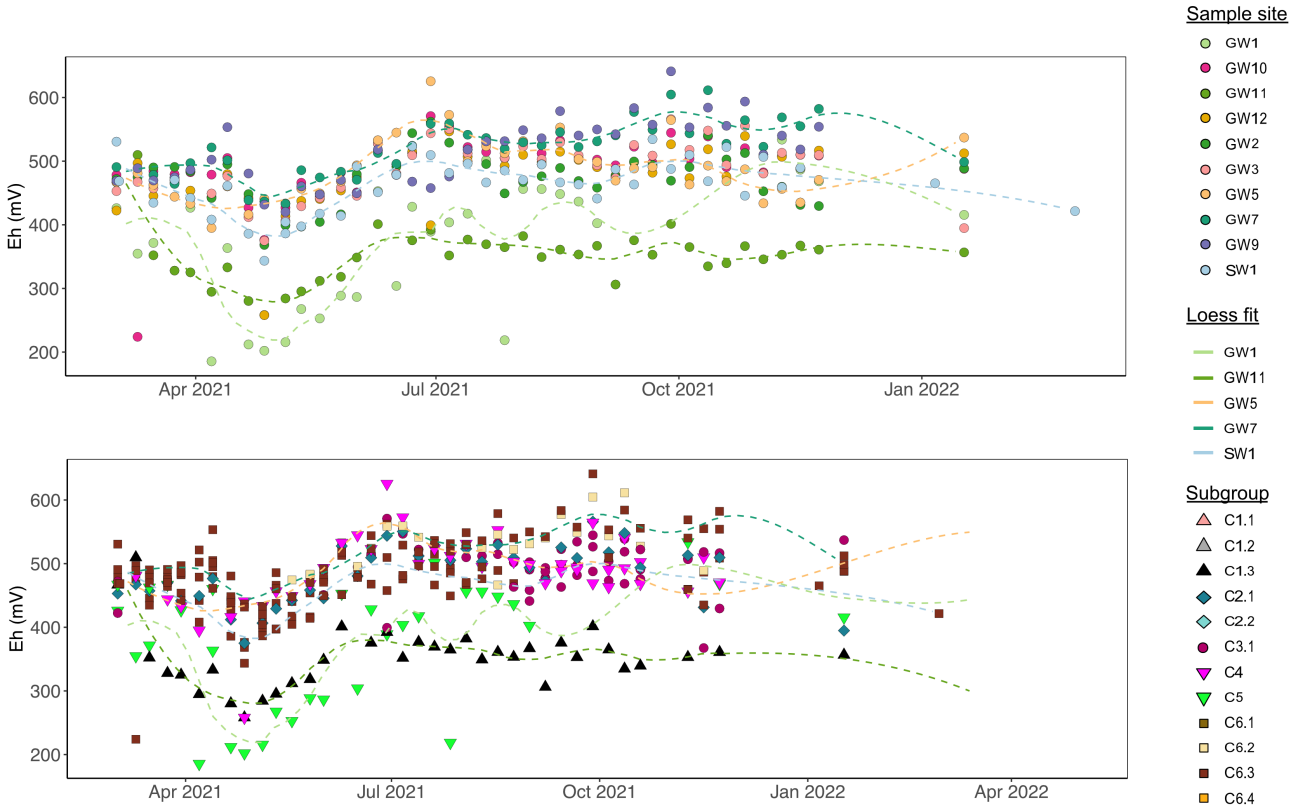

Figure B.10: Time series of the E_h (mg/L) for the 10 sample sites, with a loess curve fit to show trends. The figure highlights the two distinct signals present in the redox trends, one of a reductive environment and one of a more variable oxic zone.

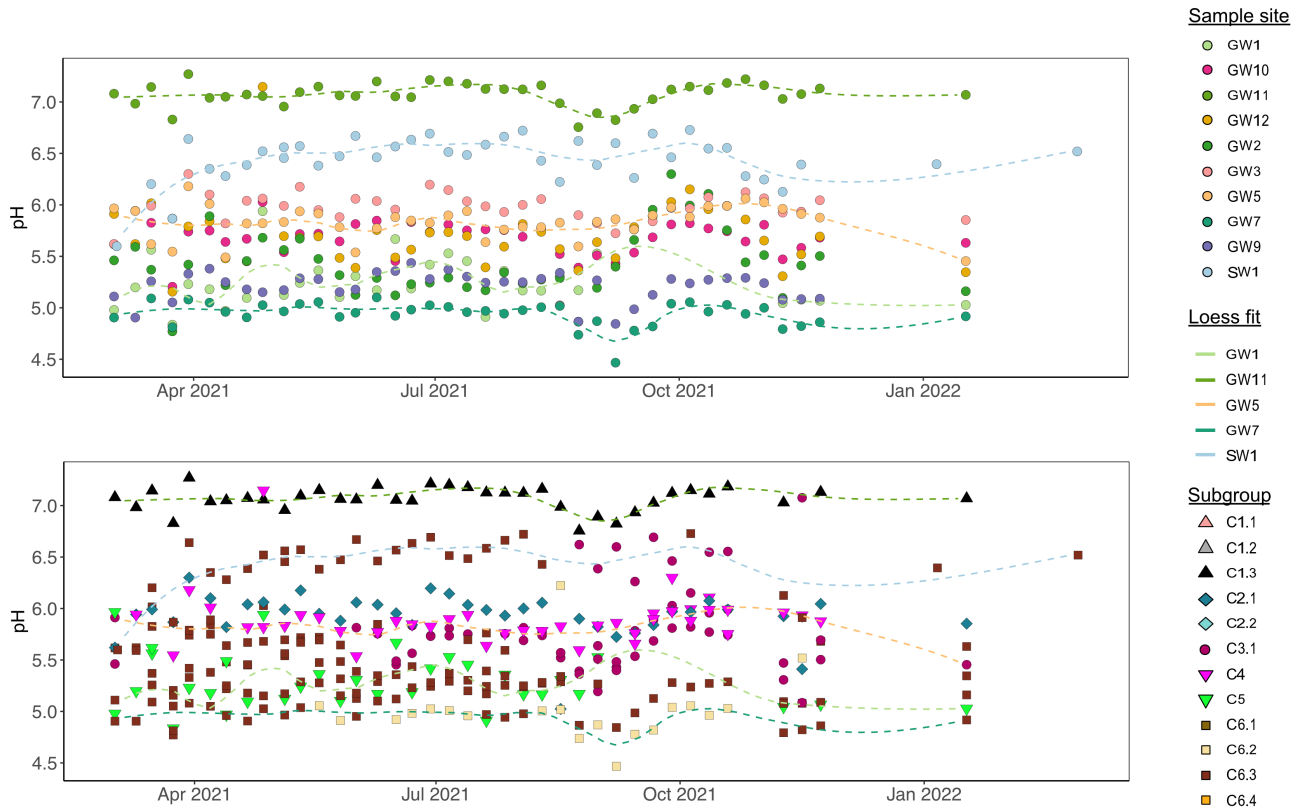

Figure B.11: Time series of the pH for the five sample sites, with a loess curve fit to display trends.

Appendix C

Additional information about Chapter 6

C.1 Random forest classifier metrics

A random forest machine learning model was developed in this study with an accuracy of 93%. The `randomForest` package in R was utilized with 500 trees and default settings, including a maximum of 2 variable splits. The model was trained using k-fold cross-validation with 5 folds and 3 repeats. The out-of-bag (OOB) estimate of error rate was 6.95%. The confusion matrix is shown below in table C.1.

Table C.1: Confusion matrix

Subgroup	*C1.1*	*C1.2*	*C1.3*	*C2.1*	*C2.2*	*C3.1*	*C3.2*	*C4*	*C5*	*C6.1*	*C6.2*	*C6.3*	*C6.4*	Error
C1.1	87	0	0	0	0	0	0	2	0	0	0	0	0	0.022
C1.2	0	46	1	0	2	0	0	1	0	0	0	0	0	0.080
C1.3	0	0	87	0	0	0	0	1	0	0	0	0	0	0.011
C2.1	0	0	0	197	3	0	0	0	6	0	0	0	0	0.044
C2.2	0	1	1	8	45	0	0	0	1	0	0	0	0	0.196
C3.1	0	0	0	0	0	261	0	3	2	0	1	21	0	0.094
C3.2	0	0	0	2	0	2	21	0	1	0	0	4	1	0.323
C4	1	0	0	0	0	3	0	89	0	0	0	0	0	0.043
C5	0	0	0	1	1	4	0	2	123	0	0	0	0	0.061
C6.1	0	0	0	0	0	0	0	2	4	10	0	0	2	0.444
C6.2	0	0	0	0	0	1	0	0	0	0	108	5	0	0.053
C6.3	0	0	0	0	0	22	1	0	0	0	3	546	2	0.049
C6.4	0	0	0	0	0	1	0	0	0	0	1	6	68	0.105

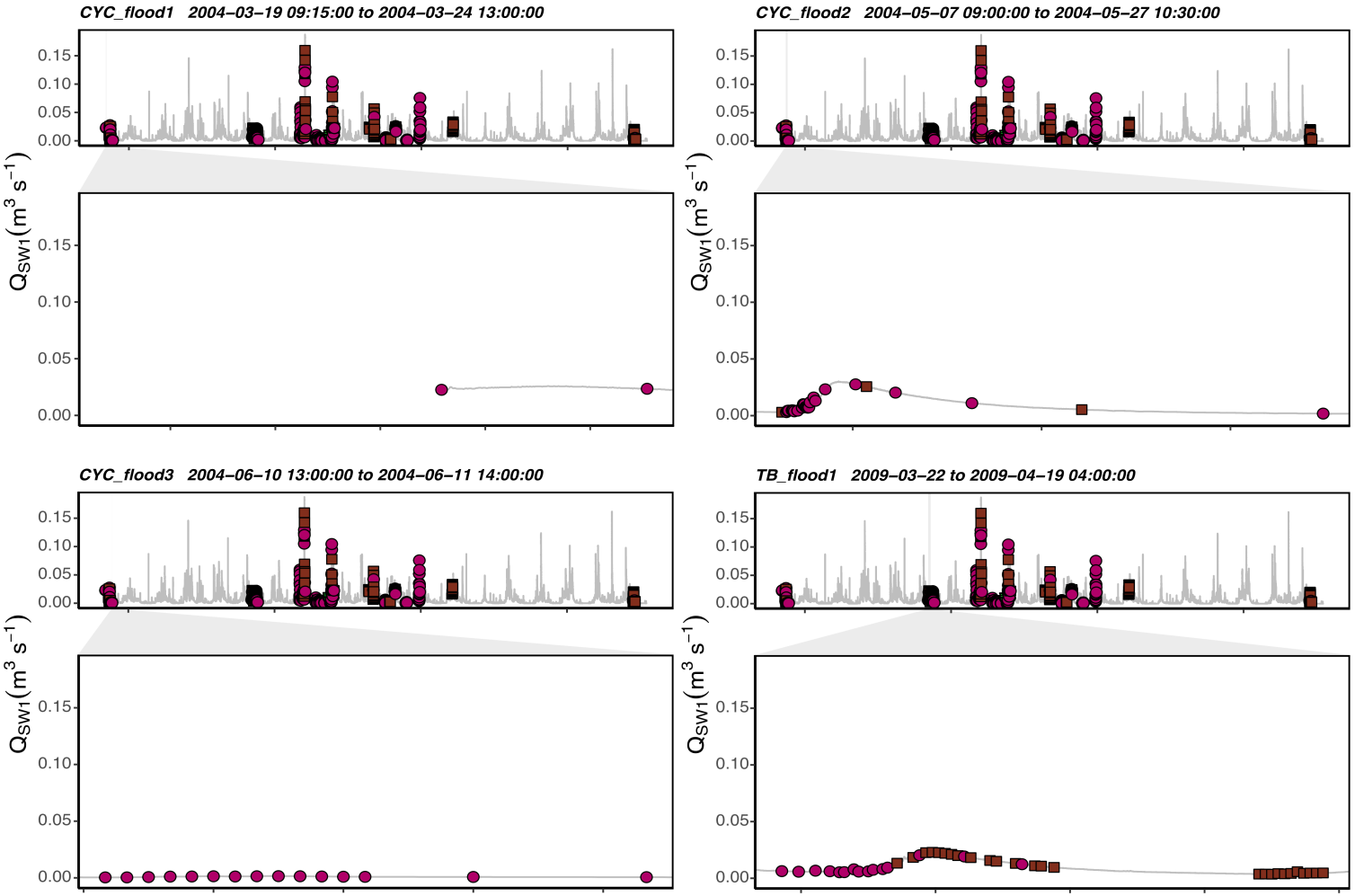

Figure C.1: Flood: `CYC_flood1` to `TB_flood1`.

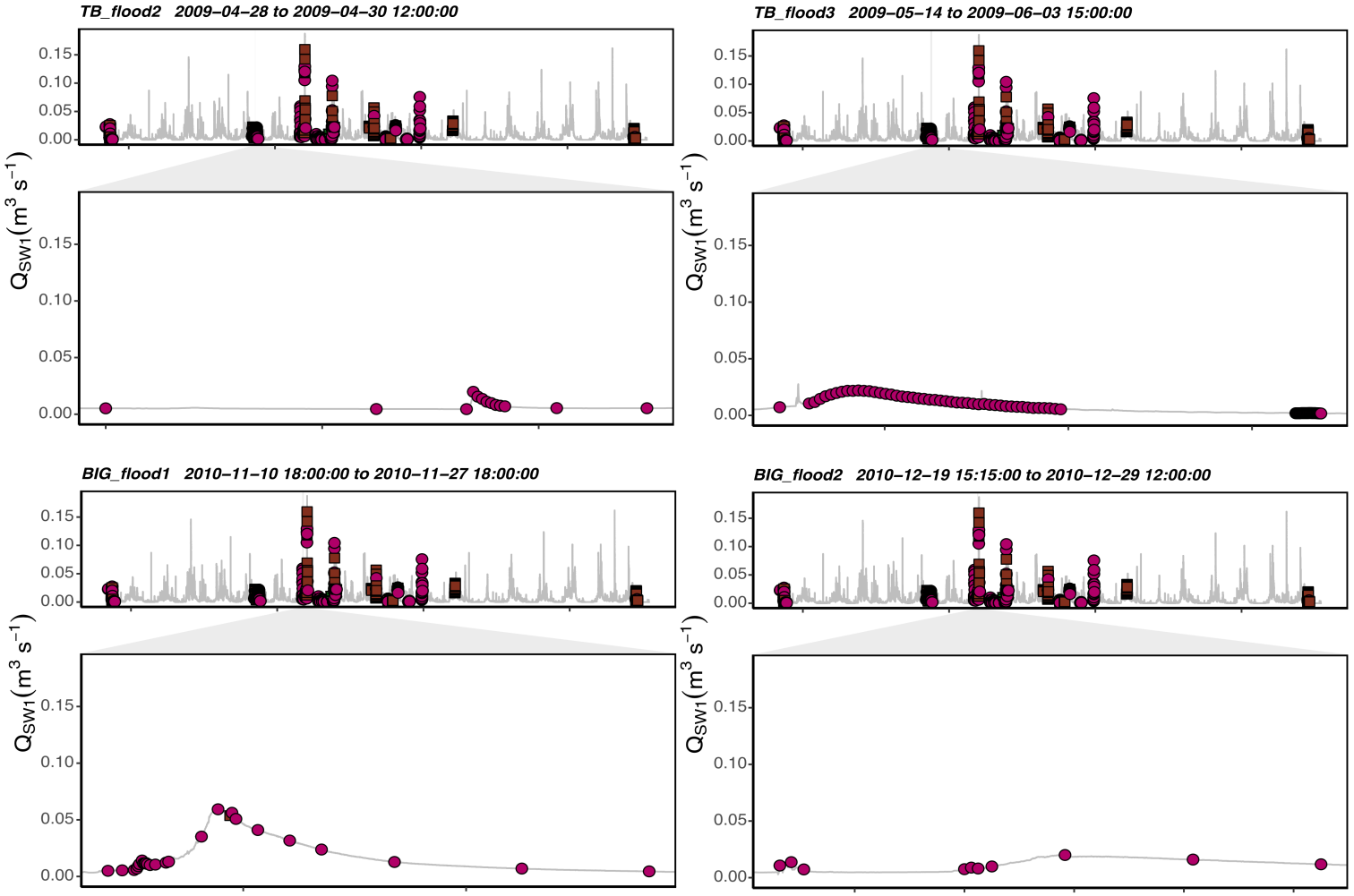

Figure C.2: Flood: `TB_flood2` to `BIG_flood2`.

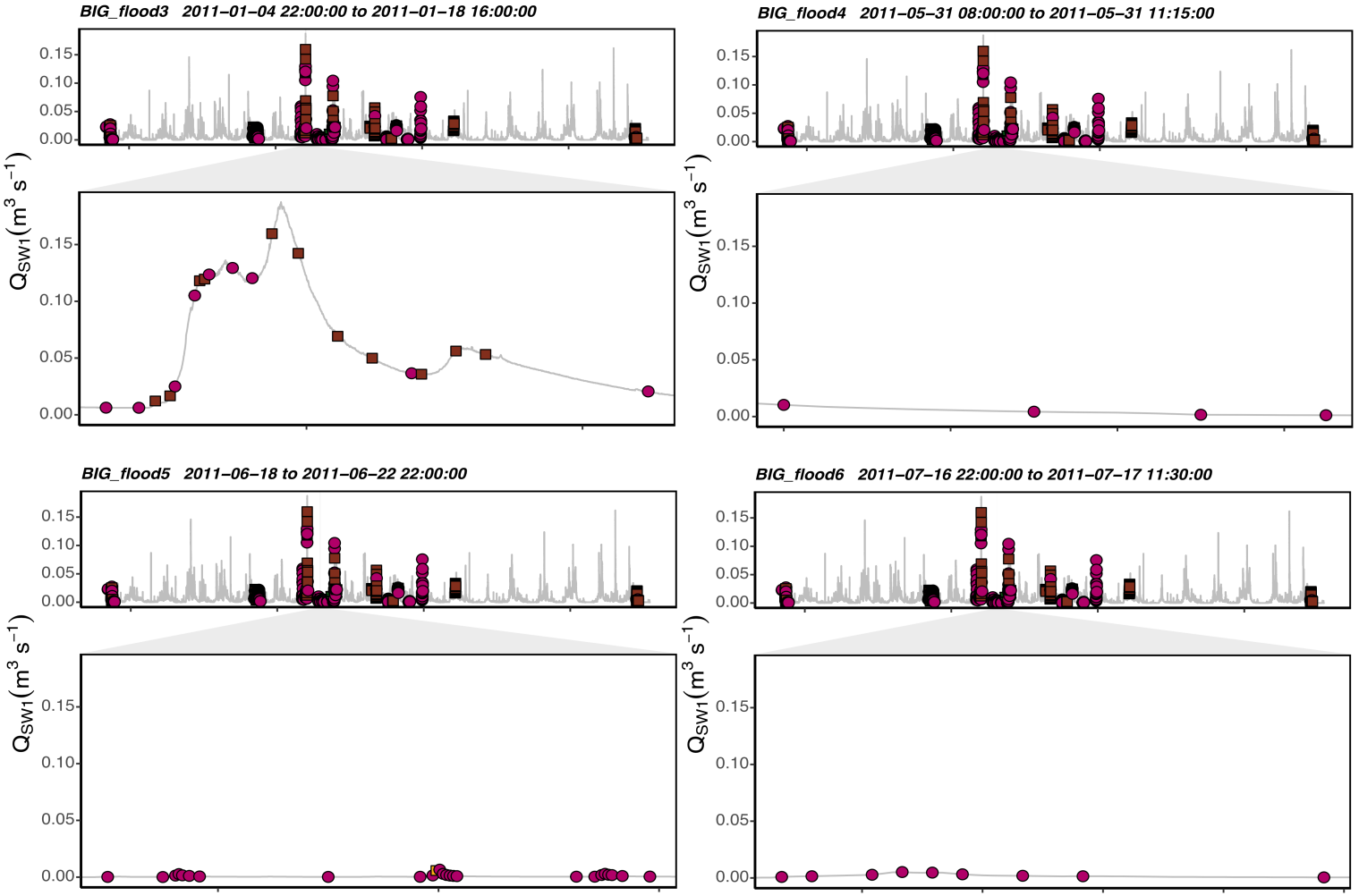

Figure C.3: Flood: `BIG_flood3` to `BIG_flood6`.

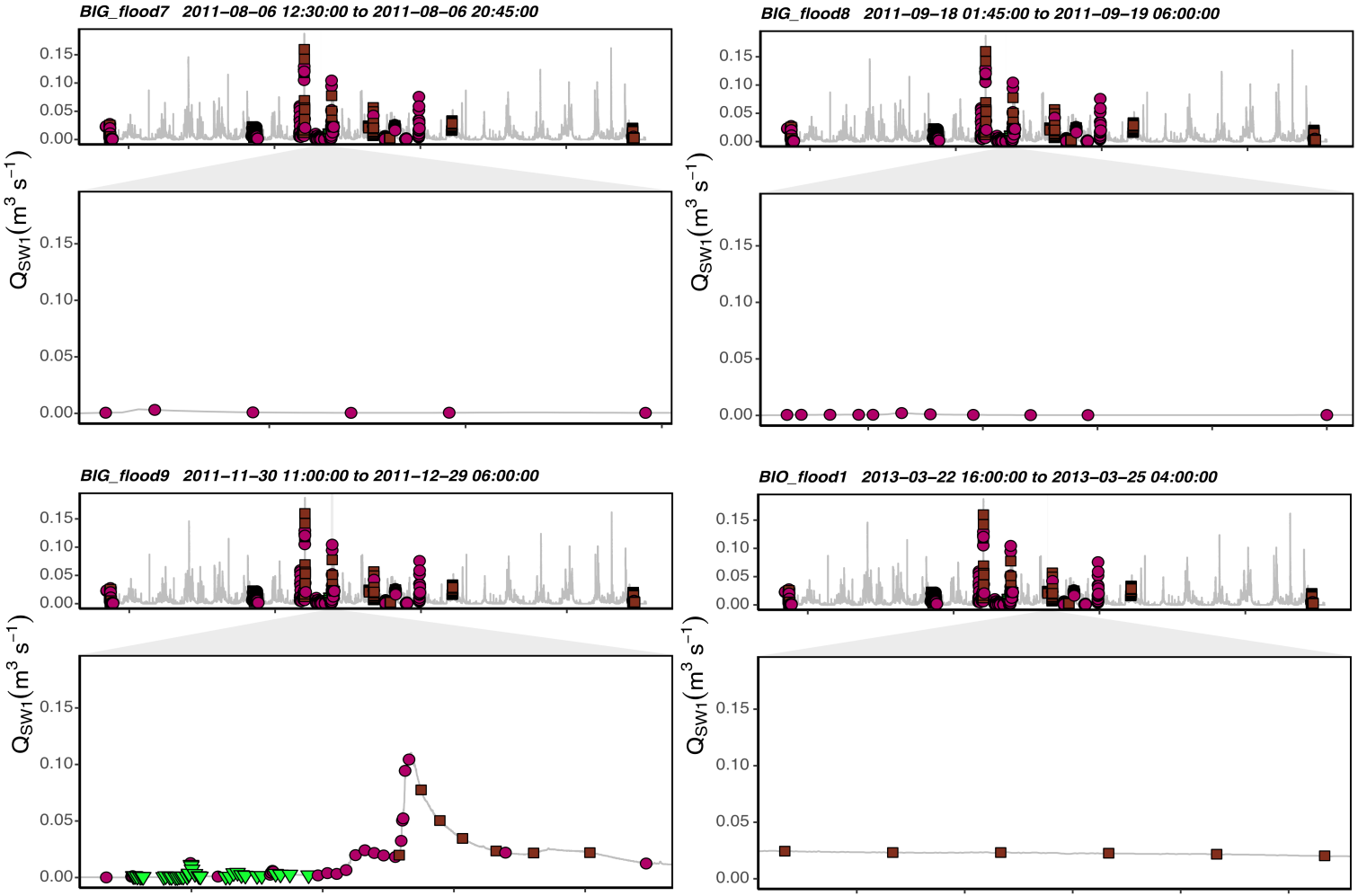

Figure C.4: Flood: `BIG_flood7` to `BIO_flood1`.

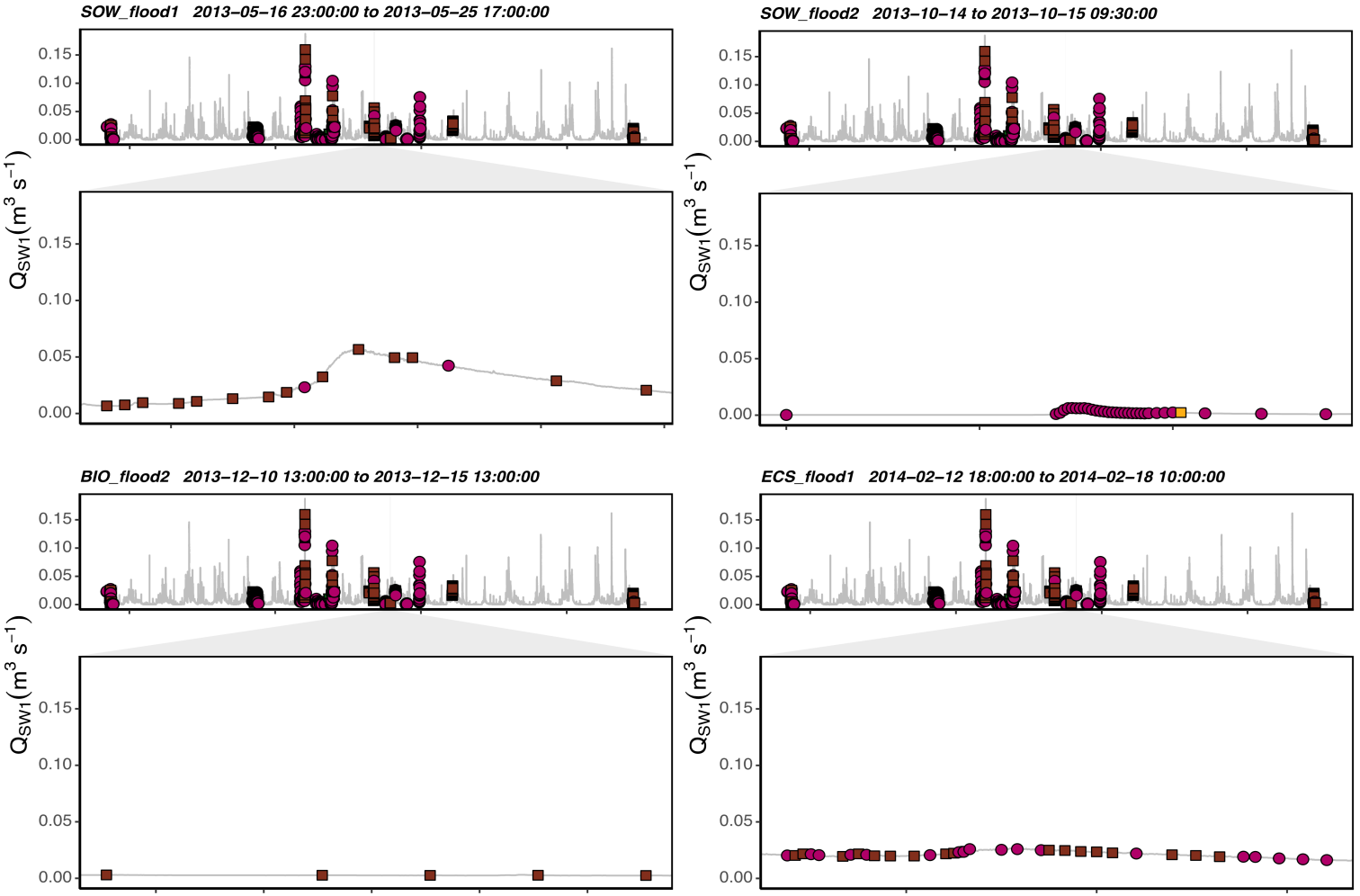

Figure C.5: Flood: `SOW_flood1` to `ECS_flood1`.

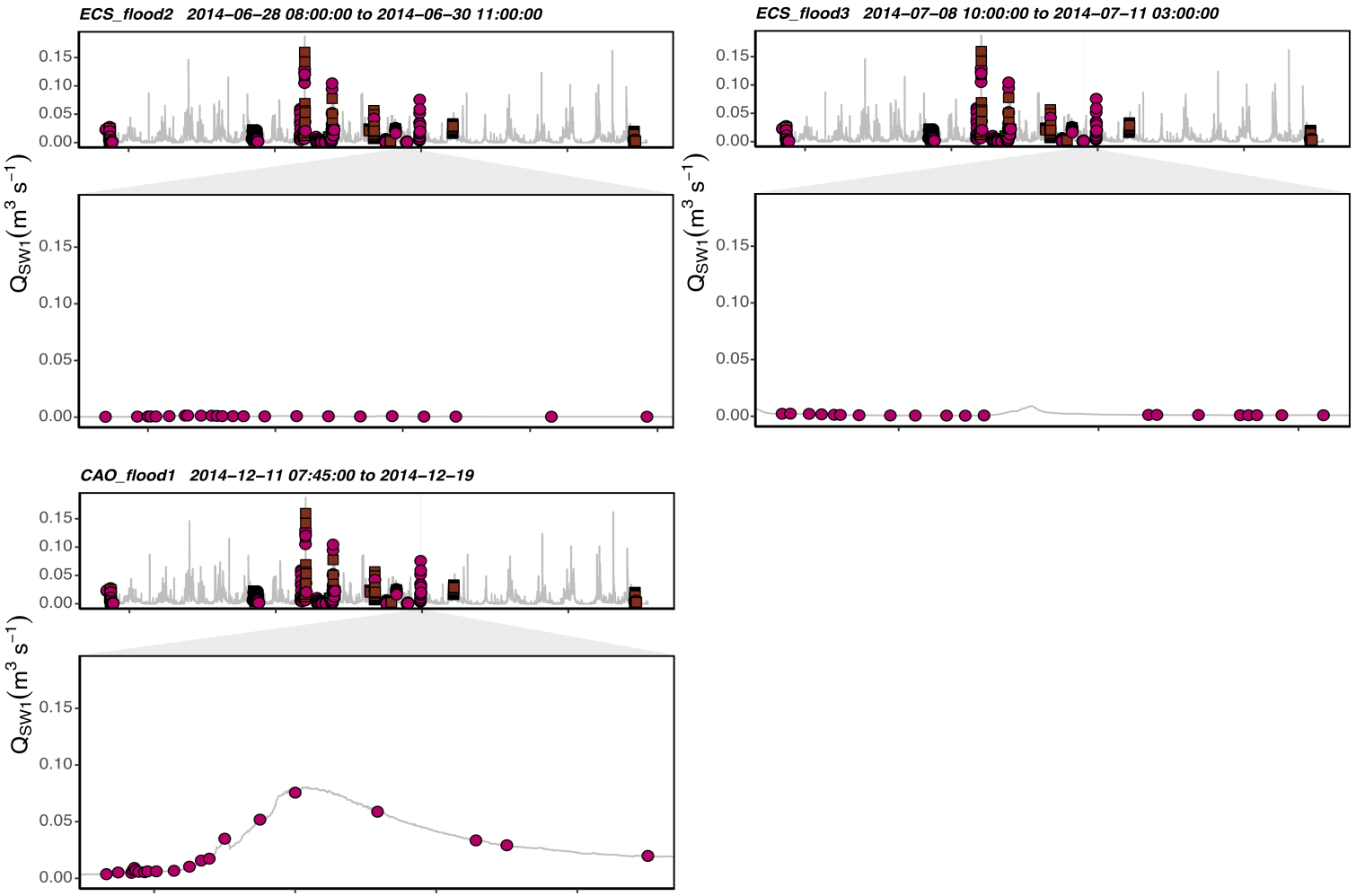

Figure C.6: `ECS_flood2` to `CAO_flood1`.

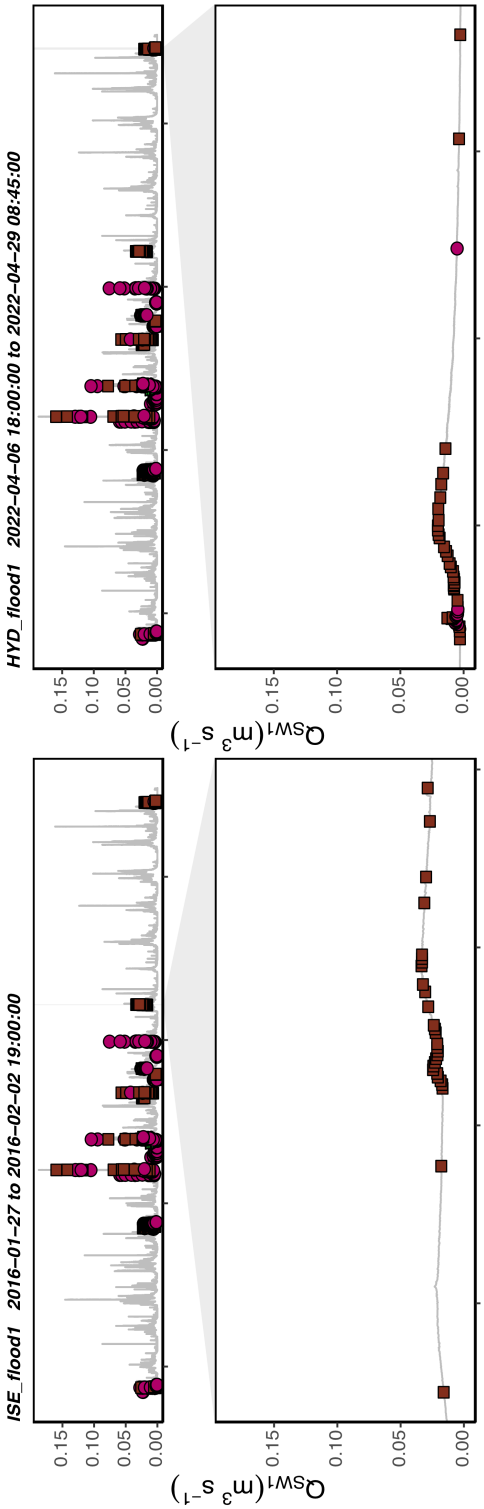

Figure C.7: `ISE_flood1` to `HYD_flood1`.

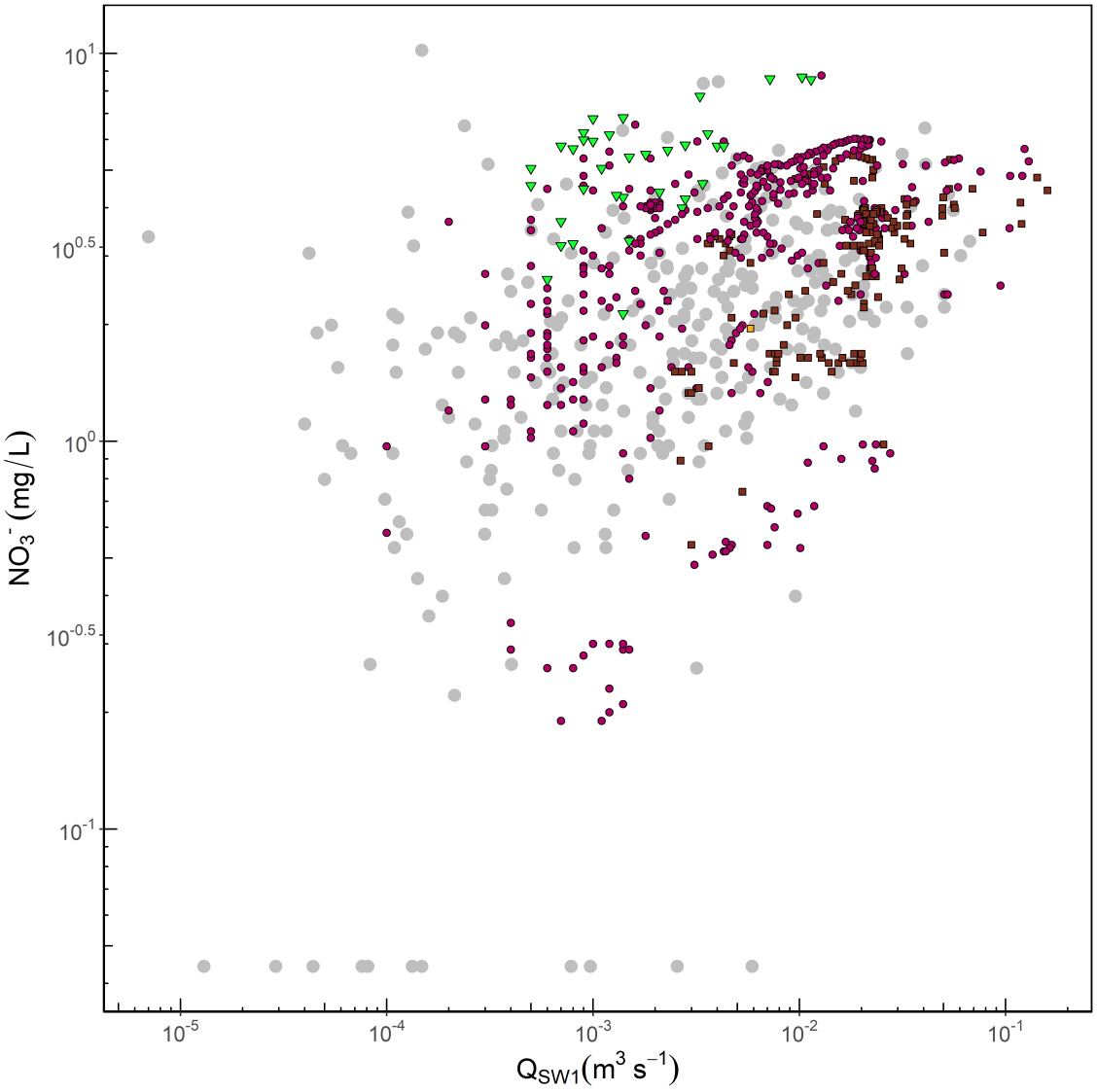

Figure C.8: $c - Q$ plot of NO_3^- for the 27 flood events

References

Abbott, B. W., J. B. Jones, E. A. Schuur, F. S. Chapin, W. B. Bowden, M. S. Bret-Harte, H. E. Epstein, M. D. Flannigan, T. K. Harms, T. N. Hollingsworth, M. C. Mack, A. D. McGuire, S. M. Natali, A. V. Rocha, S. E. Tank, M. R. Turetsky, J. E. Vonk, K. P. Wickland, G. R. Aiken, H. D. Alexander, R. M. Amon, B. W. Benscoter, Y. Bergeron, K. Bishop, O. Blarquez, B. Bond-Lamberty, A. L. Breen, I. Buffam, Y. Cai, C. Carcaillet, S. K. Carey, J. M. Chen, H. Y. Chen, T. R. Christensen, L. W. Cooper, J. H. C. Cornelissen, W. J. De Groot, T. H. Deluca, E. Dorrepaal, N. Fetcher, J. C. Finlay, B. C. Forbes, N. H. French, S. Gauthier, M. P. Girardin, S. J. Goetz, J. G. Goldammer, L. Gough, P. Grogan, L. Guo, P. E. Higuera, L. Hinzman, F. S. Hu, G. Hugelius, E. E. Jafarov, R. Jandt, J. F. Johnstone, J. Karlsson, E. S. Kasischke, G. Kattner, R. Kelly, F. Keuper, G. W. Kling, P. Kortelainen, J. Kouki, P. Kuhry, H. Laudon, I. Laurion, R. W. MacDonald, P. J. Mann, P. J. Martikainen, J. W. McClelland, U. Molau, S. F. Oberbauer, D. Olefeldt, D. Paré, M. A. Parisien, S. Payette, C. Peng, O. S. Pokrovsky, E. B. Rastetter, P. A. Raymond, M. K. Raynolds, G. Rein, J. F. Reynolds, M. Robards, B. M. Rogers, C. Schdel, K. Schaefer, I. K. Schmidt, A. Shvidenko, J. Sky, R. G. Spencer, G. Starr, R. G. Striegl, R. Teisserenc, L. J. Tranvik, T. Virtanen, J. M. Welker, and S. Zimov (2016). "Biomass offsets little or none of permafrost carbon release from soils, streams, and wildfire: An expert assessment". *Environmental Research Letters* 11.3. DOI: 10.1088/1748-9326/11/3/034014.

Adams, F. and Z. Rawajfih (1977). "Basaluminite and Alunite: A Possible Cause of Sulfate Retention by Acid Soils". *Soil Science Society of America Journal* 41.4, 686. DOI: 10.2136/sssaj1977.03615995004100040013x.

Alban, D. H. (1982). "Effects of Nutrient Accumulation by Aspen, Spruce, and Pine on Soil Properties". *Soil Science Society of America Journal* 46.4, 853–861. DOI: 10.2136/sssaj1982.03615995004600040037x.

Albéric, P. and M. Lepiller (1998). "Oxydation de la matière organique dans un système hydrologique karstique alimenté par des pertes fluviales (Loiret, France)oxidation of organic matter in a karstic hydrologic unit supplied through stream sinks (Loiret, france)". *Water Research* 32.7, 2051–2064. DOI: 10.1016/S0043-1354(97)00439-9.

Ali, G. A., A. G. Roy, M.-C. Turmel, and F. Courchesne (2010). "Source-to-stream connectivity assessment through end-member mixing analysis". *Journal of Hydrology* 392.3-4, 119–135. DOI: 10.1016/j.jhydrol.2010.07.049.

Ameli, A. A., J. J. McDonnell, and K. Bishop (2016). "The exponential decline in saturated hydraulic conductivity with depth: a novel method for exploring its effect on water flow paths and transit time distribution". *Hydrological Processes* 30.14, 2438–2450. DOI: 10.1002/hyp.10777.

Ameli, A. A., K. Beven, M. Erlandsson, I. F. Creed, J. J. McDonnell, and K. Bishop (2017). "Primary weathering rates, water transit times, and concentration-discharge relations: A theoretical analysis for the critical zone". *Water Resources Research* 53.1, 942–960. DOI: 10.1002/2016WR019448.

Amundson, R. G. and E. A. Davidson (1990). "Carbon dioxide and nitrogenous gases in the soil atmosphere". *Journal of Geochemical Exploration* 38.1-2, 13–41. DOI: 10.1016/0375-6742(90)90091-N.

Anderson, S. P., W. E. Dietrich, R. Torres, D. R. Montgomery, and K. Loague (1997). "Concentration-discharge relationships in runoff from a steep, unchanneled catchment". *Water Resources Research* 33.1, 211–225. DOI: 10.1029/96WR02715.

Anderson, S. P., J. I. Drever, C. D. Frost, and P. Holden (2000). "Chemical weathering in the foreland of a retreating glacier". *Geochimica et Cosmochimica Acta* 64.7, 1173–1189. DOI: 10.1016/S0016-7037(99)00358-0.

André, L., M. Franceschi, P. Pouchan, and O. Atteia (2005). "Using geochemical data and modelling to enhance the understanding of groundwater flow in a regional deep aquifer, Aquitaine Basin, south-west of France". *Journal of Hydrology* 305.1-4, 40–62. DOI: 10.1016/j.jhydrol.2004.08.027.

Antić-Mladenović, S., J. Rinklebe, T. Frohne, H. J. Stärk, R. Wennrich, Z. Tomić, and V. Ličina (2011). "Impact of controlled redox conditions on nickel in a serpentine soil". *Journal of Soils and Sediments* 11.3, 406–415. DOI: 10.1007/s11368-010-0325-0.

Antonelli, M., B. Glaser, A. J. Teuling, J. Klaus, and L. Pfister (2020a). "Saturated areas through the lens: 1. Spatio-temporal variability of surface saturation documented through thermal infrared imagery". *Hydrological Processes* 34.6, 1310–1332. DOI: 10.1002/hyp.13698.

– (2020b). "Saturated areas through the lens: 2. Spatio-temporal variability of streamflow generation and its relationship with surface saturation". *Hydrological Processes* 34.6, 1333–1349. DOI: 10.1002/hyp.13607.

Antonelli, M., C. E. Wetzel, L. Ector, A. J. Teuling, and L. Pfister (2017). "On the potential for terrestrial diatom communities and diatom indices to identify anthropic disturbance in soils". *Ecological Indicators* 75, 73–81. DOI: 10.1016/J.ECOLIND.2016.12.003.

Appelo, C. A. J. and D. Postma (2006). *Geochemistry, groundwater and pollution*. CRC press.

Arkesteyn, G. (1980). "Pyrite oxidation in acid sulphate soils: The role of miroorganisms". *Plant and soil* 54.1, 119–134.

Arndt, C., T. H. Misselbrook, A. Vega, R. Gonzalez-Quintero, J. A. Chavarro-Lobo, A. M. Mazzetto, and D. R. Chadwick (2020). "Measured ammonia emissions from tropical and subtropical pastures: A comparison with 2006 IPCC, 2019 Refinement to the 2006 IPCC, and EMEP/EEA (European Monitoring and Evaluation Programme and European Environmental Agency) inventory estimates". *Journal of dairy science* 103.7, 6706–6715.

Aubert, D., A. Probst, P. Stille, and D. Viville (2002). "Evidence of hydrological control of Sr behavior in stream water (Strengbach catchment, Vosges mountains, France)". *Applied Geochemistry* 17.3, 285–300. DOI: 10.1016/S0883-2927(01)00080-4.

Augusto, L., J. Ranger, D. Binkley, and A. Rothe (2002). "Impact of several common tree species of European temperate forests on soil fertility". *Annals of forest science* 59.3, 233–253.

Back, W., B. B. Hanshaw, L. N. Plummer, P. H. Rahn, C. T. Rightmire, and M. Rubin (1983). "Process and rate of dedolomitization: mass transfer and 14C dating in a regional carbonate aquifer". *Geological Society of America Bulletin* 94.12, 1415–1429.

Bao, C., L. Li, Y. Shi, and C. Duffy (2017). "Understanding watershed hydrogeochemistry: 1. Development of RT-Flux-PIHM". *Water Resources Research* 53.3, 2328–2345. DOI: 10.1002/2016WR018934.

Barthold, F. K., C. Tyralla, K. Schneider, K. B. Vaché, H.-G. Frede, and L. Breuer (2011). "How many tracers do we need for end member mixing analysis (EMMA)? A sensitivity analysis". *Water Resources Research* 47.8, 1–14. DOI: 10.1029/2011WR010604.

Bartlett, P., Y. Freund, W. S. Lee, and R. E. Schapire (1998). "Boosting the margin: a new explanation for the effectiveness of voting methods". *The Annals of Statistics* 26.5, 1651–1686. DOI: 10.1214/aos/1024691352.

Bastviken, D., F. Thomsen, T. Svensson, S. Karlsson, P. Sandén, G. Shaw, M. Matucha, and G. Öberg (2007). "Chloride retention in forest soil by microbial uptake and by natural chlorination of organic matter". *Geochimica et Cosmochimica Acta* 71.13, 3182–3192. DOI: 10.1016/j.gca.2007.04.028.

Battin, T. J., L. A. Kaplan, S. Findlay, C. S. Hopkinson, E. Marti, A. I. Packman, J. D. Newbold, and F. Sabater (2009). "Erratum: Biophysical controls on organic carbon fluxes in fluvial networks (Nature Geoscience (2008) 1 (95-100))". *Nature Geoscience* 2.8, 595. DOI: 10.1038/ngeo602.

Beaulieu, E., Y. Goddëris, Y. Donnadieu, D. Labat, and C. Roelandt (2012). "High sensitivity of the continental-weathering carbon dioxide sink to future climate change". *Nature Climate Change* 2.5, 346–349. DOI: 10.1038/nclimate1419.

Beaulieu, E., Y. Goddéris, D. Labat, C. Roelandt, D. Calmels, and J. Gaillardet (2011). "Modeling of water-rock interaction in the Mackenzie basin: Competition between sulfuric and carbonic acids". *Chemical Geology* 289.1-2, 114–123. DOI: 10.1016/j.chemgeo.2011.07.020.

Beeson, S. and M. C. Cook (2004). "Nitrate in groundwater: a water company perspective". *Quarterly Journal of Engineering Geology and Hydrogeology* 37.4, 261–270.

Bellman, R. (1961). "Curse of dimensionality". *Adaptive control processes: a guided tour. Princeton, NJ* 3.2.

Benettin, P., N. B. Rodriguez, M. Sprenger, M. Kim, J. Klaus, C. J. Harman, Y. V. D. Velde, M. Hrachowitz, and G. Botter (2022). "Transit time estimation in catchments : Recent developments and future directions". 2006, 1–36. DOI: 10.1029/2022WR033096.

Berghuijs, W. R. and J. W. Kirchner (2017). "The relationship between contrasting ages of groundwater and streamflow". *Geophysical Research Letters* 44.17, 8925–8935. DOI: 10.1002/2017GL074962.

Berner, E. and R. Berner (1996). "Global environment water, air, and geochemical cycles Prentice-Hall". *Englewood Cliffs, NewJersey*.

Berner, E. K. and R. A. Berner (1987). "Global water cycle: geochemistry and environment". *Prentice-Hall, Inc., Englewood Cliffs New Jersey. 1987. 397*.

Berner, R. A. and K. A. Maasch (1996). "Chemical weathering and controls on atmospheric O2 and CO2: Fundamental principles were enunciated by J.J. Ebelmen in 1845". *Geochimica et Cosmochimica Acta* 60.9, 1633–1637. DOI: 10.1016/0016-7037(96)00104-4.

Berner, R. A. and J. L. Rao (1996). "Alkalinity buildup during silicate weathering under a snow cover". *Aquatic Geochemistry* 2.4, 301–312. DOI: 10.1007/bf00115974.

BernerR, L. et al. (1983). "Thecarbonate silicate geochemicalcycleanditseffectonatmosphericcarbondioxideover thepast100million years". *American Journalofscience* 283.7, 641r683.

Beven, K. and J. Freer (2001). "Equifinality, data assimilation, and uncertainty estimation in mechanistic modelling of complex environmental systems using the GLUE methodology". *Journal of hydrology* 249.1-4, 11–29.

Bini, C., G. Sartori, M. Wahsha, and S. Fontana (2011). "Background levels of trace elements and soil geochemistry at regional level in NE Italy". *Journal of Geochemical Exploration* 109.1-3, 125–133. DOI: 10.1016/j.gexplo.2010.07.008.

Birkel, C. and C. Soulsby (2015). "Advancing tracer-aided rainfall-runoff modelling: A review of progress, problems and unrealised potential". *Hydrological Processes* 29.25, 5227–5240. DOI: 10.1002/hyp.10594.

Bishop, P. L. and T. Yu (1999). "A microelectrode study of redox potential change in biofilms". *Water science and technology* 39.7, 179–185.

Bluth, G. J. and L. R. Kump (1994). "Lithologic and climatologic controls of river chemistry". *Geochimica et Cosmochimica Acta* 58.10, 2341–2359. DOI: 10.1016/0016-7037(94)90015-9.

Böhlke, J. K. and J. M. Denver (1995). "Combined Use of Groundwater Dating, Chemical, and Isotopic Analyses to Resolve the History and Fate of Nitrate Contamination in Two Agricultural Watersheds, Atlantic Coastal Plain, Maryland". *Water Resources Research* 31.9, 2319–2339. DOI: 10.1029/95WR01584.

Bonanno, E., G. Blöschl, and J. Klaus (2021). "Flow directions of stream-groundwater exchange in a headwater catchment during the hydrologic year". *Hydrological Processes* 35.8, 1–18. DOI: 10.1002/hyp.14310.

– (2022). "Exploring tracer information in a small stream to improve parameter identifiability and enhance the process interpretation in transient storage models". *Hydrology and Earth System Sciences* 26.23, 6003–6028. DOI: 10.5194/hess-26-6003-2022.

Botter, G., A. Porporato, I. Rodriguez-Iturbe, and A. Rinaldo (2009). "Nonlinear storage-discharge relations and catchment streamflow regimes". *Water Resources Research* 45.10, 1–16. DOI: 10.1029/2008WR007658.

Bouchez, J., J. S. Moquet, J. C. Espinoza, J. M. Martinez, J. L. Guyot, C. Lagane, N. Filizola, L. Noriega, L. Hidalgo Sanchez, and R. Pombosa (2017). "River Mixing in the Amazon as a Driver of Concentration-Discharge Relationships". *Water Resources Research* 53.11, 8660–8685. DOI: 10.1002/2017WR020591.

Boudot, J. P., A. Bel Hadj Brahim, R. Steiman, and F. Seigle-Murandi (1989). "Biodegradation of synthetic organo-metallic complexes of iron and aluminium with selected metal to carbon ratios". *Soil Biology and Biochemistry* 21.7, 961–966. DOI: 10.1016/0038-0717(89)90088-6.

Boyer, E. W., G. M. Hornberger, K. E. Bencala, and D. M. Mcknight (1997). "Response characteristics of DOC flushing in an alpine catchment". *Hydrological Processes* 11.12, 1635–1647. DOI: 10.1002/(sici)1099-1085(19971015)11:12<1635::aid-hyp494>3.0.co;2-h.

Bragan, R. J., J. L. Starr, and T. B. Parkin (1997). "Shallow Groundwater Denitrification Rate Measurement by Acetylene Block". *Journal of Environmental Quality* 26.6, 1531–1538. DOI: 10.2134/jeq1997.00472425002600060012x.

Brantley, S. L., M. B. Goldhaber, and K. V. Ragnarsdottir (2007). "Crossing Disciplines and Scales to Understand the Critical Zone". *Elements* 3.5, 307–314. DOI: 10.2113/gselements.3.5.307.

Brantley, S. L., M. E. Holleran, L. Jin, and E. Bazilevskaya (2013). "Probing deep weathering in the Shale Hills Critical Zone Observatory, Pennsylvania (USA): The hypothesis of nested chemical reaction fronts in the subsurface". *Earth Surface Processes and Landforms* 38.11, 1280–1298. DOI: 10.1002/esp.3415.

Breiman, L. (2001). "Random forests". *Machine learning* 45.1, 5–32.

Brooks, P. D., J. Chorover, Y. Fan, S. E. Godsey, R. M. Maxwell, J. P. McNamara, and C. Tague (2015). "Hydrological partitioning in the critical zone: Recent advances and opportunities for developing transferable understanding of water cycle dynamics". *Water Resources Research* 51.9, 6973–6987. DOI: 10.1002/2015WR017039.

Burford, E. P., M. Fomina, and G. M. Gadd (2003). "Fungal involvement in bioweathering and biotransformation of rocks and minerals". *Mineralogical Magazine* 67.6, 1127–1155. DOI: 10.1180/0026461036760154.

Butler, T. J. and G. E. Likens (1995). "A direct comparison of throughfall plus stemflow to estimates of dry and total deposition for sulfur and nitrogen". *Atmospheric Environment* 29.11, 1253–1265. DOI: 10.1016/1352-2310(94)00339-M.

Buttle, J. M. and D. L. Peters (1997). "Inferring hydrological processes in a temperate basin using isotopic and geochemical hydrograph separation: A re-evaluation". *Hydrological Processes* 11.6, 557–573. DOI: 10.1002/(SICI)1099-1085(199705)11:6<557::AID-HYP477>3.0.CO;2-Y.

Callahan, R. P., C. S. Riebe, L. S. Sklar, S. Pasquet, K. L. Ferrier, W. J. Hahm, N. J. Taylor, D. Grana, B. A. Flinchum, J. L. Hayes, and W. S. Holbrook (2022). "Forest vulnerability to drought controlled by bedrock composition". *Nature Geoscience* 15.9, 714–719. DOI: 10.1038/s41561-022-01012-2.

Calmels, D., J. Gaillardet, A. Brenot, and C. France-Lanord (2007). "Sustained sulfide oxidation by physical erosion processes in the Mackenzie River basin: Climatic perspectives". *Geology* 35.11, 1003–1006. DOI: 10.1130/G24132A.1.

Calmels, D., J. Gaillardet, and L. François (2014). "Sensitivity of carbonate weathering to soil CO2 production by biological activity along a temperate climate transect". *Chemical Geology* 390, 74–86. DOI: 10.1016/j.chemgeo.2014.10.010.

Campbell, D. H., D. W. Clow, G. P. Ingersoll, M. A. Mast, N. E. Spahr, and J. T. Turk (1995). "Processes Controlling the Chemistry of Two Snowmelt-Dominated Streams in the Rocky Mountains". *Water Resources Research* 31.11, 2811–2821. DOI: 10.1029/95WR02037.

Canfield, D. E., B. Thamdrup, and J. W. Hansen (1993). "The anaerobic degradation of organic matter in Danish coastal sediments: iron reduction, manganese reduction, and sulfate reduction". *Geochimica et Cosmochimica Acta* 57.16, 3867–3883.

Capaccioni, B., M. Didero, C. Paletta, and P. Salvadori (2001). "Hydrogeochemistry of groundwaters from carbonate formations with basal gypsiferous layers: an example from the Mt Catria–Mt Nerone ridge (Northern Appennines, Italy)". *Journal of Hydrology* 253.1-4, 14–26.

Cardenal, J., J. Benavente, and J. Cruz-Sanjulian (1994). "Chemical evolution of groundwater in Triassic gypsum-bearing carbonate aquifers (Las Alpujarras, southern Spain)". *Journal of Hydrology* 161.1-4, 3–30.

Carrer, G. E., J. Klaus, and L. Pfister (2019). "Assessing the Catchment Storage Function Through a Dual-Storage Concept". *Water Resources Research* 55.1, 476–494. DOI: 10.1029/2018WR022856.

Carrera, J., E. Vázquez-Suñé, O. Castillo, and X. Sánchez-Vila (2004). "A methodology to compute mixing ratios with uncertain end-members". *Water Resources Research* 40.12, 1–11. DOI: 10.1029/2003WR002263.

Cattell, R. B. (1966). "The scree test for the number of factors". *Multivariate behavioral research* 1.2, 245–276.

Centrella, S., G. Hoareau, N. E. Beaudoin, G. Motte, P. Lanari, F. Piccoli, J. P. Callot, E. Gomez-Rivas, and J. D. Martın-Martın (2023). "Estimating the fluid composition after dolomitization using mass balance equation: comparison of examples from Spain, Canada and France". *Global and Planetary Change* 220, 104016.

Champ, D. R., J. Gulens, and R. E. Jackson (1979). "Oxidation–reduction sequences in ground water flow systems". *Canadian Journal of earth sciences* 16.1, 12–23.

Chanat, J. G., K. C. Rice, and G. M. Hornberger (2002). "Consistency of patterns in concentration-discharge plots". *Water Resources Research* 38.8, 22–1. DOI: 10.1029/2001WR000971.

Chandra, A. P. and A. R. Gerson (2010). "The mechanisms of pyrite oxidation and leaching: A fundamental perspective". *Surface Science Reports* 65.9, 293–315. DOI: 10.1016/j.surfrep.2010.08.003.

Chapelle, F. H., P. M. Bradley, D. R. Lovley, and D. A. Vroblesky (1996a). "Measuring rates of biodegradation in a contaminated aquifer using field and laboratory methods". *Groundwater* 34.4, 691–698.

Chapelle, F. H., S. K. Haack, P. Adriaens, M. A. Henry, and P. M. Bradley (1996b). "Comparison of E h and H2 measurements for delineating redox processes in a contaminated aquifer". *Environmental Science & Technology* 30.12, 3565–3569.

Chapelle, F. H. and D. R. Lovley (1990). "Rates of microbial metabolism in deep coastal plain aquifers". *Applied and Environmental Microbiology* 56.6, 1865–1874.

Chapelle, F. H., P. B. McMahon, N. M. Dubrovsky, R. F. Fujii, E. T. Oaksford, and D. A. Vroblesky (1995). "Deducing the distribution of terminal electron-accepting processes in hydrologically diverse groundwater systems". *Water Resources Research* 31.2, 359–371.

Chebotarev, I. (1955). "Metamorphism of natural waters in the crust of weathering—1". *Geochimica et Cosmochimica Acta* 8.1-2, 22–48.

Cherry, J. A. and R. A. Freeze (1979). *Groundwater*. Englewood Cliffs, NJ: Prentice-Hall.

Chiodini, G., R. Cioni, M. Guidi, B. Raco, and L. Marini (1998). "Soil CO2 flux measurements in volcanic and geothermal areas". *Applied Geochemistry* 13.5, 543–552. DOI: 10.1016/S0883-2927(97)00076-0.

Chiodini, G., F. Frondini, D. M. Kerrick, J. Rogie, F. Parello, L. Peruzzi, and A. R. Zanzari (1999). "Quantification of deep CO2 fluxes from Central Italy. Examples of carbon balance for regional aquifers and of soil diffuse degassing". *Chemical Geology* 159.1-4, 205–222. DOI: 10.1016/S0009-2541(99)00030-3.

Chorover, J., L. A. Derry, and W. H. McDowell (2017). "Concentration-discharge relations in the critical zone: Implications for resolving critical zone structure, function, and evolution". *Water Resources Research* 53.11, 8654–8659.

Christensen, T. H., P. L. Bjerg, S. A. Banwart, R. Jakobsen, G. Heron, and H.-J. Albrechtsen (2000). "Characterization of redox conditions in groundwater contaminant plumes". *Journal of Contaminant hydrology* 45.3-4, 165–241.

Christophersen, N. and R. P. Hooper (1992). "Multivariate analysis of stream water chemical data: The use of principal components analysis for the end-member mixing problem". *Water Resources Research* 28.1, 99–107. DOI: 10.1029/91WR02518.

Christophersen, N., C. Neal, R. P. Hooper, R. D. Vogt, and S. Andersen (1990). "Modelling streamwater chemistry as a mixture of soilwater end-members—a step towards second-generation acidification models". *Journal of Hydrology* 116.1-4, 307–320.

Christophersen, N., C. Neal, and R. P. Hooper (1993). "Modelling the hydrochemistry of catchments: a challenge for the scientific method". *Journal of Hydrology* 152.1-4, 1–12. DOI: 10.1016/0022-1694(93)90138-Y.

Churka Blum, S., J. Lehmann, D. Solomon, E. F. Caires, and L. R. F. Alleoni (2013). "Sulfur forms in organic substrates affecting S mineralization in soil". *Geoderma* 200-201, 156–164. DOI: 10.1016/j.geoderma.2013.02.003.

Clough, A. and J. Skjemstad (2000). "Physical and chemical protection of soil organic carbon in three agricultural soils with different contents of calcium carbonate". *Soil Research* 38.5, 1005–1016.

Cloutier, V., R. Lefebvre, R. Therrien, and M. M. Savard (2008). "Multivariate statistical analysis of geochemical data as indicative of the hydrogeochemical evolution of groundwater in a sedimentary rock aquifer system". *Journal of Hydrology* 353.3-4, 294–313. DOI: 10.1016/j.jhydrol.2008.02.015.

Clow, D. W. and M. A. Mast (2010). "Mechanisms for chemostatic behavior in catchments: Implications for CO2 consumption by mineral weathering". *Chemical Geology* 269.1-2, 40–51.

Correa, A., D. Windhorst, D. Tetzlaff, P. Crespo, R. Célleri, J. Feyen, and L. Breuer (2017). "Temporal dynamics in dominant runoff sources and flow paths in the Andean Páramo". *Water Resources Research* 53.7, 5998–6017. DOI: 10.1002/2016WR020187.

D'Amario, S. C., D. C. Rearick, C. Fasching, S. W. Kembel, E. Porter-Goff, D. E. Spooner, C. J. Williams, H. F. Wilson, and M. A. Xenopoulos (2019). "The prevalence of nonlinearity and detection of ecological breakpoints across a land use gradient in streams". *Scientific Reports* 9.1, 1–11. DOI: 10.1038/s41598-019-40349-4.

Davis, J. C. and R. J. Sampson (1986). *Statistics and data analysis in geology*. Vol. 646. Wiley New York.

Davis, S. N. and R. J. De Wiest (1966). *Hydrogeology*. Vol. 463. Wiley New York.

De Lucia, M. and M. Kühn (2013). "Coupling R and PHREEQC: Efficient programming of geochemical models". *Energy Procedia* 40, 464–471. DOI: 10.1016/j.egypro.2013.08.053.

DeLaune, R. and K. Reddy (2005). *Encyclopedia of Soils in the Environment*.

Delsman, J. R., G. H. P. O. Essink, K. J. Beven, and P. J. Stuyfzand (2013). "Uncertainty estimation of end-member mixing using generalized likelihood uncertainty estimation (GLUE), applied in a lowland catchment". *Water Resources Research* 49.8, 4792–4806. DOI: 10.1002/wrcr.20341.

Dhiman, S. D. and A. K. Keshari (2006). "GIS assisted inverse geochemical modeling for plausible phase transfers in aquifers". *Environmental Geology* 50.8, 1211–1219. DOI: 10.1007/s00254-006-0293-2.

Dijkstra, F. A. and M. M. Smits (2002). "Tree species effects on calcium cycling: The role of calcium uptake in deep soils". *Ecosystems* 5.4, 385–398. DOI: 10.1007/s10021-001-0082-4.

Dixon, D. G. and J. L. Hendrix (1993). "A mathematical model for heap leaching of one or more solid reactants from porous ore pellets". *Metallurgical Transactions B* 24.6, 1087–1102.

Draaijers, G. P., J. W. Erisman, T. Spranger, and G. P. Wyers (1996). "The application of throughfall measurements for atmospheric deposition monitoring". *Atmospheric Environment* 30.19, 3349–3361. DOI: 10.1016/1352-2310(96)00030-1.

Druschel, G. K., B. J. Baker, T. M. Gihring, and J. F. Banfield (2004). "Acid mine drainage biogeochemistry at Iron Mountain, California". *Geochemical Transactions* 5.2, 13–32. DOI: 10.1063/1.1769131.

Du Laing, G., E. Meers, M. Dewispelaere, J. Rinklebe, B. Vandecasteele, M. G. Verloo, and F. M. G. Tack (2009). "Effect of Water Table Level on Metal Mobility at Different Depths in Wetland Soils of the Scheldt Estuary (Belgium)". *Water, Air, and Soil Pollution* 202.1-4, 353–367. DOI: 10.1007/s11270-009-9982-2.

Duckworth, O. W., J. R. Bargar, and G. Sposito (2008). "Sorption of ferric iron from ferrioxamine B to synthetic and biogenic layer type manganese oxides". *Geochimica et Cosmochimica Acta* 72.14, 3371–3380. DOI: 10.1016/j.gca.2008.04.026.

Ebel, B. A. and K. Loague (2006). "Physics-based hydrologic-response simulation: Seeing through the fog of equifinality". *Hydrological Processes* 20.13, 2887–2900. DOI: 10.1002/hyp.6388.

Eberts, S. M. and L. L. George (2000). *Regional ground-water flow and geochemistry in the Midwestern basins and arches aquifer system in parts of Indiana, Ohio, Michigan, and Illinois*. US Department of the Interior, US Geological Survey.

Edmunds, W. M. and C. B. Gaye (1994). "Estimating the spatial variability of groundwater recharge in the Sahel using chloride". *Journal of Hydrology* 156.1-4, 47–59. DOI: 10.1016/0022-1694(94)90070-1.

Eriksson, E. (1960). "The Yearly Circulation of Chloride and Sulfur in Nature; Meteorological, Geochemical and Pedological Implications. Part II". *Tellus* 12.1, 64–109. DOI: 10.3402/tellusa.v12i1.9341.

Etiope, G. (1999). "Faulted area Unfaulted". 104, 889–894.

Evans, C. and T. D. Davies (1998). "Causes of concentration/discharge hysteresis and its potential as a tool for analysis of episode hydrochemistry". *Water Resources Research* 34.1, 129–137. DOI: 10.1029/97WR01881.

Everitt, B. and T. Hothorn (2011). *An Introduction to Applied Multivariate Analysis with R - 4 Multidimensional Scaling*, 61–74.

Fabiani, G., R. Schoppach, D. Penna, and J. Klaus (2022). "Transpiration patterns and water use strategies of beech and oak trees along a hillslope". *Ecohydrology* 15.2, 1–18. DOI: 10.1002/eco.2382.

Fan, Y., M. Clark, D. M. Lawrence, S. Swenson, L. E. Band, S. L. Brantley, P. D. Brooks, W. E. Dietrich, A. Flores, G. Grant, J. W. Kirchner, D. S. Mackay, J. J. McDonnell, P. C. Milly, P. L. Sullivan, C. Tague, H. Ajami, N. Chaney, A. Hartmann, P. Hazenberg, J. McNamara, J. Pelletier, J. Perket, E. Rouholahnejad-Freund, T. Wagener, X. Zeng, E. Beighley, J. Buzan, M. Huang, B. Livneh, B. P. Mohanty, B. Nijssen, M. Safeeq, C. Shen, W. van Verseveld, J. Volk, and D. Yamazaki (2019). "Hillslope Hydrology in Global Change Research and Earth System Modeling". *Water Resources Research*, 1737–1772. DOI: 10.1029/2018WR023903.

Farmer, S. (1971). "An investigation into the results of principal component analysis of data derived from random numbers". *Journal of the Royal Statistical Society: Series D (The Statistician)* 20.4, 63–72.

Farnham, I. M., A. K. Singh, K. J. Stetzenbach, and K. H. Johannesson (2002). "Treatment of nondetects in multivariate analysis of groundwater geochemistry data". *Chemometrics and Intelligent Laboratory Systems* 60.1-2, 265–281. DOI: 10.1016/S0169-7439(01)00201-5.

Feast, N., K. Hiscock, P. Dennis, and J. Andrews (1998). "Nitrogen isotope hydrochemistry and denitrification within the Chalk aquifer system of north Norfolk, UK". *Journal of Hydrology* 211.1-4, 233–252.

Fenicia, F., D. Kavetski, H. H. Savenije, M. P. Clark, G. Schoups, L. Pfister, and J. Freer (2014). "Catchment properties, function, and conceptual model representation: Is there a correspondence?" *Hydrological Processes* 28.4, 2451–2467. DOI: 10.1002/hyp.9726.

Fiedler, S., M. J. Vepraskas, and J. Richardson (2007). "Soil Redox Potential: Importance, Field Measurements, and Observations". In: *Advances in Agronomy*. Vol. 94. 06, 1–54. DOI: 10.1016/S0065-2113(06)94001-2.

Finzi, A. C., N. Van Breemen, and C. D. Canham (1998a). "Canopy tree-soil interactions within temperate forests: Species effects on soil carbon and nitrogen". *Ecological Applications* 8.2, 440–446. DOI: 10.1890/1051-0761(1998)008[0440:CTSIWT]2.0.CO;2.

– (1998b). "Canopy tree-soil interactions within temperate forests: Species effects on soil carbon and nitrogen". *Ecological Applications* 8.2, 440–446. DOI: 10.1890/1051-0761(1998)008[0440:CTSIWT]2.0.CO;2.

Fisher, R. S. and W. F. Mullican (1997). *Hydrochemical evolution of sodium-sulfate and sodium-chloride groundwater beneath the Northern Chihuahuan Desert, Trans-Pecos, Texas, USA*. DOI: 10.1007/s100400050102.

Floriancic, M. G., B. M. Fischer, P. Molnar, J. W. Kirchner, and I. H. van Meerveld (2019). "Spatial variability in specific discharge and streamwater chemistry during low flows: Results from snapshot sampling campaigns in eleven Swiss catchments". *Hydrological Processes* 33.22, 2847–2866. DOI: 10.1002/hyp.13532.

Fogler, H. (2020). *Elements of Chemical Reaction Engineering*. International the Physical and. Pearson.

Fowler, D. (1980). "Wet and dry deposition of sulphur and nitrogen compounds from the atmosphere". In: *Effects of acid precipitation on terrestrial ecosystems*. Springer, 9–27.

Freney, J., G. Melville, and C. Williams (1975). "Soil organic matter fractions as sources of plant-available sulphur". *Soil Biology and Biochemistry* 7.3, 217–221.

Frohne, T., J. Rinklebe, R. A. Diaz-Bone, and G. Du Laing (2011). "Controlled variation of redox conditions in a floodplain soil: Impact on metal mobilization and biomethylation of arsenic and antimony". *Geoderma* 160.3-4, 414–424. DOI: 10.1016/j.geoderma.2010.10.012.

Fu, H., H. Zhang, Y. Sui, N. Hu, D. Ding, Y. Ye, G. Li, Y. Wang, and Z. Dai (2018). "Transformation of uranium species in soil during redox oscillations". *Chemosphere* 208, 846–853. DOI: 10.1016/j.chemosphere.2018.06.059.

Gaillardet, J., B. Dupré, P. Louvat, and C. J. Allègre (1999). "Global silicate weathering and CO2 consumption rates deduced from the chemistry of large rivers". *Chemical Geology* 159.1-4, 3–30. DOI: 10.1016/S0009-2541(99)00031-5.

Gaillardet, J., R. Millot, and B. Dupré (2003). "Chemical denudation rates of the western Canadian orogenic belt: The Stikine terrane". *Chemical Geology* 201.3-4, 257–279. DOI: 10.1016/j.chemgeo.2003.07.001.

Galloway, J. N. and G. E. Likens (1978). "The collection of precipitation for chemical analysis". *Tellus* 30.1, 71–82. DOI: 10.1111/J.2153-3490.1978.TB00819.X.

Galloway, J. N., J. Thornton, S. A. Norton, H. L. Volchok, and R. A. McLean (1982). "Trace metals in atmospheric deposition: A review and assessment". *Atmospheric Environment (1967)* 16.7, 1677–1700. DOI: 10.1016/0004-6981(82)90262-1.

Galy, A. and C. France-Lanord (1999). "Weathering processes in the Ganges-Brahmaputra basin and the riverine alkalinity budget". *Chemical Geology* 159.1-4, 31–60. DOI: 10.1016/S0009-2541(99)00033-9.

Garrels, R. M. and F. T. MacKenzie (1967). "Origin of the chemical compositions of some springs and lakes". In: ACS Publications.

Genuer, R., J. M. Poggi, C. Tuleau-Malot, and N. Villa-Vialaneix (2017). "Random Forests for Big Data". *Big Data Research* 9, 28–46. DOI: 10.1016/j.bdr.2017.07.003.

Ghasemizade, M. and M. Schirmer (2013). "Subsurface flow contribution in the hydrological cycle: Lessons learned and challenges ahead-a review". *Environmental Earth Sciences* 69.2, 707–718. DOI: 10.1007/s12665-013-2329-8.

Gibbs, R. J. (1970). "Mechanisms Controlling World Water Chemistry". *Science* 170.3962, 1088–1090. DOI: 10.1126/science.170.3962.1088.

Gillet, M., C. Le Gal La Salle, P. A. Ayral, S. Khaska, P. Martin, and P. Verdoux (2021). "Identification of the contributing area to river discharge during low-flow periods". *Hydrology and Earth System Sciences* 25.12, 6261–6281. DOI: 10.5194/hess-25-6261-2021.

Gillham, R. and J. Cherry (1978). "Field evidence of denitrification in shallow groundwater flow systems". *Water Quality Research Journal* 13.1, 53–72.

Glaser, B., M. Antonelli, M. Chini, L. Pfister, and J. Klaus (2018). "Technical note: Mapping surface-saturation dynamics with thermal infrared imagery". *Hydrology and Earth System Sciences* 22.11, 5987–6003. DOI: 10.5194/HESS-22-5987-2018.

Glaser, B., M. Antonelli, L. Hopp, and J. Klaus (2020). "Intra-catchment variability of surface saturation - Insights from physically based simulations in comparison with biweekly thermal infrared image observations". *Hydrology and Earth System Sciences* 24.3, 1393–1413. DOI: 10.5194/hess-24-1393-2020.

Glaser, B., L. Hopp, D. Partington, P. Brunner, R. Therrien, and J. Klaus (2021). "Sources of Surface Water in Space and Time: Identification of Delivery Processes and Geographical Sources With Hydraulic Mixing-Cell Modeling". *Water Resources Research* 57.12, 1–24. DOI: 10.1029/2021WR030332.

Glaser, B., C. Jackisch, L. Hopp, and J. Klaus (2019). "How Meaningful are Plot-Scale Observations and Simulations of Preferential Flow for Catchment Models?" *Vadose Zone Journal* 18.1, 1–18. DOI: 10.2136/vzj2018.08.0146.

Glaser, B., J. Klaus, S. Frei, J. Frentress, L. Pfister, and L. Hopp (2016). "On the value of surface saturated area dynamics mapped with thermal infrared imagery for modeling the hillslope-riparian-stream continuum". *Water Resources Research* 52.10, 8317–8342. DOI: 10.1002/2015WR018414.

Glassley, W. E., A. M. Simmons, and J. R. Kercher (2002). "Mineralogical heterogeneity in fractured, porous media and its representation in reactive transport models". *Applied Geochemistry* 17.6, 699–708. DOI: 10.1016/S0883-2927(02)00031-8.

Goddéris, Y., S. L. Brantley, L. M. François, J. Schott, D. Pollard, M. Déqué, and M. Dury (2013). "Rates of consumption of atmospheric CO2 through the weathering of loess during the next 100 yr of climate change". *Biogeosciences* 10.1, 135–148. DOI: 10.5194/bg-10-135-2013.

Goddéris, Y., L. M. François, A. Probst, J. Schott, D. Moncoulon, D. Labat, and D. Viville (2006). "Modelling weathering processes at the catchment scale: The WITCH numerical model". *Geochimica et Cosmochimica Acta* 70.5, 1128–1147. DOI: 10.1016/j.gca.2005.11.018.

Godsey, S. E., J. W. Kirchner, and D. W. Clow (2009). "Concentration-discharge relationships reflect chemostatic characteristics of US catchments". *Hydrological Processes* 23.13, 1844–1864. DOI: 10.1002/hyp.7315.

Goll, D. S., N. Moosdorf, J. Hartmann, and V. Brovkin (2014). "Climate-driven changes in chemical weathering and associated phosphorus release since 1850: Implications for the land carbon balance". *Geophysical Research Letters* 41.10, 3553–3558. DOI: 10.1002/2014GL059471.

Goren, O., B. Lazar, A. Burg, and I. Gavrieli (2012). "Mobilization and retardation of reduced manganese in sandy aquifers: Column experiments, modeling and implications". *Geochimica et Cosmochimica Acta* 96, 259–271. DOI: 10.1016/j.gca.2012.06.032.

Gourdol, L., R. Clement, J. Juilleret, L. Pfister, and C. Hissler (2021). "Exploring the regolith with electrical resistivity tomography in large-scale surveys: Electrode spacing-related issues and possibility". *Hydrology and Earth System Sciences* 25.4, 1785–1812. DOI: 10.5194/hess-25-1785-2021.

Grathwohl, P., H. Rügner, T. Wöhling, K. Osenbrück, M. Schwientek, S. Gayler, U. Wollschläger, B. Selle, M. Pause, J. O. Delfs, M. Grzeschik, U. Weller, M. Ivanov, O. A. Cirpka, U. Maier, B. Kuch, W. Nowak, V. Wulfmeyer, K. Warrach-Sagi, T. Streck, S. Attinger, L. Bilke, P. Dietrich, J. H. Fleckenstein, T. Kalbacher, O. Kolditz, K. Rink, L. Samaniego, H. J. Vogel, U. Werban, and G. Teutsch (2013). "Catchments as reactors: A comprehensive approach for water fluxes and solute turnover". *Environmental Earth Sciences* 69.2, 317–333. DOI: 10.1007/s12665-013-2281-7.

Griethuysen, C. van, M. Luitwieler, J. Joziasse, and A. A. Koelmans (2005). "Temporal variation of trace metal geochemistry in floodplain lake sediment subject to dynamic hydrological conditions". *Environmental Pollution* 137.2, 281–294. DOI: 10.1016/j.envpol.2005.01.023.

Güler, C. and G. D. Thyne (2004). "Hydrologic and geologic factors controlling surface and groundwater chemistry in Indian Wells-Owens Valley area, southeastern California, USA". *Journal of Hydrology* 285.1-4, 177–198. DOI: 10.1016/j.jhydrol.2003.08.019.

Güler, C., G. D. Thyne, J. E. McCray, and K. A. Turner (2002). "Evaluation of graphical and multivariate statistical methods for classification of water chemistry data". *Hydrogeology Journal* 10.4, 455–474. DOI: 10.1007/s10040-002-0196-6.

Hagen, J. S., E. Leblois, D. Lawrence, D. Solomatine, and A. Sorteberg (2021). "Identifying major drivers of daily streamflow from large-scale atmospheric circulation with machine learning". *Journal of Hydrology* 596.January, 126086. DOI: 10.1016/j.jhydrol.2021.126086.

Hagmaier, J. L. (1971). "Groundwater flow, hydrochemistry, and uranium deposition in the Powder River Basin, Wyoming".

Hale, V. C. and J. J. McDonnell (2016). "Effect of bedrock permeability on stream base flow mean transit time scaling relations: 1. A multiscale catchment intercomparison". *Water Resources Research* 52.2, 1358–1374. DOI: 10.1002/2014WR016124.

Handley-Sidhu, S., P. J. Worsfold, F. R. Livens, D. J. Vaughan, J. R. Lloyd, C. Boothman, M. Sajih, R. Alvarez, and M. J. Keith-Roach (2009). "Biogeochemical Controls on the Corrosion of Depleted Uranium Alloy in Subsurface Soils". *Environmental Science & Technology* 43.16, 6177–6182. DOI: 10.1021/es901276e.

Hanson, P. J., N. T. Edwards, C. T. Garten, and J. A. Andrews (2000). "Separating root and soil microbial contributions to soil respiration: A review of methods and observations". *Biogeochemistry* 48.1, 115–146. DOI: 10.1023/A:1006244819642.

Hartigan, J. A. (1975). *Clustering algorithms*. John Wiley & Sons, Inc.

Hartmann, J., N. Jansen, H. H. Dürr, S. Kempe, and P. Köhler (2009). "Global CO2-consumption by chemical weathering: What is the contribution of highly active weathering regions?" *Global and Planetary Change* 69.4, 185–194. DOI: 10.1016/j.gloplacha.2009.07.007.

Hartmann, M., P. Gomez-Pereira, C. Grob, M. Ostrowski, D. J. Scanlan, and M. V. Zubkov (2014). "Efficient CO2 fixation by surface Prochlorococcus in the Atlantic Ocean". *ISME Journal* 8.11, 2280–2289. DOI: 10.1038/ismej.2014.56.

Hastie, T. e. a. (2009). "Springer Series in Statistics The Elements of Statistical Learning". *The Mathematical Intelligencer* 27.2, 83–85.

Hercod, D. J., P. V. Brady, and R. T. Gregory (1998). "Catchment-scale coupling between pyrite oxidation and calcite weathering". *Chemical Geology* 151.1-4, 259–276. DOI: 10.1016/S0009-2541(98)00084-9.

Herman, J. S. and M. M. Lorah (1987). "CO2 outgassing and calcite precipitation in Falling Spring Creek, Virginia, U.S.A." *Chemical Geology* 62.3-4, 251–262. DOI: 10.1016/0009-2541(87)90090-8.

Herndon, E. M., A. L. Dere, P. L. Sullivan, D. Norris, B. Reynolds, and S. L. Brantley (2015). "Landscape heterogeneity drives contrasting concentration–discharge relationships in shale headwater catchments". *Hydrology and Earth System Sciences* 19.8, 3333–3347. DOI: 10.5194/hess-19-3333-2015.

Higashi, T. (1983). "Characterization of Al/Fe-humus complexes in dystrandepts through comparison with synthetic forms". *Geoderma* 31.4, 277–288. DOI: 10.1016/0016-7061(83)90041-1.

Hikov, A. (2004). "Geochemistry of strontium in advanced argillic alteration systems–possible guide to exploration". *Proceedings, Annual Scientific Conference, Sofia*, 16–17.

Hill, A. R. (2019). "Groundwater nitrate removal in riparian buffer zones: a review of research progress in the past 20 years". *Biogeochemistry* 143.3, 347–369. DOI: 10.1007/s10533-019-00566-5.

Hissler, C., N. Martínez-Carreras, F. Barnich, L. Gourdol, J. F. Iffly, J. Juilleret, J. Klaus, and L. Pfister (2021). "The Weierbach experimental catchment in Luxembourg: A decade of critical zone monitoring in a temperate forest - from hydrological investigations to ecohydrological perspectives". *Hydrological Processes* 35.5, 1–7. DOI: 10.1002/hyp.14140.

Hoagland, B., T. A. Russo, and S. L. Brantley (2017). "Relationships in a Headwater Sandstone Stream". *Water Resources Research RESEARCH* 53, 4643–4667. DOI: 10.1002/2016WR019717.Received.

Hobbie, S. E., P. B. Reich, J. Oleksyn, M. Ogdahl, R. Zytkowiak, C. Hale, and P. Karolewski (2006). "Tree species effects on decomposition and forest floor dynamics in a common garden". *Ecology* 87.9, 2288–2297. DOI: 10.1890/0012-9658(2006)87[2288:TSEODA]2.0.CO;2.

Hockmann, K., M. Lenz, S. Tandy, M. Nachtegaal, M. Janousch, and R. Schulin (2014). "Release of antimony from contaminated soil induced by redox changes". *Journal of Hazardous Materials* 275, 215–221. DOI: 10.1016/j.jhazmat.2014.04.065.

Hockmann, K., S. Tandy, M. Lenz, R. Reiser, H. M. Conesa, M. Keller, B. Studer, and R. Schulin (2015). "Antimony retention and release from drained and waterlogged shooting range soil under field conditions". *Chemosphere* 134, 536–543. DOI: 10.1016/j.chemosphere.2014.12.020.

Høgh-Jensen, H., R. Loges, F. V. Jørgensen, F. P. Vinther, and E. S. Jensen (2004). "An empirical model for quantification of symbiotic nitrogen fixation in grass-clover mixtures". *Agricultural Systems* 82.2, 181–194. DOI: 10.1016/j.agsy.2003.12.003.

Hooper, R. P., N. Christophersen, and N. E. Peters (1990). "Modelling streamwater chemistry as a mixture of soilwater end-members - An application to the Panola Mountain catchment, Georgia, U.S.A." *Journal of Hydrology* 116.1-4, 321–343. DOI: 10.1016/0022-1694(90)90131-G.

Hopp, L., C. Harman, S. L. Desilets, C. B. Graham, J. J. McDonnell, and P. A. Troch (2009). "Hillslope hydrology under glass: Confronting fundamental questions of soil-water-biota co-evolution at Biosphere 2". *Hydrology and Earth System Sciences* 13.11, 2105–2118. DOI: 10.5194/hess-13-2105-2009.

Hotelling, H. (1933). "Analysis of a complex of statistical variables into principal components." *Journal of educational psychology* 24.6, 417.

Hrachowitz, M., P. Benettin, B. M. van Breukelen, O. Fovet, N. J. Howden, L. Ruiz, Y. van der Velde, and A. J. Wade (2016). "Transit times—the link between hydrology and water quality at the catchment scale". *Wiley Interdisciplinary Reviews: Water* 3.5, 629–657. DOI: 10.1002/wat2.1155.

Hrachowitz, M., O. Fovet, L. Ruiz, and H. H. Savenije (2015). "Transit time distributions, legacy contamination and variability in biogeochemical 1/fα scaling: How are hydrological response dynamics linked to water quality at the catchment scale?" *Hydrological Processes* 29.25, 5241–5256. DOI: 10.1002/hyp.10546.

Ibarra, D. E., J. K. Caves, S. Moon, D. L. Thomas, J. Hartmann, C. P. Chamberlain, and K. Maher (2016). "Differential weathering of basaltic and granitic catchments from concentration–discharge relationships". *Geochimica et Cosmochimica Acta* 190, 265–293. DOI: 10.1016/j.gca.2016.07.006.

Jackisch, C., S. K. Hassler, T. L. Hohenbrink, T. Blume, H. Laudon, H. McMillan, P. Saco, and L. Van Schaik (2021). "Preface: Linking landscape organisation and hydrological functioning: From hypotheses and observations to concepts, models and understanding". *Hydrology and Earth System Sciences* 25.9, 5277–5285. DOI: 10.5194/hess-25-5277-2021.

Jadhav, M. S., K. C. Khare, and A. S. Warke (2015). "Water Quality Prediction of Gangapur Reservoir (India) Using LS-SVM and Genetic Programming". *Lakes and Reservoirs: Research and Management* 20.4, 275–284. DOI: 10.1111/lre.12113.

Jaremalm, M., S. Köhler, and F. Lidman (2013). "Precipitation of barite in the biosphere and its consequences and Simpevarp". *SKB TR-13-28. 82 s* December.

Jin, L., D. I. Siegel, L. K. Lautz, M. J. Mitchell, D. E. Dahms, and B. Mayer (2010). "Calcite precipitation driven by the common ion effect during groundwater-surface-water mixing: A potentially common process in streams with geologic settings containing

gypsum". *Bulletin of the Geological Society of America* 122.7-8, 1027–1038. DOI: 10.1130/B30011.1.

Johnson, N. M., G. E. Likens, F. H. Bormann, D. W. Fisher, and R. S. Pierce (1969). "A Working Model for the Variation in Stream Water Chemistry at the Hubbard Brook Experimental Forest, New Hampshire". *Water Resources Research* 5.6, 1353–1363. DOI: 10.1029/WR005i006p01353.

Johnson, T. M. and D. J. DePaolo (1994). "Interpretation of isotopic data in groundwater-rock systems: Model development and application to Sr isotope data from Yucca Mountain". *Water Resources Research* 30.5, 1571–1587. DOI: 10.1029/94WR00157.

Jolliffe, I. T. (2002). *Principal component analysis for special types of data*. Springer.

Jones, D. L. and A. C. Edwards (1998). "Influence of sorption on the biological utilization of two simple carbon substrates". *Soil Biology and Biochemistry* 30.14, 1895–1902. DOI: 10.1016/S0038-0717(98)00060-1.

Judd, A. G. (1980). "The use of cluster analysis in the derivation of geotechnical classifications". *Bulletin of the Association of Engineering Geologists* 17.4, 193–211.

Juilleret, J., S. Dondeyne, K. Vancampenhout, J. Deckers, and C. Hissler (2016). "Mind the gap: A classification system for integrating the subsolum into soil surveys". *Geoderma* 264, 332–339. DOI: 10.1016/j.geoderma.2015.08.031.

Kaiser, H. F. (1958). "Psychometrika". *Springer) The Varimax Criterion for Analytic Rotation in Factor Analysis* 23, 187.

Kaiser, K. and G. Guggenberger (2003). "Mineral surfaces and soil organic matter". *European Journal of Soil Science* 54.2, 219–236. DOI: 10.1046/j.1365-2389.2003.00544.x.

Kaiser, K., K. Eusterhues, C. Rumpel, G. Guggenberger, and I. Kögel-Knabner (2002). "Stabilization of organic matter by soil minerals - Investigations of density and particle-size fractions from two acid forest soils". *Journal of Plant Nutrition and Soil Science* 165.4, 451–459. DOI: 10.1002/1522-2624(200208)165:4<451::AID-JPLN451>3.0.CO;2-B.

Kaiser, K. and W. Zech (1998). "Soil Dissolved Organic Matter Sorption as Influenced by Organic and Sesquioxide Coatings and Sorbed Sulfate". *Soil Science Society of America Journal* 62.1, 129–136. DOI: 10.2136/sssaj1998.03615995006200010017x.

Kaleem, M., S. Naseem, E. Bashir, B. Shahab, and T. Rafique (2021). "Discrete geochemical behavior of Sr and Ba in the groundwater of Southern Mor Range, Balochistan, a tracer for igneous and sedimentary rocks weathering and related environmental issues". *Applied Geochemistry* 130.December 2020, 104996. DOI: 10.1016/j.apgeochem.2021.104996.

Karim, A. and J. Veizer (2000). "Weathering processes in the Indus River Basin: Implications from riverine carbon, sulfur, oxygen, and strontium isotopes". *Chemical Geology* 170.1-4, 153–177. DOI: 10.1016/S0009-2541(99)00246-6.

Kaste, J. M., A. M. Heimsath, and B. C. Bostick (2007). "Short-term soil mixing quantified with fallout radionuclides". *Geology* 35.3, 243–246. DOI: 10.1130/G23355A.1.

Kaufman, L. and P. J. Rousseeuw (2009). *Finding groups in data: an introduction to cluster analysis*. John Wiley & Sons.

Kavetski, D., F. Fenicia, and M. P. Clark (2011). "Impact of temporal data resolution on parameter inference and model identification in conceptual hydrological modeling: Insights from an experimental catchment". *Water Resources Research* 47.5, 1–25. DOI: 10.1029/2010WR009525.

Keller, C. K. and D. H. Bacon (1998). "Soil respiration and georespiration distinguished by transport analyses of vadose CO2, 13CO2, and 14CO2". *Global Biogeochemical Cycles* 12.2, 361–372. DOI: 10.1029/98GB00742.

Kim, H., J. K. Bishop, W. E. Dietrich, and I. Y. Fung (2014). "Process dominance shift in solute chemistry as revealed by long-term high-frequency water chemistry observations of groundwater flowing through weathered argillite underlying a steep forested hillslope". *Geochimica et Cosmochimica Acta* 140, 1–19. DOI: 10.1016/j.gca.2014.05.011.

King, A. C., M. Raiber, and M. E. Cox (2014). "Analyse statistique multi variables de données hydro chimiques pour caractériser une connexion aquifère-cours d'eau alluvial durant sécheresse et hautes eaux: Cressbrook Creek, Sud-Est du Queensland, Australie". *Hydrogeology Journal* 22.2, 481–500. DOI: 10.1007/s10040-013-1057-1.

Kirchner, J. W. (2003). "A double paradox in catchment hydrology and geochemistry". *Hydrological Processes* 17.4, 871–874. DOI: 10.1002/hyp.5108.

– (2009). "Catchments as simple dynamical systems: Catchment characterization, rainfall-runoff modeling, and doing hydrology backward". *Water Resources Research* 45.2, 1–34. DOI: 10.1029/2008WR006912.

Klaus, J. and J. McDonnell (2013). "Hydrograph separation using stable isotopes: Review and evaluation". *Journal of Hydrology* 505, 47–64. DOI: 10.1016/j.jhydrol.2013.09.006.

Klaus, J., C. E. Wetzel, N. Martínez-Carreras, L. Ector, and L. Pfister (2015). "A tracer to bridge the scales: On the value of diatoms for tracing fast flow path connectivity from headwaters to meso-scale catchments". *Hydrological Processes* 29.25, 5275–5289. DOI: 10.1002/hyp.10628.

Kleber, A. (1997). "Cover-beds as soil parent materials in midlatitude regions". *CATENA* 30.2-3, 197–213. DOI: 10.1016/S0341-8162(97)00018-0.

Kleber, M., R. Mikutta, M. S. Torn, and R. Jahn (2005). "Poorly crystalline mineral phases protect organic matter in acid subsoil horizons". *European Journal of Soil Science* 56.6, 050912034650054. DOI: 10.1111/j.1365-2389.2005.00706.x.

Knapp, J. L., C. Neal, A. Schlumpf, M. Neal, and J. W. Kirchner (2019). "New water fractions and transit time distributions at Plynlimon, Wales, estimated from stable

water isotopes in precipitation and streamflow". *Hydrology and Earth System Sciences* 23.10, 4367–4388. DOI: 10.5194/hess-23-4367-2019.

Kohfahl, C., C. Sprenger, J. B. Herrera, H. Meyer, F. F. Chacón, and A. Pekdeger (2008). "Recharge sources and hydrogeochemical evolution of groundwater in semiarid and karstic environments: A field study in the Granada Basin (Southern Spain)". *Applied Geochemistry* 23.4, 846–862. DOI: 10.1016/j.apgeochem.2007.09.009.

Kölle, W., P. Werner, O. Strebel, and J. Böttcher (1983). "Denitrifikation in einem reduzierenden Grundwasserleiter". *Vom Wasser* 61, 125–147.

Kong, M., L. Huang, L. Li, Z. Zhang, S. Zheng, and M. K. Wang (2014). "Effects of oxalic and citric acids on three clay minerals after incubation". *Applied Clay Science* 99, 207–214. DOI: 10.1016/j.clay.2014.06.035.

Korom, S. F. (1992). "Natural denitrification in the saturated zone: A review". *Water Resources Research* 28.6, 1657–1668. DOI: 10.1029/92WR00252.

Kusonwiriyawong, C., M. Bigalke, F. Abgottspon, M. Lazarov, and W. Wilcke (2016). "Response of Cu partitioning to flooding: A δ65Cu approach in a carbonatic alluvial soil". *Chemical Geology* 420, 69–76. DOI: 10.1016/j.chemgeo.2015.11.005.

Laaksoharju, M., M. Gascoyne, and I. Gurban (2008). "Understanding groundwater chemistry using mixing models". *Applied Geochemistry* 23.7, 1921–1940. DOI: 10.1016/j.apgeochem.2008.02.018.

Ladouche, B., A. Probst, D. Viville, S. Idir, D. Baqué, M. Loubet, J.-L. Probst, and T. Bariac (2001). "Hydrograph separation using isotopic, chemical and hydrological approaches (Strengbach catchment, France)". *Journal of Hydrology* 242.3-4, 255–274. DOI: 10.1016/S0022-1694(00)00391-7.

Land, M., J. Ingri, P. S. Andersson, and B. Öhlander (2000). "Ba/Sr, Ca/Sr and 87Sr/86Sr ratios in soil water and groundwater: Implications for relative contributions to stream water discharge". *Applied Geochemistry* 15.3, 311–325. DOI: 10.1016/S0883-2927(99)00054-2.

Langbein, W. and D. Dawdy (1964). "Occurrence of dissolved solids in surface waters". *US Geol. Survey Prof. Paper*, 116–117.

Langfelder, P. and S. Horvath (2012). "Fast R Functions for Robust Correlations and Hierarchical Clustering". *Journal of Statistical Software* 46.11, 1–7. DOI: 10.18637/jss.v046.i11.

Lasaga, A. C. (1984). "Chemical kinetics of water-rock interactions". *Journal of geophysical research: solid earth* 89.B6, 4009–4025.

Lee, M. H., J. L. Payeur-Poirier, J. H. Park, and E. Matzner (2016). "Variability in runoff fluxes of dissolved and particulate carbon and nitrogen from two watersheds of different tree species during intense storm events". *Biogeosciences* 13.18, 5421–5432. DOI: 10.5194/bg-13-5421-2016.

Lee, R. W. (1981). *Geochemistry of water in the Fort Union Formation of the northern Powder River Basin, southeastern Montana*. US Government Printing Office.

Lelong, F., C. Dupraz, P. Durand, and J. F. Didon-Lescot (1990). "Effects of vegetation type on the biogeochemistry of small catchments (Mont Lozere, France)". *Journal of Hydrology* 116.1-4, 125–145. DOI: 10.1016/0022-1694(90)90119-I.

Lequy, É., A. Legout, S. Conil, and M.-P. Turpault (2013). "Aeolian dust deposition rates in Northern French forests and inputs to their biogeochemical cycles". *Atmospheric Environment* 80, 281–289. DOI: 10.1016/j.atmosenv.2013.07.075.

Lerman, A., L. Wu, and F. T. Mackenzie (2007). "CO2 and H2SO4 consumption in weathering and material transport to the ocean, and their role in the global carbon balance". *Marine Chemistry* 106.1-2 SPEC. ISS. 326–350. DOI: 10.1016/j.marchem.2006.04.004.

Lerner, D., A. Issar, and I. Simmers (1990). "Groundwater recharge: a guide to understanding and estimating natural recharge. Int. Contrib. Hydrogeol. 8". *International Association of Hydrogeologists, Goring, UK*.

Levitan, D. M., C. E. Zipper, P. Donovan, M. E. Schreiber, R. R. Seal, M. A. Engle, J. A. Chermak, R. J. Bodnar, D. K. Johnson, and J. G. Aylor (2015). "Statistical analysis of soil geochemical data to identify pathfinders associated with mineral deposits: An example from the Coles Hill uranium deposit, Virginia, USA". *Journal of Geochemical Exploration* 154, 238–251. DOI: 10.1016/j.gexplo.2014.12.012.

Li, D. D., A. D. Jacobson, and D. J. McInerney (2014). "A reactive-transport model for examining tectonic and climatic controls on chemical weathering and atmospheric CO2 consumption in granitic regolith". *Chemical Geology* 365, 30–42. DOI: 10.1016/j.chemgeo.2013.11.028.

Li, F. and J. Zeng (2017). "Characterization of Origin and Evolution of Formation Water in Buried Hill of Jizhong Depression, China, Using Multivariate Statistical Analysis of Geochemical Data". *Geofluids* 2017. DOI: 10.1155/2017/5290686.

Li, L., C. Bao, P. L. Sullivan, S. Brantley, Y. Shi, and C. Duffy (2017). "Understanding watershed hydrogeochemistry: 2. Synchronized hydrological and geochemical processes drive stream chemostatic behavior". *Water Resources Research* 53.3, 2346–2367. DOI: 10.1002/2016WR018935.

Li, L., P. L. Sullivan, P. Benettin, O. A. Cirpka, K. Bishop, S. L. Brantley, J. L. Knapp, I. van Meerveld, A. Rinaldo, J. Seibert, H. Wen, and J. W. Kirchner (2021). "Toward catchment hydro-biogeochemical theories". *Wiley Interdisciplinary Reviews: Water* 8.1. DOI: 10.1002/wat2.1495.

Li, S. L., D. Calmels, G. Han, J. Gaillardet, and C. Q. Liu (2008). "Sulfuric acid as an agent of carbonate weathering constrained by δ13CDIC: Examples from Southwest China". *Earth and Planetary Science Letters* 270.3-4, 189–199. DOI: 10.1016/j.epsl.2008.02.039.

Liaw, A. and M. Wiener (2002). "Classification and Regression by randomForest". *R News* 2.3, 18–22.

Lindberg, R. D. and D. D. Runnells (1984). "Ground Water Redox Reactions: An Analysis of Equilibrium State Applied to Eh Measurements and Geochemical Modeling". *Science* 225.4665, 925–927. DOI: 10.1126/science.225.4665.925.

Lindberg, S. E., G. M. Lovett, D. A. Schaefer, and M. Bredemeier (1988). "Dry deposition velocities and surface-to-canopy scaling factors for aerosol calcium from forest canopy throughfall". *Journal of Aerosol Science* 19.7, 1187–1190. DOI: 10.1016/0021-8502(88)90132-2.

Lindberg, S. E., G. M. Lovett, D. Richter, and D. W. Johnson (1986). "Atmospheric deposition and canopy interactions of major ions in a forest". *Science* 231.4734, 141–145.

Lindberg, S. E. and G. M. Lovett (1985). "Field measurements of particle dry deposition rates to foliage and inert surfaces in a forest canopy". *Environmental Science & Technology* 19.3, 238–244. DOI: 10.1021/es00133a003.

Liu, Z., G. L. Macpherson, C. Groves, J. B. Martin, D. Yuan, and S. Zeng (2018). "Large and active CO2 uptake by coupled carbonate weathering". *Earth-Science Reviews* 182.December 2017, 42–49. DOI: 10.1016/j.earscirev.2018.05.007.

Lopez-Chicano, M., M. Bouamama, A. Vallejos, and A. Pulido-Bosch (2001). "Factors which determine the hydrogeochemical behaviour of karstic springs. A case study from the Betic Cordilleras, Spain". *Applied Geochemistry* 16.9-10, 1179–1192.

Lovett, G. M. and S. E. Lindberg (1993). "Atmospheric deposition and canopy interactions of nitrogen in forests". *Canadian Journal of Forest Research* 23.8, 1603–1616.

Lützow, M. V., I. Kögel-Knabner, K. Ekschmitt, E. Matzner, G. Guggenberger, B. Marschner, and H. Flessa (2006). "Stabilization of organic matter in temperate soils: Mechanisms and their relevance under different soil conditions - A review". *European Journal of Soil Science* 57.4, 426–445. DOI: 10.1111/j.1365-2389.2006.00809.x.

Macpherson, G. L., J. A. Roberts, J. M. Blair, M. A. Townsend, D. A. Fowle, and K. R. Beisner (2008). "Increasing shallow groundwater CO2 and limestone weathering, Konza Prairie, USA". *Geochimica et Cosmochimica Acta* 72.23, 5581–5599. DOI: 10.1016/j.gca.2008.09.004.

Maher, K. (2010). "The dependence of chemical weathering rates on fluid residence time". *Earth and Planetary Science Letters* 294.1-2, 101–110. DOI: 10.1016/j.epsl.2010.03.010.

– (2011). "The role of fluid residence time and topographic scales in determining chemical fluxes from landscapes". *Earth and Planetary Science Letters* 312.1-2, 48–58. DOI: 10.1016/j.epsl.2011.09.040.

Maher, K. and C. P. Chamberlain (2014). "Hydrologic regulation of chemical weathering and the geologic". *Science* 343.6178, 1502–1504. DOI: 10.1126/science.1250770.

Małoszewski, P. and A. Zuber (1982). "Determining the turnover time of groundwater systems with the aid of environmental tracers. 1. Models and their applicability". *Journal of Hydrology* 57.3-4, 207–231. DOI: 10.1016/0022-1694(82)90147-0.

Mansfeldt, T. (2003). "In situ long-term redox potential measurements in a dyked marsh soil". *Journal of Plant Nutrition and Soil Science* 166.2, 210–219. DOI: 10.1002/jpln.200390031.

Mansfeldt, T., S. Schuth, W. Häusler, F. E. Wagner, S. Kaufhold, and M. Overesch (2012). "Iron oxide mineralogy and stable iron isotope composition in a Gleysol with petrogleyic properties". *Journal of Soils and Sediments* 12.1, 97–114. DOI: 10.1007/s11368-011-0402-z.

Marandi, A. and P. Shand (2018). "Groundwater chemistry and the Gibbs Diagram". *Applied Geochemistry* 97.July, 209–212. DOI: 10.1016/j.apgeochem.2018.07.009.

Markelova, E. (2016). "Redox potential and mobility of contaminant oxyanions (As, Sb, Cr) in argillaceous rock subjected to oxic and anoxic cycles". Theses. Université Grenoble Alpes ; University of Waterloo (Canada).

Martínez-Carreras, N., C. E. Wetzel, J. Frentress, L. Ector, J. J. McDonnell, L. Hoffmann, and L. Pfister (2015). "Hydrological connectivity inferred from diatom transport through the riparian-stream system". *Hydrology and Earth System Sciences* 19.7, 3133–3151. DOI: 10.5194/hess-19-3133-2015.

Martínez-Carreras, N., C. Hissler, L. Gourdol, J. Klaus, J. Juilleret, J. F. Iffly, and L. Pfister (2016). "Storage controls on the generation of double peak hydrographs in a forested headwater catchment". *Journal of Hydrology* 543, 255–269. DOI: 10.1016/j.jhydrol.2016.10.004.

McDonnell, J. J., M. K. Stewart, and I. F. Owens (1991). "Effect of Catchment-Scale Subsurface Mixing on Stream Isotopic Response". *Water Resources Research* 27.12, 3065–3073. DOI: 10.1029/91WR02025.

McDonnell, J. J. and K. Beven (2014). "Debates-The future of hydrological sciences: A (common) path forward? A call to action aimed at understanding velocities, celerities and residence time distributions of the headwater hydrograph". *Water Resources Research* 50.6, 5342–5350. DOI: 10.1002/2013WR015141.

McGuire, J. T., E. W. Smith, D. T. Long, D. W. Hyndman, S. K. Haack, M. J. Klug, and M. A. Velbel (2000). "Temporal variations in parameters reflecting terminal-electron-accepting processes in an aquifer contaminated with waste fuel and chlorinated solvents". *Chemical Geology* 169.3-4, 471–485.

McGuire, K. J. and J. J. McDonnell (2006). "A review and evaluation of catchment transit time modeling". *Journal of Hydrology* 330.3-4, 543–563. DOI: 10.1016/j.jhydrol.2006.04.020.

McLaughlin, C. and L. A. Kaplan (2013). "Biological lability of dissolved organic carbon in stream water and contributing terrestrial sources". *Freshwater Science* 32.4, 1219–1230. DOI: 10.1899/12-202.1.

McMahon, P. B. and F. H. Chapelle (2008). "Redox processes and water quality of selected principal aquifer systems". *Ground Water* 46.2, 259–271. DOI: 10.1111/j.1745-6584.2007.00385.x.

McMahon, P. B., J. Böhlke, and S. Christenson (2004). "Geochemistry, radiocarbon ages, and paleorecharge conditions along a transect in the central High Plains aquifer, southwestern Kansas, USA". *Applied Geochemistry* 19.11, 1655–1686.

McMahon, P. B., F. H. Chapelle, and P. M. Bradley (2011). "Evolution of redox processes in groundwater". In: *Aquatic Redox Chemistry*. ACS Publications, 581–597.

McNab Jr., W. W. (2014). "A Monte Carlo-Based Approach for Groundwater Chemistry Inverse Modeling". *Open Journal of Modern Hydrology* 04.04, 112–120. DOI: 10.4236/ojmh.2014.44011.

Melloul, A. and M. Collin (1992). "The 'principal components' statistical method as a complementary approach to geochemical methods in water quality factor identification; application to the Coastal Plain aquifer of Israel". *Journal of Hydrology* 140.1-4, 49–73. DOI: 10.1016/0022-1694(92)90234-M.

Metropolis, N., A. W. Rosenbluth, M. N. Rosenbluth, A. H. Teller, and E. Teller (1953). "Equation of state calculations by fast computing machines". *The Journal of Chemical Physics* 21.6, 1087–1092. DOI: 10.1063/1.1699114.

Meybeck, M. and F. Moatar (2012). "Daily variability of river concentrations and fluxes: Indicators based on the segmentation of the rating curve". *Hydrological Processes* 26.8, 1188–1207. DOI: 10.1002/hyp.8211.

Mikutta, R., C. Mikutta, K. Kalbitz, T. Scheel, K. Kaiser, and R. Jahn (2007). "Biodegradation of forest floor organic matter bound to minerals via different binding mechanisms". *Geochimica et Cosmochimica Acta* 71.10, 2569–2590. DOI: 10.1016/j.gca.2007.03.002.

Millot, R., J. Gaillardet, B. Dupré, and C. J. Allégre (2003). "Northern latitude chemical weathering rates: Clues from the Mackenzie River Basin, Canada". *Geochimica et Cosmochimica Acta* 67.7, 1305–1329. DOI: 10.1016/S0016-7037(02)01207-3.

Mitchell, M. J. and R. D. Fuller (1988). "Models of sulfur dynamics in forest and grassland ecosystems with emphasis on soil processes". *Biogeochemistry* 5.1, 133–163.

Moatar, F., B. W. Abbott, C. Minaudo, F. Curie, and G. Pinay (2017). "Elemental properties, hydrology, and biology interact to shape concentration-discharge curves for carbon, nutrients, sediment, and major ions". *Water Resources Research* 53.2, 1270–1287. DOI: 10.1002/2016WR019635.

Montemagno, A., C. Hissler, V. Bense, A. J. Teuling, J. Ziebel, and L. Pfister (2022). "Dynamics of rare earth elements and associated major and trace elements during

Douglas-fir (Pseudotsuga menziesii) and European beech (Fagus sylvatica L.) litter degradation". *Biogeosciences* 19.13, 3111–3129. DOI: 10.5194/BG-19-3111-2022.

Moragues Quiroga, C. (2018). "Water mixing processes in the critical zone: evidence from trace elements and Sr-Nd-Pb-U isotopes". PhD thesis. Strasbourg.

Moragues-Quiroga, C., J. Juilleret, L. Gourdol, E. Pelt, T. Perrone, A. Aubert, G. Morvan, F. Chabaux, A. Legout, P. Stille, and C. Hissler (2017). "Genesis and evolution of regoliths: Evidence from trace and major elements and Sr-Nd-Pb-U isotopes". *CATENA* 149, 185–198. DOI: 10.1016/J.CATENA.2016.09.015.

Moses, C. O., D. K. Nordstrom, J. S. Herman, and A. L. Mills (1987). "Aqueous pyrite oxidation by dissolved oxygen and by ferric iron". *Geochimica et Cosmochimica Acta* 51.6, 1561–1571.

Mudd, S. M. and D. J. Furbish (2006). "Using chemical tracers in hillslope soils to estimate the importance of chemical denudation under conditions of downslope sediment transport". *Journal of Geophysical Research: Earth Surface* 111.2, 1–18. DOI: 10.1029/2005JF000343.

Mulholland, P. J., G. V. Wilson, and P. M. Jardine (1990). "Hydrogeochemical Response of a Forested Watershed to Storms: Effects of Preferential Flow Along Shallow and Deep Pathways". *Water Resources Research* 26.12, 3021–3036. DOI: 10.1029/WR026i012p03021.

Muneer, M. and J. Oades (1989). "The role of Ca-organic interactions in soil aggregate stability .II. Field studies with 14C-labeled straw, CaCO3 and CaSO4.2.H2O". *Soil Research* 27.2, 401. DOI: 10.1071/SR9890401.

Murphy, E. and J. Schramke (1998). "Estimation of microbial respiration rates in groundwater by geochemical modeling constrained with stable isotopes". *Geochimica et Cosmochimica Acta* 62.21-22, 3395–3406.

Musolff, A., C. Schmidt, B. Selle, and J. H. Fleckenstein (2015). "Catchment controls on solute export". *Advances in Water Resources* 86, 133–146. DOI: 10.1016/j.advwatres.2015.09.026.

Nordstrom, D. K., L. N. Plummer, D. Langmuir, E. Busenberg, H. M. May, B. F. Jones, and D. L. Parkhurst (1990). "Revised chemical equilibrium data for major water—mineral reactions and their limitations". In: ACS Publications.

Oades, J. M. (1988). "The retention of organic matter in soils". *Biogeochemistry* 5.1, 35–70. DOI: 10.1007/BF02180317.

Öberg, G. and P. Sandén (2005). "Retention of chloride in soil and cycling of organic matter-bound chlorine". *Hydrological Processes* 19.11, 2123–2136. DOI: 10.1002/hyp.5680.

Ocampo, C. J., C. E. Oldham, M. Sivapalan, and J. V. Turner (2006). "Hydrological versus biogeochemical controls on catchment nitrate export: a test of the flushing mechanism". *Hydrological Processes* 20.20, 4269–4286. DOI: 10.1002/hyp.6311.

Oostra, S., H. Majdi, and M. Olsson (2006). "Impact of tree species on soil carbon stocks and soil acidity in southern Sweden". *Scandinavian Journal of Forest Research* 21.5, 364–371. DOI: 10.1080/02827580600950172.

Oren, O., I. Gavrieli, A. Burg, J. Guttman, and B. Lazar (2007). "Manganese mobilization and enrichment during soil aquifer treatment (SAT) of effluents, the Dan Region Sewage Reclamation Project (Shafdan), Israel". *Environmental Science and Technology* 41.3, 766–772. DOI: 10.1021/es060576+.

Orth, P. and K. Schügerl (1972). "Distribution of residence times and contact times in packed bed reactors: influence of the chemical reaction". *Chemical Engineering Science* 27.3, 497–510.

Oste, L. A., E. J. Temminghoff, and W. H. Van Riemsdijk (2002). "Solid-solution partitioning of organic matter in soils as influenced by an increase in pH or Ca concentration". *Environmental Science and Technology* 36.2, 208–214. DOI: 10.1021/es0100571.

Otero, N., A. Soler, and À. Canals (2008). "Controls of δ34S and δ18O in dissolved sulphate: Learning from a detailed survey in the Llobregat River (Spain)". *Applied Geochemistry* 23.5, 1166–1185. DOI: 10.1016/j.apgeochem.2007.11.009.

Paerl, H. W. (1997). "Coastal eutrophication and harmful algal blooms: Importance of atmospheric deposition and groundwater as 'new' nitrogen and other nutrient sources". *Limnology and Oceanography* 42.5 II, 1154–1165. DOI: 10.4319/lo.1997.42.5{_}part{_}2.1154.

Pansu, M. and J. Gautheyrou (2006). "Handbook of Soil Analysis: Mineralogical, Organic and Inorganic Methods". In:

Parkhurst, D. L. and S. R. Charlton (2008). *NetpathXL, an Excel Interface to the Program NETPATH*. US Department of the Interior, US Geological Survey.

Parkhurst, D. L. and C. Appelo (2013). "Description of input and examples for PHREEQC Version 3 — A computer program for speciation, batch-reaction, one-dimensional transport, and inverse geochemical calculations". *U.S. Geological Survey Techniques and Methods, book 6, chapter A43*, 6–43.

Paschke, S. S., L. J. Kauffman, S. M. Eberts, and S. R. Hinkle (2007). "Overview of regional studies of the Transport of Anthropogenic and Natural Contaminants to public-supply wells". *US Geological Survey Professional Paper* 1737 A, 1–17.

Pawellekl, F., F. Frauenstein, and J. Veizer (2002). "Hydrochemistry and isotope geochemistry of the upper Danube River". *Geochimica et Cosmochimica Acta* 66.21, 3839–3853. DOI: 10.1016/S0016-7037(01)00880-8.

Pearson, K. (1901). "Principal components analysis". *The London, Edinburgh, and Dublin Philosophical Magazine and Journal of Science* 6.2, 559.

Pelizardi, F., S. A. Bea, J. Carrera, and L. Vives (2017). "Identifying geochemical processes using End Member Mixing Analysis to decouple chemical components for mixing ratio

calculations". *Journal of Hydrology* 550, 144–156. DOI: 10.1016/j.jhydrol.2017.04.010.

Peng, F., J. Wen, Y. Zhang, and J. Jin (2020). "Monthly Streamflow Prediction Based on Random Forest Algorithm and Phase Space Reconstruction Theory". *Journal of Physics: Conference Series* 1637.1. DOI: 10.1088/1742-6596/1637/1/012091.

Penn, C. J. and J. J. Camberato (2019). "A critical review on soil chemical processes that control how soil ph affects phosphorus availability to plants". *Agriculture (Switzerland)* 9.6, 1–18. DOI: 10.3390/agriculture9060120.

Petelet-Giraud, E., P. Négrel, and J. Casanova (2018). "Tracing surface water mixing and groundwater inputs using chemical and isotope fingerprints (δ18O-δ2H, 87Sr/86Sr) at basin scale: The Loire River (France)". *Applied Geochemistry* 97.March, 279–290. DOI: 10.1016/j.apgeochem.2018.08.028.

Petsch, S. T. and R. A. Berner (1998). "Coupling the geochemical cycles of C, P, Fe, and S; the effect on atmospheric O 2 and the isotopic records of carbon and sulfur". *American Journal of Science* 298.3, 246–262.

Pfister, L., N. Martínez-Carreras, C. Hissler, J. Klaus, G. E. Carrer, M. K. Stewart, and J. J. McDonnell (2017). "Bedrock geology controls on catchment storage, mixing, and release: A comparative analysis of 16 nested catchments". *Hydrological Processes* 31.10, 1828–1845. DOI: 10.1002/HYP.11134.

Pfister, L., J. J. McDonnell, C. Hissler, and L. Hoffmann (2010). "Ground-based thermal imagery as a simple, practical tool for mapping saturated area connectivity and dynamics". *Hydrological Processes* 24.21, 3123–3132. DOI: 10.1002/hyp.7840.

Pinay, G., S. Peiffer, J. R. De Dreuzy, S. Krause, D. M. Hannah, J. H. Fleckenstein, M. Sebilo, K. Bishop, and L. Hubert-Moy (2015). "Upscaling Nitrogen Removal Capacity from Local Hotspots to Low Stream Orders' Drainage Basins". *Ecosystems* 18.6, 1101–1120. DOI: 10.1007/s10021-015-9878-5.

Piper, A. M. (1944). "A graphic procedure in the geochemical interpretation of water-analyses". *Eos, Transactions American Geophysical Union* 25.6, 914–928.

Plummer, B. L. N., E. C. Prestemon, and D. L. Parkhurst (1991a). "An interactive code (NETPATH) for modeling net geochemical reactions along a flow path". *U.S Geological survey*, 231.

Plummer, L. N., E. C. Prestemon, and D. L. Parkhurst (1994). "An interactive code (NETPATH) for modeling NET geochemical reactions along a flow PATH, version 2.0. USGS Water-Resources Investigations Report, 94- 4169, 130 p." *Water-Resources Investigations Report*, 130 p.

Plummer, L. N. (1992). "Geochemical modeling of water-rock interaction; Past, present, future". In: *International symposium on water-rock interaction*, 23–33.

Plummer, L. N., E. C. Prestemon, and D. L. Parkhurst (1991b). *An interactive code (NETPATH) for modeling net geochemical reactions along a flow path*. 91-4078. Department of the Interior, US Geological Survey.

Plummer, L. N., J. F. Busby, R. W. Lee, and B. B. Hanshaw (1990). "Geochemical Modeling of the Madison Aquifer in Parts of Montana, Wyoming, and South Dakota". *Water Resources Research* 26.9, 1981–2014. DOI: 10.1029/WR026i009p01981.

Postma, D., C. Boesen, H. Kristiansen, and F. Larsen (1991). "Nitrate reduction in an unconfined sandy aquifer: water chemistry, reduction processes, and geochemical modeling". *Water resources research* 27.8, 2027–2045.

Puckett, L. J., T. K. Cowdery, P. B. McMahon, L. H. Tornes, and J. D. Stoner (2002). "Using chemical, hydrologic, and age dating analysis to delineate redox processes and flow paths in the riparian zone of a glacial outwash aquifer-stream system". *Water Resources Research* 38.8, 9–1.

Racine, J. S. (2012). *RStudio: a platform-independent IDE for R and Sweave*.

Raich, J. W. and C. S. Potter (1995). "Global patterns of carbon dioxide emissions from soils". *Global Biogeochemical Cycles* 9.1, 23–36. DOI: 10.1029/94GB02723.

Reardon, E. J., G. B. Allison, and P. Fritz (1979). "Seasonal chemical and isotopic variations of soil Co2 at Trout Creek, Ontario". *Developments in Water Science* 12.C, 355–371. DOI: 10.1016/S0167-5648(09)70026-7.

Reddy, K. R. and R. D. DeLaune (2008). *Biogeochemistry of wetlands: science and applications*. CRC press.

Rehage, H. and M. Kind (2021). "The first Damköhler number and its importance for characterizing the influence of mixing on competitive chemical reactions". *Chemical Engineering Science* 229, 116007. DOI: 10.1016/j.ces.2020.116007.

Reich, P. B., J. Oleksyn, J. Modrzynski, P. Mrozinski, S. E. Hobbie, D. M. Eissenstat, J. Chorover, O. A. Chadwick, C. M. Hale, and M. G. Tjoelker (2005). "Linking litter calcium, earthworms and soil properties: A common garden test with 14 tree species". *Ecology Letters* 8.8, 811–818. DOI: 10.1111/j.1461-0248.2005.00779.x.

Reimann, C., P. Filzmoser, R. Garrett, and R. Dutter (2011). *Statistical data analysis explained: applied environmental statistics with R*. John Wiley & Sons.

Rickard, D. and G. W. Luther (2007). "Chemistry of Iron Sulfides". *Chemical Reviews* 107.2, 514–562. DOI: 10.1021/cr0503658.

Rinklebe, J., S. Antić-Mladenović, T. Frohne, H. J. Stärk, Z. Tomić, and V. Ličina (2016). "Nickel in a serpentine-enriched Fluvisol: Redox affected dynamics and binding forms". *Geoderma* 263, 203–214. DOI: 10.1016/j.geoderma.2015.09.004.

Rivett, M. O., S. R. Buss, P. Morgan, J. W. Smith, and C. D. Bemment (2008). "Nitrate attenuation in groundwater: a review of biogeochemical controlling processes". *Water research* 42.16, 4215–4232.

Robertson, W. D., J. A. Cherry, and S. L. Schiff (1989). "Atmospheric sulfur deposition 1950-1985 inferred from sulfate in groundwater". *Water Resources Research* 25.6, 1111–1123. DOI: 10.1029/WR025i006p01111.

Rodriguez, N. B. and J. Klaus (2019). "Catchment Travel Times From Composite StorAge Selection Functions Representing the Superposition of Streamflow Generation Processes". *Water Resources Research* 55.11, 9292–9314. DOI: 10.1029/2019WR024973.

Roelandt, C., Y. Godderis, M. P. Bonnet, and F. Sondag (2010). "Coupled modeling of biospheric and chemical weathering processes at the continental scale". *Global Biogeochemical Cycles* 24.2, 1–18. DOI: 10.1029/2008GB003420.

Roland, M., P. Serrano-Ortiz, A. S. Kowalski, Y. Goddéris, E. P. Sánchez-Cañete, P. Ciais, F. Domingo, S. Cuezva, S. Sanchez-Moral, B. Longdoz, D. Yakir, R. Van Grieken, J. Schott, C. Cardell, and I. A. Janssens (2013). "Atmospheric turbulence triggers pronounced diel pattern in karst carbonate geochemistry". *Biogeosciences* 10.7, 5009–5017. DOI: 10.5194/bg-10-5009-2013.

Romero-Mujalli, G., J. Hartmann, J. Börker, J. Gaillardet, and D. Calmels (2019). "Ecosystem controlled soil-rock pCO2 and carbonate weathering – Constraints by temperature and soil water content". *Chemical Geology* 527, 118634. DOI: 10.1016/j.chemgeo.2018.01.030.

Sacks, L. A., J. S. Herman, and S. J. Kauffman (1995). "Controls on high sulfate concentrations in the Upper Floridan aquifer in southwest Florida". *Water Resources Research* 31.10, 2541–2551.

Sahraei, A., A. Chamorro, P. Kraft, and L. Breuer (2021). "Application of Machine Learning Models to Predict Maximum Event Water Fractions in Streamflow". *Frontiers in Water* 3.June, 1–21. DOI: 10.3389/frwa.2021.652100.

Sakaa, B., A. Elbeltagi, S. Boudibi, H. Chaffaï, A. R. M. T. Islam, L. C. Kulimushi, P. Choudhari, A. Hani, Y. Brouziyne, and Y. J. Wong (2022). "Water quality index modeling using random forest and improved SMO algorithm for support vector machine in Saf-Saf river basin". *Environmental Science and Pollution Research* 29.32, 48491–48508. DOI: 10.1007/s11356-022-18644-x.

Saraceno, J. F., B. A. Pellerin, B. D. Downing, E. Boss, P. A. Bachand, and B. A. Bergamaschi (2009). "High-frequency in situ optical measurements during a storm event: Assessing relationships between dissolved organic matter, sediment concentrations, and hydrologic processes". *Journal of Geophysical Research: Biogeosciences* 114.4. DOI: 10.1029/2009JG000989.

Saunders, J. A. and L. E. Toran (1994). "Evidence for dedolomitization and mixing in Paleozoic carbonates near Oak Ridge, Tennessee". *Groundwater* 32.2, 207–214.

Saylor, R. D., B. D. Baker, P. Lee, D. Tong, L. Pan, and B. B. Hicks (2019). "The particle dry deposition component of total deposition from air quality models: right,

wrong or uncertain?" *Tellus B: Chemical and Physical Meteorology* 71.1, 1550324. DOI: 10.1080/16000889.2018.1550324.

Scaini, A., M. Audebert, C. Hissler, F. Fenicia, L. Gourdol, L. Pfister, and K. J. Beven (2017). "Velocity and celerity dynamics at plot scale inferred from artificial tracing experiments and time-lapse ERT". *Journal of Hydrology* 546, 28–43. DOI: 10.1016/J.JHYDROL.2016.12.035.

Scaini, A., C. Hissler, F. Fenicia, J. Juilleret, J. F. Iffly, L. Pfister, and K. Beven (2018). "Hillslope response to sprinkling and natural rainfall using velocity and celerity estimates in a slate-bedrock catchment". *Journal of Hydrology* 558, 366–379. DOI: 10.1016/j.jhydrol.2017.12.011.

Schlesinger, W. H., J. T. Gray, and F. S. Gilliam (1982). "Atmospheric deposition processes and their importance as sources of nutrients in a chaparral ecosystem of southern California". *Water Resources Research* 18.3, 623–629. DOI: 10.1029/WR018i003p00623.

Schoeller, H. (1960). "Salinity of groundwater, evapotranspiration and recharge of aquifers". *IASH Pulls., France*.

Schoeneberger, P. J. and D. A. Wysocki (2005). "Hydrology of soils and deep regolith: A nexus between soil geography, ecosystems and land management". *Geoderma* 126.1-2 SPEC. ISS. 117–128. DOI: 10.1016/j.geoderma.2004.11.010.

Schot, P. and J. Van der Wal (1992). "Human impact on regional groundwater composition through intervention in natural flow patterns and changes in land use". *Journal of Hydrology* 134.1-4, 297–313.

Schulz-Zunkel, C., J. Rinklebe, and H. R. Bork (2015). "Trace element release patterns from three floodplain soils under simulated oxidized-reduced cycles". *Ecological Engineering* 83, 485–495. DOI: 10.1016/j.ecoleng.2015.05.028.

Schwab, M., J. Klaus, L. Pfister, and M. Weiler (2017). "How runoff components affect the export of DOC and nitrate: a long-term and high-frequency analysis". *Hydrology and Earth System Sciences Discussions* July, 1–21.

Schwab, M. P., J. Klaus, L. Pfister, and M. Weiler (2018). "Diel fluctuations of viscosity-driven riparian inflow affect streamflow DOC concentration". *Biogeosciences* 15.7, 2177–2188. DOI: 10.5194/bg-15-2177-2018.

Scott, K. and C. Pain (2009). *Regolith science*. Csiro Publishing.

Seeboonruang, U. and T. R. Ginn (2006a). "Upscaling heterogeneity in aquifer reactivity via exposure-time concept: Forward model". *Journal of Contaminant Hydrology* 84.3-4, 127–154. DOI: 10.1016/j.jconhyd.2005.12.011.

– (2006b). "Upscaling heterogeneity in aquifer reactivity via the exposure-time concept: Inverse model". *Journal of Contaminant Hydrology* 84.3-4, 155–177. DOI: 10.1016/j.jconhyd.2005.12.010.

Seibert, J., T. Grabs, S. Köhler, H. Laudon, M. Winterdahl, and K. Bishop (2009). "Linking soil- and stream-water chemistry based on a Riparian Flow-Concentration Integration Model". *Hydrology and Earth System Sciences* 13.12, 2287–2297. DOI: 10.5194/hess-13-2287-2009.

Semmel, A. and B. Terhorst (2010). "The concept of the Pleistocene periglacial cover beds in central Europe: A review". *Quaternary International* 222.1-2, 120–128. DOI: 10.1016/j.quaint.2010.03.010.

Serrano-Ortiz, P., M. Roland, S. Sanchez-Moral, I. A. Janssens, F. Domingo, Y. Goddéris, and A. S. Kowalski (2010). "Hidden, abiotic CO2 flows and gaseous reservoirs in the terrestrial carbon cycle: Review and perspectives". *Agricultural and Forest Meteorology* 150.3, 321–329. DOI: 10.1016/j.agrformet.2010.01.002.

Sharif, M. U., R. K. Davis, K. F. Steele, B. Kim, T. M. Kresse, and J. A. Fazio (2008). "Inverse geochemical modeling of groundwater evolution with emphasis on arsenic in the Mississippi River Valley alluvial aquifer, Arkansas (USA)". *Journal of Hydrology* 350.1-2, 41–55. DOI: 10.1016/j.jhydrol.2007.11.027.

Smith, R. L. and J. H. Duff (1988). "Denitrification in a sand and gravel aquifer". *Applied and Environmental Microbiology* 54.5, 1071–1078. DOI: 10.1128/aem.54.5.1071-1078.1988.

Spalding, R. F. and M. E. Exner (1993). "Occurrence of nitrate in groundwater—a review". *Journal of environmental quality* 22.3, 392–402.

Spence, J. and K. Telmer (2005). "The role of sulfur in chemical weathering and atmospheric CO2 fluxes: Evidence from major ions, δ13CDIC, and δ34SSO4 in rivers of the Canadian Cordillera". *Geochimica et Cosmochimica Acta* 69.23, 5441–5458. DOI: 10.1016/j.gca.2005.07.011.

Stadler, S., K. Osenbrück, K. Knöller, A. Suckow, J. Sültenfuß, H. Oster, T. Himmelsbach, and H. Hötzl (2008). "Understanding the origin and fate of nitrate in groundwater of semi-arid environments". *Journal of Arid Environments* 72.10, 1830–1842. DOI: 10.1016/j.jaridenv.2008.06.003.

Stallard, R. F. and S. F. Murphy (2014). "A Unified Assessment of Hydrologic and Biogeochemical Responses in Research Watersheds in Eastern Puerto Rico Using Runoff-Concentration Relations". *Aquatic Geochemistry* 20.2-3, 115–139. DOI: 10.1007/s10498-013-9216-5.

Starr, R. C. and R. W. Gillham (1993). "Denitrification and organic carbon availability in two aquifers". *Groundwater* 31.6, 934–947.

Steefel, C. I. and K. Mäher (2009). "Fluid-rock interaction: A reactive transport approach". *Reviews in Mineralogy and Geochemistry* 70.July 2014, 485–532. DOI: 10.2138/rmg.2009.70.11.

Stewart, B., J. B. Shanley, J. W. Kirchner, D. Norris, T. Adler, C. Bristol, A. A. Harpold, J. N. Perdrial, D. M. Rizzo, G. Sterle, K. L. Underwood, H. Wen, and L. Li (2022). "Streams as Mirrors: Reading Subsurface Water Chemistry From Stream Chemistry". *Water Resources Research* 58.1. DOI: 10.1029/2021WR029931.

Stiff, H. A. (1951). "The interpretation of chemical water analysis by means of patterns". *Journal of petroleum technology* 3.10, 15–3.

Strebel, O., J. Böttcher, and W. Kölle (1985). "Stoffbilanzen im Grundwasser eines Einzugsgebietes als Hilfsmittel bei Klärung und Prognose von Grundwasserqualitätsproblemen (Beispiel Fuhrberger Feld)". *Zeitschrift der Deutschen Geologischen Gesellschaft*, 533–541.

Stumm, W., J. J. Morgan, and J. I. Drever (1996). "Aquatic chemistry". *Journal of environmental quality* 25.5, 1162.

Stumm, W. and J. J. Morgan (1970). "Aquatic Chemistry: Chemical Equilibria and Rates in Natural Waters". In:

Svensson, T., G. M. Lovett, and G. E. Likens (2012). "Is chloride a conservative ion in forest ecosystems?" *Biogeochemistry* 107.1-3, 125–134. DOI: 10.1007/s10533-010-9538-y.

Szramek, K. and L. M. Walter (2004). "Impact of Carbonate Precipitation on Riverine Inorganic Carbon Mass Transport from a Mid-continent, Forested Watershed". *Aquatic Geochemistry* 10.1/2, 99–137. DOI: 10.1023/B:AQUA.0000038960.63501.5b.

Tabatabai, M. A. (1987). "Physicochemical Fate of Sulfate in Soils". *JAPCA* 37.1, 34–38. DOI: 10.1080/08940630.1987.10466197.

Tang, G., M. A. Mayes, J. C. Parker, and P. M. Jardine (2010). "CXTFIT/Excel-A modular adaptable code for parameter estimation, sensitivity analysis and uncertainty analysis for laboratory or field tracer experiments". *Computers and Geosciences* 36.9, 1200–1209. DOI: 10.1016/j.cageo.2010.01.013.

Tank, S. E., R. G. Striegl, J. W. McClelland, and S. V. Kokelj (2016). "Multi-decadal increases in dissolved organic carbon and alkalinity flux from the Mackenzie drainage basin to the Arctic Ocean". *Environmental Research Letters* 11.5, 1–10. DOI: 10.1088/1748-9326/11/5/054015.

Team, R. et al. (n.d.). *CR Core Team R: A Language and Environment for Statistical Computing*.

Templ, M., P. Filzmoser, and C. Reimann (2008). "Cluster analysis applied to regional geochemical data: problems and possibilities". *Applied Geochemistry* 23.8, 2198–2213.

Tesoriero, A. J., H. Liebscher, and S. E. Cox (2000). "Mechanism and rate of denitrification in an agricultural watershed: Electron and mass balance along groundwater flow paths". *Water resources research* 36.6, 1545–1559.

Theis, C. V. (1935). "The relation between the lowering of the piezometric surface and the rate and duration of discharge of a well using ground-water storage". *Eos, Transactions American Geophysical Union* 16.2, 519–524.

Thompson, A., O. A. Chadwick, D. G. Rancourt, and J. Chorover (2006). "Iron-oxide crystallinity increases during soil redox oscillations". *Geochimica et Cosmochimica Acta* 70.7, 1710–1727. DOI: 10.1016/j.gca.2005.12.005.

Thurman, E. M. (2012). *Organic geochemistry of natural waters*. Vol. 2. Springer Science & Business Media.

Thyne, G., C. Güler, and E. Poeter (2004). "Sequential analysis of hydrochemical data for watershed characterization". *Ground Water* 42.5, 711–723. DOI: 10.1111/j.1745-6584.2004.tb02725.x.

Tipper, E. T., E. I. Stevenson, V. Alcock, A. C. Knight, J. J. Baronas, R. G. Hilton, M. J. Bickle, C. S. Larkin, L. Feng, K. E. Relph, and G. Hughes (2020). "Global silicate weathering flux overestimated because of sediment-water cation exchange". *Proceedings of the National Academy of Sciences of the United States of America* 118.1. DOI: 10.1073/pnas.2016430118.

Tonkin, M. and J. Doherty (2009). "Calibration-constrained Monte Carlo analysis of highly parameterized models using subspace techniques". *Water Resources Research* 45.1, 1–17. DOI: 10.1029/2007WR006678.

Toride, N. and F. J. Leij (1995). "Parameters from Laboratory or Field". *Transport* 137, 1–131.

Torres, M. A., A. J. West, and G. Li (2014). "Sulphide oxidation and carbonate dissolution as a source of CO2 over geological timescales". *Nature* 507.7492, 346–349. DOI: 10.1038/nature13030.

Turchyn, A. V., E. T. Tipper, A. Galy, J. K. Lo, and M. J. Bickle (2013). "Isotope evidence for secondary sulfide precipitation along the Marsyandi River, Nepal, Himalayas". *Earth and Planetary Science Letters* 374, 36–46. DOI: 10.1016/j.epsl.2013.04.033.

Tuttle, M. L., G. N. Breit, and I. M. Cozzarelli (2009). "Processes affecting δ34S and δ18O values of dissolved sulfate in alluvium along the Canadian River, central Oklahoma, USA". *Chemical Geology* 265.3-4, 455–467. DOI: 10.1016/j.chemgeo.2009.05.009.

Van Beek, C., H. Boukes, D. Van Rijsbergen, and R. Straatman (1988). "The threat of the Netherlands waterworks by nitrate in the abstracted groundwater, as demonstrated on the well field Vierlingsbeek." *Water Supply* 6.3, 313–318.

Viers, J., B. Dupre, J. J. Braun, R. Freydier, S. Greenberg, J. N. Ngoupayou, and L. S. Mkamdjou (2001). "Evidence for non-conservative behaviour of chlorine in humid tropical environments". *Aquatic Geochemistry* 7.2, 127–154. DOI: 10.1023/A:1017930106507.

Von Blanckenburg, F., J. Bouchez, D. E. Ibarra, and K. Maher (2015). "Stable runoff and weathering fluxes into the oceans over Quaternary climate cycles". *Nature Geoscience* 8.7, 538–542. DOI: 10.1038/ngeo2452.

Walker, J. C., P. Hays, and J. F. Kasting (1981). "A negative feedback mechanism for the long-term stabilization of Earth's surface temperature". *Journal of Geophysical Research: Oceans* 86.C10, 9776–9782.

Ward, J. H. (1963). "Hierarchical Grouping to Optimize an Objective Function". *Journal of the American Statistical Association* 58.301, 236. DOI: 10.2307/2282967.

Watanabe, M., T. Takamatsu, M. K. Koshikawa, S. Yamamura, and K. Inubushi (2008). "Dry deposition of acidic air pollutants to tree leaves, determined by a modified leaf-washing technique". *Atmospheric Environment* 42.32, 7339–7347. DOI: 10.1016/j.atmosenv.2008.07.015.

Wei, W., X. Zhang, J. Cui, and Z. Wei (2011). "Interaction between low molecular weight organic acids and hydroxyapatite with different degrees of crystallinity". *Colloids and Surfaces A: Physicochemical and Engineering Aspects* 392.1, 67–75. DOI: 10.1016/j.colsurfa.2011.09.034.

Welch, L. A. and D. M. Allen (2014). "Caractéristiques de la conductivité hydraulique en région de montagne et implications pour la conceptualisation des écoulements souterraines dans la roche en place". *Hydrogeology Journal* 22.5, 1003–1026. DOI: 10.1007/s10040-014-1121-5.

Wen, H. and L. Li (2018). "An upscaled rate law for mineral dissolution in heterogeneous media: The role of time and length scales". *Geochimica et Cosmochimica Acta* 235, 1–20. DOI: 10.1016/j.gca.2018.04.024.

White, A. F. and A. E. Blum (1995). "Effects of climate on chemical, weathering in watersheds". *Pergamon Geochimica et Cosmochimica Acta* 59.9, 1729–1747.

Williams, M. W., A. D. Brown, and J. M. Melack (1993). "Geochemical and hydrologic controls on the composition of surface water in a high-elevation basin. Sierra Nevada, California". *Limnology and Oceanography* 38.4, 775–797. DOI: 10.4319/lo.1993.38.4.0775.

Winter, T., S. Mallory, T. Allen, and D. Rosenberry (2000). "The use of principal component analysis for interpreting ground water hydrographs". *Groundwater* 38.2, 234–246.

Winterdahl, M., M. Erlandsson, M. N. Futter, G. A. Weyhenmeyer, and K. Bishop (2014). "Intra-annual variability of organic carbon concentrations in running waters: Drivers along a climatic gradient". *Global Biogeochemical Cycles* 28.4, 451–464.

Wood, W. W. (1999). "Use and misuse of the chloride-mass balance method in estimating ground water recharge". *Ground water* 37.1, 2–5.

– (2019). "Geogenic groundwater solutes: the myth". *Hydrogeology Journal* 27.8, 2729–2738. DOI: 10.1007/s10040-019-02057-1.

Wood, W. W. and W. E. Sanford (1995). "Chemical and Isotopic Methods for Quantifying Ground-Water Recharge in a Regional, Semiarid Environment". *Ground Water* 33.3, 458–468. DOI: 10.1111/j.1745-6584.1995.tb00302.x.

Woodruff, L., W. F. Cannon, D. B. Smith, and F. Solano (2015). "The distribution of selected elements and minerals in soil of the conterminous United States". *Journal of Geochemical Exploration* 154, 49–60. DOI: 10.1016/j.gexplo.2015.01.006.

Wrede, S., F. Fenicia, N. Martínez-Carreras, J. Juilleret, C. Hissler, A. Krein, H. H. Savenije, S. Uhlenbrook, D. Kavetski, and L. Pfister (2015). "Towards more systematic perceptual model development: A case study using 3 Luxembourgish catchments". *Hydrological Processes* 29.12, 2731–2750. DOI: 10.1002/hyp.10393.

Wymore, A. S., R. L. Brereton, D. E. Ibarra, and W. H. Mcdowell (2017). "Critical zone structure controls concentration-discharge relationships and solute generation in forested tropical montane watersheds", 6279–6295. DOI: 10.1002/2016WR020016.Received.

Xiao, D., S. L. Brantley, and L. Li (2021). "Vertical Connectivity Regulates Water Transit Time and Chemical Weathering at the Hillslope Scale". *Water Resources Research* 57.8, 1–21. DOI: 10.1029/2020WR029207.

Xu, J., Q. Wei, Y. Yu, S. Peng, and S. Yang (2013). "Influence of water management on the mobility and fate of copper in rice field soil". *Journal of Soils and Sediments* 13.7, 1180–1188. DOI: 10.1007/s11368-013-0716-0.

Yoshimura, K., Z. Liu, J. Cao, D. Yuan, Y. Inokura, and M. Noto (2004). "Deep source CO2 in natural waters and its role in extensive tufa deposition in the Huanglong Ravines, Sichuan, China". *Chemical Geology* 205.1-2, 141–153. DOI: 10.1016/j.chemgeo.2004.01.004.

Yoshimura, K., S. Nakao, M. Noto, Y. Inokura, K. Urata, M. Chen, and P. W. Lin (2001). "Geochemical and stable isotope studies on natural water in the Taroko Gorge karst area, Taiwan- Chemical weathering of carbonate rocks by deep source CO2 and sulfuric acid". *Chemical Geology* 177.3-4, 415–430. DOI: 10.1016/S0009-2541(00)00423-X.

Yu, F. and A. G. Hunt (2017). "Damköhler Number Input to Transport-Limited Chemical Weathering Calculations". *ACS Earth and Space Chemistry* 1.1, 30–38. DOI: 10.1021/acsearthspacechem.6b00007.

Yu, T. and P. L. Bishop (1998). "Stratification of microbial metabolic processes and redox potential change in an aerobic biofilm studied using microelectrodes". *Water Science and Technology* 37.4-5, 195–198.

Yuan, F. and B. Mayer (2012). "Chemical and isotopic evaluation of sulfur sources and cycling in the Pecos River, New Mexico, USA". *Chemical Geology* 291, 13–22. DOI: 10.1016/j.chemgeo.2011.11.014.

Zarnetske, J. P., R. Haggerty, S. M. Wondzell, and M. A. Baker (2011). "Dynamics of nitrate production and removal as a function of residence time in the hyporheic zone". *Journal of Geophysical Research: Biogeosciences* 116.1, 1–12. DOI: 10.1029/2010JG001356.

Zhang, Z. and A. Furman (2021). "Soil redox dynamics under dynamic hydrologic regimes - A review". *Science of the Total Environment* 763, 143026. DOI: 10.1016/j.scitotenv.2020.143026.

Zhi, W., L. Li, W. Dong, W. Brown, J. Kaye, C. Steefel, and K. H. Williams (2019). "Distinct Source Water Chemistry Shapes Contrasting Concentration-Discharge Patterns". *Water Resources Research* 55.5, 4233–4251. DOI: 10.1029/2018WR024257.

Zhu, C., G. Anderson, et al. (2002). *Environmental applications of geochemical modeling*. Cambridge University Press.

Zimmer, M. A. and J. P. Gannon (2018). "Run-off processes from mountains to foothills: The role of soil stratigraphy and structure in influencing run-off characteristics across high to low relief landscapes". *Hydrological Processes* 32.11, 1546–1560. DOI: 10.1002/hyp.11488.

Zimmer, M. A. and B. L. McGlynn (2017). "Time-lapse animation of hillslope groundwater dynamics details event-based and seasonal bidirectional stream-groundwater gradients". *Hydrological Processes* 31.10, 1983–1985. DOI: 10.1002/hyp.11124.

Zimmermann, F., K. Plessow, R. Queck, C. Bernhofer, and J. Matschullat (2006). "Atmospheric N-and S-fluxes to a spruce forest—Comparison of inferential modelling and the throughfall method". *Atmospheric Environment* 40.25, 4782–4796.

Acknowledgements

As I reflect on the close of my PhD journey here in Luxembourg, I can scarcely believe it's come to an end. When I first began with LIST, the thought of a four-year tenure felt like a lifetime, a far-off endpoint. Yet, before I knew it, the finish line was upon me.

The past four years have been a whirlwind of experiences, both professionally and personal. I was fortunate to start my PhD with a cohort of 14 others in the DTU at LIST, a rare occurrence at a research institute. This large group of peers fostered a sense of camaraderie as we navigated our academic pursuits together. I formed bonds with fellow PhD students that I know will last a lifetime. I special thanks to the OG members of the A008 office. You know who you are! One of these individuals, who I was lucky enough to call my best friend before embarking on this journey, was also completing her PhD in Munich. Her understanding of the struggles we faced only solidified her place as an honorary member of our group. I was lucky enough to marry her in March 2023. These past four years have had a profound impact on me, shaping me both professionally and personally. I would like to dedicate this section of the thesis to extend my heartfelt gratitude to the institutions and people who made this PhD journey possible.

I am deeply thankful for the support of the FNR and LIST throughout my PhD journey. The funding from the FNR allowed me to focus solely on my research without any financial worries. The resources and state-of-the-art facilities, along with the chance to work in the Weierbach Experimental Catchment, provided by LIST were vital to the success of my work and I am forever grateful for their assistance. My journey would not have been complete without the ERIN and CAT group at LIST. Their interdisciplinary and collaborative atmosphere fostered a wealth of ideas, motivating me to push beyond the limits of my research. I am particularly grateful for the opportunities they provided to present my work and receive insightful feedback. I am humbled by their unwavering support and guidance throughout my PhD journey, and I am forever grateful for their impact on my academic and professional growth. I am also thankful to my fellow PhD students, the ones that came before me and the ones that shared the journey with me. Your success was an inspiration to me to keep at it, keep going forward and reach the finish line.

I express my heartfelt gratitude to the HOST team - Jeff, Viola, and Jérôme - for their invaluable support throughout my fieldwork. Their help with pre-processing water samples

and the wonderful memories created during the rainy days in the Weierbach will always hold a special place in my heart. I am truly grateful for their technical proficiency and wealth of knowledge, which greatly enriched my research. I will always be thankful for their support and guidance. Additionally, I extend my sincere appreciation to François Barnich and Loic Leonard. Their tireless effort in assisting me with the daunting task of analysing the hundreds of samples collected during my fieldwork was greatly appreciated. I will always cherish the early morning coffee and pain au chocolate with Loic, a fond memory that will bring a smile to my face.

I would now like to extend my gratitude to my supervisors. These individuals played a significant role in my work both technically and personally. Firstly, I would like to thank Laurent Pfister for his support and technical inputs throughout my PhD journey. He was always available to listen and resolve any professional or personal problems I encountered. I am deeply grateful for all that he has done for me. Next, I would like to express my gratitude to Erwin Zehe. Thank you for the time and attention you gave to me and my work. Your clear and knowledgeable assessments during meetings always helped me improve my work. Your well-thought-out critiques were informative, kind, and always aimed at bettering my work. I would also like to thank Laurent Gourdol, who, even though he was not an official member of my CET committee, made a significant contribution to my PhD. Thank you for all your help on the technical aspects I had little knowledge of when starting my PhD. I have learned a great deal from you, and I am forever grateful.

Lastly, Christophe Hissler, what can I say? "The man, the myth, the legend!" Christophe, as I am writing this and reflecting on the time at LIST, I am feeling relieved to have reach this point, but also sad that it will come to an end. It was for me a great pleasure to be your student. I have started a PhD very late in my life compared to my peers, and I thought it would be a cake walk. Hard was the fall! Thank you for being my mentor on this journey. Thank you for all you have done for me and for choosing me for this project. Thank you that you kept believing in me even though at stages it looked like my PhD campaign was a lost cause. I am forever in your debt.

I guess that that wraps up most of it. I would now like to write a personal acknowledgement to my loved ones. This journey was one of great sacrifice to me. My parents are in are now in the in their twilight years and I am mindful of the value of time and that it is finite. I would like to thank them for all the support and understanding. Also, I would like to express my sadness that I had to spend so much time not seeing them in pursuit of this goal. I could not have reached this point if it were not for the sacrifices, they made in their lives to provide me with opportunities. As I get older myself, I come to understand things that was not clear to me in my youth. My two dear brothers, thank you for all your support, there is no bond stronger than brotherhood.

I would like to give special thanks to my lovely supporting wife. Serita, thank you for all the support, all the sacrifice and all the help. You could understand what I had to overcome because you already went through it. Sometimes I think you are the older and wiser one. I feel very privileged to have had you by my side and look forward to the next chapter of the adventures we will share.

I would like to conclude by saying that I could not have accomplished any of this without the Grace of the God of Abraham, Isaac, and Jacob.

This work is part of the doctoral unit HYDRO-CSI project and was supported by the Luxembourg National Research Fund (FNR) in the framework of the FNR/PRIDE research programme (contract no. PRIDE15/10623093/HYDRO-CSI/Pfister).

Fonds National de la Recherche Luxembourg

LUXEMBOURG INSTITUTE OF SCIENCE AND TECHNOLOGY | LIST

UNIVERSITÉ DU LUXEMBOURG

KIT Karlsruher Institut für Technologie

Catchment and Ecohydrology Research Group

HYDRO CSI DOCTORAL TRAINING UNIT